Spectral Fatigue Analysis Techniques

Zhihua Hu

A Dissertation submitted for the Degree of
Doctor of Philosophy

Department of Mechanical Engineering
University College London

November 1994

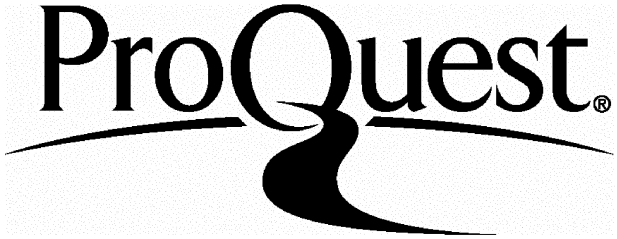

Abstract

This thesis presents a practical design tool for wind turbine blades which was developed from existing theory on spectral fatigue analysis previously used for offshore platform design. The usual aim with spectral fatigue analysis techniques is to estimate fatigue damage or some related function such as rainflow ranges from spectral statistics. Monitored structural responses from different wind turbines were used to assess these existing techniques. The best two methods (suitable only for Gaussian stationary and random responses) were found to be Dirlik's empirical formula and Bishop's theoretical solution. Various parameters involved in the computation such as cutoff frequency and clipping ratio were examined. Guidelines for selection of these parameters are also given.

A method based on Bishop's theoretical solution is extended to include the influence of mean stress. The joint PDF of rainflow cycle and mean stress can be obtained from the response PSD using this method. Because the global mean level information is usually not provided by the PSD, only the relative mean of each rainflow cycle is calculated using this method. The global mean level can then be provided by the designer during the structural analysis stage. This new method was used to analyse the mean stress influence for wind turbine blades using the two monitored structural response histories mentioned above.

A number of possible approaches for the spectral fatigue analysis of non-Gaussian response histories are discussed. A method based on Bishop's theoretical solution is extended to calculate the PDF of rainflow ranges from non-Gaussian response histories specified as a peak trough transition matrix. Although this is only a partial solution to the overall problem it still represents a significant breakthrough. It may, for instance, be of use for estimating rainflow ranges from standardised load sequences specified as turning point matrices. Restricted by the complexity of non-Gaussian processes, especially the limited information provided by PSD's, a universal solution for the transition matrix and the peak number of the process in unit time is currently not available.

As part of the continual development of wind turbines, blade diameters are continuing to increase. The blade response can then sometimes contain a huge deterministic component, caused by gravity, which makes the edgewise response process not only non-Gaussian but also not random. Existing methods can not deal with this situation. By numerical simulation from selected spectra and deterministic component parameters, a mathematical model for the rainflow cycle PDF has been established. Least square techniques were employed for curve fitting to obtain a set of model parameters. These parameters were used to train a back propagation neural network. Finally, a neural network toolbox was developed for the fatigue analysis of wind turbine blades subjected to both Gaussian stationary random flapwise responses and edgewise responses with a deterministic component. In principle, the method can easily be extended to cover more then one deterministic components. Verification of the technique has been carried out using measured responses from a Howden HWP330 wind turbines.

Table of Contents

List of Figures

List of Tables

List of Symbols and Abbreviations

PSD	Power Spectral Density
PDF	Probability Density Function
DFT	Discrete Fourier Transform
FFT	Fast Fourier Transform
RAT	Reverse Arrangement Test
rms	root mean square
S	cycle range
N	cycle number
b	inverse slope of *S-N* curve
k	*S-N* curve intercept

Chapter 2

a	crack length
ΔK	stress (strain) intensity factor
D,n	material constants
Y	specimen geometry and loading factor
$\delta\sigma$	cycle stress range
n_s	number of cycles with range S
E[D]	expected fatigue damage
E[P]	expected peak number in unit time
E[0]	expected zero crossing in unit time
T	time duration
p(S)	cycle range probability density function
y(t)	response series
t^+	time forwards
t^-	time backwards
x(t)	random process
P(x)	probability distribution of x
p(x)	probability density function of x
α_n	nth order moment
μ_n	nth order central moment
$\overline{x}$	mean value of random process
σ	root mean square
$E\{.\}$	mathematical expectation
$\phi(u)$	characteristic function
R_{xy}	cross-correlation function
τ	time lag
R_x	autocorrelation function
R_{xx}	autocorrelation function
a_n, b_n	Fourier constants
ω_n	radius frequency
$X(\omega)$	Fourier integral
$A(\omega)$	real part of $X(\omega)$
$B(\omega)$	imaginary part of $X(\omega)$
$S(\omega)$	two sided spectrum
$G(f)$	one sided spectrum
X	stochastic process
$\dot{X}$	first order differential process
$\ddot{X}$	second order differential process
$G_k(f)$	power spectral density function
L_s	duration of signal
Δt	time interval width of signal
m_n	nth order moment of PSD
γ	irregularity factor
f_m	"mean" frequency
M	mass matrix
C	damping matrix
K	stiffness matrix
V	deformation
$p(\tau)$	loading
T_p	period of load
$h(\cdot)$	unit impulse response function
$P(i\omega)$	Fourier transform of load *p(t)*
v(t)	time domain response
$V(i\omega)$	frequency domain response
$H(\omega)$	frequency response function
$S(i\omega)$	response spectrum
$u[\cdot]$	unit step function
$N()$	number of level crossing
$r(0)$	number of zero crossing
$M()$	number of extrema
$q_+()$	number of extrema per unit time

Chapter 3

$E[D]_{RR}$	expected damage by rainflow cycle
$E[D]_{NB}$	expected damage by narrow band solution
$\lambda(\cdot,\cdot)$	correction factor
a,c	constants
ϵ	$= \sqrt{1-\gamma^2}$

$\Gamma(\cdot)$	Gamma function
S_h	equivalent stress
$erf(\cdot)$	error function
z	normalised cycle range ($= S/2\sqrt{m_0}$)
$p_{RR}(z)$	rainflow cycle range PDF
C_1	coefficients in Dirlik's formula
C_2	coefficients in Dirlik's formula
C_3	coefficients in Dirlik's formula
τ	factor of exponential distribution
α	factor of Rayleigh distribution
Y_1	first event in rainflow cycle
Y_2	second event in rainflow cycle
Y_3	third event in rainflow cycle
$Y_1()$	probabilities of Y_1
$Y_2()$	probabilities of Y_2
$Y_3()$	probabilities of Y_3
ip	peak level
kp	trough level
dh	level interval width
$X(t)$	stochastic signal
$Z(t)$	deterministic component
$Y(t)$	combined time history $X(t)+Y(t)$
$g_x()$	bandwidth correction term
$M(\cdot,\cdot,\cdot)$	confluent hypergeometric function
N_u	number of mean upcrossings of deterministic component in one period
N_p	number of peaks of deterministic component in one period
σ_X	standard deviation of stochastic process
σ_Z	standard deviation of deterministic component
c_k	amplitudes of sine waves
$\phi(t)$	standard normal distribution
$\psi(t)$	$= \int_\infty^t \phi(p)dp = erf(t)$
$\xi(t)$	$= \phi(t) - t\psi(-t)$
$\gamma(t)$	deterministic component of the combined signal

Chapter 4

N	number of signal blocks
A	acceptable range for RAT
χ^2	chi-square distribution
X^2	calculated value of chi-square test
K	class intervals
f_i	observed frequency
F_i	expected frequency
n	number of freedom
α	significance level
$\chi^2_{n;\alpha}$	chi-square value with number of degrees n with significance level α

Chapter 5

ρ	clipping ratio
X_{max}	assumed maximum value of random process

Chapter 6

S_a	cycle range with mean
S_{a0}	cycle range with zero mean
S_m	mean stress of cycle
S_{ult}	ultimate tensile stress
S_y	yield stress
$f(\cdot\|\cdot)$	conditional probability
α_1	trough level
α_2	peak level
$P_{min,max}()$	peak-trough transition probability
P	transition probability matrix
p_{ij}	element of P
C	absorption state
T	transient state
R	transition probability from T to C
Q	transition probability within T
I	transition probability within C, unit matrix
O	transition probability out of C, null matrix
Π	equilibrium distribution of transition probability
f_j^i	long run probability of transition from i to it j

Chapter 7

$H_k()$	Hermite series
$P(\omega)$	Fourier transform of $p(x)$
H_p	entropy of PDF
C_k	coefficient
R_{xxx}	bi-correlation
t_k	time argument
R_{xxxx}	tri-correlation
$S_{xxx}(\cdot,\cdot)$	bi-spectrum
$S_{xxxx}(\cdot,\cdot,\cdot)$	tri-spectrum
F_x	cumulative distribution of process $X(t)$
Φ_u	cumulative distribution of process $U(t)$
$g(\cdot)$	transferring function from Φ_u to F_x
$\xi,\ \dot{\xi}$	random process and its first order differential
$p(\xi,\dot{\xi})$	joint PDF of ξ and $\dot{\xi}$
$F(\hat{\xi})$	peak probability distribution of ξ
$N(\cdot)$	number of level crossings

Chapter 8

$x(t)$	stationary Gaussian process
$X(\omega)$	Fourier transform of $x(t)$
$S(\omega)$	PSD function of $x(t)$
$X^*(\omega)$	orthogonal function of $X(\omega)$
$G(\omega)$	one-sided PSD
ψ	phase angle information
$Y(t)$	complex random process
$A,\ Q$	constants for defining spectra
f_1, f_2	constants for defining spectra
f_c	constants for defining spectra
p_1, p_2	constants for defining spectra
A	amplitude of sine wave
$p_x(x)$	PDF of sine wave $x(t)$ with random phase
$p_y(y)$	Gaussian distribution process $y(t)$
$p(z)$	PDF of process $z(t)=x(t)+y(t)$
f_{RR}	model function for rainflow cycle PDF
C_1	constants in model equation
C_2	constants in model equation
C_3	constants in model equation
τ	coefficient in exponential distribution
α	coefficient in Rayleigh distribution
$\mu,\ \beta$	coefficient in Gaussian distribution
θ	model parameter
$f(x,\theta)$	model equation
$e_i(\theta)$	residual of ith observation
$\Phi(\theta)$	least square error (sum of squares of the residual)
ρ_i	iterate step length
v_i	iterate direction
θ^*	target value of θ
R_i	coefficient matrix
q_i	gradient vector
$H_{ij}(\theta)$	Hessian matrix
N_{ij}	approximation of H_{ij}
$h_j(\theta)$	constraint equation
$\zeta_j(\theta)$	penalty function
α_j	penalty factor
$\Phi^\dagger(\theta)$	extended objective function
$E(\theta)$	objective function for the model of rainflow cycle PDF
$p_{RR}(z)$	rainflow cycle PDF counted from simulated signal
$\xi(z)$	weight function
net_{pj}	input to neuron j from system input p
w_{ij}	weight factor of neuron i to neuron j
o_{pi}	output of neuron i for system input p
δ_{pk}	error at neuron k for system input p
E_p	total error of output layer
μ	coefficient of sigmoid function
δ^o_{pk}	intermediate quantity
η	upgrading step size

Chapter 9

$X(t)$	response of wind turbulence
$Y(t)$	response of gravity
$Z(t)$	sum of $X(t)$ and $Y(t)$
A	amplitude of gravity response
ϕ	azimuth of turbine blade
ξ	phase of gravity response

Acknowledgements

I would like to express my thanks to my supervisor, Dr. Neil Bishop. The thesis is fulfilled with his excellent supervision and encouragement.

With special thanks to my wife, Wang Qin, for her companionship and understanding during this difficult time in the last four years, which makes all this possible.

I will not forget the support from my parents and two sisters. They sustained all the hardship in the past fifteen years after I left home in 1979.

I would also like to express my appreciation to Professor Fang Shanfeng and other Professors in the Department of Civil and Structural Engineering, Wuhan University of Hydraulic and Electric Engineering, P.R. China, for their guidance and help during my time in China before I came to study in Britain.

Finally, thanks to the Chinese government and British Council for their sponsorship of the work.

Declaration

This dissertation is submitted in support of an application for the Degree of Doctor of Philosophy in Engineering Science, from University College London.

No part of the work contained in the thesis has been submitted for any other Degree or Diploma from this University or any other Institution.

All the computation work in this thesis was performed by me with my own programs. All the programs used in this thesis are coded and developed by me. The work contained in this thesis is original and my own unless otherwise stated in the text.

I hereby declare that this declaration is true in every respect.

Zhihua Hu

Chapter 1

Introduction

Spectral fatigue analysis is a very new topic. Basic techniques were developed for very limited situations in the 1960's and 1970's. More advanced techniques for stationary Gaussian and random loadings were developed in the late 1980's and early 1990's. The original objectives of the work in this thesis were to extend the techniques to cover loading situations not satisfying these assumptions and these objectives have been satisfied through the development of solutions to cover non-Gaussian loadings and non-random (deterministic) components. In addition, further goals have been achieved such as a solution for the range-mean distribution for a random signal specified in the frequency domain as a Power Spectral Density (PSD) function.

Fatigue is defined as the process of structural change occurring in a material subjected to conditions which produce fluctuating stresses and strains at some point or points and which may culminate in cracks or complete fracture after a sufficient number of fluctuations [1]. Fatigue failures were starting to worry engineers over a hundred years ago [2] [3]. Research on fatigue was then started. Early research during 1850 to 1875 involved conducting experiments to establish a safe alternating stress below which failure would not occur. Full scale axles as well as smaller laboratory specimens were employed to establish the endurance limit concept for design. Among the early researches, August Wöhler first pointed out many important aspects of fatigue behaviour. The most important one being that fatigue depends more on the range of stress than the maximum stress and the life of specimens reduces when the amplitudes of repeated loading increases. He also introduced the concept of a stress versus life *(S-N)* diagram.

After the initial research from 1850 to 1875, more experimental work was conducted to establish a clearer understanding of the fatigue phenomena, i.e., the process of crack propagation under cyclic loading. The importance of cyclic deformation was clearly established in 1932 [4]. Research in fatigue during the 1930's and 1940's was largely devoted to experimentally establishing the effects of

the many factors that influence the long-life fatigue strength. Tests were usually conducted in rotating bending and the life range of interest was about 10^6 cycles and greater.

The quantitative relationships between plastic strain and fatigue life was established in the 1950's. In the 1960's fracture mechanics was developed as a practical engineering tool for fatigue analysis. Paris quantified the relationships for fatigue crack propagation in "Twenty Years of Reflection on Questions Involving Fatigue Crack Growth". By the 1970's fatigue analysis became an established engineering tool in many industrial applications.

Based on this research, various analysis techniques [5] [6] have emerged to deal with different design requirements. They include:

(i) The nominal stress approach. The amplitude of some representative stress in the component is used to predict its life. The stress is often a nominal stress and local features such as holes and notches are dealt with by introducing stress concentration factors. Failure may be taken as the appearance of a crack, a specific length of crack, or total failure depending on the test data available.

(ii) The fracture mechanics approach [7]. Crack propagation is assumed to depend on a fracture mechanics parameter, usually the range of crack tip stress intensity factor ΔK. Life is then calculated by assuming an initial crack length and finding how many cycles are needed to make this crack grow to an unacceptable size.

(iii) The local stress-strain or critical location approach [8] [9]. The strain history of some critical location is estimated from the loading history, including plasticity effects. Life is then estimated from test data taken under strain controlled conditions.

The nominal stress approach was used in this thesis. It was chosen because methods such as the ones described above, either have no relevant influence on the focus of the present study, or are unsuitable for dealing with the loading problem investigated because there is a need to define a stress (or strain) "cycle" for the loading conditions which are more complex than constant amplitude.

For a constant amplitude loading history, the S-N curve can be reliably used to predict fatigue life. However, when a structure or component is subjected to normal service loadings this approach has to be adapted to account for the fact

that the loadings will not be of constant amplitude. For such situations, firstly there must be a way to count the accumulation of fatigue damage, and secondly a method must be used to extract the "cycles" which contribute to such damage from the loading time history. For the first problem, Miner's law is generally adopted. This law assumes a linear fatigue accumulation and ignores the order of cycles of different range and their interactive effects [10]. For the second problem, many methods of "cycle" defining or counting have been proposed. Among them, the rainflow cycle counting method is generally used because it is believed that this method gives the best correlation with test results.

For stochastic loading, it is hard to express the loading history using a mathematical formula. A more common way is to express the loading in the frequency domain as a PSD, as with, for instance, wind loading, sea wave loading, etc. The structural analysis for such loading histories is also conducted using frequency domain techniques. Using a linear assumption, the input-output relationship is described with the so-called transfer function. This analysis technique has many advantages. The most important one is that, the tedious and time consuming computing work in the time domain can be avoided and the response spectrum can be obtained without knowing the time history of the loading (actually it is very difficult to know). With most Finite Element packages used for structural analysis, such spectra can be obtained directly.

It is for this reason that considerable attention has focused on the spectral fatigue analysis approach for structures and/or components subjected to stochastic loadings [1]. This approach uses the frequency domain information describing structural response to predict the fatigue damage, rather than relying on the more traditional deterministic or time domain solutions.

Work by S. O. Rice [11] and then J.S. Bendat [12] produced relationships for calculating the number of peaks and zero crossings per unit time from the joint probability density function of the process and its first and second order differential processes. For a Gaussian signal, this joint probability density function can be determined from the frequency domain representations of the loading. This relationship provides the basic foundation for spectral fatigue analysis.

The first frequency domain approach was the so-called narrow band solution which assumes that the response has a narrow frequency band of one predominant frequency. However, this is not always the situation, especially when taking account of possible nonlinearities and the fact that structures are nearly always multi-degree of freedom systems. Other methods were developed to modify it to

deal with more general loading situations and to use the rainflow cycle definition. Some methods have also been developed to calculate the rainflow cycle probability density function directly, either using numerical simulation [13] or Markov chain theory [1]. Most of the work up to present date assumes that the response processes are stationary, random and Gaussian. Perhaps there are two reasons for this assumption. The first is that, according to the central limit theorem, most structural responses should be Gaussian. The second is that, the Power Spectral Density functions can only provide enough information about the distribution of Gaussian processes. It is known that the distribution of the process and its first and second order differential processes is essential for such analysis. For non-Gaussian responses, there is currently no efficient way to perform the fatigue analysis using frequency domain information. Actually, non-Gaussian processes are too wide a class of distributions to deal with as a whole.

The first large scale application of frequency domain fatigue analysis was for offshore engineering. Much material has been published on the spectral fatigue design of offshore platforms. This technique has been applied for railway engineering design [14]. This technique has also been applied to wind turbine blade design. However, the loading on wind turbine blades does not satisfy the Gaussian assumption as the gravity component in the edgewise direction becomes bigger. This deterministic (gravity) component is applied predominantly in the blades edgewise direction although there is some coupling into the flapwise direction. In all but the purely flapwise direction there is therefore a combined stochastic (wind loading) and deterministic (gravity) mixed signal. Such a deterministic component makes the response not only non-Gaussian but not purely random as well. This thesis develops a fatigue design tool for such structures.

Chapter 2 gives the theoretical background necessary for spectral fatigue analysis, such as Miner's law, rainflow cycle counting, the theory of stochastic processes, spectral analysis etc. This chapter also presents Rice's work for deriving the number of peaks and zero-crossings of a stochastic process in unit time.

Chapter 3 presents most of the present methods using frequency domain information. Among them are the narrow band solution and the so-called correction factor methods, Tunna's method, Dirlik's empirical formula, Madsen's formula, and Biship's theoretical solution.

Chapter 4 assesses most of the present methods with two sets of monitored structural response data. First of all, a statistical analysis of the time histories is performed in order to check stationarity and normality. Then, using the PSD's

calculated directly from these signals, the fatigue damage is calculated using the frequency domain methods. Rainflow cycle counting is also performed on these time signals directly and the results are taking as a reference solution with which to compare the frequency domain approaches. It was found that the narrow band solution always gives an over conservative prediction while Dirlik's empirical formula and Biship's theoretical solution give the most consistent results with the time domain solution. It was also found that the existence of a deterministic component in the response causes great problems for the fatigue analysis as expected.

Chapter 5 presents the computational considerations required when performing the calculations in **Chapter 4**. Some problems concerning practical calculations are discussed in this chapter. The first problem discussed is the selection of the cutoff frequency of the PSD function, which is related to the monitoring noise problem or the truncation of response spectra. The frequency cutoff point is the integration limit used when computing the moments of the PSD. Since higher moments are used to determine the probability distribution of the second order differential process, the cutoff frequency problem is sometimes very serious. The length of the signal required for fatigue analysis is also discussed here. This can also be taken as a guide for response monitoring for the purpose of fatigue analysis. The selection of clipping ratio is also an important issue. This chapter finds practical ways of selecting these parameters based on frequency domain information for the first time. The influence of S-N curve slope b is also discussed here. It was found that the so-called equivalent stress parameter should be used with great care.

Chapter 6 presents a method to include the mean stress in spectral fatigue analysis. This method is based on Bishop's theoretical solution [1]. Since the global mean information is not available from the PSD, the relative mean of each cycle is used. This is not usually a problem at the design stage because such global mean information is then often available. For research purposes, this information can be obtained from the corresponding time series. The fatigue damage can then be calculated by employing Goodman's relationship or some other formulae to transform the cycle with mean to a cycle without mean which causes the equivalent fatigue damage. The S-N curve can then be used as usual. This method is applied to the two sets of monitored response histories, i.e., WEG MS-1 and Howden HWP330 data, to assess the influence of mean stress on fatigue.

Chapter 7 gives a review of current approaches for non-Gaussian analysis.

First of all, methods for the mathematical and spectral representation of a non-Gaussian process are discussed. Some methods for the fatigue analysis of non-Gaussian signals with assumptions are also discussed. A method for calculating the rainflow cycle distribution from non-Gaussian responses is presented in this chapter, provided that the peak to trough and trough to peak transition probability matrices are known. Again, this method is based on Bishop's theoretical solution [1]. As the peak number in unit time is related to the joint probability distribution of the process and its first and second order differential processes, it is currently impossible to find a universal formula for the complete problem. The peak-trough transition matrix is also related to these differential processes. In order to make progress with this problem in this chapter an approach related to standard load sequence development is suggested as a better solution if the peak-trough and trough-peak transition matrices are available.

Chapter 8 presents a neural network toolbox for the fatigue analysis of responses which contain a deterministic component. This toolbox is based on numerical simulation. After performing rainflow cycle counting on time series simulated from selected spectra and deterministic components, a mathematical model was established to express the rainflow cycle probability density function. Curve fitting using least square techniques was then employed to calculate a set of model parameters. A neural network was established and trained to calculate the model parameters using spectral statistics and deterministic component parameters. The situation of a pure Gaussian signal is also considered in this neural network toolbox development.

Chapter 9 presents an assessment of the toolbox developed in **Chapter 8**. A first attempt is made to use the edgewise signals of the Howden HWP330 data. An attempt is made to separate the deterministic components from the response histories. A new method combining a band pass filter and a least square technique is proposed for such work. It is a more efficient way than the azimuth averaging method. The assessment gives a satisfactory result.

Chapter 10 gives a summary of the conclusions from each chapter and proposes some topics for future work.

Chapter 2

Theoretical background for spectral fatigue analysis

2.1 Introduction

Structural fatigue under constant amplitude fluctuating stresses has been studied widely for many years, both theoretically and experimentally. In theoretical studies, fracture mechanics can be employed. The theories of linear elastic fracture mechanics (LEFM), elastic-plastic fracture mechanics (EPFM), and even microstructure-based micromechanics have been developed to analyse fatigue damage at different stages of the crack growth [15]. All these theories give us a good understanding about crack propagation and the process of fatigue damage.

If the crack is relatively long (or the stress is low), LEFM is a suitable theory to describe the crack growth. This stage of crack growth is governed by the so-called Paris law as follows:

$$\frac{da}{dN} = D\Delta K^n \tag{2.1}$$

where a is the crack length, N is the cycle number, D and n are material constants, ΔK is the stress (or strain) intensity factor defined as $\Delta K = Y\delta\sigma\sqrt{(\phi a)}$ with Y as the specimen geometry and loading system factor and $\delta\sigma$ as the cyclic stress range. A suitable integral will give the relationship between the limit of stress cycle number N (fatigue life) and the stress cycle ranges S, which is the widely used S-N curve. In the log-log plane, they are generally straight lines, as shown in Figure 2.1. The so-called Basquin equation $N = kS^{-b}$ can then be used to mathematically represent the relationship.

These curves meet well with experimental results [2] [4] [16]. Actually, the S-N curve was first discovered experimentally at an early stage of research in fatigue (See Introduction).

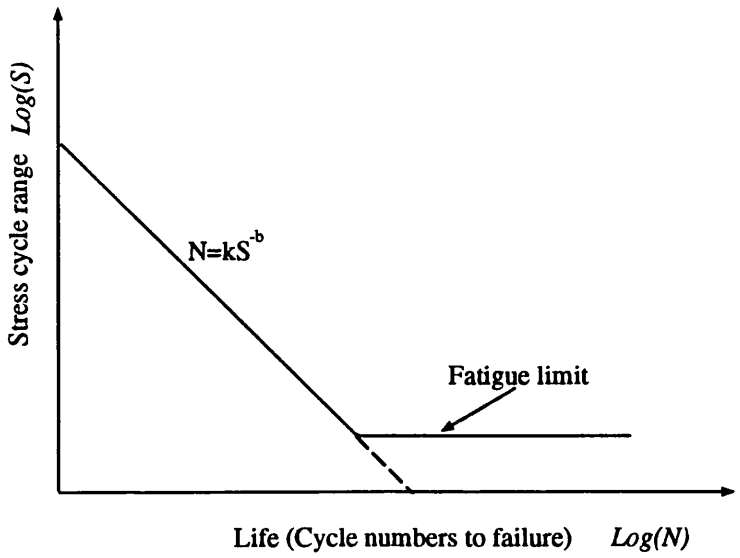

Figure 2.1: A typical S-N curve

Most existing structures, however, experience the action of random loads, such as automobiles, offshore platforms, windmills, air fighters etc. The loads for such structures are neither constant nor even deterministic. There is no way to simply translate the results of constant amplitude fatigue theory for these circumstances even though this is the practical environment under which the structure is operating.

Fatigue damage analysis under such circumstances is very difficult to perform in the time domain at the structural design stage. However, because of the development of random vibration theory, especially the development of frequency domain techniques, this analysis has now become possible using frequency domain information which is much easier to obtain in relation to the structural analysis.

Much research work has been done concerning the task of estimating fatigue life using frequency domain techniques. The ability to estimate fatigue damage from the PSD of stress or strain at some critical location is now a valuable design tool in the offshore, aerospace, and wind engineering industries. The next section gives a brief introduction to the theory necessary for spectral fatigue analysis, such as extracting the stress cycles from complex stress histories, fatigue accumulation, and spectral analysis of structures.

2.2 Fatigue damage accumulation

Two difficulties arise when attempting to use the fracture mechanics approach for design purposes. First, the initial characteristics of the crack or flaws must be

known, and second, the order of different cycles in the lifetime calculation must also be known. This information is often not available for the designer. Indeed, when the loads are stochastic, the ordering can not be known in a deterministic sense. Thus, it is necessary to propagate the statistics of the crack lengths and the loading through the nonlinear differential Equation 2.1, and this is a very difficult task.

In order to overcome these difficulties, the somewhat simpler Palmgren-Miner approach has been extended to cover the case of irregular load histories [17][18]. Two basic assumptions lie at the heart of this approach. First, it is assumed that the damage increment for each load cycle is characterised by the corresponding closed hysteresis path in the local plastic stress-strain diagram shown as in Figure 2.2. Thus, any given (closed loop) load cycle is equivalent to a sinusoidal cycle with the same stress or strain range. In this thesis, it will be assumed that the cycle can be characterised by either the stress or the strain range.

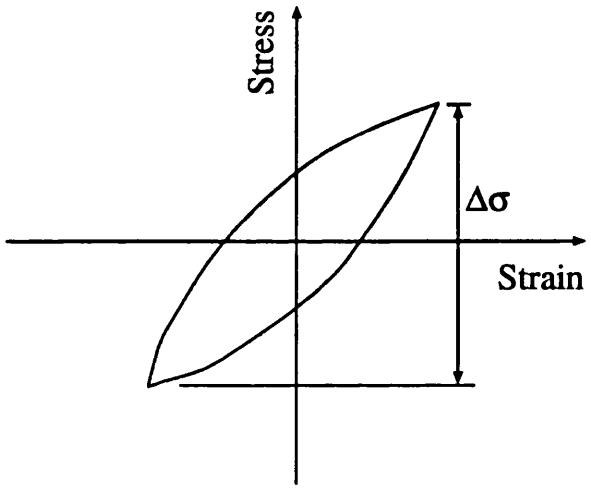

Figure 2.2: The stress-strain hysteresis cycle

The second main assumption is that the effect of the sequencing of the hysteresis cycles can be neglected. It is assumed that each cycle causes an increment of damage which depends on its stress range regardless of the previous load history[19]. With these two assumptions, the cumulative damage caused by stochastic loading can be estimated by assuming that at final failure,

$$\sum \frac{n_s}{N} = 1.0 \tag{2.2}$$

where n_s is the number of cycles counted with a particular stress range band(s) and N is the fatigue life from $S-N$ curve $N = kS^{-b}$ corresponding to this stress range.

The second assumption is of course not precisely correct. However, it has been argued heuristically that in the case of stochastic loading, the random sequencing tends to reduce the influence of cycle order. In other words, sequences causing increased damage (as determined by their order and not the stress range content) are equally as likely to occur as sequences causing decreased damage [20].

The basic idea behind the Palmgren-Miner approach to fatigue analysis is to find a set of sinusoidal load cycles, which does the same fatigue damage as the given history, and then, the results from constant amplitude fatigue testing can be used. The process of finding this set of sinusoidal cycles is generally referred to as the "cycle counting" and will be discussed in the next section.

This linear accumulation law is sometimes found to be not true for some complicated stress situations [15] [21]. Some alternative formula have also been proposed to replace this law [21]. However, no other method has been found to work better for the universal situation.

Using the Palmgren-Miner's law, for a given time series with cycles counted from it, the expected fatigue damage *E[D]* can be estimated using

$$E[D] = \sum \frac{n_s}{N} \tag{2.3}$$

The expected fatigue life is then the reciprocal of *E[D]*.

The number of stress cycle ranges from S to $S + dS$ during time T can be expressed as :

$$n_s = T \cdot E[P] \cdot p(S) \cdot dS \tag{2.4}$$

where, $E[P]$ is the expected number of peaks in unit time and $p(S)$ is the PDF of cycle ranges.

By substituting Equation 2.4 and the Basquin equation into Equation 2.3, yields the expected damage caused by the whole loading history:

$$E[D] = E[P] \cdot \frac{T}{k} \int_0^\infty S^b p(S) dS \tag{2.5}$$

Thus, to calculate the fatigue damage the probability density of cycle distribution and the number of peaks in unit time must be calculated first. The important tasks of spectral fatigue analysis are therefore to calculate both the peak rate and cycle PDF in the frequency domain. This has been achieved by some research groups but with many important assumptions.

Another way of expressing the above damage equation is by using an equivalent stress range parameter. It is a single stress range which produces the same

fatigue damage. It can be expressed as :

$$S_h = [\int_0^\infty S^b p(S) dS]^{\frac{1}{b}} \tag{2.6}$$

2.3 Stress (Strain) cycle counting

Stress cycle definition, or choosing a suitable cycle counting method, is the first problem encounted in random fatigue analysis. As pointed out in the previous section, the cycle counting process is actually trying to find a set of sinusoidal cycles which has the same fatigue damage as the original stochastic sequence. Up to now, there are more than ten types of counting methods which have been reported in the literatures [22][23][24][1]. Some of them are listed below.

(i) **Peak count method.** The number of peaks and/or troughs at particular levels are counted.

(ii) **Mean-crossing peak count method.** As (i) above except that only the maximum peak or minimum trough is counted between zero crossings.

(iii) **Ordinary range count.** The height of ranges between adjacent peaks and troughs is counted. From this a probability density of ordinary ranges can be calculated.

(iv) **Range-mean Count.** This method is identical to (iii), except that the mean value of each ordinary range is also counted.

(v) **Level crossing count.** The number of upwards (or downwards) crossings of particular levels are counted.

(vi) **Fatiguemeter count.** A technique developed in the aeronautics industry to measure variations of acceleration. This is a similar technique to (v) except that small variations in the signal, such as noise, are removed by using a gate or trigger level. Signal excursions from the previous recorded level are only recorded if the trigger level is exceeded [25].

(vii) **Range-pair count** [22].

(viii) **Wetzel's method** [26].

(ix) **Rainflow method** [27][28].

Among all of them, the last three have generally been accepted as better methods of calculating fatigue damage from random signals [18]. Among the last three, the rainflow counting method is now widely accepted as the one which gives the most consistent prediction compared to the actual life result [18][29]. It is for this reason that, rainflow cycle counting is accepted as the default counting method in the whole of this thesis.

The rainflow cycle counting method was first proposed by Matsuishi and Endo [27] [30] in 1968. The original definition of a rainflow cycle was fairly complicated. It simulated the phenomena of rain dripping down rooftops, and so it was called the "Pagoda Roof method". Several equivalent versions of the rainflow counting method have evolved [31] [32] [33]. The minor differences which led to the creation of these methods have now been resolved and all give identical cycle counts if the time history starts and ends at either the highest peak or the lowest trough. The first alternative and more useful definition was made by Rychlik as given below[34].

Definition 1. Let $y(\tau)$, $-T < \tau < T$, be a load function (Figure 2.3), and suppose it has a local maximum at time t with height $y(t) = u$. Let t^+ be the time for the first upcrossing after t of the level u, (or $t^+ = T$ if no such upcrossing exists for $t < \tau < T$), t^- be the time for the first upcrossing before t of the level u, (or $t^- = T$ if no such upcrossing exists for $-T < \tau < t$). Define two ranges at $(t, y(t))$,

$$S^+ = \max_{t<\tau<t^+} (y(t) - y(\tau))$$
$$S^- = \max_{t^-<\tau<t} (y(t) - y(\tau))$$

The amplitude of a rainflow cycle originating at $(t, y(t))$ is defined by :

$$S = \min(S^-, S^+)$$

If the load history is a stationary ergodic time signal, a symmetric about $t = 0$ exists. For this reason, another restriction of $S^- \geq S^+$ can be applied to the definition. Every cycle counted then should be considered as two cycles with the same amplitude. This modified the definition as [1]:

Definition 2. For a rainflow cycle valued S to exist at a current peak, the signal must have the following configuration as in Figure 2.4:

i). takes the signal forwards ($+ve$ time) from point 1 to point 2, a distance S below it.

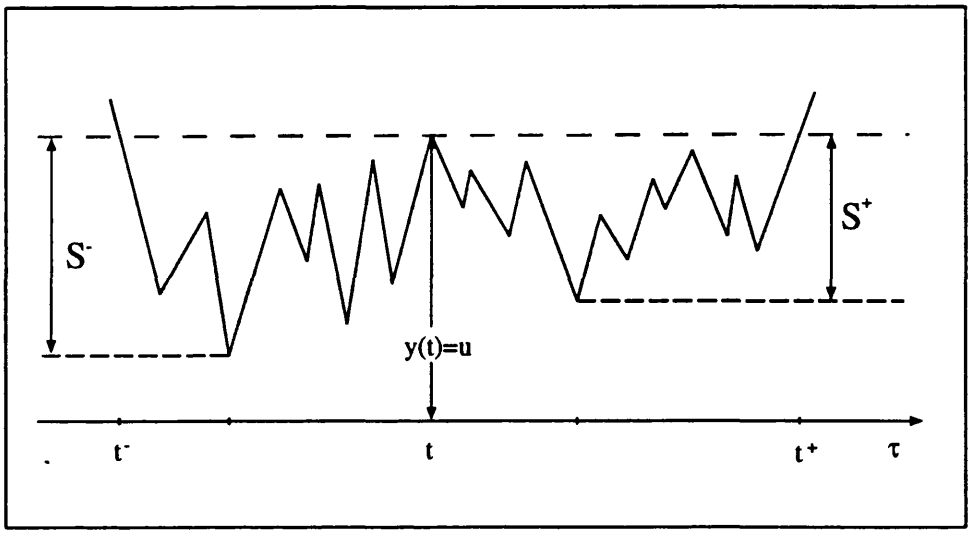

Figure 2.3: Rychlik's definition for rainflow cycle

ii). takes the signal forwards from point 2 to point 3, some level at or above point 1.

iii). takes the signal backwards (*-ve* time) from point 1 to point 4, some level at or below point 2.

iv). takes the signal backwards from point 4 to point 5, some level at or above point 1.

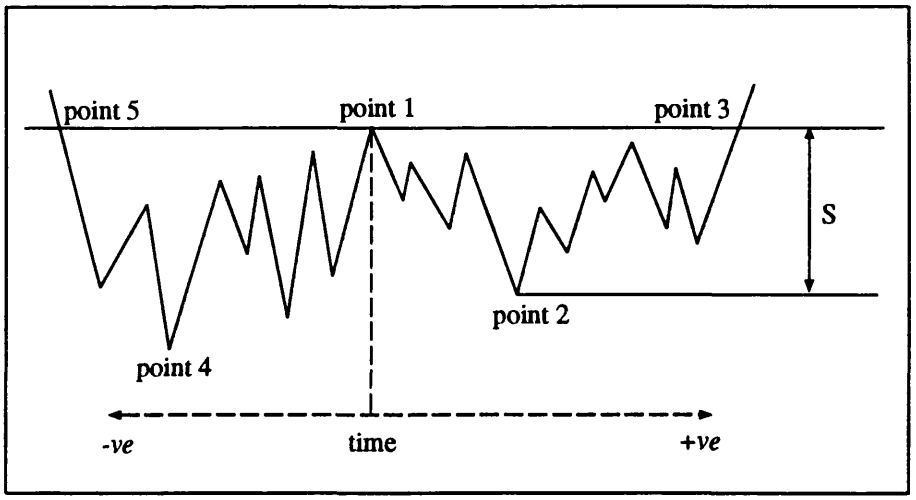

Figure 2.4: Modified definition for rainflow cycle

However, for stationary ergodic signals, when considering the long term distribution of the signal, event iv) of this definition is redundant. Because if the signal comes from below the level of point 2 there is a probability of *1.0* that it

originally came from a level above point 1 prior to this (given that it could go to any level below point 2 during this process).

Based on above analysis, a new definition was made by Bishop[35] and is given as below (Figure 2.5):

Definition 3. For a rainflow cycle valued S to be defined from a particular peak the following events must happen:

i). Y_1 The signal must have come from a level at least S below the level of point 1 without at any time going above the level of point 1 (with any number of extreme points in between).

ii). Y_2 The signal must then go from the level of point 1 to some level a distance S below without at any time between going back to the level of point 1 or below the level of point 2 (with any number of extreme points in between).

iii). Y_3 The signal must then go from the level of point 2 to some level at or above point 1 without at any time going back to the level of point 2 (with any number of extreme points in between).

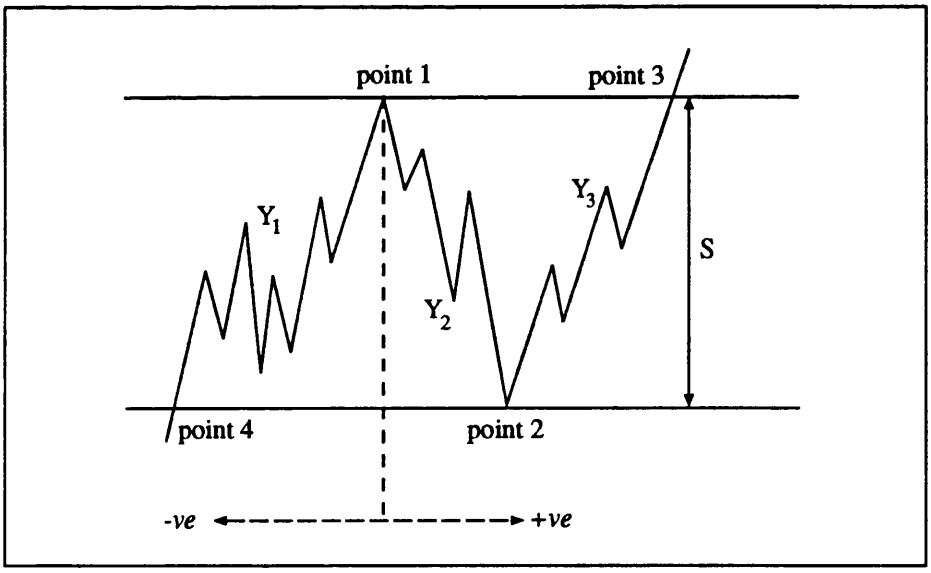

Figure 2.5: Bishop's definition for rainflow cycle

The essential idea of rainflow cycle counting is to characterise the stress (or strain) history over a long time period. That is, to allow the hysteresis cycle to be closed after a long time interval by using the stress-strain "memory" information. The transitions in-between can then be processed separately. The advantage is

therefore that large cycles which can be missed very easily by ordinary counting methods is counted by this method. Figure 2.6 shows such an example. Figure 2.6(a) shows a typical strain history. The initial strain excursion, from O to A, uses the cyclic stress-strain curve. The strain range O to A is plotted on the strain axis, and the stress at point A is calculated from the equation for the cyclic stress-strain curve. Point A is then taken as an origin, the stress range from A to B is then calculated from the hysteresis curve. The actual stress at B then is obtained by subtracting the stress range A to B from the value at point A. By continuing this plotting process until the end of the local strain history, the stress-strain hysteresis history can be derived as shown in Figure 2.6(b).

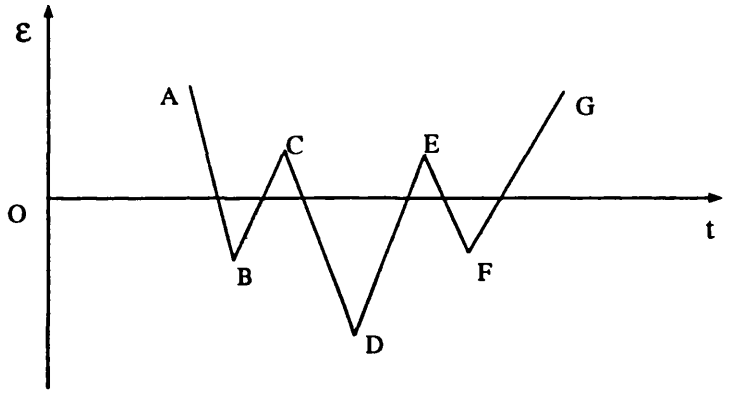

(a). A typical local train history

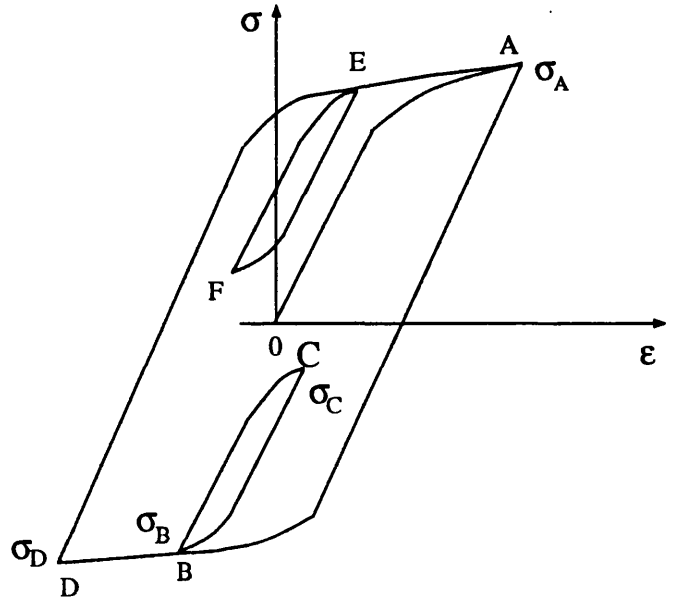

(b). The stress-strain hysteresis loop for strain history (a)

Figure 2.6: An example of rainflow cycle counting

As seen from this stress-strain history, apart from two closed hysteresis loops ranged as E-F and B-C, there exists a large cycle which has the range A-D, which could easily be missed by other counting methods.

2.4 Stochastic process

2.4.1 General assumptions

The time process $x(t)$, in general terms can be classified as either **deterministic** or **random**. A deterministic process can be thought of as one where future states into which the process may fall can be predicted accurately, and with certainty. This type of process can generally be expressed explicitly in mathematical form. Such a process can be either periodic or nonperiodic. A random process is one where the future movements of the process can not be represented by any mathematical expression with certainty at any particular time.

A **stationary** random process is one where the statistical properties measured across a set of records, or ensemble, at a particular time, are identical with the statistics measured across the ensemble at any other time. In addition to being stationary, the process can be termed **ergodic** if the statistics measured along any one sample or record are representative of the statistics measured along any other sample. It is much more convenient for statistical computation if the process has such a property because the statistics can then be obtained from one sample.

2.4.2 Probability and moments

If the process is stationary, it can best be described by its probability distribution function *P(x)* or the probability density function (PDF) *p(x)*, which are independent of time *t*. The moments of the process are defined by its probability density function *p(x)* as:

$$\alpha_n = E\{X^n\} = \int_{-\infty}^{\infty} x^n p(x) dx$$

The central moments are similarly defined as:

$$\mu_n = E\{(X - \overline{x})^n\} = \int_{-\infty}^{\infty} (x - \overline{x})^n p(x) dx$$

in which $\overline{x}$ denotes the global mean value of the process. The variance of the process is then given by the second order central moment, and its square root gives the so-called root mean square (or standard deviation).

The characteristic function of the process is defined as

$$\phi(u) = E\{e^{iux}\} = \int_{-\infty}^{\infty} e^{iux} p(x) dx \tag{2.7}$$

Thus, the PDF is obtained by applying a Fourier transformation to the characteristic function.

$$p(x) = \frac{1}{2\pi} \int_{-\infty}^{\infty} e^{-iux} \phi(u) du \tag{2.8}$$

The characteristic function can be expanded as a MacLaurin series as follows

$$\phi(u) = \phi(0) + \phi'(0)u + \phi''(0)\frac{u^2}{2} + ... = \sum_{j=0}^{n} \frac{\alpha_j}{j!}(iu)^j + O(u^n) \tag{2.9}$$

From Equation 2.7,

$$\phi^{(n)}(0) = i^n \int_{-\infty}^{\infty} x^n p(x) dx = i^n \alpha_n$$

For the situation of more than one random variables, the parameters are defined similarly.

It is obvious that for a general stochastic process, the probability distribution of the process should be described by all the moments of the process. In other words, finite order moments of the process are never enough to fully describe the process. Any truncation causes errors unless the higher order moments can be expressed as functions of lower order moments. The widely used Gaussian distribution with the PDF expressed as

$$p(x) = \frac{1}{\sqrt{2\pi}\sigma} e^{\frac{x^2}{2\sigma^2}}$$

is a good example of where all higher order moments can be calculated from the lower order moments as:

$$\mu_n = (n-1)\sigma^2 \mu_{n-2} \qquad n = 2, 4, 6, \cdots$$

while the odd moments vanish.

2.4.3 Correlation function

The cross-correlation function gives a measurement of the amount by which two functions are related to each other. For two random variables *x(t)* and *y(t)*, their cross-correlation function is given by:

$$R_{xy} = \lim_{T \to \infty} \frac{1}{2T} \int_{-T}^{T} x(t) y(t+\tau) dt \tag{2.10}$$

The autocorrelation function gives a measurement of the amount by which a signal is correlated with itself. It is defined as the average value of the product $x(t)x(t+\tau)$. Provided that the process is stationary, the value of $E[x(t)x(t+\tau)]$ is independent of time t and will depend only on the time separation τ:

$$R_{xx}(\tau) = E[x(t)x(t+\tau)]$$

or, alternatively

$$R_{xx}(\tau) = \lim_{T\to\infty} \frac{1}{2T} \int_{-T}^{T} x(t)x(t+\tau)dt = R(\tau) \tag{2.11}$$

2.4.4 Fourier analysis and spectrum

As well as describing any process in the time domain, it can also be described by its Fourier components in the frequency domain [36] [37]. If *x(t)* is a periodic function of time t, with period T, it can be expressed as an infinite Fourier series of the form

$$x(t) = a_0 + \sum_{k=1}^{\infty} (a_k \cos\omega_n t + b_k \sin\omega_n t) \tag{2.12}$$

where $\omega_n = n\omega_1 = n\frac{2\pi}{T}$, and the Fourier constants are given by

$$\begin{cases} a_0 = \frac{1}{T}\int_0^T x(t)dt \\ a_n = \frac{2}{T}\int_0^T x(t)\cos(\omega_n t)dt \qquad n = 1,2,3,\cdots \\ b_n = \frac{2}{T}\int_0^T x(t)\sin(\omega_n t)dt \qquad n = 1,2,3,\cdots \end{cases}$$

This series expression can also be put in integral form as:

$$X(\omega) = A(\omega) - iB(\omega) = \frac{1}{2\pi}\int_{-\infty}^{\infty} x(t)e^{-i\omega t}dt \tag{2.13}$$

where $A(\omega)$ and $B(\omega)$ denote the Fourier constants a_n and b_n except that a_0 is put to zero.

An inverse transform would give:

$$x(t) = \int_{-\infty}^{\infty} X(\omega)e^{i\omega t}d\omega \tag{2.14}$$

The most important condition for this expansion to hold is that the function must decay to zero when $|t| \to \infty$, that is,

$$\int_{-\infty}^{\infty} |x(t)|dt < \infty \tag{2.15}$$

If the process $x(t)$ is random instead of periodic, it can not be represented by a discrete Fourier series. Also, for a stationary process, Equation 2.15 is not satisfied, so that the Fourier analysis can not be applied to the sample function directly. This difficulty can be overcome by analysing, not sample functions of the process itself, but its autocorrelation function. Provided the mean value of a process is adjusted to zero and the process has no periodic components, the autocorrelation function does satisfy:

$$R(\tau \to \infty) = 0$$

and then the condition

$$\int_{-\infty}^{\infty} |R(\tau)| d\tau < \infty$$

is satisfied. The Fourier transform can be applied to $R(\tau)$.

$$S(\omega) = \frac{1}{2\pi} \int_{-\infty}^{\infty} R(\tau) e^{-i\omega\tau} d\tau \tag{2.16}$$

This function is called the spectral density function of the process in radians. It consists of a Fourier transform pair with correlation function as:

$$R(\tau) = \int_{-\infty}^{\infty} S(\omega) e^{i\omega\tau} d\omega \tag{2.17}$$

The spectral density function defined in this way is known as the two-sided spectral density function. It gives a "negative frequency" which only makes some sense mathematically. More generally, the one-sided spectral density function is defined to give just positive frequency components and can still give the same mean square value of the process. If the frequency (f) is defined in Hz, it is related to the two-sided spectral density function (in radians ω) as:

$$G(f) = 2S(f) = 4\pi S(\omega)$$

The spectra of the stochastic process X and its derivate $\dot{X}$ are connected by

$$S_{\dot{X}}(\omega) = \omega^2 S_X(\omega) \tag{2.18}$$

Similarly,

$$S_{\ddot{X}}(\omega) = \omega^4 S_X(\omega) \tag{2.19}$$

2.4.5 Fast Fourier Transform

In practical calculations, the transform is generally performed on the discrete time series $\{x_r\}$ as:

$$X_k = \frac{1}{N} \sum_{r=0}^{N-1} x_r e^{-i2\pi(\frac{kr}{N})}, \qquad k = 0, 1, 2, ..N-1 \tag{2.20}$$

The one sided Power Spectral Density (PSD) is given by :

$$G_k(f) = 2L_s||X_k||^2 \tag{2.21}$$

where, $L_s = (N \cdot \Delta t)$ and Δt is the time interval between each time point in $\{x_r\}$. The PSD defined in this way takes the energy information from the time series but discards the phase information.

The computation of the discrete Fourier transform of Equation 2.20 is time consuming, especially when N is big. The Fast Fourier Transform (FFT) is therefore generally adopted for this computation. The methodology is that the work can be performed by partitioning the whole sequence $\{x_r\}$ into a number of shorter sequences. Then, combination of these subsequences together will yield the full DFT of the original sequence.

Suppose that $\{x_r\}$, $r = 0, 1, 2, \cdots (N-1)$ is the sequence where N is an even number and that this is partitioned into two shorter sequences $\{y_r\}$ and $\{z_r\}$ where[36][38]

$$\begin{cases} y_r = x_{2r} \\ \\ z_r = x_{2r+1} \end{cases} \qquad r = 0, 1, 2, \cdots, (N/2-1)$$

The DFT's of these two short sequences are Y_k and Z_k given as:

$$\begin{cases} Y_k = \dfrac{1}{N/2} \displaystyle\sum_{r=0}^{N/2-1} y_r e^{-i2\pi(\frac{kr}{N/2})} \\ \\ Z_k = \dfrac{1}{N/2} \displaystyle\sum_{r=0}^{N/2-1} z_r e^{-i2\pi(\frac{kr}{N/2})} \end{cases} \qquad k = 0, 1, 2, \cdots, (N-1) \tag{2.22}$$

Recombination of Equation 2.20 would give:

$$\begin{aligned} X_k &= \frac{1}{N} \sum_{r=0}^{N-1} x_r e^{-i2\pi(\frac{kr}{N})} \\ &= \frac{1}{N} \{ \sum_{r=0}^{N/2-1} x_{2r} e^{-i2\pi(\frac{k(2r)}{N})} + \sum_{r=0}^{N/2-1} x_{2r+1} e^{-i2\pi(\frac{k(2r+1)}{N})} \} \end{aligned} \tag{2.23}$$

It is found from Equation 2.22 and 2.23 that

$$X_k = \frac{1}{2}\{Y_k + e^{-i(2\pi k/N)} Z_k\} \qquad k = 0, 1, 2, \cdots, (N/2-1) \tag{2.24}$$

The DFT of the original sequence can therefore be obtained directly from the DFT's of the two half-sequences Y_k and Z_k according to Equation 2.24. If the original length N of sequence $\{x_r\}$ is a power of 2, then the half-sequences $\{y_r\}$

and $\{z_r\}$ may themselves be partitioned into quarter-sequences, and so on, until eventually the last sub-sequences have only one term each. As Y_k and Z_k are periodic in k with period $N/2$, the full computation is[36]:

$$\begin{cases} X_k = \frac{1}{2}\{Y_k + W^k Z_k\} \\ X_{k+N/2} = \frac{1}{2}\{Y_k - W^k Z_k\} \end{cases} \qquad k = 0, 1, 2, \cdots, (N/2 - 1) \tag{2.25}$$

in which $W = e^{-i(2\pi/N)}$

2.4.6 Statistics in the frequency domain

For the purpose of this thesis the spectrum is characterised by its moments as shown in Figure 2.7. These are actually the weighted sums of the spectrum.

$$m_n = \int_0^\infty f^n G(f) df = \sum_{k=1}^{m} f_k^n G_k(f_k) \delta f \tag{2.26}$$

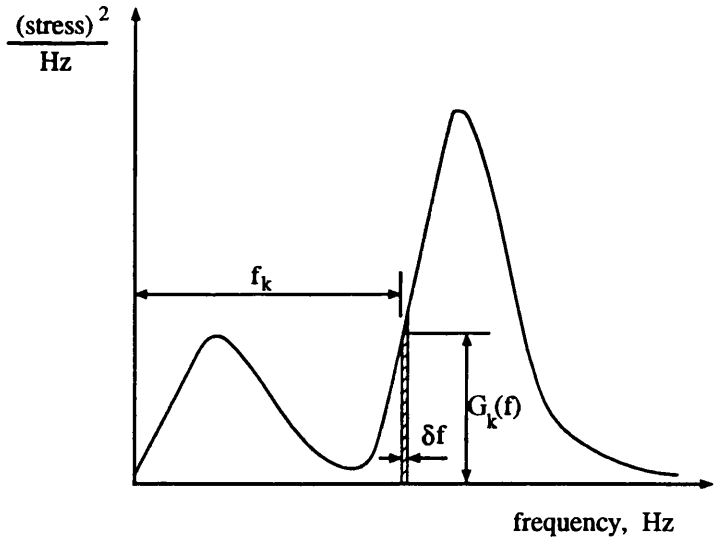

Figure 2.7: PSD moments calculation

The even order moments can be calculated from both one-sided and two-sided PSD's. The odd order moments are generally only defined for one-sided PSD's.

From Equation 2.18 and 2.26, the zeroth order moment from the spectrum gives the standard deviation of the original process. The *2nd* order moment gives the standard deviation of the first order differential process.

Much of the work on statistics of the spectrum relies heavily on the work of S.O.Rice [11] and J.S.Bendat [12]. Some details related to the calculation of these

statistics are shown in the next section. If the signal is stationary, ergodic and Gaussian, results were produced for the number of zero crossings and number of peaks per unit time.

The number of zero crossings and number of peaks per unit time (peak rate) are given as:

$$E[0] = \sqrt{m_2/m_0} \tag{2.27}$$

$$E[P] = \sqrt{m_4/m_2} \tag{2.28}$$

Using the number of zero crossings and number of peaks, the irregularity factor is defined as:

$$\gamma = E[0]/E[P] = m_2/\sqrt{m_0 m_4} \tag{2.29}$$

The irregularity factor is generally taken as an indication of the frequency band width of the signal and its spectrum. It can take any value between 0.0 and 1.0. When γ approaches 1.0, the signal becomes more like a regular sine wave. In this limiting case the signal is said to be **narrow band** and its probability density function of peaks becomes Rayleigh; Cycle counting in this case is relatively easy. As the irregularity factor approaches 0.0 the signal becomes more like shot noise. In this limiting case the signal is said to be completely **wide band**, and its probability density function of peaks becomes Gaussian. In practice the response is rarely narrow nor completely wide band but somewhere between.

In some circumstances, the centroid of the spectrum is taken as a measurement of the frequency level of the spectrum and is defined as "mean frequency" and is made dimensionless by normalisation using the peak rate [13].

$$f_m = m_1/m_0/E[P]$$

2.5 Spectral analysis and structural dynamics

From the theory of structural dynamics, the motion equation of structures can be written as [39] :

$$M\ddot{v} + C\dot{v} + Kv = F(\Omega, t) \tag{2.30}$$

where M, C, and K are mass, damping, and stiffness matrices respectively, v is the structural response, Ω is the space in which the structure is defined. Under the circumstances that the structure is under the action of deterministic dynamic loading, structural analysis can be performed in the time domain using suitable numerical integration methods, such as Newmark method, wilson-θ method, etc. For the case of arbitrary dynamic loading, Duhamel's integral equation can be

taken as the general solution for structural response in time domain. For single degree of freedom systems, this integral can be expressed as:

$$v(t) = \int_0^t p(\tau)h(t-\tau)d\tau \tag{2.31}$$

where, $h(t-\tau)$ is the unit-impulse response function and is expressed as:

$$h(t-\tau) = \frac{1}{m\omega}\sin\omega(t-\tau) \tag{2.32}$$

for undamped single degree of freedom systems.

Most systems are of multi-degree of freedom. If the loading in coordinate j is a general time varying load $p_j(t)$, the dynamic response in coordinate i could be obtained by superposing the effects of a succession of impulses as specified using Duhamel's integral, assuming zero initial conditions. The generalised expression for the response in coordinate i to the load at j is the integral as follows:

$$v_{ij}(t) = \int_0^t p_j(\tau)h_{ij}(t-\tau)d\tau \qquad i = 1, 2, \cdots, N \tag{2.33}$$

where N is the total number of degrees of freedom. $h_{ij}(t)$ denotes the response at coordinate i to the unit-impulse loading in coordinate j. The total response in coordinate i produced by a general loading involving all components of the load vector $p(t)$ is obtained by summing the contributions from all load components:

$$v_i(t) = \sum_{j=1}^{N}[\int_0^t p_j(\tau)h_{ij}(t-\tau)d\tau] \qquad i = 1, 2, \cdots, N \tag{2.34}$$

This type of time domain analysis is complex and time consuming but is possible. However, if the loading is stochastic instead of deterministic in type, this analysis method is generally invalid because the history of the loading is unknown except for some statistical characteristics. Frequency domain analysis then becomes quite useful.

To perform a frequency domain analysis, the variables (load and response) must be expressed as Fourier series. For the periodic loading $p(t)$ with period T, the Fourier series form is given by Equation 2.12 and 2.13.

$$p(t) = \sum_{n=-\infty}^{\infty} P(i\omega_n)\exp(i\omega_n t)$$

where the complex amplitude coefficients are given by

$$P(i\omega_n) = \frac{1}{T}\int_{-T/2}^{T/2} p(t)\exp(-i\omega_n t)dt$$

with $n\omega_1 = \omega_n = n \cdot 2\pi/T$.

When *p(t)* is an arbitrary nonperiodic loading, the above equations can still be used by letting $T \to \infty$, as in integral form

$$\begin{cases} p(t) = \dfrac{1}{2\pi}\displaystyle\int_{-\infty}^{\infty} P(i\omega)\exp(i\omega t)d\omega \\ P(i\omega) = \displaystyle\int_{-\infty}^{\infty} p(t)\exp(-i\omega t)dt \end{cases} \tag{2.35}$$

which is the Fourier transform pair.

The Fourier series expression of the response can then be connected with the Fourier series of the loading by the complex frequency response function $H(i\omega)$, which is the invrese Fourier transform of $h(t)$, as

$$V(i\omega) = \int_{-\infty}^{\infty} v(t)\exp(-i\omega t)dt = H(i\omega)P(i\omega)$$

When the case of multi-degree of freedom is considered, the loading and its Fourier series become a vector $\mathbf{p(t)}$ and $\mathbf{P(i\omega)}$, and the frequency response function becomes a matrix $\mathbf{H(i\omega)}$. Their components in coordinate j are :

$$P_j(i\omega) = \int_{-\infty}^{\infty} p_j(t)\exp(-i\omega t)dt$$

and

$$V_{ij}(i\omega) = \int_{-\infty}^{\infty} v(t)\exp(-i\omega t)dt = H_{ij}(i\omega)P_j(i\omega) \tag{2.36}$$

The response in coordinate i can be obtained as

$$v_i(t) = \sum_{j=1}^{N} v_{ij}(t) = \sum_{j=1}^{N}[\int_0^t p_j(\tau)h_{ij}(t-\tau)d\tau] \tag{2.37}$$

The unit impulse and the complex frequency response functions are two transfer function in time and frequency domains respectively. They are related as a Fourier transform pair:

$$\begin{cases} H(i\omega) = \displaystyle\int_{-\infty}^{\infty} h(t)\exp(-i\omega t)dt \\ h(t) = \dfrac{1}{2\pi}\displaystyle\int_{-\infty}^{\infty} H(i\omega)\exp(i\omega t)d\bar{\omega} \end{cases} \tag{2.38}$$

In multi-degree of freedom cases, this relationship becomes:

$$\begin{cases} H_{ij}(i\omega) = \displaystyle\int_{-\infty}^{\infty} h_{ij}(t)\exp(-i\omega t)dt \\ h_{ij}(t) = \dfrac{1}{2\pi}\displaystyle\int_{-\infty}^{\infty} H_{ij}(i\omega)\exp(i\omega t) \end{cases} \tag{2.39}$$

In the point view of the spectrum, the input and output spectrum are connected by the relationship

$$S_v(i\omega) = H(-i\omega)H(i\omega)S_p(i\omega) = |H(\omega)|^2 S_p(i\omega) \tag{2.40}$$

2.6 Some useful results from the PSD

The expected number of zeros of a stochastic process $X(t)$ within a given interval $[t_1, t_2]$ or, more generally, the expected number of crossing of $X(t)$ at some arbitrary level x_0 in $[t_1, t_2]$ is of considerable interest. When Miner's law is used for random fatigue analysis, the expected number of peaks in unit time is also an important parameter for the damage accumulative computation. Together with the zero crossing rate, it should be calculated from the spectrum[40].

2.6.1 Zero crossings

Let $X(t)$, $t \in T$, be a m.s. differentiable stochastic process[1]. The formulation of the threshold-crossing problem for $X(t)$ is facilitated by defining a new process

$$Y(t) = u[X(t) - x_0], \qquad t \in T \tag{2.41}$$

where u[] is a unit step function. It is seen that the formal derivative of $Y(t)$ can be in the form

$$\dot{Y}(t) = \dot{X}(t)\delta[X(t) - x_0], \qquad t \in T \tag{2.42}$$

where $\delta[]$ is the Dirac delta function. It has the weight $\frac{1}{\dot{X}(t)}$. A typical function of $X(t)$ along with its corresponding sample functions $Y(t)$ and $\dot{Y}(t)$ are shown in Figure 2.8. The sample function of $\dot{Y}(t)$ consists of unit impulses. these impulses are directed upward or downward depending upon whether the crossings of its associated $x(t)$ at x_0 occur with positive or negative slopes.

If $N(x_0; t_1, t_2)$ denotes the random variable whose value is the number of crossings of $X(t)$ at x_0 within the interval $[t_1, t_2]$, it thus can be denoted by

$$N(x_0; t_1, t_2) = \int_{t_1}^{t_2} |\dot{X}(t)|\delta[X(t) - x_0]dt \tag{2.43}$$

The number of zeros of $X(t)$ within the interval $[t_1, t_2]$ is simply $N(0; t_1, t_2)$.

Hence, the expected number of crossings of $X(t)$ at x_0 within the interval $[t_1, t_2]$ is given by

$$E[N(x_0; t_1, t_2)] = \int_{t_1}^{t_2}\int_{-\infty}^{\infty}\int_{-\infty}^{\infty} |\dot{x}|\delta(x - x_0)f(x, t; \dot{x}, t)dxd\dot{x}dt \tag{2.44}$$

$$= \int_{t_1}^{t_2}\int_{-\infty}^{\infty} |\dot{x}|f(x_0, t; \dot{x}, t)d\dot{x}dt \tag{2.45}$$

[1] A second-order stochastic process $X(t), t \in T$, has a *mean square derivative* or *m.s. derivative* $\dot{X}(t)$ at t if

$$\lim_{\tau \to 0}[X(t + \tau) - X(t)]/\tau = \dot{X}(t)$$

Higher order m.s. derivatives are defined analogously. Here, *lim* refers to limit in mean square.

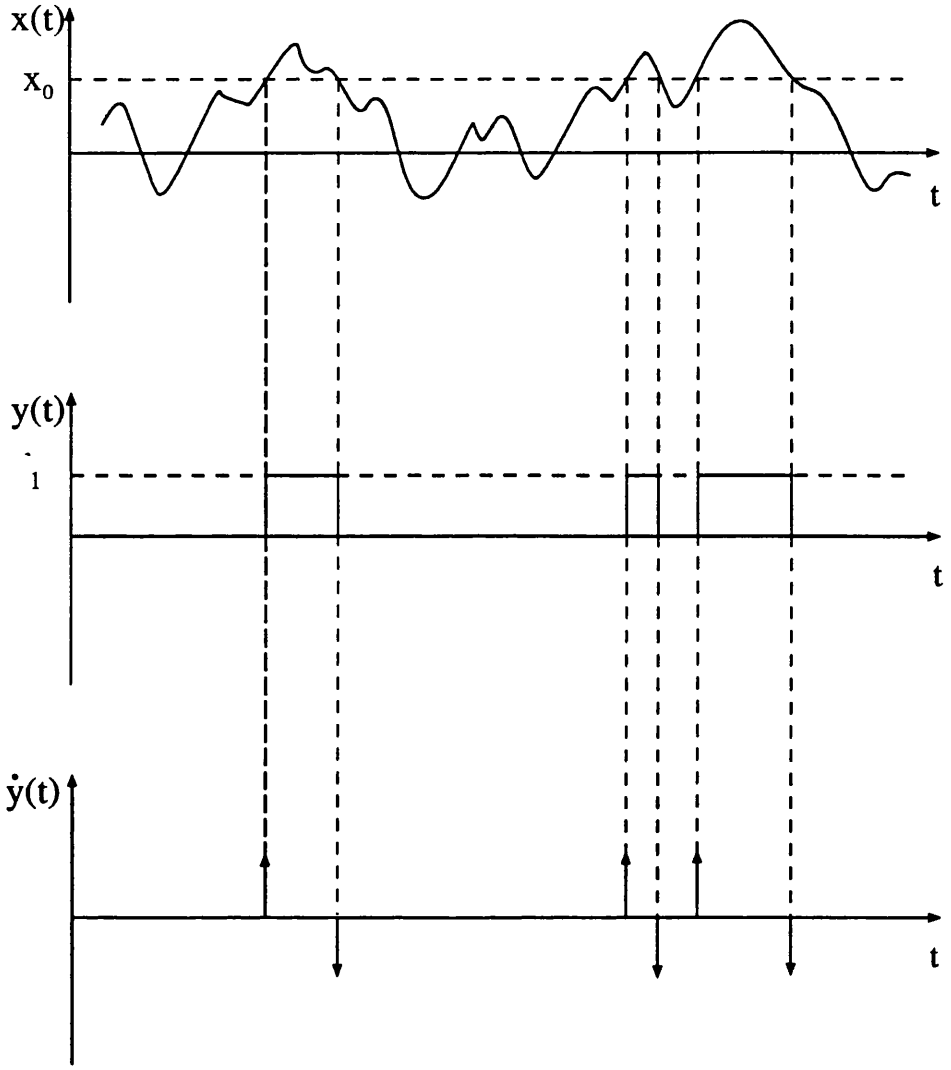

Figure 2.8: A typical sample function of $X(t)$ and its associated sample functions

This gives the information on expected number of zero-crossings and threshold-crossings within an interval by the joint density function of $X(t)$ and $\dot{X}(t)$ at t over the interval.

If $N_+(x_0; t_1, t_2)$ is the number of crossings of $X(t)$ at x_0 with positive slopes with an interval $[t_1, t_2]$, then it can be easily obtained by changing the integral boundary

$$E[N_+(x_0; t_1, t_2)] = \int_{t_1}^{t_2} \int_0^{\infty} \dot{x} f(x_0, t; \dot{x}, t) d\dot{x} dt \tag{2.46}$$

The problem of threshold crossings with negative slopes can also be easily obtained

$$E[N_-(x_0; t_1, t_2)] = -\int_{t_1}^{t_2} \int_{-\infty}^{0} \dot{x} f(x_0, t; \dot{x}, t) d\dot{x} dt \tag{2.47}$$

As seen from Equation 2.45, the integral

$$r(x_0,t) = \int_{-\infty}^{\infty} |\dot{x}| f(x_0,t;\dot{x},t) d\dot{x} \tag{2.48}$$

may be regarded as the expected rate of crossing at $x_0(t)$. This rate becomes independent of t if the stochastic process $X(t)$ is stationary, and $r(x_0,t) = r(x_0)$ gives the expected number of crossings at x_0 per unit time in this case.

Consider the case where $X(t)$ is a stationary, once m.s. differentiable, and Gaussian process with mean zero and correlation function $R_{XX}(\tau)$. The joint density function of $X(t)$ and $\dot{X}(t)$ at t then takes the form

$$f(x,t;\dot{x},t) = f(x,\dot{x}) = \frac{1}{2\pi\sigma_X\sigma_{\dot{X}}} exp[-\frac{1}{2}(\frac{x^2}{\sigma_X^2} + \frac{\dot{x}^2}{\sigma_{\dot{X}^2}})] \tag{2.49}$$

where $\sigma_X^2 = R_{XX}(0)$ and

$$\sigma_{\dot{X}}^2 = R_{\dot{X}\dot{X}} = -d^2 R_{XX}(\tau)/d\tau^2|_{\tau=0} \tag{2.50}$$

The expected rate of crossing at x_0 is constant and can be obtained by substituting Equation 2.49 into 2.48

$$r(x_0) = (\sigma_{\dot{X}}/\pi\sigma_X) exp(-x_0^2/2\sigma_X^2) \tag{2.51}$$

The expected rate of zero crossings has the simple form

$$r(0) = \sigma_{\dot{X}}/\pi\sigma_X, \qquad r_+(0) = r_-(0) = r(0)/2 \tag{2.52}$$

If the spectral density function of the process is $S_X(f)$, then $S_{\dot{X}} = (2\pi f)^2 S_X(f)$. The expected rate of zero crossings can be expressed as

$$r(0) = \sigma_{\dot{X}}/\pi\sigma_X = 2[\int_0^{\infty} f^2 S_X(f) df / \int_0^{\infty} S_X(f) df]^{1/2} \tag{2.53}$$

In terms of the moments of the spectrum, it can be expressed as

$$r_-(0) = r_+(0) = r(0)/2 = \sqrt{(m_2/m_0)} \tag{2.54}$$

2.6.2 Distribution of Extrema

The problem of determining the expected number of extremes (maxima and minima) of a stochastic process *X(t)* within a given interval is a direct analogy with the zero-crossing problem. A maximum in a sample function $x(t)$ of $X(t)$ occurs when its first derivative $\dot{x}(t)$ is zero and the second derivative is negative; a minimum occurs when $\dot{x}(t) = 0$ and $\ddot{x}(t)$ is positive. The number of extrema of

the sample function within a given interval is then equal to the number of zero crossings of $\dot{x}(t)$ in that interval.

Let $X(t), t \in T$ be at least twice m.s. differentiable. As in the zero-crossing problem, we consider a new stochastic process defined by

$$Y(t) = u[\dot{X}(t)], \quad t \in T$$

Formally differentiating *Y(t)* we obtain

$$\dot{Y}(t) = \ddot{X}(t)\delta[\dot{X}(t)], \quad t \in T$$

Hence, the number of extrema of *X(t)* within the interval $[t_1, t_2]$ is given by

$$\int_{t_1}^{t_2} |\ddot{X}(t)|\delta[\dot{X}(t)]dt$$

If only the number of extrema above level x_0 of *X(t)* in the interval $[t_1, t_2]$ is concerned, it can be denoted by random variable $M(x_0; t_1, t_2)$ and be expressed as

$$M(x_0; t_1, t_2) = \int_{t_1}^{t_2} |\ddot{X}(t)|\delta[\dot{X}(t)]u[X(t) - x_0]dt \tag{2.55}$$

The mean is given by

$$\begin{aligned} E\{M(x_0; t_1, t_2)\} &= \int_{t_1}^{t_2}\int_{-\infty}^{\infty}\int_{-\infty}^{\infty} |\ddot{x}|\delta(\dot{x})u(x - x_0)f(x, t; \dot{x}, t; \ddot{x}, t)dxd\dot{x}d\ddot{x}dt \\ &= \int_{t_1}^{t_2} dt \int_{-\infty}^{\infty} d\ddot{x} \int_{x_0}^{\infty} |\ddot{x}|f(x, t; 0, t; \ddot{x}, t)dx \end{aligned} \tag{2.56}$$

It is seen that then the information about the expected number of extrema in a given interval is in general contained in the joint density function of $X(t)$, $\dot{X}(t)$,and $\ddot{X}(t)$ at t over the interval. From this equation, the *maxima* of *X(t)* above x_0 in the interval $[t_1, t_2]$ is expressed as

$$E\{M_+(x_0; t_1, t_2)\} = \int_{t_1}^{t_2} dt \int_{-\infty}^{0} d\ddot{x} \int_{x_0}^{\infty} |\ddot{x}|f(x, t; 0, t; \ddot{x}, t)dx \tag{2.57}$$

As seen from the above, we get

$$q_+(x_0, t) = -\int_{-\infty}^{0} d\ddot{x} \int_{x_0}^{\infty} \ddot{x}f(x, t; 0, t; \ddot{x}, t)dx \tag{2.58}$$

For a stationary, twice m.s. differentiable Gaussian process $X(t)$ with zero mean, the joint density function of $X(t)$, $\dot{X}(t)$, and $\ddot{X}(t)$ takes the form

$$f(\mathbf{x}, t) = (2\pi)^{-3/2}|\Lambda|^{-1/2}\exp[-\frac{1}{2}\mathbf{x}^T\Lambda^{-1}\mathbf{x}] \tag{2.59}$$

where $\mathbf{x}^T = [x\ \dot{x}\ \ddot{x}]$ and

$$\Lambda = \begin{vmatrix} \sigma_X^2 & 0 & -\sigma_{\dot{X}}^2 \\ 0 & \sigma_{\dot{X}}^2 & 0 \\ -\sigma_{\dot{X}}^2 & 0 & \sigma_{\ddot{X}}^2 \end{vmatrix}$$

By substituting the joint probability density function 2.59 into Equation 2.58, the integral can be obtained as:

$$\begin{aligned} q_+(x_0,t) = q_+(x_0) = \ & (2\pi)^{-3/2}(\sigma_X\sigma_{\dot{X}})^{-2}\int_{x_0}^{\infty}\{|\Lambda|^{-1/2}exp[-\tfrac{1}{2|\Lambda|}\sigma_{\dot{X}}^2\sigma_{\ddot{X}}^2x^2] \\ & +(\pi/2)^{1/2}(\sigma_{\dot{X}}^3x/\sigma_X)exp(-x^2/2\sigma_X^2) \\ & \times[1+erf(\sigma_{\dot{X}}^3x/\sqrt{2}\sigma_X|\Lambda|^{1/2})]\}dx \end{aligned} \tag{2.60}$$

where *erf()* is the error function defined by

$$erf(x) = (2/\sqrt{\pi})\int_0^x exp(-u^2)du$$

The expected total number of maxima per unit time $q_+(-\infty)$ is expressed as

$$q_+(-\infty) = (1/2\pi)(\sigma_{\ddot{X}}/\sigma_{\dot{X}}) \tag{2.61}$$

In terms of spectrum moments it has the form

$$q_+(-\infty) = \sqrt{(m_4/m_2)} \tag{2.62}$$

It is also noted that, this formula can be easily derived from Equation 2.53 by noting the equivalence between the zero crossings of $\dot{X}(t)$ with negative slope and the maxima of *X(t)*.

2.7 Discussion

From the theory of fatigue accumulation, the two factors to be calculated from frequency domain information are the peak rate of the random process and the rainflow cycle probability density function. Since the phase information in the complex spectrum is discarded when the PSD is calculated, there is always the question of whether the PSD can provide enough information for a complete fatigue analysis.

The answer to this question can be found by looking at the probability distribution of the time process. The PSD must at least provide enough information for the joint probability distribution of the process and its first and second order differential processes. This necessity is required from Equation 2.58 for calculating the peak rate. If the probability distribution of the process is Gaussian, it can be proven that the joint probability distribution of the process and its first and second order differential processes is Gaussian as well [40]. For this special situation,

the zeroth, second and fourth moments of the PSD can completely determine the joint probability distribution function as $\sigma_X, \sigma_{\dot{X}}, \sigma_{\ddot{X}}$ can be calculated directly from these three moments. This means that spectral fatigue analysis is valid for the situation under which the process has a Gaussian distribution. Perhaps this is the most important reason why a Gaussian distribution is assumed by most of the present methods in use.

However, if the Gaussian assumption does not hold, it is hard to say whether the PSD can provide enough information for spectral analysis. Actually, knowing the distribution of the process itself is not enough because the joint probability distribution can not be decided if the process distribution is not Gaussian. This simply means that some assumptions then have to be made about the joint probability distribution itself. It has still not been proven whether the PSD itself can provide enough information for determining such distributions. Chapter 7 of this thesis covers the topic of non-Gaussian signals in more detail.

Chapter 3

Present methods in use

3.1 General background

Spectral fatigue analysis has been widely used in aircraft, offshore platform [41] [42] and welded joint design [43]. More recently it has been adopted in wind engineering for the fatigue analysis of wind turbine blades. Currently, most of the available techniques assumes that the response is random, stationary, ergodic and Gaussian.

The first spectral fatigue solution was the so-called narrow band solution. Some correction factor methods were then developed to adapt it for wide band situations by incorporating rainflow cycle counting. Theoretical analysis was less prominent than digital simulation work. This is perhaps because of the complexity of the rainflow cycle configuration.

3.2 Narrow band solution

The narrow band solution was the first for resolving the random fatigue damage problem using frequency domain information. It was formulated using the fact that the stress peaks have a Rayleigh distribution if the process is Gaussian and narrow-banded [40]. In particular, each stress range(s) is taken to be twice the stress peak amplitude(s) of the random process. In this case, the probability density of peaks for Gaussian signals with irregularity factor approaching *1.0* is given by :

$$p_{peak}(s) = \frac{s}{m_0} e^{-\frac{s^2}{2m_0}} \tag{3.1}$$

The distribution of peaks can be related to the distribution of cycle ranges because the probability of a range greater than or equal to $S(\equiv 2s)$ is the same as the probability of a peak greater than or equal to s. Thus

$$P[range \geq S] = P[peak \geq s] = \int_0^s p_{peak}(s)ds$$

This integral can be evaluated directly from Equation 3.1 with the result that

$$P[range \geq S] = 1 - \exp\{\frac{-s^2}{2m_0}\} = 1 - \exp\{\frac{-S^2}{8m_0}\}$$

Differentiating this probability distribution gives the PDF for stress ranges in a narrow band Gaussian signal

$$p(S) = \frac{S}{4m_0}\exp\{\frac{-S^2}{8m_0}\} \tag{3.2}$$

The rate of occurrence of cycles for narrow band signal is taken as the rate of occurrence of zero-crossings $E[P] = E[0]$, as $\gamma = E[0]/E[P] = 1$. This gives a conservative result as :

$$E[D]_{NB} = E[P]\frac{T}{k}\int_0^\infty S^b p(S)dS = E[0]\frac{T}{k}\int_0^\infty S^b \frac{S}{4m_0}e^{-\frac{S^2}{8m_0}}dS \tag{3.3}$$

Note here that the damage equation is completely defined using m_0, m_2 and m_4 (if *E[P]* rather than *E[0]* is used).

Further integration gives:

$$E[D]_{NB} = E[0]\frac{T}{k}(2\sqrt{2m_0})^b\Gamma(\frac{b}{2}+1)$$

where $\Gamma(\cdot)$ is the gamma function expressed as:

$$\Gamma(z) = 2\int_0^\infty y^{2z-1}e^{-y^2}dy \qquad z > 0 \tag{3.4}$$

Because numerical integration is now a relatively straightforward task use of Gamma function is less common.

The assumptions leading to this equation are strictly correct only for very narrow-banded Gaussian processes, but the equation is used in a much wider range of situations. For this reason, some methods have been developed to "correct" the narrow band solution into a rainflow solution suitable for wider band situations.

3.3 Correction factor methods

3.3.1 Wirsching's correct factor

The model developed by Wirsching [44][45], was adequate for narrow band loading, but required an empirical function in order to accommodate wide band stress histories as expressed by

$$E[D]_{RR} = E[D]_{NB} \cdot \lambda(b, \epsilon) \tag{3.5}$$

where $\lambda(b,\epsilon)$ is a correction factor for the bandwidth. It was obtained by simulating signals from wide band spectra which were then compared with the rainflow cycle counting results and narrow band results. Regression analysis produced the following expression.

$$\lambda(b,\epsilon) = a + (1-a)(1-\epsilon)^c$$

where

$$a = 0.926 - 0.033b \qquad c = 1.587b - 2.323 \qquad \epsilon = \sqrt{1-\gamma^2}$$

In terms of equivalent stress, it can be written as :

$$S_h = 2\sqrt{2m_0}[\lambda(b,\epsilon)\Gamma(\frac{b}{2}+1)]^{\frac{1}{b}} \tag{3.6}$$

3.3.2 Chaudhury and Dover equations

An equation was proposed by Chaudhury and Dover [46]. After extensive study of the peak distribution in different power spectra, two general solutions for the narrow band and the wide band spectra were determined. Based on the assumption that the equivalent stress range solution always lies between the narrow and wide band solutions, the following semi-theoretical solution was proposed,

$$S_h = 2\sqrt{2m_0}[\frac{\epsilon^{b+2}}{2\sqrt{\pi}}\Gamma(\frac{b+1}{2}) + \frac{\gamma}{2}\Gamma(\frac{b+2}{2})]^{\frac{1}{b}} \tag{3.7}$$

Later, after J.C.P. Kam and W.D.Dover [41] studied this formula using sea state stress response spectra, a new empirical procedure was proposed. It is expressed as:

$$S_h = 2\sqrt{2m_0}[\frac{\epsilon^{b+2}}{2\sqrt{\pi}}\Gamma(\frac{b+1}{2}) + \frac{\gamma}{2}\Gamma(\frac{b+2}{2}) + erf(\gamma)\Gamma(\frac{b+2}{2})]^{\frac{1}{b}} \tag{3.8}$$

The error function $erf(\gamma)$ can be expressed by

$$\begin{aligned} erf(\gamma) &= 0.3012\gamma + 0.4916\gamma^2 + 0.9181\gamma^3 - 2.3534\gamma^4 - 3.3307\gamma^5 \\ &+ 15.6524\gamma^6 - 10.784\gamma^7 \qquad for \quad 0.13 < \gamma < 0.96 \end{aligned}$$

3.3.3 Hancock's equations

Two equations, developed by Hancock *et al* [47], incorporate curve fitting parameters into the Weibull distribution. Thus obtained the expression for equivalent stress. They are expressed as:

Handcock A :

$$S_h = 2\sqrt{2m_0}[\gamma\Gamma(\frac{b}{2}+1)]^{\frac{1}{b}} \tag{3.9}$$

Handcock B :

$$S_h = \gamma\sqrt{2m_0}(2-\xi^2)[\Gamma(\frac{b}{2-\epsilon^2}+1]^{\frac{1}{b}} \tag{3.10}$$

in which ξ is the damping factor.

3.4 Tunna's formula

J. M. Tunna developed two formulae for Gaussian random loads situations [48] [14]. One is used for the narrow band load case, which is exactly the same as formula 3.2. Another one is used for wide band situation, which is expressed as:

$$p(S) = \frac{S}{4\gamma\sigma^2}\exp\frac{-S^2}{8\gamma\sigma^2} \tag{3.11}$$

This formula actually contains the narrow band solution as $\gamma = 1$ for narrow band signals. The range here is defined as the Range Mean cycle instead of rainflow cycle.

3.5 Dirlik's formula

Dirlik conducted extensive computer simulation on the rainflow cycle distribution of random Gaussian stress histories. He studied seventy spectra of various shapes, with γ in the range *0.160* to *0.988* [13]. Seventy Gaussian stationary stress histories were then simulated from these spectra. Both countings for ordinary range and rainflow range cycles were performed on the simulated signals. The rainflow cycle PDF was modelled by using the following expression:

$$p_{RR}(z) = C_1\frac{1}{\tau}e^{-\frac{z}{\tau}} + C_2\frac{z}{\alpha^2}e^{-\frac{z^2}{2\alpha^2}} + C_3 z e^{-\frac{z^2}{2}} \tag{3.12}$$

where cycle range $S = 2z\sqrt{m_0}$. z is therefore a normalised range parameter.

This model used three combined PDF's, exponential, Rayleigh and standard Rayleigh distributions, to fit the probability density of low, middle and high range cycles respectively. By minimising the cost function (mean square error of the model equation with the time domain counting result) and regression analysis,

the parameters were derived in terms of the spectrum moments,

$$
\begin{aligned}
f_m &= \frac{m_1}{m_0}[\frac{m_2}{m_4}]^{\frac{1}{2}} \\
C_1 &= \frac{2(f_m - \gamma^2)}{1+\gamma^2} \\
C_2 &= \frac{1-\gamma-C_1+C_1^2}{1-\alpha} \\
C_3 &= 1 - C_1 - C_2 \\
\tau &= \frac{1.25(\gamma - C_3 - C_2\alpha)}{C_1} \\
\alpha &= \frac{\gamma - f_m - C_1^2}{1-\gamma-C_1+C_1^2}
\end{aligned}
$$

This important empirical formula was the first to directly link the rainflow cycle distribution with the spectrum moments. Because of the wide range covered by the selected irregularity factor and mean frequency, the formula works very well for Gaussian stress/strain histories [49][50][51]. The simulation process here seems to have worked quite successfully. The phases used for simulating the time histories from the spectra are assumed to have a uniform distribution in $0 - 2\pi$, the Gaussian assumption was therefore implicitly adopted.

3.6 Bishop's theoretical solution

Dr. Bishop carried out theoretical studies on the connection between the spectrum and rainflow cycle distribution[1] [52]. For a rainflow cycle as defined in Definition 3 in previous section, the three events which constitute a rainflow cycle can be separated and considered as three single events. The probability of a rainflow cycle existing was therefore considered to be equal to the probability of these three events occurring together. This consideration significantly simplified the computation of rainflow cycles because each event was dealt with as a series of transitions of the signal from a peak to a trough or from a trough to a peak rather than the complicated configuration associated with the original definition. The rainflow cycle PDF then can be expressed as:

$$
p_{RR}(h) = \frac{2.0}{dh} \sum_{ip=h+1}^{\infty} Y_1(ip, ip-h) Y_2(ip, ip-h) Y_3(ip, ip-h) p(ip) \qquad (3.13)
$$

where, $Y_1(ip, ip-h)$, $Y_2(ip, ip-h)$, and $Y_3(ip, ip-h)$ are the probabilities of events Y_1, Y_2 and Y_3, respectively and can be calculated by Markov process theory. dh is the interval width used to divide the signal and $p(ip)$ is the probability of

the signal being at peak *ip*. The coefficient 2.0 occurs because there exists a symmetry about *t=0* for stationarity.

To calculate the probability of the signal transition from peak to trough and from trough to peak, the peak-trough series can be assumed as a Markov chain. The probability of the above three events can then be calculated using Markov stochastic process theory. The complete PDF of rainflow ranges can therefore be obtained.

Theoretically, this method can be taken as a universal method and is suitable for any type of signals either Gaussian or non-Gaussian. As will be seen later, however, this method needs a one step signal transition matrix to set up the Markov model matrix. This transition matrix is generally very difficult to derive except for a Gaussian distribution. So, this method is restricted mainly to the Gaussian signals. However, due to its clear theoretical background, this method can be easily used for some special non-Gaussian situations once the heavy mathematical work is done to produce the required one step transition matrix. Additionally, this is the only method which offers the possibility of retaining the information about the relative mean of the rainflow cycles. This is obviously needed if the influence of mean stress is to be considered. This is covered in more detail in Chapter 6.

3.7 Madsen formula

The work of Madsen *et al* [53] was derived specifically for application to wind turbines. It deals with signals which combine stochastic and deterministic loads. These two components of signal are treated separately. For a random stationary stochastic process, damage is assumed to be a constant function of time, the value of the constant being dependent on the signal characteristics. For a zero-mean, Gaussian, narrow band stochastic process, a Rayleigh distribution of peaks applies and each range is taken as a half cycle as before. For this idealised signal, Madsen proposes a dimensionless damage parameter, which is equal to the actual damage of the signal, normalised by dividing by the damage due to a constant amplitude signal having the same *rms*. This was shown to be a function of the slope of *S-N* curve.

For more complex and realistic wide band processes, Madsen assumes a Gaussian distribution, and hence a solution for the distribution of the peaks. referencing Wirsching [44], he uses the assumption that each peak will eventually pair

with an equal and opposite trough to form a closed cycle. This is exceptionally conservative, and so a 'bandwidth correction factor' is proposed. Madsen proposes a formula, independent of *S-N* curve slope, and supports it by reference to published fatigue test data. His basis for the formula is a comparison of fatigue lives, rather than the signal statistics themselves.

For the deterministic component of load, the simple case of two superimposed sine waves is considered, and a constant amplitude sine wave of equivalent damage is proposed, as a function of *S-N* curve slope. Making the assumption of uniform distribution of phase between the two original sine waves, he fitted an empirical relationship to calculate the equivalent constant amplitude stress range as a function of irregularity factor and *S-N* curve slope.

For the general case of a sum of periodic and stochastic terms, Madsen builds from the special case of a sinusoid plus a narrow band stochastic process. He proposes to view the confluent hypergeometric function as an interpolating function between the purely periodic signal and the Gaussian stochastic signal. To allow for wide band processes, the periodic *rms* and stochastic *rms* are each corrected for irregularity.

theory

Throughout the theory of Madsen, the expected damage rate is defined as

$$E[D] = E[0](\frac{S_h}{k})^b \tag{3.14}$$

where *E[0]* is the zero-crossing rate with positive slope, k the stress intercept and b the fixed inverse slope of *S-N* curve, and S_h an equivalent constant amplitude stress range calculated for the signal.

Stochastic Loading

For a purely stochastic signal,*X(t)*,

$$S_h = 2\sqrt{2}g_x(\gamma_x)\sigma_x[\Gamma(1+\frac{b}{2})]^{1/b} \tag{3.15}$$

where the bandwidth correction term is defined as

$$g_x(\gamma) = 0.93 + 0.07\gamma^5$$

Deterministic Loading

The equivalent stress range for the deterministic component, $Z(t)$ is

$$S_h = 2\sqrt{2}g_z(\gamma_z)\sigma_z \tag{3.16}$$

with bandwidth correction correction factor

$$g_z(\gamma) = 1.24 - (0.325 - 0.025b)(2.2\gamma - \gamma^2)$$

The bandwidth (irregularity factor) is defined as $\gamma = N_u/N_p$, where N_u is the number of mean up-crossing, and N_p the number of peaks, in one time period ($T_0 = 2\pi/\omega_0$). By defining γ in this form, Madsen believed that some information on the relative phase between the Fourier components is retained, whereas all such information is lost in the spectral moment parameters.

The standard deviation is calculated as

$$\sigma_Z = (\frac{1}{2}\sum_{k=1}^{K} c_k^2)^{1/2}$$

where c_k is the amplitude of the sine waves.

Combined Loading

For the combined time history, *Y(t)=X(t)+Z(t)*,

$$S_h = 2\sqrt{2}g_x(\gamma_y)\sigma_x[\Gamma(1+\frac{b}{2})M(-\frac{b}{2},1,-\beta^2)]^{1/b} \tag{3.17}$$

with $\beta = \frac{g_z(\gamma_y)\sigma_z}{g_x(\gamma_y)\sigma_x}$
$M(\cdot,\cdot,\cdot)$ is a confluent hypergeometric function satisfying

$$M(-\frac{b}{2},1,-\beta^2)|_{\beta=0} = 1$$

and

$$M(-\frac{b}{2},1,-\beta^2)|_{\beta\to\infty} = \frac{\beta^b}{\Gamma(1+\frac{b}{2})}$$

The combined model therefore also includes the previous models as special cases.

The correction for irregularity is applied using the bandwidth parameter,

$$\gamma_y = E[0]^y/E[P]^y$$

defined for the combined signal from

$$\nu_0^y = E[0]_x \cdot \frac{1}{T}\int_0^{T_0} \phi(\frac{\gamma}{\sigma_x})\xi(\frac{\dot{\gamma}}{\sigma_{\dot{x}}})dt$$

and

$$\nu_m^y = E[P]_x \cdot \frac{1}{T}\int_0^{T_0} \phi(\frac{\dot{\gamma}}{\sigma_{\dot{x}}})\xi(\frac{\ddot{\gamma}}{\sigma_{\ddot{x}}})dt$$

where

$$\begin{cases} \phi(t) = \frac{1}{\sqrt{2\pi}} e^{-t^2/2} \\ \xi(t) = \phi(t) - t\psi(t) \\ \psi(t) = \int_{-\infty}^{t} \phi(p)dp = erf(t) \end{cases}$$

with $\sigma_{\dot{x}} = \sqrt{m_2}$ and $\sigma_{\ddot{x}} = \sqrt{m_4}$

The function $\gamma(\cdot)$ is derived by subtracting the deterministic time-history from the mean of the combined signal, $\mu_y = c_0$, so that

$$\gamma(t) = \mu_y - Z(t) = -\sum_{k=1}^{K} c_k \sin(k\omega_0 t + \theta_k)$$

3.8 Discussion

The methods discussed in this chapter are mainly of three classes. The first is the narrow band solution, which introduces a rigorous assumption on the frequency distribution of the response history. The second class is that of correction factor methods which try to adapt the narrow band solutions to a wide frequency band and introduce rainflow cycle counting in the damage estimation. The third class includes the methods which involve more numerical simulation and theoretical studies such as Dirlik's formula and the theoretical method. Because of the order in which they were developed, the second class generally work better than the first and the third class are expected to be the best. Assessment in the following chapter proves this point. Apart from the methods described in this chapter, there are also some other methods developed to predict the rainflow cycle PDF, say [34], [54], [54]. However, they are not widely used.

Although madsen made an attempt to solve the deterministic component problem here, it is far from satisfactory. The damage he derived for the stochastic part is still based on a correction to the narrow band solution. The interpolation he uses involving hypergeometric functions also has no theoretical background.

All these methods assume the response histories are Gaussian. Such assumptions should be reasonable for most engineering situations. The fatigue life prediction for most engineering structures should then have reasonable results. Non-Gaussian situations will be discussed in **Chapter 7**.

Chapter 4

Fatigue Analysis of WEG MS-1 and Howden data

4.1 Introduction

For all of the methods described in the previous chapter, the best way of assessing how well they can work is to apply them to the analysis of monitored structural response histories. The monitored times series would then be able to provide a time domain solution which can be taken as a reference solution with which to compare the frequency domain solution. The work presented in this chapter performs this assessment. The power spectral density functions used for the fatigue analysis are calculated from the response history directly.

Two sets of data from WEG MS-1 and Howden HWP330 wind turbine machines were used. They are monitored response histories of the wind turbine blades during operation. Since most of the methods are developed for fatigue analysis of offshore structures other than wind turbine blades, it is useful to perform fatigue analysis on these monitored turbine responses in order to assess the validity of applying these methods to turbine blade fatigue analysis.

This chapter presents the results from such an analysis. The problems revealed by the analysis and some possible solutions are presented in later chapters.

4.2 Analysis program

A program was developed to perform fatigue analysis calculations on the random stress history in both the time and frequency domains. In the time domain analysis, rainflow counting is performed on the time series to obtain the time domain fatigue life estimation. This estimation is then taken as the reference solution. This is because it is the result that all the frequency domain approaches are trying to estimate. When working in the frequency domain, the spectrum is computed from the given time series or read from a data file which stores the

spectrum. If the later is the case, there would be no reference solution with which to compare the frequency domain solutions. Most of the methods described in the previous chapter are implemented in the program. They are:

- Narrow band solution
- Wirsching's modification
- Hancock A and B
- Chaudhury and Dover's modification
- Dirlik's empirical formula
- Bishop's theoretical solution

As far as the deterministic element of the signal is concerned, only one significant component caused by gravity was discovered in the Howden edgewise signals. The WEG MS-1 data files did not contain edgewise signals whilst the Howden data are combined deterministic and stochastic response histories.

The rainflow cycle PDF's predicted by all the frequency domain methods are calculated first. The damages from these rainflow cycle PDF's are then compared with the one from the time domain analysis. The ratio of the frequency domain damages with the time domain solution is defined as the damage rate in this thesis. A value greater than *1.0* implies that the frequency domain result is conservative, i.e., gives a damage value greater than the time domain solution. Conversely, a value less than *1.0* implies that the frequency domain result is unconservative. The program is presented in Appendix A.

As part of its initial development the program was first used for the analysis of a set of computer simulated data, denoted as *nbdata, nbdatb, nbdatc* and *nbdatd.* For a typical data set, *nbdata*, the PSD function is shown in Figure 4.1.

The rainflow cycle PDF's counted from the time series and predicted by the frequency domain methods mentioned above are shown in Figure 4.2. Since the signal is a simulated Gaussian time history, it was found that most of the methods agree well with the time domain analysis results. The narrow band solution, as expected, is definitely conservative as the middle and high range part of the probability density are over predicted. This part of the PDF contributes most to the total fatigue damage because of the nonlinear Basquin equation.

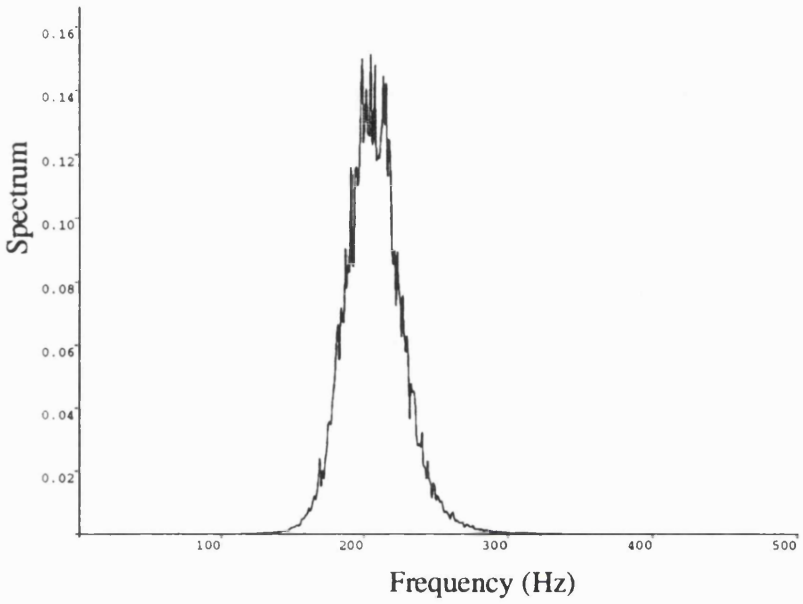

Figure 4.1: Spectrum of nbdata

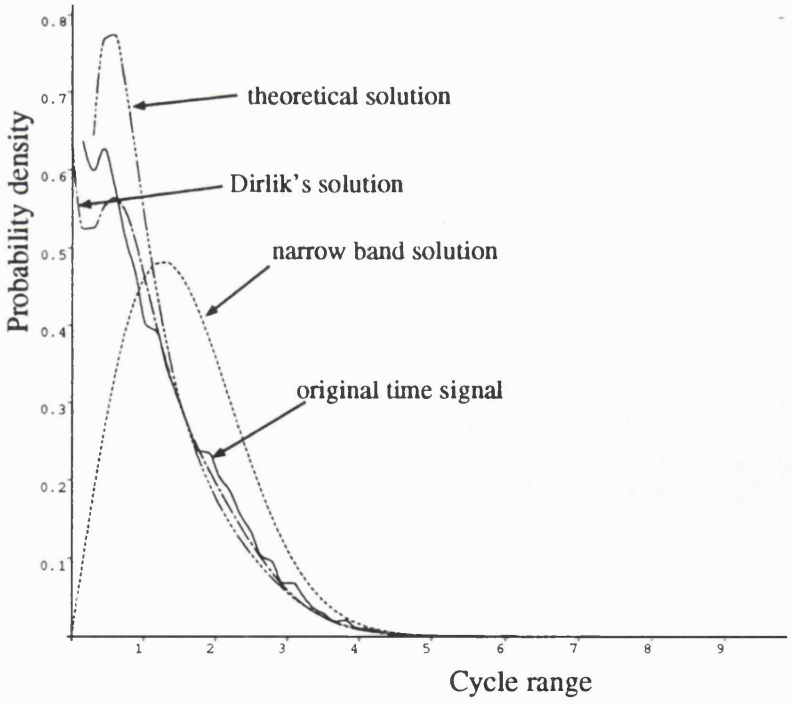

Figure 4.2: Rainflow cycle distribution of nbdata

4.3 Analysis of WEG MS-1 data

4.3.1 The WEG MS-1 data

The WEG MS-1 data was recorded from a WEG MS-1 wind turbine on Orkney. This machine has a two-bladed steel rotor, 20 meters in diameter and is rated at 50kw.

Six load cases were examined, two for freely teetered operation and four with fixed hub, covering a wide range of wind speeds. Four radial locations were considered in each case: at 1.35m, 3.28m, 4.94m and 7.24m measured from the blade root (and denoted as case 12, 19, 27 and 35), respectively. The load cases are defined in Table 4.1.

The data given are not the stress time histories. Instead, they are the flapwise moments at each section. As known from beam theory, dividing the bending moment history by the sectional bending resistance module can easily produce the stress history. But it does not have to be done because what is concerned here is the PDF of the cycles. The transformation from bending moment cycle range into stress cycle range does not change the shape of the probability density function. The fatigue damage, of course, has changed. But if one is only trying to compare the damage with a time domain result, the ratio will remain unchanged. Thus, all the work here is performed directly on the bending moment histories.

Table 4.1: MS-1 load cases

Case	wind speed (m/s)	Yaw (deg.)	Turb. Int. (%)	Hub Config.	Campaign dur.(secs)	Length (points)
A	18.4	7.1	9.7	Fixed	300	37500
B	23.7	3.0	11.1	Fixed	240	30028
C	11.1	-12.5	8.9	Fixed	300	37500
D	16.5	2.5	10.1	Fixed	300	37500
E	15.6	-3.1	6.6	Teetered	102	12823
F	11.3	12.3	15.0	Teetered	300	37500

4.3.2 $S-N$ curve

The $S-N$ curve used in the damage calculation should be based on BS5400 weld specification [55]. It is CLASS D and defined as,

$$N = 10^7(\sigma_0)^b \qquad for \quad \sigma_r \geq \sigma_0$$

$$N = 10^7(\sigma_0)^{b+2} \qquad for \quad \sigma_r < \sigma_0$$

where σ_0 is the stress range corresponding to $N = 1 \times 10^7$. For convenience of analysis, a single inverse slope $b = 5.0$ was used in this section.

4.3.3 Statistical analysis

Two types of statistical check were performed on the WEG data. First of all, the Reverse Arrangement Test (RAT) [56] was carried out to check for trend and stationarity. The Reverse Arrangement Test is a test on the independence of the observations in a time series. The signal is first divided into different blocks and the statistical parameters such as the mean and root mean square are calculated for each block. Then the mean or *rms* calculated from each block is taken as a sequence x_i, $i = 1, 2, ..N$, and the number of times that $x_i > x_j$ for $i < j$ is counted thus obtained the *number of reverse arrangements.* If the sequence of observations is independent (i.e., no trend is present) then the number of reverse arrangements is a random variable with a mean value and variance as follows

$$\mu = \frac{N(N-1)}{4}$$

$$\sigma = \frac{N(N-1)(2N+5)}{72}$$

The actual distribution from the signal can then be compared with a theoretical value. Given a tolerance (significance) level, an acceptable region for the stationarity of the signal can be determined.

When performing this test for the MS-1 data, the signals were divided into different blocks, with each block containing about 15 seconds of data except for load case E. The block number is 20 for load cases A,C,D and F, 16 for B, and 10 for E. The mean and root mean square are calculated for each block. For a given confidence level of *0.01*, the acceptable regions for the hypothesis that the observations are independent are :

$$N = 20 : 59 \leq A \leq 130$$

$$N = 16 : 34 \leq A \leq 85$$

$$N = 10 : 9 \leq A \leq 35$$

The results from the RAT test applied to the MS-1 data are listed in Table 4.2. They are also presented in Figure 4.3, together with the acceptable regions for all the load cases. It is clear that, except for load case A, the RAT values for

both mean and root mean square of the signals are inside the acceptable region for the confidence level of *0.01*. Thus, the conclusion from the stationarity check of the WEG MS-1 data is that, load case A of WEG data is a nonstationary time series for a confidence level of *0.01*, but all the other signals can be taken as stationary.

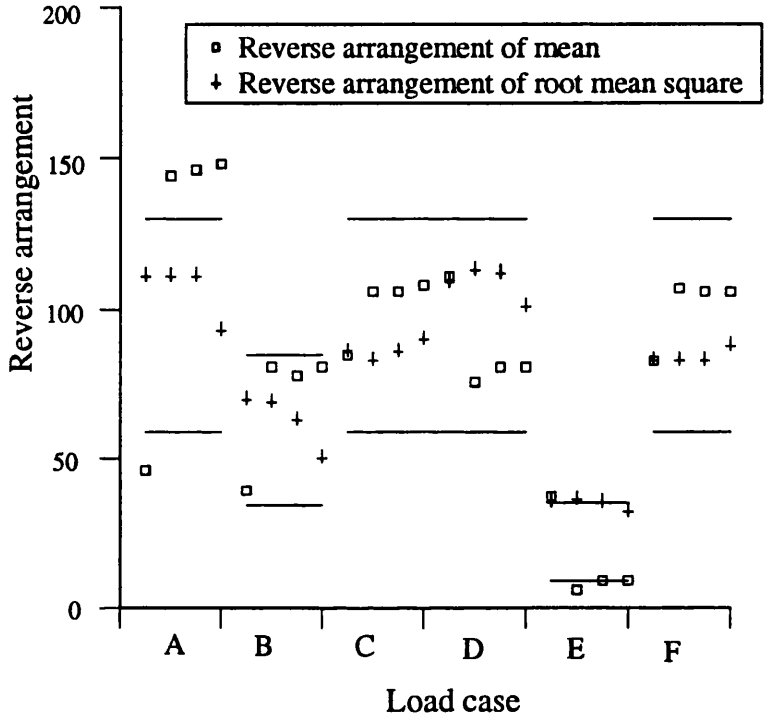

Figure 4.3: Reverse arrangement test of WEG MS-1 data

The chi-square χ^2 and kurtosis values are used for the check of normality. X^2 is defined as [56] [57]:

$$X^2 = \sum_{i=1}^{K} \frac{(f_i - F_i)^2}{F_i}$$

where K is the number of *class intervals* which the observations are grouped into, f_i is the *observed frequency* and F_i is the *expected frequency*. The distribution for X^2 is approximately the same as for χ_n^2 with the number of degree $n = K - 3$. Given a significance level α, the observations are accepted as normal if

$$X^2 \leq \chi_{n;\alpha}^2$$

Kurtosis(Coefficient of Excess) is defined as

$$Kurtosis = \frac{\mu_4}{\mu_2^2} - 3$$

where μ_2 and μ_4 are defined as the second and fourth central moments of the signal. It can be used as a measure of the flattening of a distribution near its centre. The value of Kurtosis can range from *-2* to infinity with *-2* corresponding to a symmetric binary random variable ($|x| = constant$) and a value of ∞ corresponding to the distributions with slowly decaying tails. For a normal distribution, the *Kurtosis* should be zero since $E[x^4] = 3\sigma^4$ [58].

The X^2 values were calculated with *30* degrees of freedom for WEG MS-1 data. All the results are listed in Table 4.2. The normality check from χ^2 concludes that all the signals are non-Gaussian given a significance level of *0.99* and corresponding upper bound of *50.9*. Figure 4.4 presented all of the X^2 values and the upper bound for significant level *0.99*. All the values are far above the upper bound. The values of Kurtosis broadly reflect the degree of non-normality for the signals but can not provide a definite conclusion since there is no quantity acceptance region given theoretically.

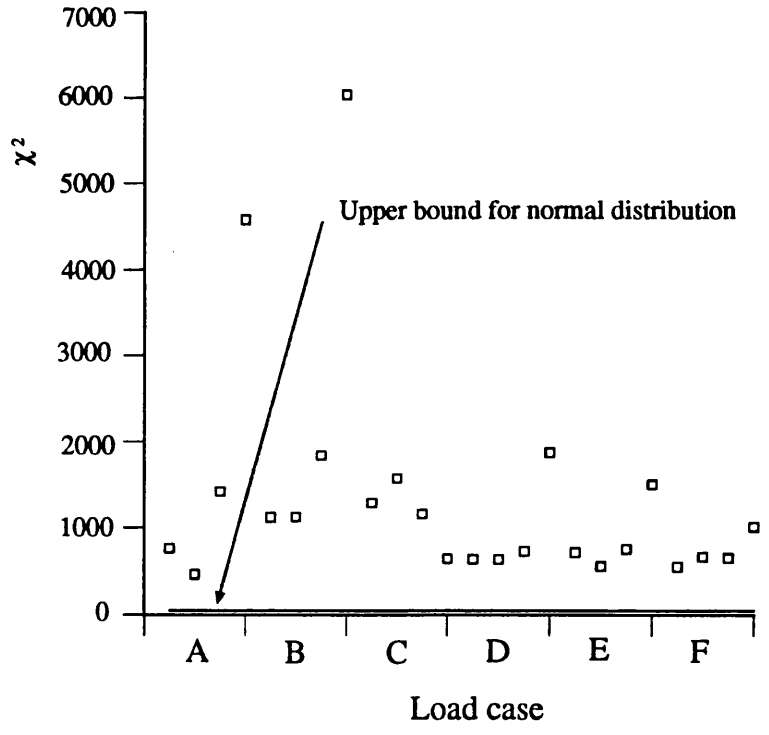

Figure 4.4: X^2 of WEG MS-1 data for degree 30

Table 4.2: Statistical analysis for WEG MS-1 data

data	*mean*	*ratm*	*rms*	*Ratr*	$E[p]$	$E[0]$	γ	X^2_{30}	Kts
y12a	-132.78	46	32.04	111	4805	859	0.18	760.1	-0.035
y19a	43.56	144	31.57	111	4936	857	0.17	462.1	0.028
y27a	44.78	146	36.85	111	5140	764	0.15	1417.5	-0.059
y35a	68.78	148	55.87	93	5231	548	0.11	4574.6	-0.205
y12b	-67.83	39	29.03	70	3361	1023	0.30	1118.7	-0.375
y19b	-9.02	81	28.51	69	3339	1041	0.31	1118.9	0.363
y27b	-50.81	78	29.39	63	3636	1122	0.31	1835.9	0.544
y35b	-93.33	81	38.19	50	4258	1035	0.24	6038.5	0.895
y12c	-90.27	85	21.75	86	6063	867	0.14	1282.8	-0.177
y19c	19.32	106	21.06	83	6162	942	0.15	1571.0	0.193
y27c	6.76	106	19.68	86	6212	1105	0.18	1160.4	0.193
y35c	42.08	108	18.23	90	6604	1316	0.20	643.6	0.163
y12d	-168.95	111	22.37	109	5084	1134	0.22	633.6	-0.003
y19d	77.05	76	21.76	113	5144	1154	0.22	632.8	-0.036
y27d	68.30	81	21.48	112	5448	1287	0.24	724.3	-0.105
y35d	114.85	81	24.02	101	5843	1379	0.24	1869.0	-0.442
y12e	-184.18	37	18.31	35	2013	476	0.24	714.4	0.493
y19e	68.50	6	19.35	36	1915	489	0.26	554.5	-0.285
y27e	50.88	9	19.98	35	1851	547	0.30	751.5	-0.377
y35e	106.58	9	23.79	32	1869	580	0.31	1498.3	-0.772
y12f	-149.26	83	19.02	83	6299	1148	0.18	551.0	0.073
y19f	66.92	107	18.05	83	6265	1185	0.19	663.7	-0.139
y27f	46.37	106	17.80	83	5858	1381	0.24	651.6	-0.240
y35f	90.41	106	18.55	88	5971	1525	0.26	1006.3	-0.255

4.3.4 Fatigue analysis

The MS-1 data was acquired using a frequency *125Hz*, giving a Nyquist frequency of *62.5Hz*. Since the rotor speed of the MS-1 machine is *88* RPM. This implies a *1P* frequency of *1.47Hz*. The first *10* harmonics were used to obtain a maximum stochastic frequency of *15.625Hz*. The cutoff frequency was then set at *15.625Hz* [59].

The rainflow cycle PDF's of *y12a* from both time and frequency domain analysises are presented in Figure 4.5*a*. It is clear that the narrow band solution over estimates the middle and high range cycles. However, Dirlik's formula and the theoretical solution give a reasonably good prediction for the cycles in these ranges. In terms of fatigue, the middle and high range cycles always contribute most to the fatigue damage, as shown in Figure 4.5*b*.

The fatigue analysis from the WEG MS-1 data was performed in both the time and frequency domains. In the frequency domain analysis, the narrow band solution, Wirsching's modified solution, Chaudhury and Dover's solution, and Hancock A were used, together with Dirlik's empirical formula and Bishop's theoretical solution. They are all listed in Table 4.3 in terms of damage rates[49][50].

The most consistent frequency domain results were obtained using Dirlik's empirical formula and Neil Bishop's theoretical solution. These two approaches are far more accurate than the alternative approaches. However, although the averages for the 24 load cases are close to *1.00* for both methods, estimates of less than *1.00* for individual locations are quite possible.

The fluctuation of the results listed here can be partly explained as simple stochastical scatter. The damage rates for *y35a* and *y35b* are the two highest in this table. They have most serious level of non-normality in the normality check. The nonnormality of *y35b* is more serious than *y35a* but has a better fatigue damage rate. This may be caused by the nonstationarity existing in *y35a*. Because the normality check on the whole signal indicated that all the data is non-Gaussian the fatigue damage results are surprisingly good. There may be several reasons for this. One of the most important is that the spectra are calculated using rectangular windows. The non-stationarity and non-normality in each window (block) is not as serious as for the whole data sample and thus the data inside each window is a better approximation to the Gaussian signal.

Further discussion on this topic is presented in the next chapter.

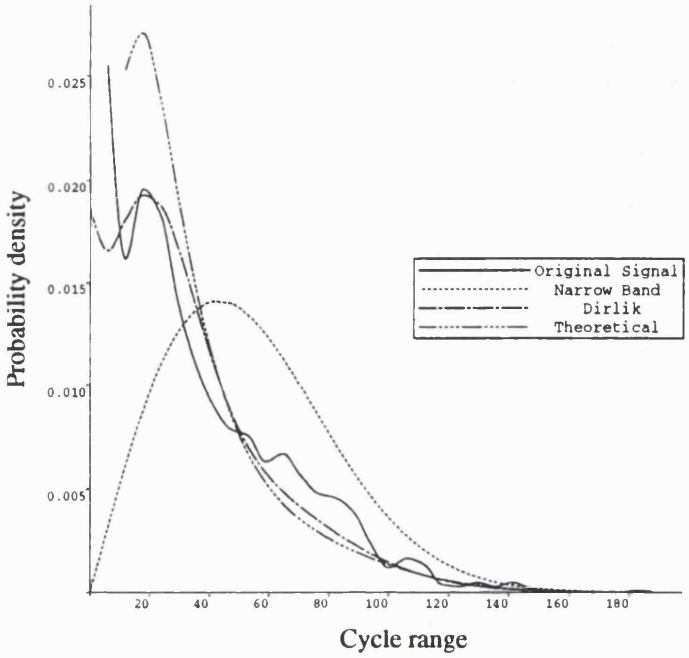

(a). Rainflow cycle probability density

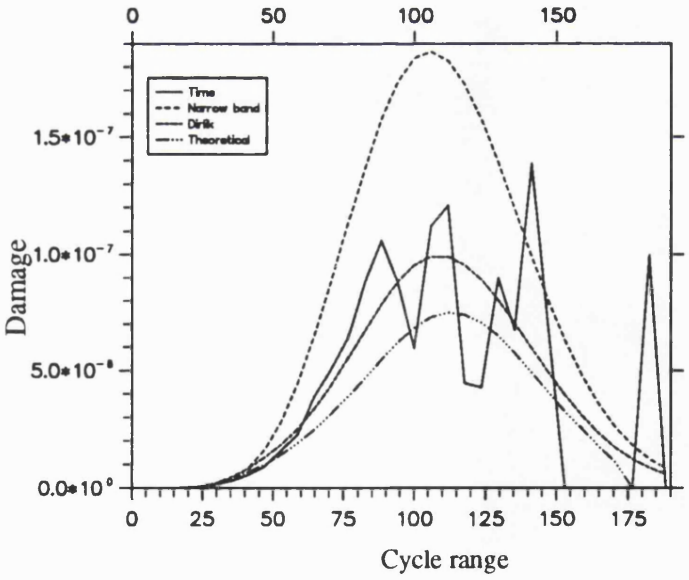

(b). Damage distribution

Figure 4.5: Rainflow cycle probability density and damage distribution for WEG MS-1 data y12a

Table 4.3: Fatigue damage rates for WEG MS-1 data

load	narrow-band	Dirlik	Wirsching	Bishop	Chaudhury	Hancock
y12a	5.14	1.03	3.91	1.07	2.13	2.75
y19a	5.15	1.00	3.92	1.09	2.14	2.77
y27a	14.34	1.59	10.91	1.23	5.12	5.83
y35a	81.87	2.34	62.23	1.37	30.08	25.08
y12b	1.91	0.77	1.46	0.79	0.98	1.25
y19b	1.98	0.81	1.50	0.86	1.04	1.31
y27b	3.67	1.07	2.79	0.91	1.47	1.92
y35b	18.34	1.48	13.95	1.30	5.68	6.10
y12c	1.98	0.76	1.51	0.61	0.95	1.25
y19c	1.87	0.73	1.43	0.61	0.92	1.20
y27c	2.03	0.74	1.54	0.51	0.87	1.14
y35c	3.22	0.76	2.45	0.46	1.15	1.42
y12d	2.09	0.84	1.59	0.81	1.03	1.33
y19d	2.03	0.83	1.54	0.83	1.02	1.31
y27d	2.92	1.01	2.22	0.81	1.23	1.62
y35d	7.50	1.12	5.70	0.87	2.75	3.29
y12e	2.80	0.99	2.13	0.90	1.50	1.95
y19e	3.06	1.01	2.33	1.02	1.64	2.12
y27e	3.50	1.03	2.67	1.08	1.65	2.16
y35e	8.81	1.11	6.71	1.41	3.31	4.15
y12f	3.86	0.98	2.93	1.01	1.66	2.18
y19f	3.97	1.00	3.02	1.13	1.78	2.33
y27f	3.96	1.01	3.01	1.11	1.76	2.31
y35f	5.59	0.98	4.25	1.17	2.17	2.80
avrg	7.98	1.04	6.08	0.96	3.08	3.32

4.4 Analysis of Howden HWP330 data

4.4.1 HOWDEN HWP330 data

The Howden HWP330 data was monitored from a 33m wind turbine in Altamont, Pass, California. The data was stored on tapes labeled 18, 26, 27 and 30. Each tape contained bending moment histories from the blade at 3, 8 and 13 meters from the hub. The load cases are summarised in Table 4.4.

Table 4.4: Load case of Howden HWP330 data

Tape	Windspeed (m/s)	Turbulence Intensity(%)	Mean yaw (deg)	Duration (s)	Length (points)
18	10.68	19.6	-11.7	2560	102000
26	14.07	9.2	-6.5	3260	130400
27	16.86	10.7	-11.8	3863	154518
30	8.51	15.3	2.4	3512	140398

4.4.2 $S-N$ curve

The $S-N$ slope values used for the Howden HWP330 data were *b=4.0, 8.0* and *12.0.* Of course, only as a means of comparing fatigue analysis results for research purposes is it acceptable to use different $S-N$ slope values.

4.4.3 Statistical analysis

The same statistical analysis calculations as with the WEG MS-1 data was performed on the Howden HWP330 data. For the stationarity check the signals were divided into 50, 60, 70 and 70 blocks for tape 18, 26, 27 and 30 respectively. The results are listed in Table 4.5. The acceptance regions for a given confidence level *0.01* are as follow

$$N = 50 : 473 \leq A \leq 751$$

$$N = 60 : 702 \leq A \leq 1067$$

$$N = 70 : 977 \leq A \leq 1437$$

The RAT test applied to the mean and root mean square is presented in Figure 4.6. It is seen from the table and the figure that nearly all the Howden HWP330 data is nonstationary. The nonstationarity of a few signals such as the 3m edgewise and 8m flapwise of tape 18, and the 3m edgewise of tape 26 is not

as severe as for the rest.

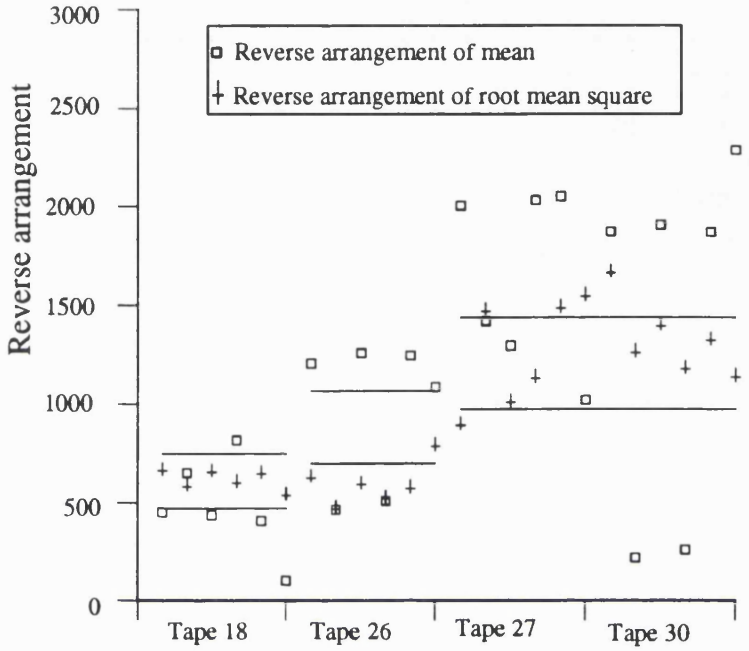

Figure 4.6: Reverse arrangement test of Howden HWP330 data

The X^2 values were calculated with 30 degrees of freedom. The upper bound for accepting the signal as Gaussian is *50.9*, given a significance level of *0.99*. From the normality test, all the data show a very strong non-Gaussian property. The normality test for nonstationary signals, of course, does not make any sense. Actually, since dominant deterministic components exist in the edgewise signals, the statistical parameters are dominated by these components.

The extremely high chi-square values from the test could also be caused by the non-stationarity in the signals apart from the non-normality of the signals. As stated in [60], a chi-square test is a conventional test for the distribution but it is also a less powerful one. "They should not be recommented for use in testing for departures from normality when the full ungrouped sample of data is available" [60] pp371. As the hypotheses test is not the topic of this thesis, no further details were discussed in the test.

4.4.4 Fatigue analysis

The sampling frequency of the Howden data was *40.0Hz*, giving a cutoff frequency for the PSD of *20.0Hz*. However, it was found that the high frequency components

Table 4.5: Statistical analysis for Howden data

data	*mean*	*ratm*	*rms*	*Ratr*	$E[P]$	$E[0]$	γ	X^2_{30}	K
T18-3-f	91.80	453	11.54	664	10477	1978	0.19	4238.4	-0.47
T18-3-c	50.35	654	29.88	584	3861	1582	0.41	72978.1	-0.01
T18-8-f	29.47	438	4.92	658	11829	2502	0.21	4469.8	-0.47
T18-8-c	39.64	820	6.91	601	4900	1585	0.32	63416.6	-0.01
T18-13-f	3.08	409	0.77	649	16423	4187	0.26	3582.1	-0.37
T18-13-c	3.66	101	2.28	538	12023	1635	0.14	38723.2	0.01
T26-3-f	93.66	1207	13.10	628	11541	2675	0.23	1116.9	-0.20
T26-3-c	10.40	466	35.47	470	5916	2043	0.35	58783.5	-0.01
T26-8-f	31.49	1259	7.59	595	13885	1976	0.14	8099.7	-0.40
T26-8-c	1.41	510	12.47	521	8622	2096	0.24	49046.8	-0.01
T26-13-f	1.74	1246	2.41	573	19770	1086	0.06	44864.8	-0.58
T26-13-c	-0.20	1085	2.30	789	17547	2265	0.13	22323.4	0.0
T27-3-f	81.94	2006	15.21	895	11529	4331	0.38	1057.1	-0.08
T27-3-c	13.98	1419	35.38	1470	9618	2450	0.26	70737.7	-0.05
T27-8-f	2.86	1295	12.50	1009	12676	2538	0.20	58583.5	-0.06
T27-8-c	22.39	2033	8.53	1131	13943	4030	0.29	3036.3	0.27
T27-13-f	-2.39	2052	2.52	1486	21605	3066	0.14	21015.4	0.73
T27-13-c	-3.08	1021	2.26	1546	23549	2960	0.13	36138.1	0.10
T30-3-f	71.71	1873	15.74	1664	12380	1875	0.15	2727.6	-0.14
T30-3-c	8.14	219	35.47	1261	4923	2174	0.44	84744.0	-0.02
T30-8-f	27.27	1907	6.22	1394	15060	2217	0.15	3181.1	-0.14
T30-8-c	1.14	261	12.30	1177	5895	2178	0.37	79738.8	-0.02
T30-13-f	3.36	1869	0.85	1320	21133	4015	0.19	1587.3	-0.33
T30-13-c	0.13	2287	2.21	1137	14780	2208	0.15	40965.3	0.01

in the signal have a great influence on the final damage estimation (which will be discussed in the following chapter). For the work in this thesis the cutoff frequency was set at the point at which m_0 reached *99.5%* of its whole value. This takes most of the signal into account but eliminates the influence of high frequency components.

The computed rainflow cycle PDF's for the 3m flapwise and edgewise edgewise load cases of tape 26 are plotted in Figure 4.7. The fatigue estimations are listed in Table 4.6, 4.7 and 4.8 for $S-N$ slopes of $b = 4.0,\ 8.0$ and 12.0 respectively. For simplicity, only the damage estimations from Dirlik's formula and Bishop's theoretical solution are listed.

Although Dirlik's empirical formula and Bishop's theoretical solution give good agreement in the fatigue analysis of the WEG MS-1 data, both of them fail to give a satisfactory result for the Howden data. This could be caused by the nonstationarity of the time histories or their non-normality. The existence of a strong deterministic component also contributes a lot to the discrepancies in the edgewise signals.

Table 4.6: Fatigue damage rates for Howden data b=4.0

chnl	tape 18		tape 26		tape 27		tape 30	
	Dirlik	Bishop	Dirlik	Bishop	Dirlik	Bishop	Dirlik	Bishop
5	0.825	0.905	0.858	0.852	0.854	0.971	1.012	0.927
6	1.702	1.965	1.616	0.832	1.581	0.519	1.758	2.324
7	0.740	0.740	0.841	0.840	1.466	0.397	0.811	0.844
8	1.625	1.140	1.548	0.493	0.830	0.860	1.693	1.822
9	0.773	0.323	1.108	0.163	1.113	0.290	0.839	0.357
10	1.495	0.660	1.334	0.294	1.281	0.306	1.483	0.896

Table 4.7: Fatigue damage rates for Howden data b=8.0

chnl	tape 18		tape 26		tape 27		tape 30	
	Dirlik	Bishop	Dirlik	Bishop	Dirlik	Bishop	Dirlik	Bishop
5	0.416	0.581	0.366	0.446	0.575	0.730	0.808	0.838
6	16.508	18.147	13.959	8.377	12.594	5.107	18.149	23.338
7	0.278	0.332	0.334	0.452	9.477	3.341	0.407	0.478
8	14.604	12.665	11.691	4.620	0.488	0.596	16.098	16.301
9	0.299	0.161	0.697	0.145	0.500	0.177	0.170	0.092
10	11.897	6.225	4.845	1.430	6.405	2.053	11.753	8.107

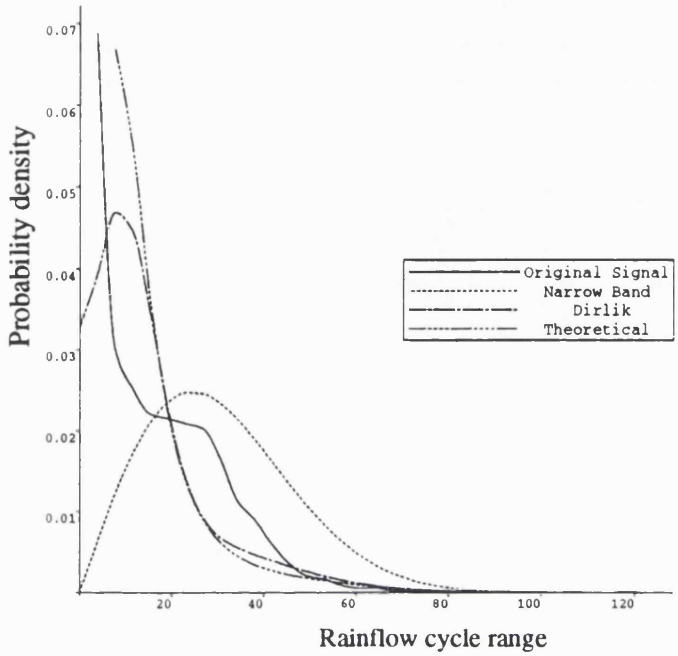

(a). Tape 26 ,3m flapwise

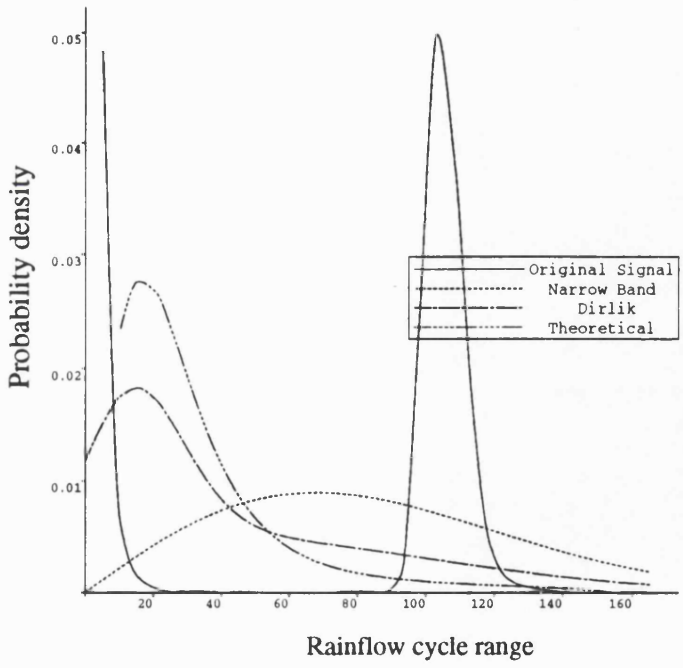

(b). Tape 26 ,3m edgewise

Figure 4.7: Rainflow cycle probability density of Howden data

Table 4.8: Fatigue damage rates for Howden data b=12.0

chnl	tape 18		tape 26		tape 27		tape 30	
	Dirlik	Bishop	Dirlik	Bishop	Dirlik	Bishop	Dirlik	Bishop
5	0.14	0.22	0.13	0.17	0.26	0.34	0.26	0.29
6	387.30	406.44	309.11	193.66	260.95	114.64	448.30	559.04
7	0.09	0.11	0.10	0.16	146.38	63.54	0.08	0.10
8	316.22	274.07	209.76	90.03	0.18	0.24	367.66	352.93
9	0.09	0.06	0.42	0.13	0.17	0.08	0.01	0.01
10	245.99	132.81	7.54	2.91	62.96	26.88	221.88	165.04

Various computational considerations except for the issue of non-stationarity will be discussed in the following chapter. To address the problem of non-stationarity, the signals were divided into blocks. The fatigue analysis was then performed on each block just as if it was an independent time history. The damage rate was then taken as the average of the rates of these blocks. It should be emphasesed that this is reasonable because the Howden data has a relatively longer duration and thus it is possible to obtain enough points for each block. For the WEG MS-1 data histories which are much shorter, this is less satisfactory. It should be stressed that the issue of sample length is a very difficult and controversial subject. The question of fatigue scatter or variance as a function of sample length has not been properly addressed before and only a qualitative approach could be adopted in this thesis.

Figure 4.8 shows the result of using blocks for tape 26 3m flapwise signals. As the number of blocks increases, the damage rate between the frequency domain and the time domain analysis approaches *1.0*. This consistent tendency might imply that the nonstationarity problem in the analysis is partly overcome. Small segments of the signal would presents less serious nonstationarity. However, here is a dilemma: a signal which is too long would be difficult to analyse because of the nonstationarity; a signal which is too short would result in the possibility of large fatigue damaging cycles being missed. This is an important problem. Future effort should be concentrated on finding a more rigorous solution.

4.5 Discussion

As seen from above, a fatigue analysis in the time domain is relatively straight forward. For the frequency domain analysis approach, all the current methods

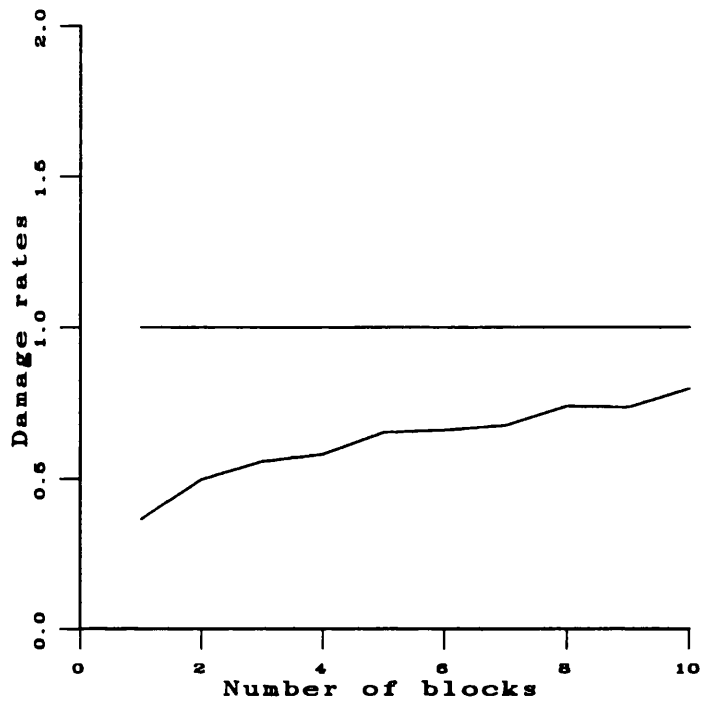

Figure 4.8: Block effect of Howden data tape 26 3m flapwise

should be used with great care. The WEG and Howden data have provided a good mechanism for verifying the present spectral analysis methods. However, because of the nonstationarity, non-normality and the strong deterministic component present in some of the signals, the frequency domain analysis techniques can not universally give acceptable results.

Analysing monitored data is quite a different task from the analysis of simulated data, or theoretical spectra. It is quite difficult to process recorded data. The results are always significantly influenced by the way the data is collected and processed, for example, the window type and window size effect on the spectrum calculated from the time signal. Different choices of cutoff frequency also produce large differences in the moments calculated from the spectrum. This may in turn produce a different peak rate expectation. However, the work presented in this chapter has enabled an overview of all the methods to be obtained and provided a guide on how they should be used in design.

In general, Dirlik's empirical formula and Bishop's theoretical solution work quite well with the damage rates close to *1.0* for WEG MS-1 data. Further computational problems are discussed in the next chapter.

Chapter 5

Computational considerations in random fatigue analysis

The fatigue analysis in the previous chapter made an overall assessment of the current methods used for random fatigue life estimation using frequency domain techniques. It was found that the computation is influenced by many factors, such as the cutoff frequency and the clipping ratio of the probability density function, etc. These parameters have to be selected carefully in the computational procedure because completely different life estimation results may otherwise be obtained. This chapter presents the results from an investigation of these parameters. Some are related to the assessment of frequency domain analysis tools and some are related to the use of these tools in design.

5.1 Effect of cutoff frequency

Theoretically, the cutoff frequency of a spectrum is generally half of the time series acquisition rate. As seen in the previous chapter, however, this cutoff frequency is decoupled from the process of calculating the moments of the spectrum when performing fatigue analysis. The reason for this is that high frequency components may cause serious problems in the calculation when often they are not structural responses but just acquisition noise. For the WEG MS-1 data the cutoff frequency was set at $15.625Hz$ to include the first 10 harmonics of the response. For the Howden data, the cutoff frequency was set at the point at which the area of the spectrum reached 99.5% of its whole area. Both these two ways of selecting the cutoff frequency are attempting to include all the structural response data in the spectra whilst excluding the noise which is either caused by acquisition error or by electronic noise during measurement.

If all the high frequency components are included in the spectrum calculation, it is possible to check how the damage changes as the point at which the cutoff frequency is varied. Figure 5.1 and 5.2 show such results from the WEG MS-1

and Howden HWP330 data. In Figure 5.1*(a)*, the PSD is plotted up to *62.5Hz*, together with the 1000 times magnified tails. The moments calculated from the spectrum are also plotted in *(b)*. It can be seen that the high frequency components have a very big influence on the higher order moments and finally on the irregularity factor as expected. The damage rates (normalised by the time domain fatigue result) of all the methods used here are plotted in *(c)*. None of them are stable until after about *27Hz*. Actually this is the point under which most of the power is included from the PSD as plotted in *(a)*.

The question which arises is, for the monitored time history or the PSD, how should the cutoff frequency be determined? The high frequency components are noise produced in data acquisition, but where should the boundary between structural response and noise be set? In other words, which part of the signal should be taken as structural response and which part as acquisition error?

The answer to this question depends partly on the bit number used in the data acquisition system. Figure 5.4 shows a simple test showing the generation of such acquisition error[38]. It is actually the acquisition error associated with a sine wave. Figure 5.4*(a)* shows the error when 5 bits are used, both the actual error and the error spectrum. Figure 5.4*(b)*, shows the error for 6 bits. A simple comparison on these two gives us a very strong impression that increasing the bit number in the data acquisition process would greatly change the error produced. Of course, the memory requirement would increase as well. Another observation is that the error is nearly white noise, distributed along the frequency axis. Fortunately, the low frequency error has a relatively small influence on the result.

Two typical results are plotted for the Howden data tape 26 in Figure 5.2, *(a)* for 3 meter flapwise and *(b)* for 3 meter edgewise. The PSD's are plotted with a log scale so that the high frequency components can be observed more clearly. It seems that the influence of these high frequency components is more serious here than with the WEG MS-1 data as seen from Figure 5.2. The high order moments and irregularity factor change more rapidly. Only the damage rates from Dirlik's formula and Bishop's theoretical solution are plotted here for simplicity.

Neither of the methods presented gives a stable solution. However, Dirlik's solution is relatively more stable in this situation. The results from Bishop's theoretical solution do not give reliable results for a signal with high frequency noise. The reason for this is that the irregularity factor becomes very low (close to zero) which makes the Kowalewski matrix used in Bishop's solution [1] ill

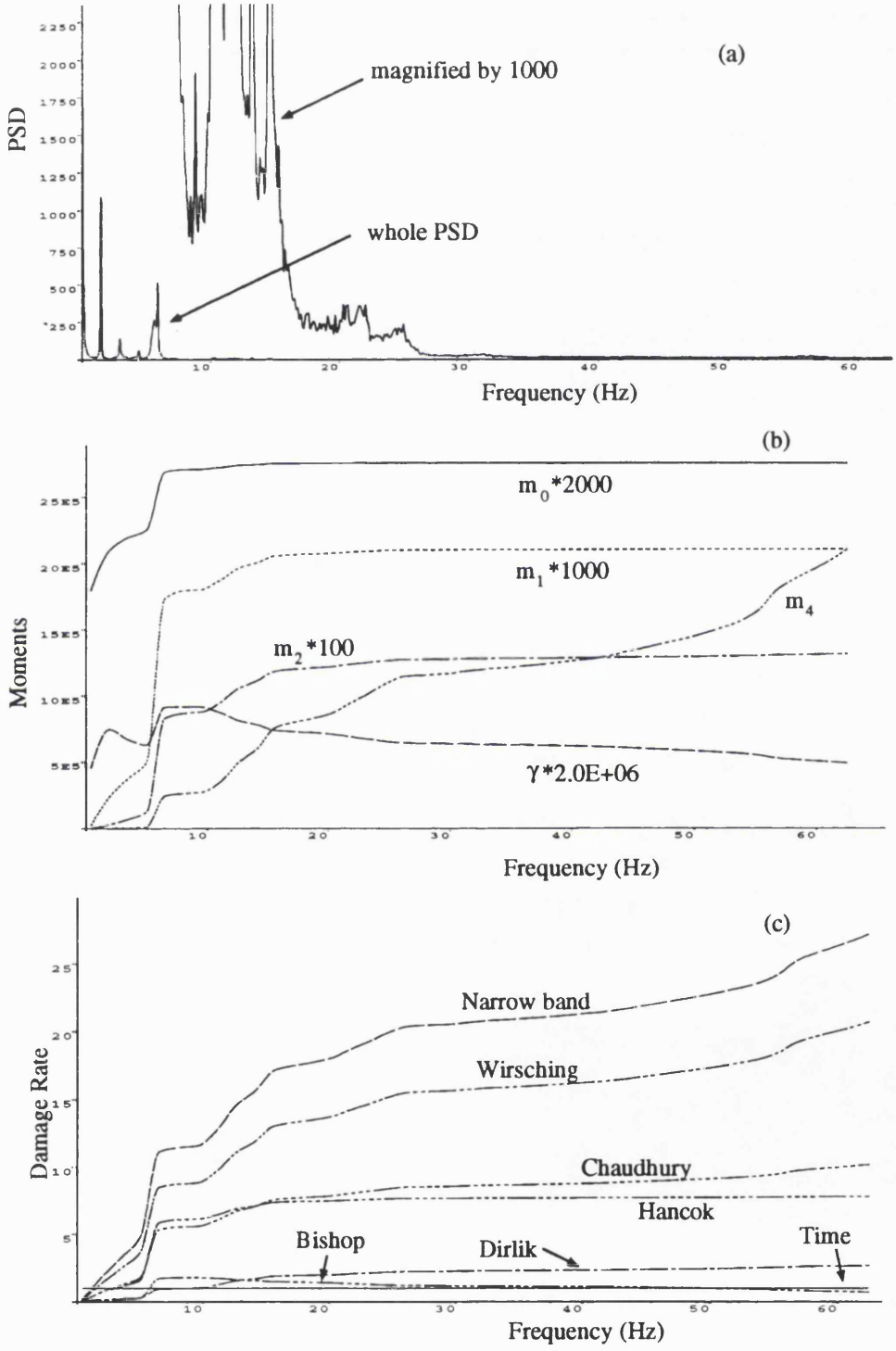

Figure 5.1: Influence of cutoff frequency of WEG MS-1 data y27a

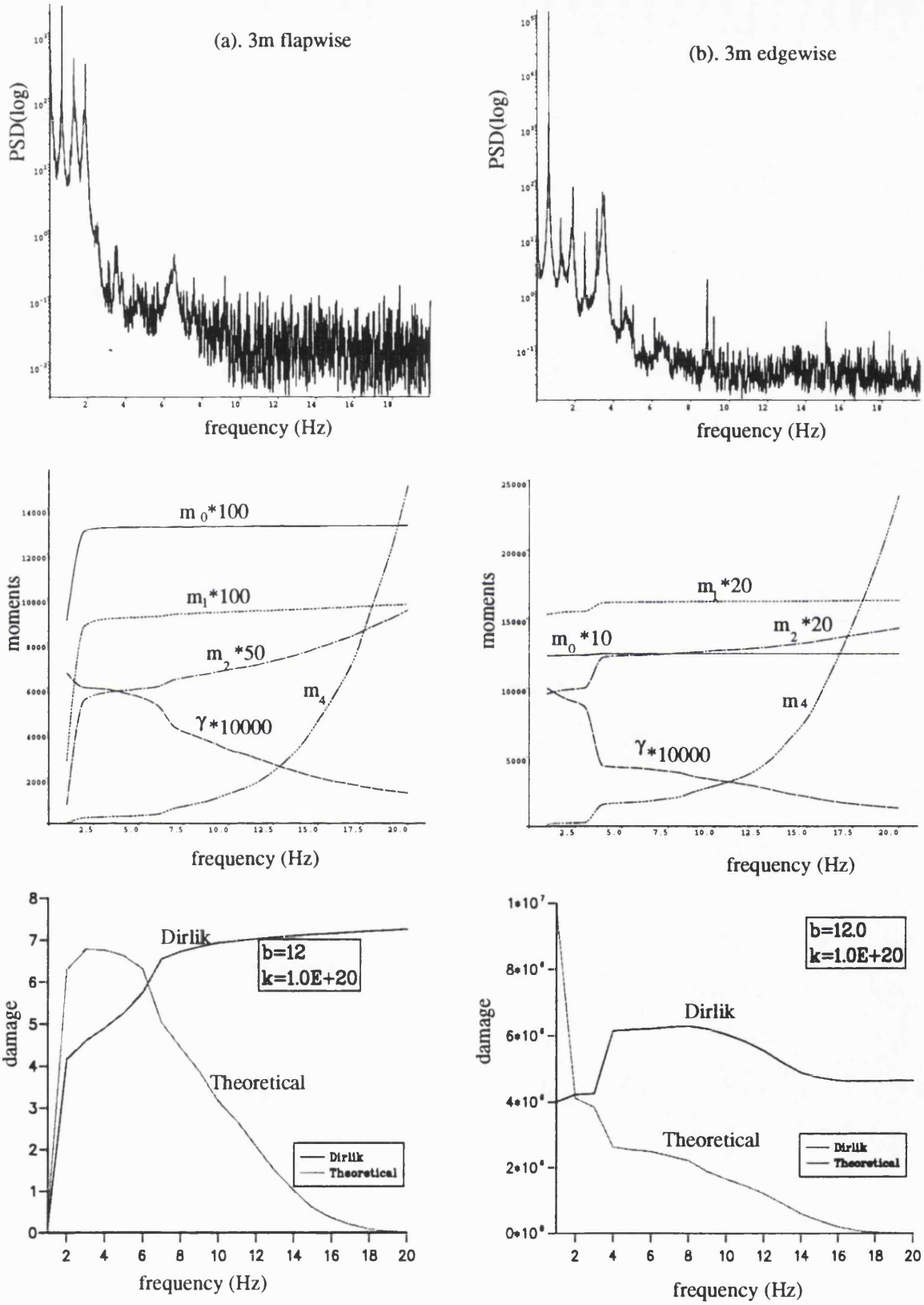

Figure 5.2: Influence of cutoff frequency of Howden data, tape 26

conditioned. Figure 5.3 shows the change of Kowalewski matrix with the change of irregularity factor. Figure 5.3*(a)* and *(b)* are the Kowalewski matrices with the following parameters respectively:

- *(a)* $m_0 = 0.406,\ m_2 = 122.959,\ m_4 = 992926.0,\ \gamma = 0.193838$
- *(b)* $m_0 = 0.406,\ m_2 = 122.708,\ m_4 = 54833.9,\ \gamma = 0.822418.$

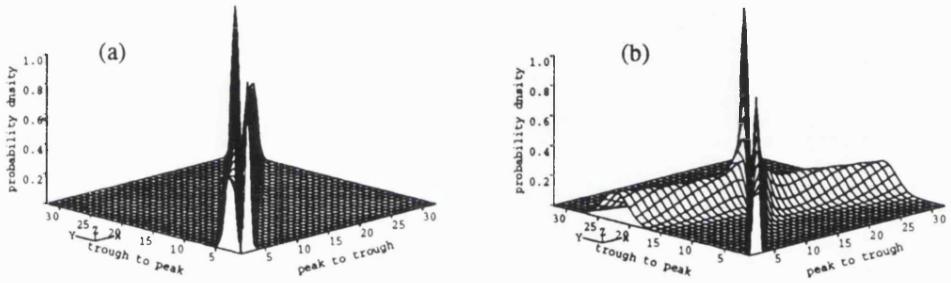

Figure 5.3: Kowalewski matrices with different cutoff frequency

These two groups of moments are from the same time series but calculated with different cutoff frequencies. It is clear from the matrix that, as the cutoff frequency increases, the probability of small cycles increases very rapidly and this makes the matrices "diagonally dominant". Since the theoretical solution generally uses a squaring method to empty the transition matrix, the squaring of this type of matrix becomes inefficient. It may even fail to converge for some extreme situations. A change of method of calculating the long-run probability would therefore help to improve the solution under these circumstances.

It is clear that the high frequency components have a big influence on the higher order moments. This increases the expected number of peaks in unit time. It would be encouraging if this increase kept the total number of higher range cycles unchanged. Since the small range cycles contributes little to the total damage, keeping the number of big cycles constant would mean the value of fatigue damage could remain the same. Unfortunately, this is not the case as shown in Figure 5.2.

The cutoff frequency issue is mainly a problem for the frequency domain tools when they are used to analyse monitored data. There is not a high frequency noise problem when a theoretical spectrum is used for structural analysis at the design stage but the spectrum truncation problem still exists. Loading spectra for some structures are provided as theoretical, empirical, or semi-theoretical formula. The sea wave load spectrum for an offshore platform, for example, is

expressed as a semi-theoretical formula which is a function of the significant wave height and the wave dominant period [46]. No matter where the spectrum comes from, the cutoff frequency has to be set by the user. This truncation problem is then the same as the cutoff frequency problem.

5.2 Length requirement

The lengths of monitored time histories are always limited by the capacity of digital recording equipment. The two sets of data analysed in this thesis, WEG MS-1 and Howden HWP330, have significant differences in this respect. For the WEG MS-1 data, the durations are 300 seconds for load cases A,C,D,F, 240 seconds for load case B and 102 seconds for E. For the Howden data, the durations are 2550, 3260, 3862, 3510 seconds for tape 18, 26, 27 and 30 respectively.

As with statistical analysis, the time series is generally required to have enough length (sample size) to be taken as a sample of the process. This requirement is also necessary for the fatigue analysis of structures under the action of random loads because each time series is taken as a representative sample of the whole stress history the structure will undergo. It has to be representative to be "qualified" as a sample for such a history.

To assess this sample length problem different lengths of time signal were used to rainflow count and estimate damage. A relationship between damage rate and signal length was therefore obtained. The results when an $S-N$ slope value of $b = 5.0$ and $k = 1.23 \times 10^{+15}$ was used are presented in Figure 5.6 for the WEG MS-1 data and Figure 5.8, 5.9 for the Howden data. The idealised data produced by computer simulation, *nbdata*, was also examined. This result is presented in Figure 5.5. For this data it can be seen that if the signal is too short, the damage rate estimated fluctuates without converging to any value. As the length increase, the damage rate converges towards the result obtained by taking the signal as a whole. For this length of signal there are enough cycles counted from the signal to form a smooth curve of the probability density function. Increasing the length of the signal further would add some cycles to the whole set of counted cycles but the PDF does not then change much. The damage rate can therefore be regarded as stable.

The result for the WEG MS-1 data in Figure 5.6, on the other hand, does not show such a tendency. The damage rate is still fluctuating even when the whole time signal is used. This clearly means that the length of the signal is still

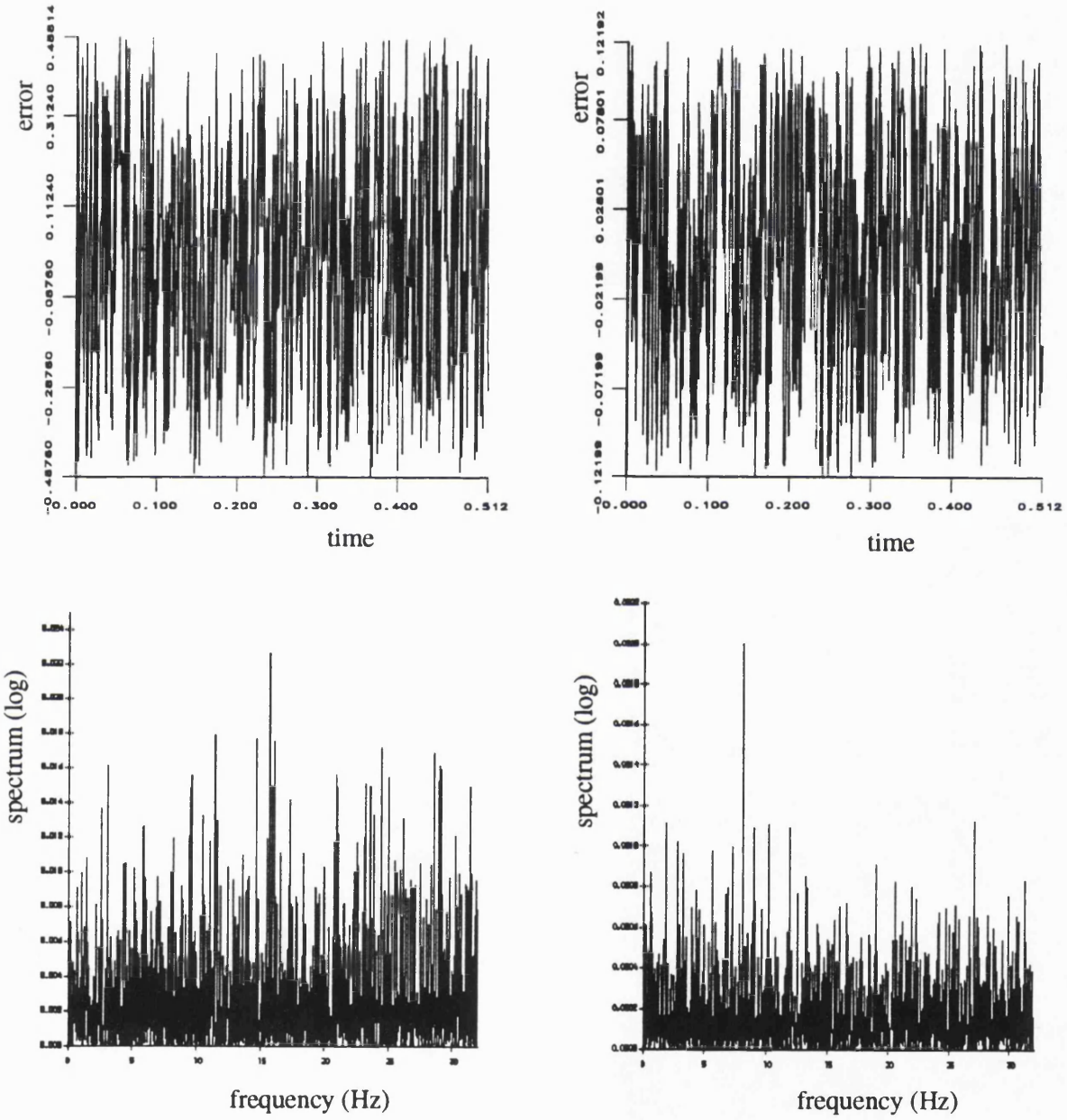

(a). 5 bit acquisition

(b). 6 bit acquisition

Figure 5.4: Noise level produced by different acquisition bit.

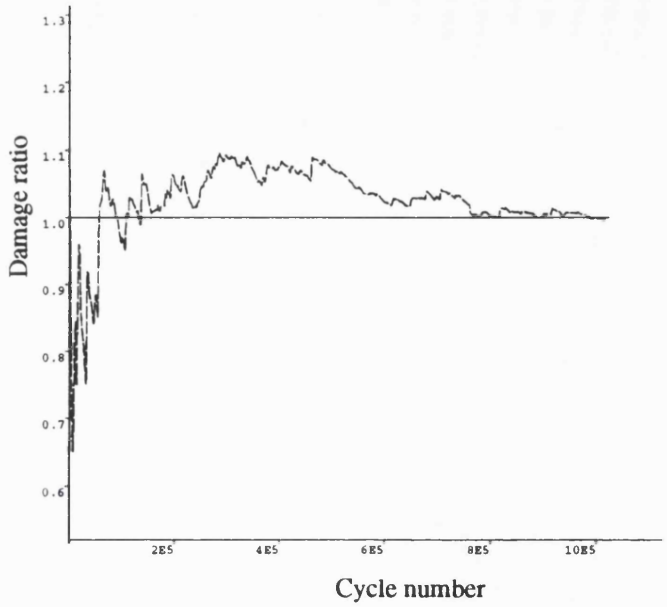

Figure 5.5: Length effect of idealised data

not enough to form a smooth PDF curve. Each time a longer signal is used, the damage is influenced by the new cycles added in. However, careful scrutiny of the maximum cycle number reveals that it is much less than for the idealised data. The general trend is therefore similar. One should be careful to realise therefore that the damage calculated at this stage can not be taken as the real structure damage because the signal can not be taken as a wholly representative sample of the structural response.

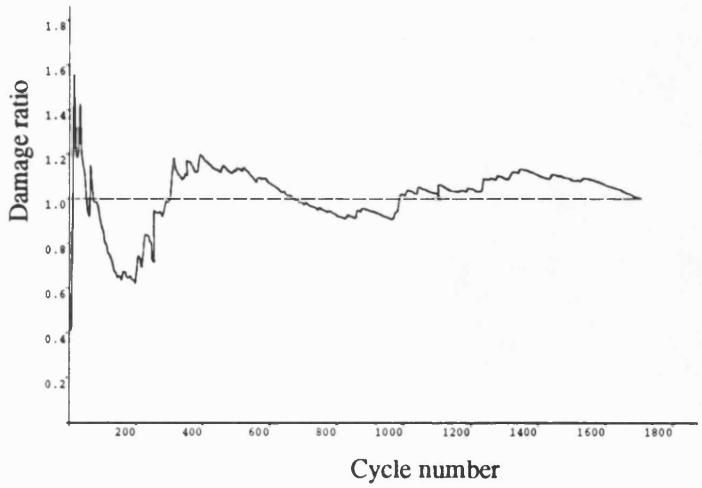

Figure 5.6: Length effect of WEG MS-1 data y12a

This phenomenon is shown more clearly in Figure 5.7, where two rainflow

cycle PDF's from simulated signals are plotted with the rainflow cycle PDF from the original signal MS-1 *y27d*. The simulated signals use the spectrum of *y27d* so that they keep the same frequency characteristics with the original signal, although one of them uses a *15.625Hz* low pass filter. It can be seen from this figure that as the signals become longer (by simulation), the rainflow cycle PDF's keep the same shape but become smoother. Then the situation in Figure 5.6 can be expected to have a significant improvement.

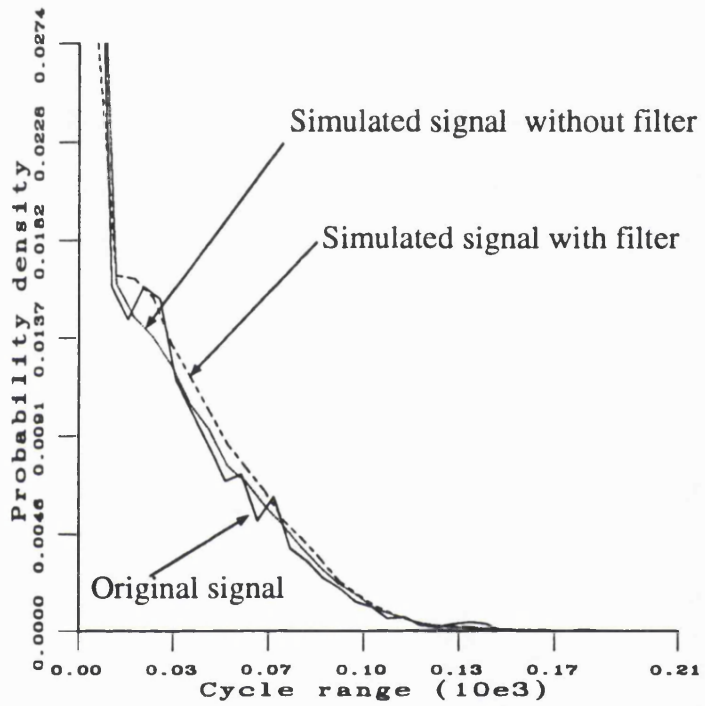

Figure 5.7: Rainflow cycle PDF's of simulated long signal

When the low pass filter is used, many small cycles produced by the high frequency noise are removed. This makes the middle and high range cycles have a relatively higher probability.

The situation for the Howden data shown in Figure 5.8 and 5.9 is quite different. The flapwise result includes several jumps to reach their final values while the edgewise results converge from the beginning. The reason for the jumps in the flapwise signal is that there exists a nonstationarity in the signal. For the edgewise signals, the damage rates are very stable due to the existence of a dominant deterministic component. This can be seen from the rainflow cycle PDF's very clearly.

It is very difficult for any method to deal with a situation where the signal is not long enough. If the signal is not long enough for rainflow counting, it is

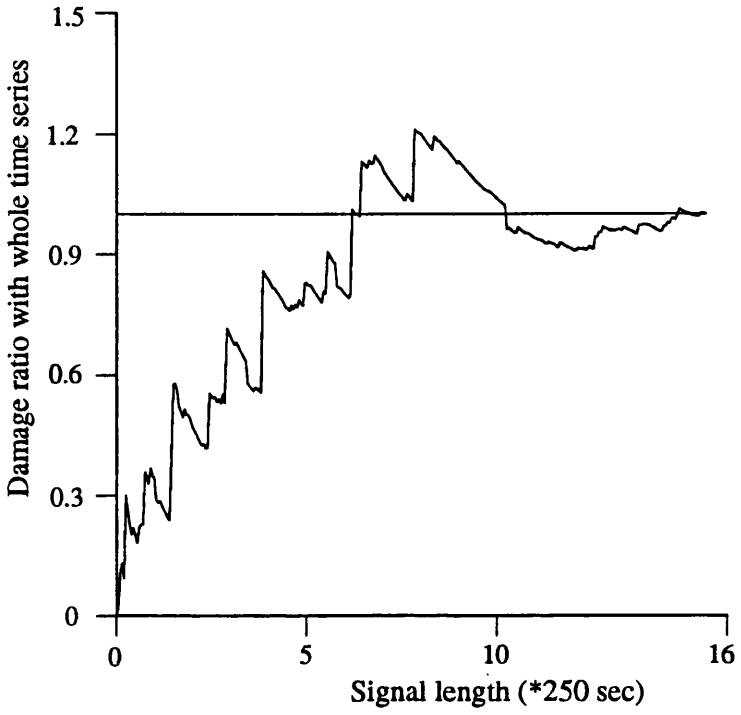

Figure 5.8: Length effect for Howden data tape 27 flapwise signal

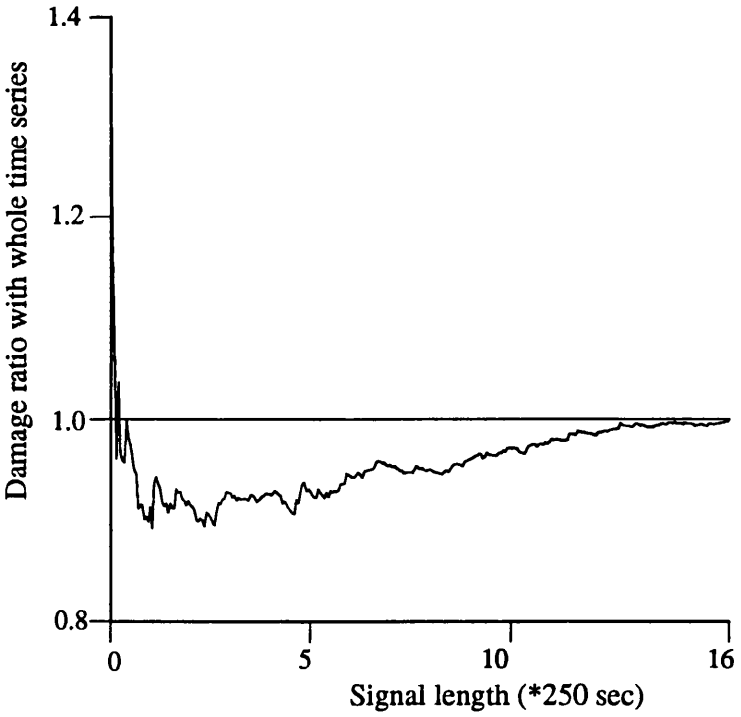

Figure 5.9: Length effect for Howden data tape 27 edgewise signal

probably true that it is not long enough to contain all the frequency information for frequency domain analysis. Actually, in general when a FFT is performed on the signal, not all the data is used in the calculation unless zeros are added to the end of the signal. When windows are used in the calculation, the problem is even more complicated because use of windows means that the data in each window can be taken as a sample and the length becomes even shorter. Actually, the size of window used has a great influence on the frequency domain estimation as shown in Figure 5.10.

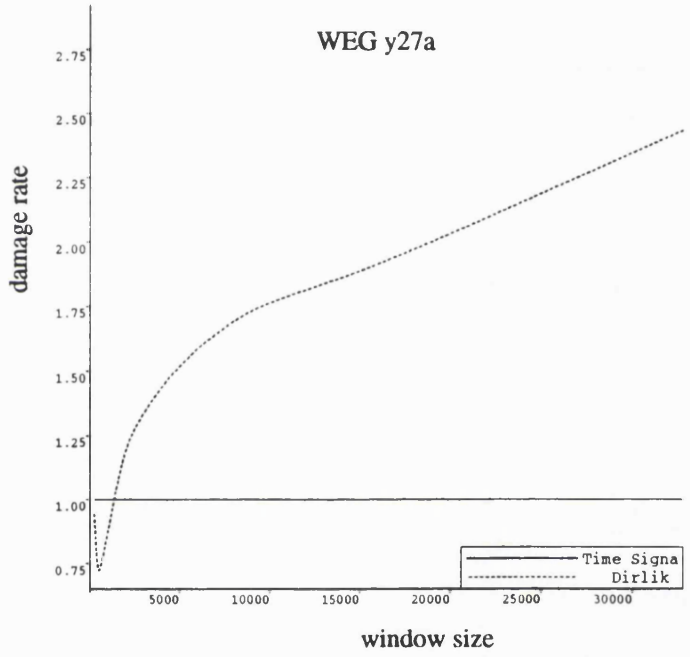

Figure 5.10: Window size effect: WEG MS-1 data y27a

It is therefore very difficult to give any quantitative instruction on the choice of sample length when trying to monitor structural response. However, the sampling frequency used for acquiring the data does not have to be too high for fatigue calculation because the peak-trough sequence is of principal concern for fatigue.

The length problem encounted with the WEG MS-1 data is also important for a statistical analysis. If the first 300 seconds of the Howden data is used for the stationarity check, it will give a stationary conclusion, which is obviously contradictory to the one drawn from the statistical check in the previous chapter. This shows that the stationarity check should also be performed on relatively longer signals.

5.3 Effect of $-$ curve slope

When two rainflow cycle probability density functions are compared with each other, it is rarely noticed that the inverse slope of the $S-N$ curve has a significant influence on the fatigue damage estimated from these two functions as in Figure 5.11. Generally speaking, the closer the two rainflow cycle PDF's are, the closer the damages derived from these two PDF's will be. In practical computation, however, it is impossible to obtain two PDF curves which are exactly the same. The difference between these two curves will then produce different damage ratios for different $S-N$ curve slope b value. The term damage ratio is used here again to represent one damage value divided by the other.

Figures 5.11 and 5.12 highlight this variance for two typical WEG MS-1 data files. They were simply derived by fixing the rainflow cycle PDF's and changing the value of b in the damage calculation. It is quite interesting to see from Figures 5.11 and 5.12 that, despite the difference in the PDF curves between the frequency domain and the time domain solutions, the fatigue damages estimated will meet at two points where the values of b are carefully selected. While for other values of b, both over-prediction and under prediction are possible. This is obviously caused by the weighted integral in the damage calculation. The importance of the difference between the PDF's from the frequency domain analysis with the one from the time domain analysis is actually changing with b.

A similar investigation on the Howden data has also been performed. Figure 5.13 and 5.14 show the results for data tape 26 3 meter flapwise and 3m edgewise respectively. The result for the 3m flapwise signal shows a similar tendency to that which appeared in the WEG MS-1 data. The result for 3m edgewise signal, on the other hand, shows a consistent upward tendency. Once again, this is because of the dominant deterministic component in the edgewise signal. The deterministic component results in cycles being concentrated in a certain range and the weighted sum is dominanted by these cycles.

This phenomena suggests that some methods which work well for one kind of material may give very poor estimation results for other kinds. The accurate prediction of both medium and higher range cycles is very important if a method is to be used for different kind of materials. It should also be noted that the term of "equivalent stress" should be understood as strictly valid only for the specified value of b which is used in its derivation. There is no universal "equivalent stress" in random fatigue estimation.

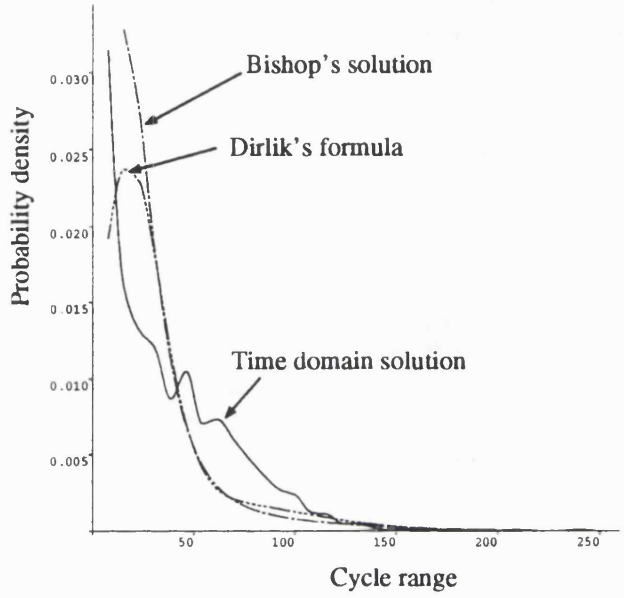

(a). Rainflow cycle PDF's from WEG data y27a

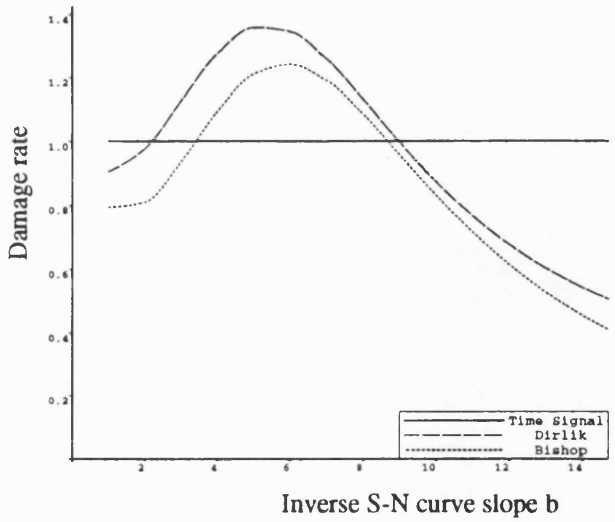

(b). Damage rates from PDF's in (a). with different b values

Figure 5.11: Effect of S-N curve slope: WEG MS-1 data y27a

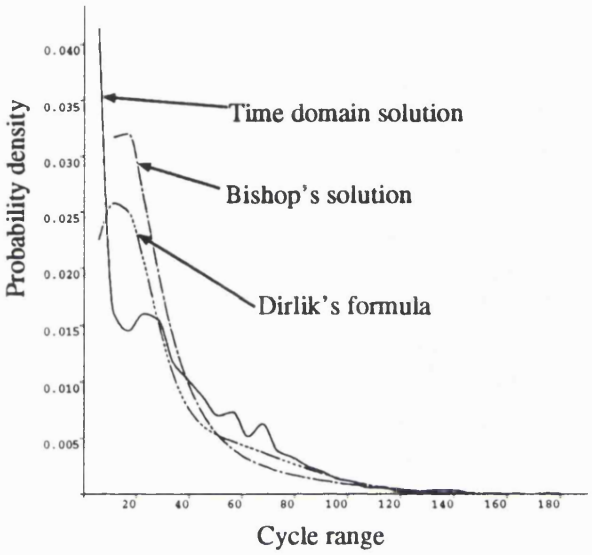

(a). Rainflow cycle PDF's from WEG data y27d

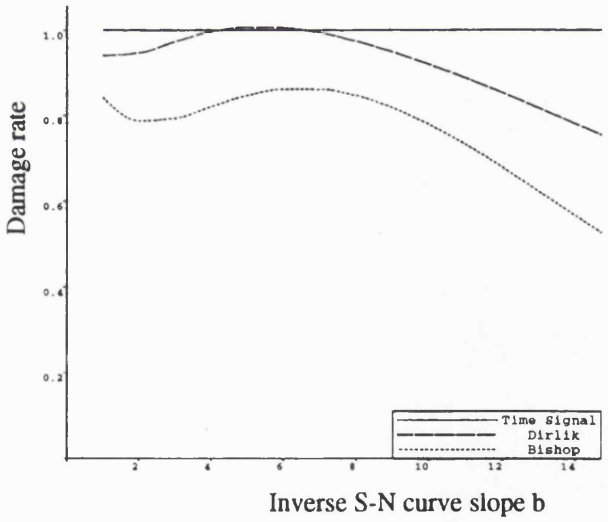

(b). Damage rates from PDF's in (a). with different b values.

Figure 5.12: Effect of S-N curve slope: WEG MS-1 data y27d

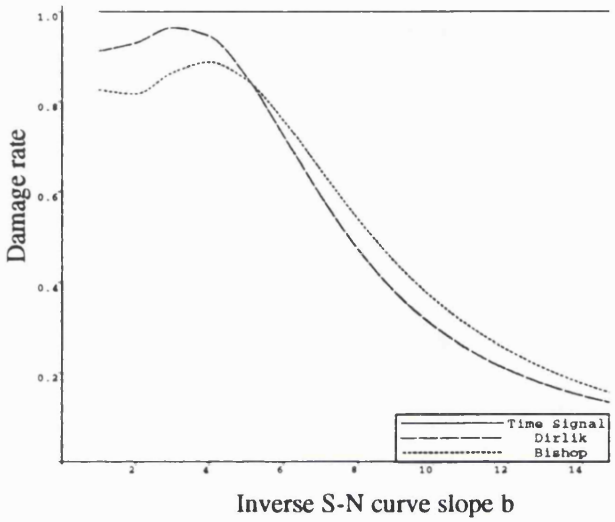

Figure 5.13: Effect of S-N curve slope: Howden data tape 26 3m flapwise

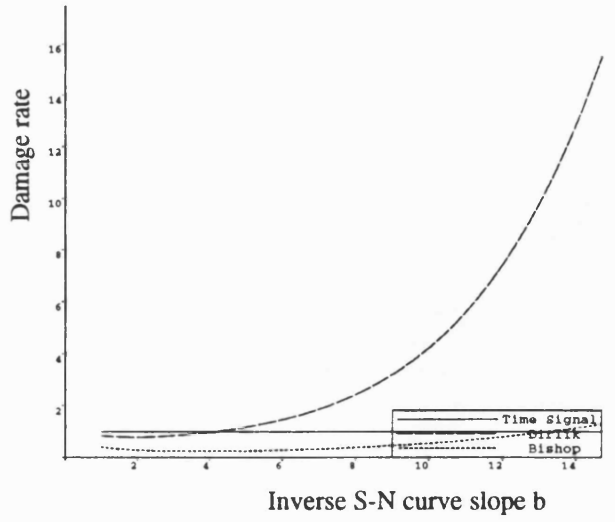

Figure 5.14: Effect of S-N curve slope: Howden data tape 26 3m edgewise

5.4 Selection of clipping ratio

When fatigue life estimation is performed in the time domain, the maximum value of the rainflow cycle can be determined easily using the difference between the highest peak and the lowest trough in the time signal. When a frequency domain analysis is performed, the range of the signal is determined from the shape of the PDF tail which theoretically goes from $-\infty$ to ∞ for a Gaussian distribution as shown in Figure 5.15. If the time series from which the spectrum is calculated is available, it is possible to derive the maximum range by referring to the time domain analysis. However this can only make sense in a research environment (and probably nonsense if one refers to Figure 4.7 in the previous chapter). A practical computation is unable to deal with this infinite range. Thus, a clipping point must be selected to set a finite maximum range other than infinity. This point is described as the so-called "clipping ratio", which is defined as the ratio of the maximum value with the root mean square. That is,

$$\rho = \frac{X_{max}}{\sigma}$$

The maximum range is $2\rho\sigma$ because of symmetry.

The principle behind the selection of clipping ratio is that it should include most of the probability inside the range determined. However, the important question is what level of probability can be truncated. Some methods used for fatigue estimation, such as Dirlik's empirical formula and Bishop's solution, can theoretically extend to infinity. A problem for practical computation is therefore to select a suitable cutoff point.

The relationship between damage rate and clipping ratio can be examined to answer this question. Figure 5.16, 5.17 and 5.18 show the typical results of this relationships when Dirlik's formula is used. The examination of the WEG MS-1 and the Howden data shows that the fatigue damage rate generally converges to the stable value for a clipping ratio range between *4.0* and *6.0*. So, selecting a clipping ratio of *6.0* would be enough from the point of view of fatigue estimation. This conclusion is also suitable for Bishop's theoretical solution.

5.5 Effect of deterministic components

Deterministic components play a very important part in wind turbine blade fatigue. As seen from the analysis of the Howden data, the deterministic component constitutes a separate peak in the rainflow cycle probability density function,

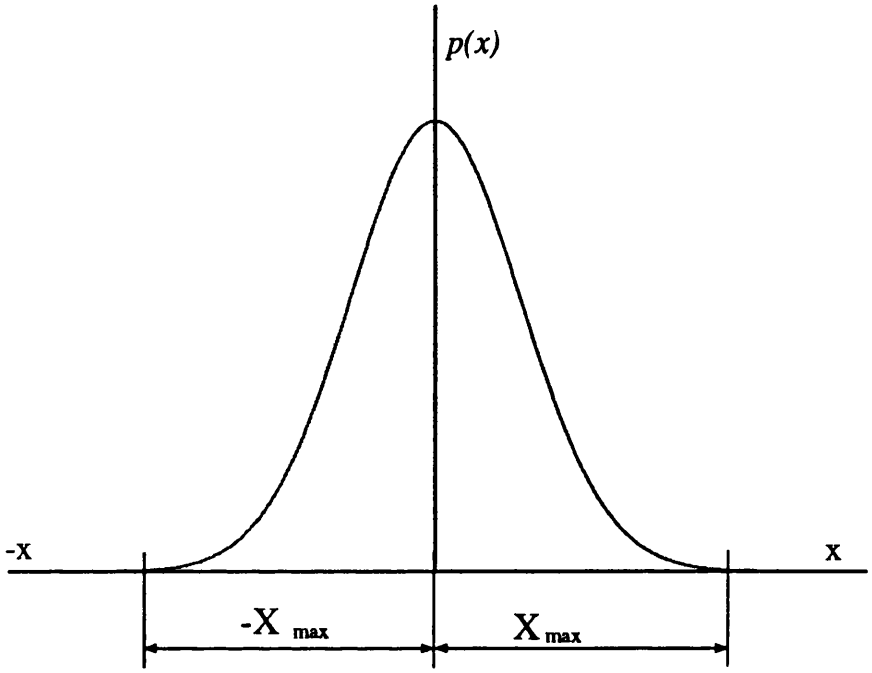

Figure 5.15: Clipping of normal distribution

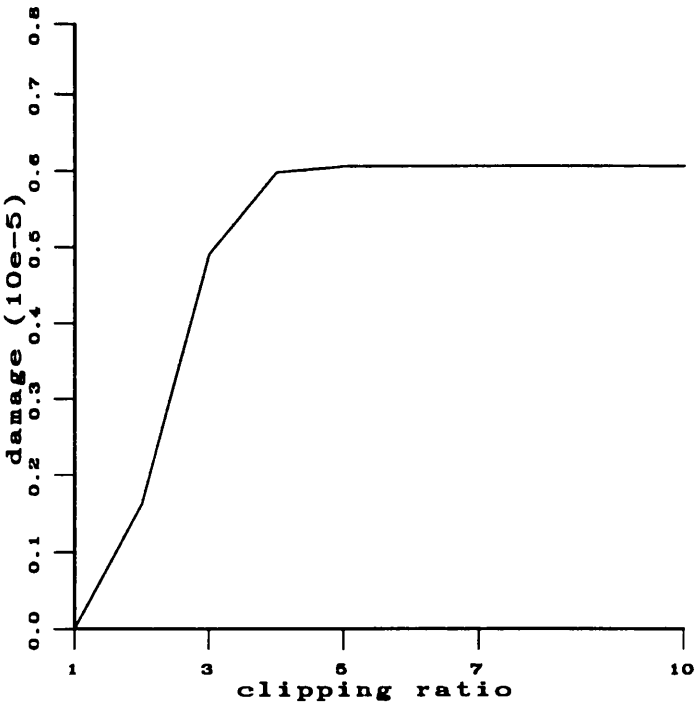

Figure 5.16: Choice of clipping ratio: WEG data y27d

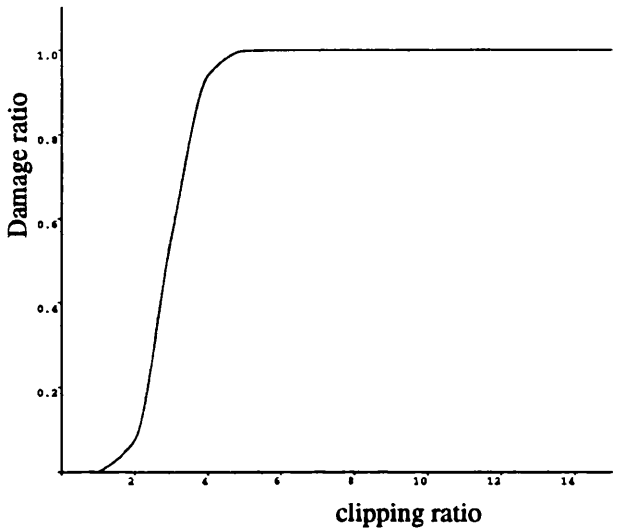

Figure 5.17: Choice of clipping ratio: Howden data tape 26 3m flapwise

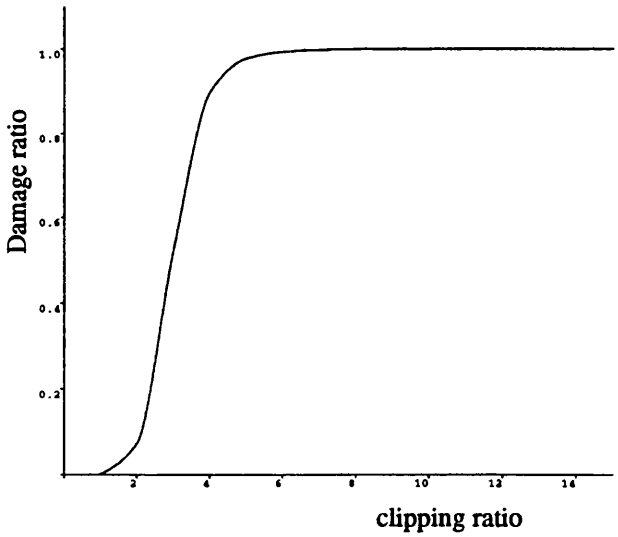

Figure 5.18: Choice of clipping ratio: Howden data tape 26 3m edgewise

which can not be predicted by any of the present methods. The fatigue damage results estimated using these methods can not, in general, be consistent with the time domain analysis even if it does sometimes by chance.

Chapter 8 deals with this problem in detail.

5.6 Discussion

Some problems which were discovered in the fatigue analysis on monitored structural response signals in previous chapters were examined in detail in this chapter. Some parameters associated with the use of present methods were investigated. This investigation provides a useful guide for the use of present methods in fatigue damage estimations.

Many problems were investigated for the first time. This will definitely help to ensure present frequency domain tools are used practically in engineering design. Some parameters, such as clipping ratio, can now be determined based on frequency domain information for the first time. The investigation of this parameter for fatigue analysis can not give a criterion on how the cutoff frequency should be selected but can raise its importance. The selection of this parameter should be based on the results from a structural random vibration analysis, that is, to separate the noise based on the analysis of structural response. The length requirement problem is mainly of concern in a time domain analysis. The analysis in this chapter provides some guidance on the monitoring of structural response histories. As with any other statistical problem, sample length is important in the analysis. As for the analysis on the effect of $S - N$ curve slope, the importance of an accurate prediction of the medium and high range cycles is raised again.

Chapter 6

Influence of Mean Stress

6.1 Introduction

It was shown in a previous chapter that both the Dirlik and Bishop methods produce very good results when the data is reasonably Gaussian, stationary and random as long as mean stress effects are ignored. For welded structures, mean stress usually has little influence on crack propagation because of the existence of residual stresses. However, wood epoxy and grp wind turbine blades have been shown to be very fatigue sensitive to mean stress [61]. The crack growth of some low alloy steels has also been found to be strongly influenced by mean stress [62].

Quite a few fracture mechanics models are proposed for considering mean stress in the analysis of crack growth. Fracture mechanics will not be discussed here since it has not been applied to the fatigue analysis of random load cases using frequency domain techniques.

Of all the spectral fatigue analysis methods, only Bishop's theoretical solution is capable of being adapted to take the mean stress into account because this method is decomposable whilst the other methods are generally given in closed forms which are impossible to separate.

It is noted that, by the very definition of rainflow cycles, they are made up of sections of signal which may be separated by a large time interval. The concept of the mean stress of a rainflow cycle then becomes rather abstract. However, since a primary characteristic of a rainflow cycle is a stress-strain hysteresis loop, the mean stress value can be associated with the mean of the loop in the stress-strain plane as shown in Figure 6.1.

Any frequency domain analysis such as the theoretical solution being described here, is generally performed without reference to the global mean of the stochastic process since its value is not part of the generally supplied spectrum. Since the so-called "mean stress" generally refers to the mean level of the cycle relative to the zero mean, the frequency domain analysis can only provide the relative

mean of each cycle when referenced to the global mean level. At the design stage, however, the global mean information is usually known as part of the structural analysis. This global mean value and information about the relative mean level of each cycle will together, decide the actual mean value of the cycle. At the research stage, if only the spectrum is supplied, it is impossible to determine the actual mean value of each cycle [4].

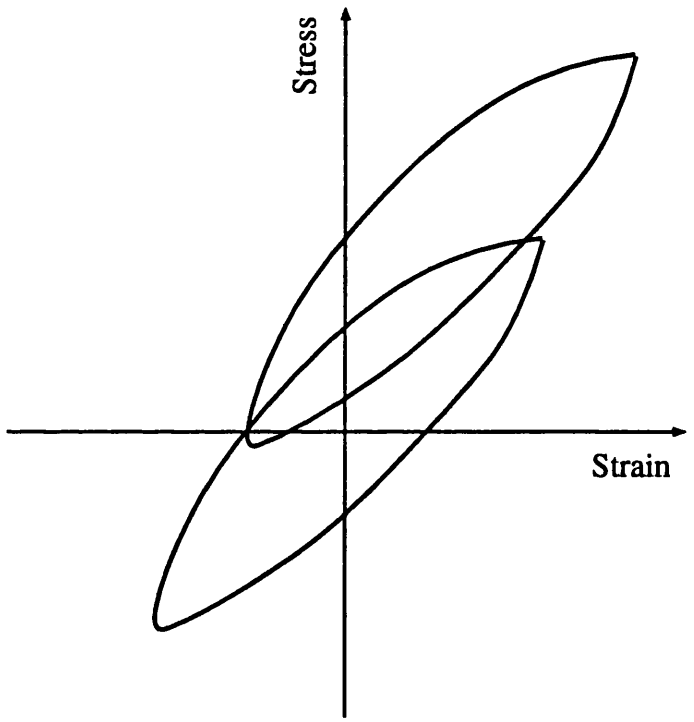

Figure 6.1: Rainflow cycles with different mean

6.2 Goodman relationship

Laboratory experiments to obtain *S-N* curves have also been conducted on different mean stress levels. Figure 6.2 shows how the *S-N* curve might change with varying mean stress level. As the tensile mean stress increases, generally the fatigue life reduces [10].

This influence has, up to now, not been included in any frequency domain approach. The relationship between fatigue damage (or life) and the mean stress and cycle range can be determined by taking a slice through Figure 6.2, the result of which is shown in Figure 6.3.

If this curve is taken as linear, the so-called Goodman relationship can be

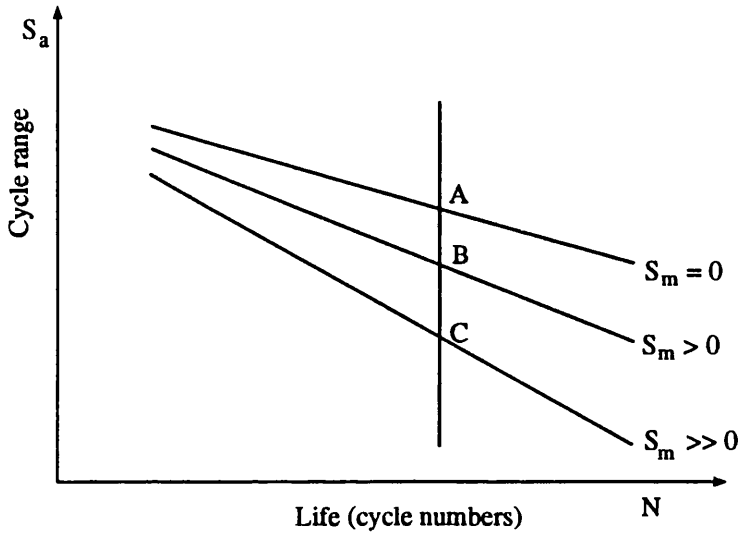

Figure 6.2: S-N curves with different mean

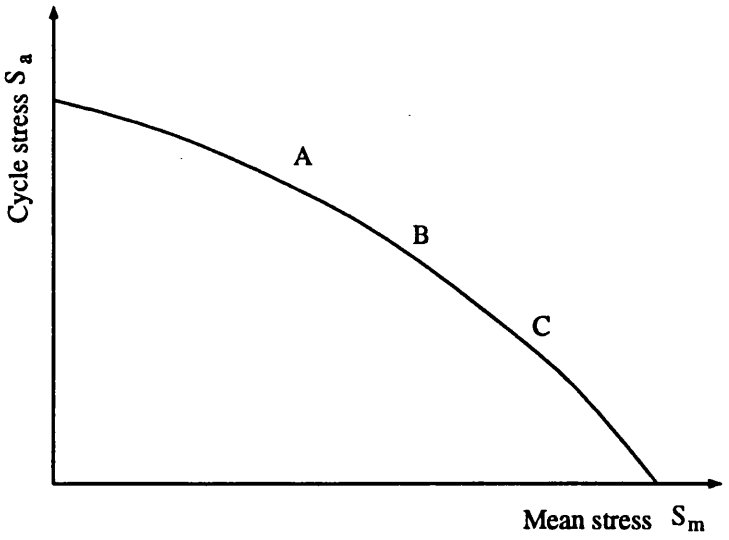

Figure 6.3: Fatigue life - cycle range - mean stress curve

obtained as given below [2]:

$$\frac{S_a}{S_{a0}} + \frac{S_m}{S_{ult}} = 1.0 \tag{6.1}$$

in which, S_{a0} is the cycle range with zero mean equivalent to cycle range S_a with mean S_m, S_{ult} is the ultimate tensile stress of the material.

Some other formulas for considering mean stress have been proposed. The non-linear Gerber relationship [2], for instance, is another one expressed as

$$\frac{S_a}{S_{ao}} + (\frac{S_m}{S_{ult}})^2 = 1$$

If the yield stress, instead of the ultimate tensile stress is used, the relationship proposed by Soderbergr in 1930 is obtained which is expressed as:

$$\frac{S_a}{S_{a0}} + \frac{S_m}{S_y} = 1.0$$

All these relationships are presented in Figure 6.4. The Goodman relationship is suitable for smooth polished specimens and is widely accepted. It is also used for all the analysis in this chapter.

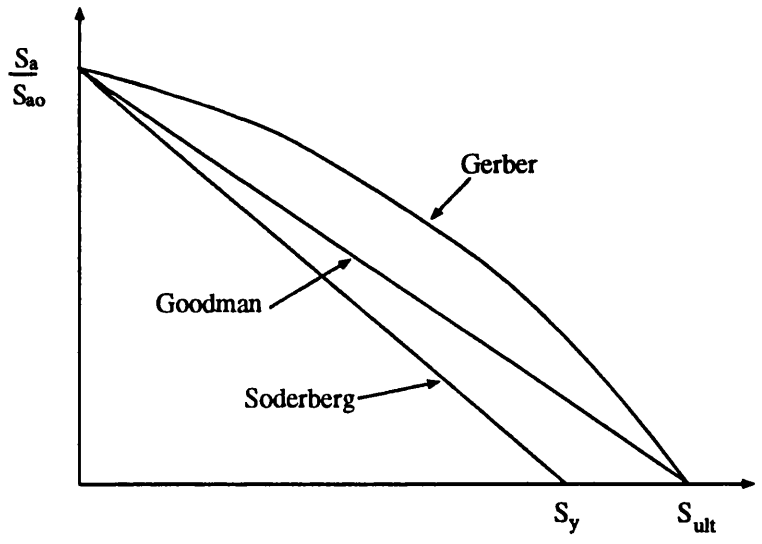

Figure 6.4: Goodman relationship

The Goodman relationship can be put into another form as:

$$S_{a0} = \frac{S_a}{(1 - \frac{S_m}{S_{ult}})} \tag{6.2}$$

This formula provides a way of converting any stress cycle with a non zero mean into a stress cycle with a zero mean which will produce the same fatigue damage. Using this conversion, the *S-N* curves, which are generally applied to constant amplitude cycles with zero mean stress, can then be used in the analysis without modification.

6.3 Theoretical solution for Gaussian signals

Before proceeding to consider mean stresses, the theoretical method developed by Dr. Bishop [1] [35] will be introduced first. This is because it is the best choice for connecting the mean value with each cycle range. The three events which make up Bishop's theoretical solution are considered separately in a way which allows modification. The mean value of each cycle can be noted down when its probability is computed. Dirlik's solution has a good overall accuracy but it is given as a closed form and so is impossible to reform.

6.3.1 Markov Process

Stochastic Process

Random variables or random vectors are adequate for describing results of random experiments which assume scalar or vector values in a given trial. In some situations, however, the outcomes of a random experiment are represented by functions. These outcomes are described by a *random function*, also known as a *stochastic process*. It is generally defined by a family of joint distribution functions of a set of random variables, which are actually member functions of the process from a finite time set.

Markov processes

A Markov process is one kind of stochastic processes classified by its memory property. Its formal definition is as follows.

Definition. A stochastic process $X(t)$, $t \in T$, is called a *Markov process* if for every n and for $t_1 < t_2 < \cdots < t_n$ in T we have the conditional PDF as

$$f(x_n, t_n | x_{n-1}, t_{n-1}; x_{n-2}, t_{n-2}; ...; x_1, t_1) = f(x_n, t_n | x_{n-1}, t_{n-1})$$

if the indicated density functions exist.

It can be seen that the Markov process is simply a stochastic process which can only "remember" its last position. In other words, only the present position is important in deciding where to go next in the process.

6.3.2 Basic formulation of the theoretical solution

The Theoretical solution assumes the peak-trough and trough-peak transitions of the time series can be represented by a Markov chain. From the associated

definition of a rainflow cycle [1], each cycle can be taken as three separate events occurring together. The probabilities of the three events then can be calculated separately. The probability for each event is actually the long run transition probability from one level to another level. If the process is Markovian, this probability can be calculated by Markov chain theory.

As shown in Figure 6.5, if the probability of being at a particular peak is defined as $p(ip)$ and a rainflow range of value h=*ip-kp* is defined, where *ip* and *kp* are the levels at point 1 and 2 respectively, the expression for the probability density function of a rainflow range value h for any peak value can be found by summing over all values of *ip*:

$$p_{RR}(h) = \frac{2.0}{dh} \sum_{ip=h+1}^{\infty} Y_1(ip, ip-h) Y_2(ip, ip-h) Y_3(ip, ip-h) p(ip) \qquad (6.3)$$

for h=*1* to *ip-1* where $Y_1(ip, ip-h)$ is the conditional probability of event Y_1, given a peak with height *ip*, $Y_2(ip, ip-h)$ is the conditional probability of event Y_2, given a peak with height *ip*, and $Y_3(ip, ip-h)$ is the conditional probability of event Y_3, given a trough with height *ip-h*. The parameter *dh* represents the interval width used to divide the total signal stress range. The value *2.0* comes from the fact that for a full set of events, rainflow ranges occurring with event Y_1 on the right hand side need to be considered. In other words, for every configuration of Y_1, Y_2, and Y_3 being considered, there is an equally likely configuration of the signal which is a reflection of the signal about *t=0*. Therefore the problem of obtaining a theoretical derivation to the rainflow range has become one of obtaining $Y_1(ip, ip-h)$, $Y_2(ip, ip-h)$, $Y_3(ip, ip-h)$ and *p(ip)*.

Two areas of theory will be required for this. A suitable method is required to model the dependence between adjacent extremes, then a theory is required to extend this to model the dependence between extremes which are not adjacent. For the first an expression by Kowalewski [63] is used and a Markov Chain model is used for the second.

6.3.3 Markov model for rainflow cycle

Markov chain models are widely used in random fatigue analysis, both for crack growth [64] and damage accumulation calculations [65]. However, this Bishop's model was the first time they were used for modelling rainflow cycles in a random response process. According to the definition of rainflow cycles, the three events needed to constitute a cycle can be modelled as in Figure 6.6. All the necessary information required to define the rainflow cycle is given by this figure. It is a

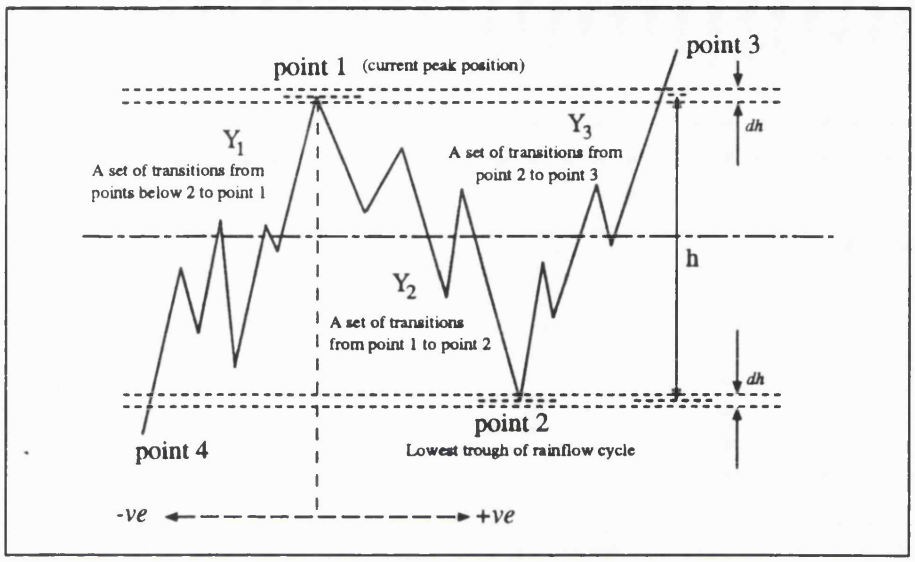

Figure 6.5: Illustration of events Y_1, Y_2, Y_3

Markov chain model with absorption states. A description of this model is given below.

State 1 (level *kp*). This is an absorption state into which transitions can occur from any level between *ip* and *ip-h*, plus *ip* itself.

State 2 (all levels below *kp*). This is also an absorption state into which transitions can occur from any level between *ip* and *ip-h*, plus *ip* itself.

State 3 (all levels above *ip*). This is an absorption state into which transitions can occur from any level between *ip* and *ip-h*. Transitions from level *ip* can not occur because a peak given trough transition can only originate from a trough at some level below it, and a trough at *ip* can only occur after a trough given peak transition from above. Such a transition is invalid. State 3 has an unusual feature. We are just interested in the probability of a set of transitions which originate from *ip* and eventually end up in either absorption state 1 or 2 without returning to level *ip* or above. Therefore, entries into level *ip* have to be transferred into state 3. This ensures that any transitions via level *ip* are prevented from accumulating to the required probability of absorption into state 1 or 2.

State 4 (levels between *ip* and *kp*). This is an transient state. Transitions to any level in this state can only occur from some other level within

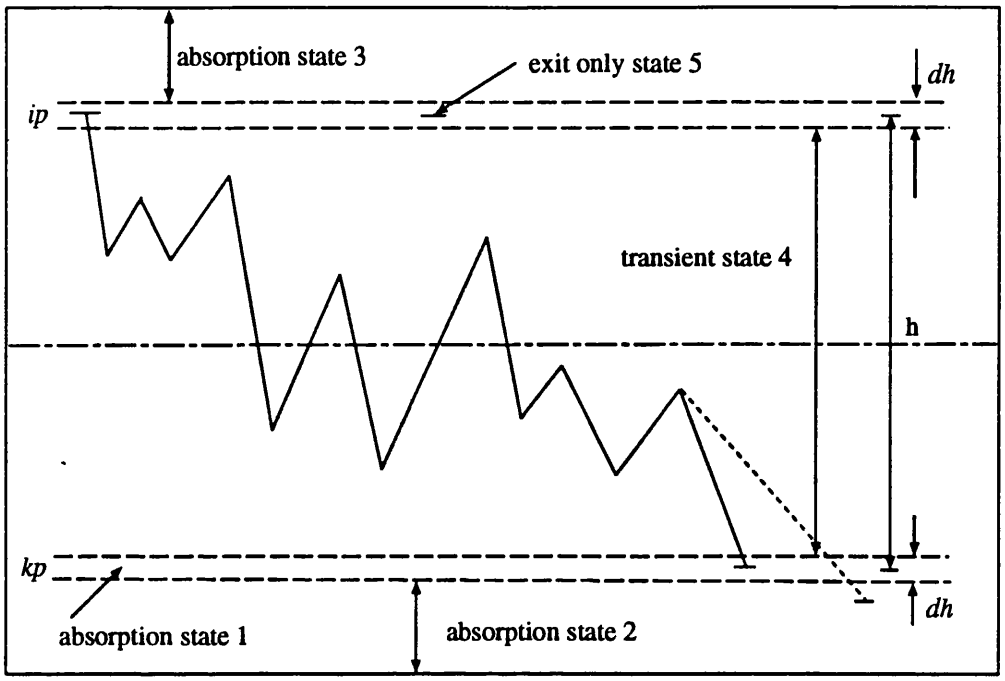

Figure 6.6: Markov model for rainflow cycle

state 4, with the exception of level *ip*, for which the initial trough given peak transition is the only possible non zero transition probability into state 4 from outside it.

State 5 (level *ip*). As explained above the only non zero transition probability out of this state is the initial trough given peak step. All transitions back into this state are transferred to state 3 in order to make subsequent transition probabilities from this state zero. Hence it is an entry only state.

6.3.4 Initial transition and Kowalewski formula

Before the long run probabilities defined by Figure 6.6 can be evaluated a one-step transition matrix is set up to model the dependency between adjacent extremes. This adjacent extremes problem can be solved by employing the Kowalewski approximate expression [63], which is valid only for stationary Gaussian signals and is expressed in terms of the zeroth,second and fourth moments of the PSD about the zero frequency axis.

$$P_{min,max}(\alpha_1,\alpha_2) = [\frac{\alpha_2-\alpha_1}{4m_0\gamma^2}][\frac{1}{(2\pi m_0(1-\gamma^2))^{1/2}}]e^{\{\frac{\alpha_1^2+\alpha_2^2+2\alpha_1\alpha_2(2\gamma^2-1)}{8m_0\gamma^2(\gamma^2-1)}\}} \qquad (6.4)$$

where α_1 is the trough level and α_2 is the peak level, m_n is the nth moment of the PSD function and $\gamma = m_2/\sqrt{m_0 m_4}$ is the irregularity factor. Figure 6.7 shows one example of this function.

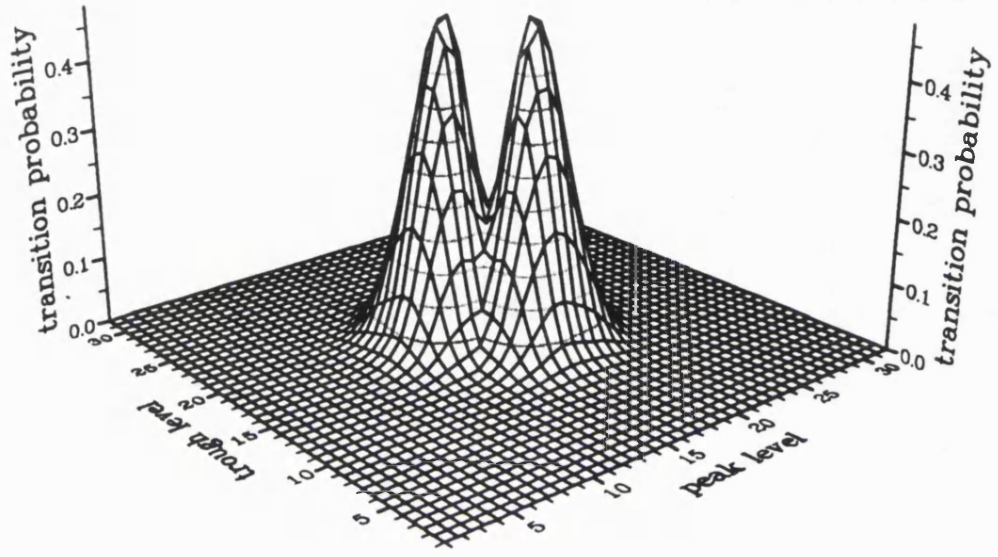

Figure 6.7: Illustration of Kowalewski's expression.

This formula should be taken as two parts: being a peak given trough part and a trough given peak part. Since the signal is considered to be Gaussian, symmetry about the diagonal exists. It can be illustrated in matrix form as in Figure 6.8.

The corresponding parts of the Markov model are shown in Figure 6.9. As state 5 is entry only, column *ip* in the matrix is transferred into column *ip+1*.

According to Markov chain theory [66], the transition matrix of the absorption problem always has the form

$$P = \{p_{ij}\} = \begin{array}{c} \\ C \\ T \end{array} \begin{array}{c} \begin{array}{cc} C & T \end{array} \\ \left| \begin{array}{cc} I & O \\ R & Q \end{array} \right| \end{array} \tag{6.5}$$

in which,

P is the transition matrix.

T denotes the transient states

C denotes the absorption states,

R is the probability of transition from T to C,

Q is the transition probability with T,

I is the transition probability within C, which is a unit matrix.

O is the transition probability out of C, which is a null matrix.

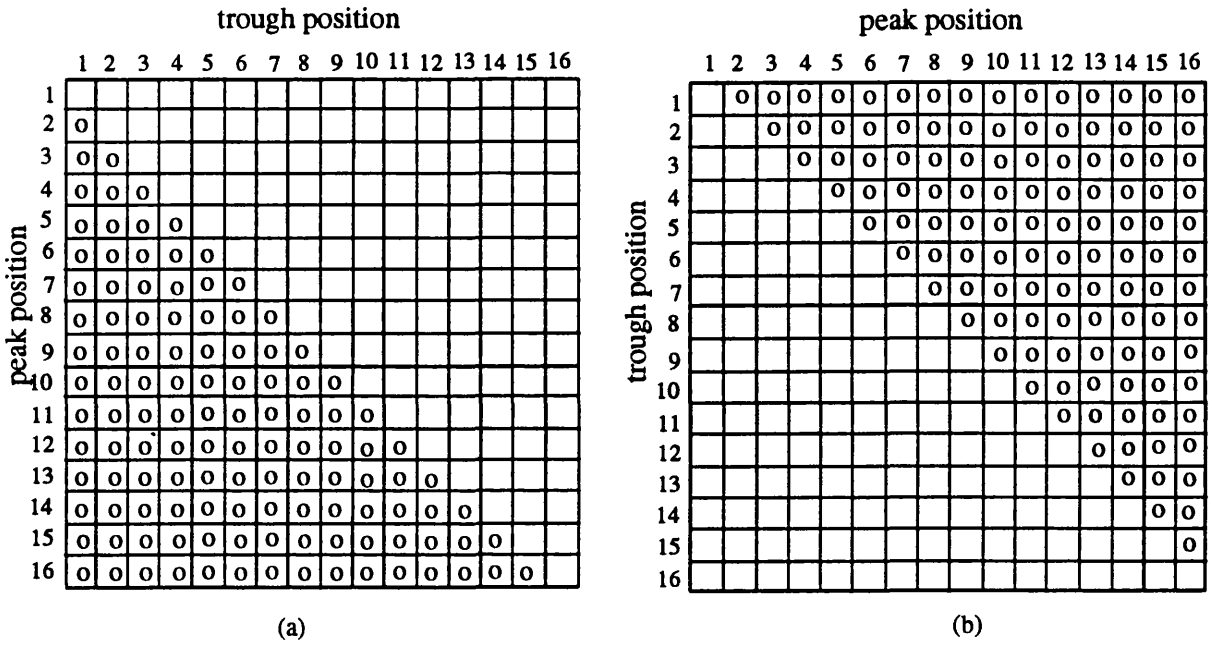

Figure 6.8: (a) The trough given peak part of Kowalewski's expression for a 16 by 16 matrix.(b) The peak given trough part of Kowalewski's expression for a 16 by 16 matrix.

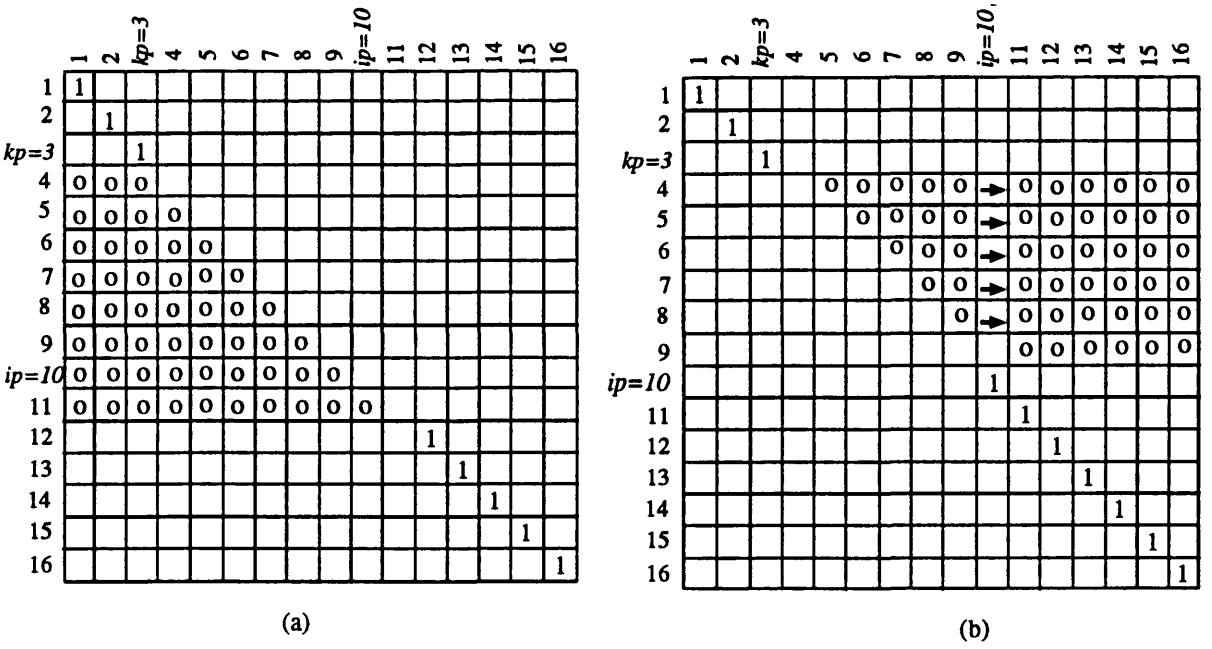

Figure 6.9: Example of one step transition matrix.(a) peak to trough, (b) trough to peak

This form is consistent with the model used here. The initial transition matrix can be obtained by multiplying the peak given trough and trough given peak matrices together. These are shown in Figure 6.10*(a)* and *(b)* in its full and condensed form. The outside part of the absorption states are removed in the condensed form.

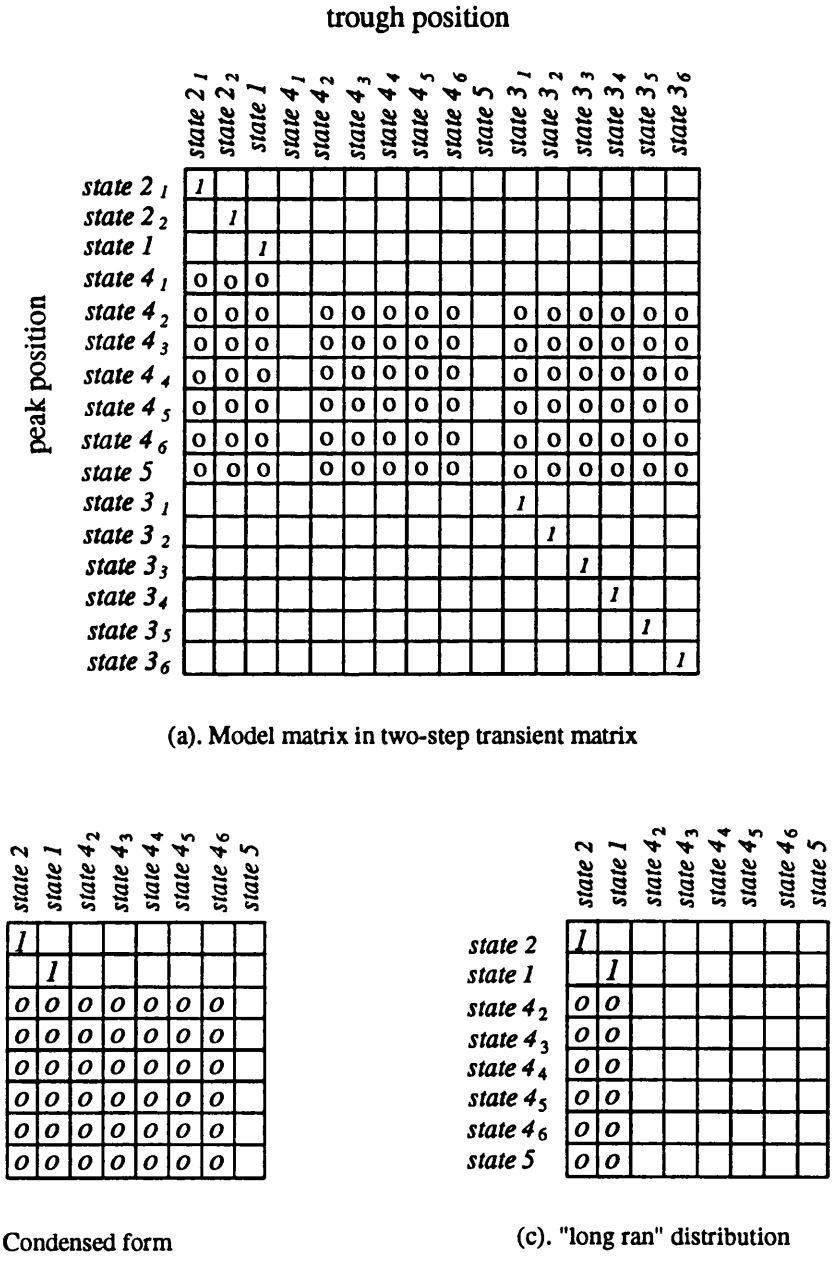

(a). Model matrix in two-step transient matrix

(b). Condensed form

(c). "long ran" distribution

Figure 6.10: Transition matrix and its equilibrium distribution

6.3.5 Long run probability

Once the initial transition matrix which models the conditions of Figure 6.6 has been set up, some appropriate method can be used to calculate the equilibrium distribution probability, i.e. the "long run" probability that the signal starts from *ip* and is absorbed into *kp* with any number of transitions in between. From the initial transition matrix in Equation 6.5, the n-step transition matrix can be expressed as

$$P^n = \begin{vmatrix} I & O \\ (I + Q + Q^2 + \cdots + Q^{n-1})R & Q^n \end{vmatrix} \tag{6.6}$$

The distribution will be in equilibrium after n becomes large enough, that is,

$$\Pi = \lim_{n\to\infty} P^n = \begin{vmatrix} I & O \\ \lim_{n\to\infty} \sum_{i=1}^{n} Q^{i-1}R & \lim_{n\to\infty} Q^n \end{vmatrix} \tag{6.7}$$

As n tends to infinity, the limit of Q^n will become null. At the same time, the series $\{Q^i\}$ will be convergent. Let the series converge to V, then

$$\Pi = \lim_{n\to\infty} P^n = \begin{vmatrix} I & O \\ V & O \end{vmatrix} \tag{6.8}$$

Because $P\Pi = \Pi$, we have

$$\begin{vmatrix} I & O \\ R & Q \end{vmatrix} \begin{vmatrix} I & O \\ V & O \end{vmatrix} = \begin{vmatrix} I & O \\ R+QV & O \end{vmatrix} = \begin{vmatrix} I & O \\ V & O \end{vmatrix} \tag{6.9}$$

So,

$$R + QV = V \tag{6.10}$$

The equilibrium distribution V satisfies

$$(I - Q)V = R$$

or

$$V = (I - Q)^{-1}R \tag{6.11}$$

The long run probability can be obtained by solving a linear equation set. In practical computation, this can also be achieved by squaring and resquaring the matrix enough times until the transient part becomes empty.

Since a Gaussian stationary process is considered, there are some symmetric relationships which can be used to simplify the computation as shown in Figure 6.11.

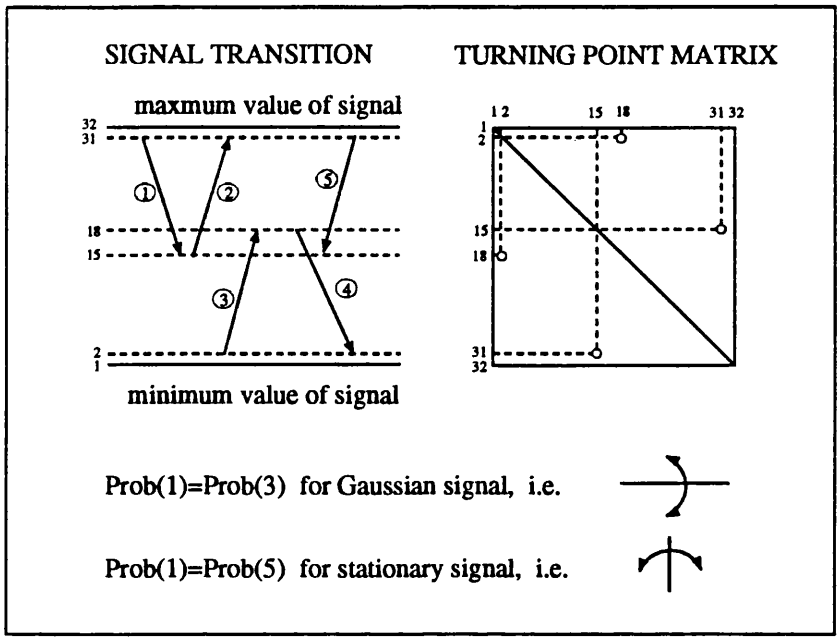

Figure 6.11: The assumption of normality and stationarity

Then if f_j^i is the"long run" probability of going to level i from level j, the three probabilities needed can be obtained as:

$$Y_1 = f_{ip}^1 + f_{ip}^2 \tag{6.12}$$

and by vertical symmetry

$$Y_2 = f_{ip}^1 \tag{6.13}$$

$$Y_3 = f_{tp-ip+h}^{1*} + f_{tp-ip+h}^{2*} \tag{6.14}$$

where *tp* is the value twice the mean signal level, state 1* is level *(tp-ip)* and state 2* is made up of levels below *tp-ip*.

6.4 Modification for considering the mean stress

The theoretical solution for Gaussian stress histories can be extended to consider the influence of mean stress. In order to do this, the solution was redefined as follows:

$$p(S, S_m) = \frac{2.0}{dS} \sum_{ip=S+1}^{\infty} Y_1(ip, ip-S) Y_2(ip, ip-S) Y_3(ip, ip-S) p(ip) \tag{6.15}$$

where S_m is the mean stress value defined by *(ip+kp)/2.*

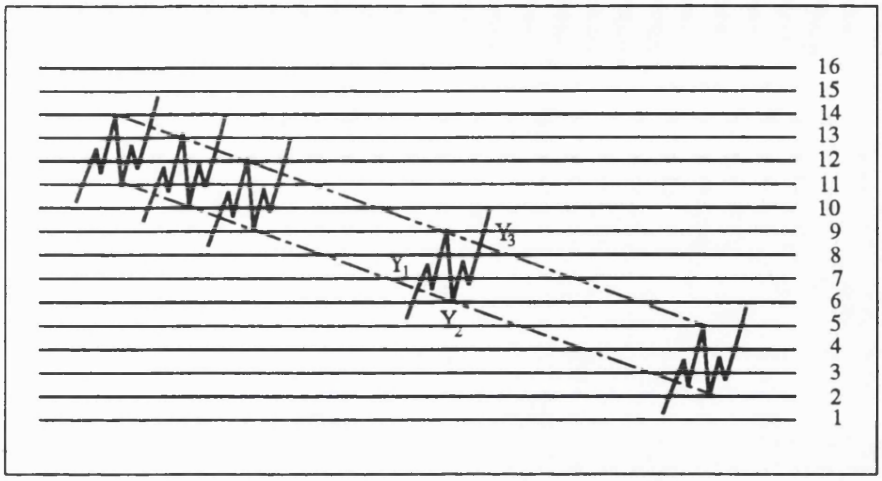

Figure 6.12: Example illustrating the method of evaluating $p_{RR}(3)$ for a 16 level process

Figure 6.12 shows an example of evaluating $p_{RR}(3)$ for a 16 level process. When the mean stress is taken into account, the probability of these cycles are grouped according to their ranges as well as mean levels.

All the parameters needed to compute Equation 6.15 are set out in the previous section.

It should be noted that the mean value included in this formula is just the relative mean of each cycle relative to the global average of the process. It is not possible to consider the absolute mean value in a frequency domain analysis.

6.5 Analysis of WEG data including mean stress

An analysis considering mean stress was performed in both the time and frequency domains for the WEG MS-1 data. A typical joint PDF is shown in Figure 6.13. As has been discussed earlier, the WEG data is not long enough to do such an analysis. This situation becomes worse when the cycles are grouped with different mean values because the limited number of cycles have to be distributed in a mean-range plane rather than along a range axis only. It is therefore very difficult to obtain a smooth PDF curve. It is unreasonable to expect the theoretical solution to give very good agreement in this situation.

The ultimate tensile stress of the material for the WEG MS-1 data was unknown for this analysis. It was therefore difficult to assess the actual influence of mean stress. In our analysis, the ratio k between the ultimate tensile stress and maximum stress range in the signal was assumed to be at different levels for the 24 load cases. Table 6.1 shows the results for k at *5, 10, 20* and *30*. The dam-

age values are normalised by the damage calculated directly from the whole time signal without considering the mean stress effect. This data shows that there is a certain amount of scatter at all the values of k. This scatter is also generally found when the load cases are analysed whilst ignoring mean stress effects (see [50]).

Table 6.1: Fatigue damage ratio for WEG MS-1 data with mean stress

data	S_{ult}/S_{max} (time dom.)				S_{ult}/S_{max} (freq. dom.)			
	5	10	20	30	5	10	20	30
y12a	3.10	1.87	1.98	1.61	3.88	2.42	2.32	1.81
y19a	2.81	1.53	1.69	1.47	3.19	1.98	1.90	1.49
y27a	3.06	1.38	1.69	1.69	3.20	1.97	1.90	1.50
y35a	3.33	1.37	1.87	1.95	1.95	1.19	1.15	0.92
y12b	2.49	1.40	1.50	1.36	1.38	0.89	0.82	0.63
y19b	2.50	1.30	1.42	1.37	1.31	0.85	0.77	0.59
y27b	2.70	1.32	1.49	1.51	1.19	0.77	0.71	0.54
y35b	3.31	1.30	1.73	1.87	1.11	0.70	0.66	0.51
y12c	2.58	1.52	1.51	1.16	1.63	1.01	0.97	0.76
y19c	2.61	1.41	1.41	1.30	1.46	0.91	0.87	0.68
y27c	2.54	1.53	1.51	1.17	1.22	0.76	0.73	0.57
y35c	2.44	1.52	1.49	1.23	1.18	0.74	0.70	0.55
y12d	2.74	1.52	1.53	1.44	2.59	1.65	1.55	1.19
y19d	3.56	1.76	1.97	1.60	2.57	1.64	1.53	1.18
y27d	3.35	1.82	1.97	1.40	2.32	1.47	1.39	1.07
y35d	2.58	1.47	1.54	1.32	2.29	1.41	1.36	1.07
y12e	2.51	1.41	1.51	1.35	2.00	1.24	1.19	0.94
y19e	3.57	1.78	1.95	1.69	2.62	1.63	1.56	1.22
y27e	1.75	0.99	0.92	1.00	2.08	1.31	1.24	0.96
y35e	3.61	1.49	2.06	2.09	2.52	1.58	1.50	1.17
y12f	2.96	1.72	1.72	1.41	2.84	1.79	1.70	1.32
y19f	2.30	1.22	1.31	1.33	2.46	1.55	1.47	1.14
y27f	3.34	1.70	1.79	1.58	3.37	2.12	2.01	1.56
y35f	2.62	1.55	1.71	1.49	2.99	1.90	1.79	1.38

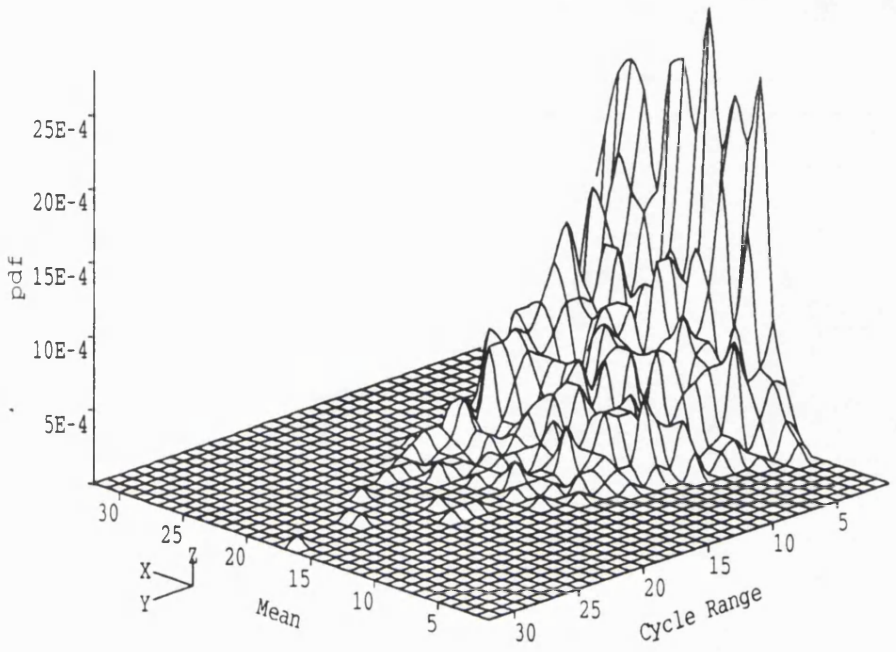

(a). Time domain analysis

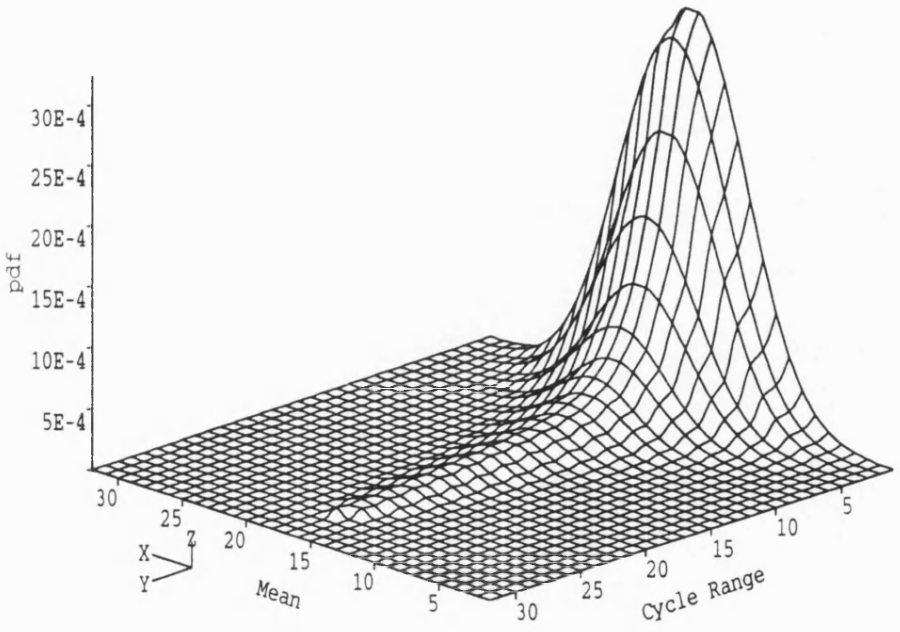

(b). Frequency domain analysis

Figure 6.13: The joint PDF of rainflow range and mean from y27a

6.6 Analysis of Howden data including mean stress

As mentioned earlier, the stress history of the Howden data is not given directly. Instead, a time series of bending moments at each section is given. Thus, rainflow cycle counting on such time signals will just give the rainflow cycle of bending moments at the sections instead of stress at the hot spots. When mean stress is considered through a Goodman type relationship in this situation, the ultimate tensile stress needs to be changed to ultimate bending moments at each corresponding section. This is allowed again because only the ratio between the mean value (stress or moment) and ultimate tensile value is important. Both ratios are actually identical. From the Goodman relationship, this ratio, $1/(1-S_m/S_{ult})$, is acting just as a magnification factor to the cycle ranged S_a with mean S_m. Since the ratios remain unchanged, the magnification factor also remains unchanged. The ultimate bending moments used for the Howden data are listed in Table 6.2.

Table 6.2: Ultimate bending moments of Howden data

Location	case 1 b=8		case 2 b=12	
3.0	325.5	452.9	538.1	902.9
8.09	170.3	166.1	277.3	329.5
13.04	40.52	31.97	64.92	62.47

Once again, rainflow counting including the mean in both the time and frequency domains using the modified theoretical solution was performed on the Howden data. Typical joint PDF's are shown in Figure 6.14 and 6.15 for both flapwise and edgewise respectively. It can be seen from the edgewise rainflow cycle PDF's that, because of the existence of a dominant deterministic component, the PDF has two finite sections in the time domain. However, the frequency domain analysis gives a PDF which is quite smooth. Generally speaking, these two different approaches will not be in agreement. This is because for the edgewise signal, as explained earlier, the assumption of randomness no longer holds.

The fatigue damage rates from both the time and frequency domain analysis are shown in Tables 6.3 and 6.4 for inverse *S-N* curve slope *b=8* and *b=12* respectively. All the damage rates are normalised by the corresponding damage rate without considering the mean stress effect. Despite the difference between the time domain and frequency domain analysis, it is very encouraging that the

frequency domain results change quite consistently with the time domain results. The prediction from the frequency domain analysis is generally in good agreement with the time domain analysis [67].

Table 6.3: Fatigue damage ratio of Howden data with mean b=8.0

Location	tape 18		tape 26		tape 27		tape 30	
	time	freq.	time	freq.	time	freq.	time	freq.
3m flap	3.910	4.394	4.680	4.554	3.781	3.712	3.029	3.090
3m edge	1.585	1.486	1.103	1.093	1.129	1.128	1.076	0.873
8m flap	2.234	2.412	2.281	2.583	2.059	1.937	2.155	2.248
8m edge	2.791	2.751	1.053	1.040	1.068	1.068	1.031	1.017
13m flap	1.394	1.443	1.080	1.225	1.010	0.973	1.314	1.496
13m edge	1.639	1.609	1.018	1.000	1.000	0.973	1.045	1.025

Table 6.4: Fatigue damage ratio of Howden data with mean b=12.0

Location	tape 18		tape 26		tape 27		tape 30	
	time	freq.	time	freq.	time	freq.	time	freq.
3m flap	35.89	52.16	65.21	57.93	43.75	32.37	17.25	19.37
3m edge	4.13	3.94	1.35	1.35	1.44	1.49	1.25	1.05
8m flap	7.53	9.48	7.38	11.39	7.23	5.36	6.63	7.86
8m edge	26.46	26.20	1.27	1.16	1.22	1.26	1.09	1.12
13m flap	2.18	2.48	1.16	1.66	1.02	0.95	1.72	2.71
13m edge	4.49	4.39	1.01	1.02	1.00	0.95	1.15	1.10

6.7 Discussion

For the first time, a theoretical method has been developed to predict both the rainflow range content and the corresponding cycle mean information from frequency domain statistics. The new method has been applied to data which is approximately Gaussian, stationary and random and the results obtained show very good agreement with the corresponding time domain result which is used as a reference value. Results for the Howden data are less good, as expected, because of the poor quality of the data in terms of it being non-Gaussian, nonstationary and not purely random.

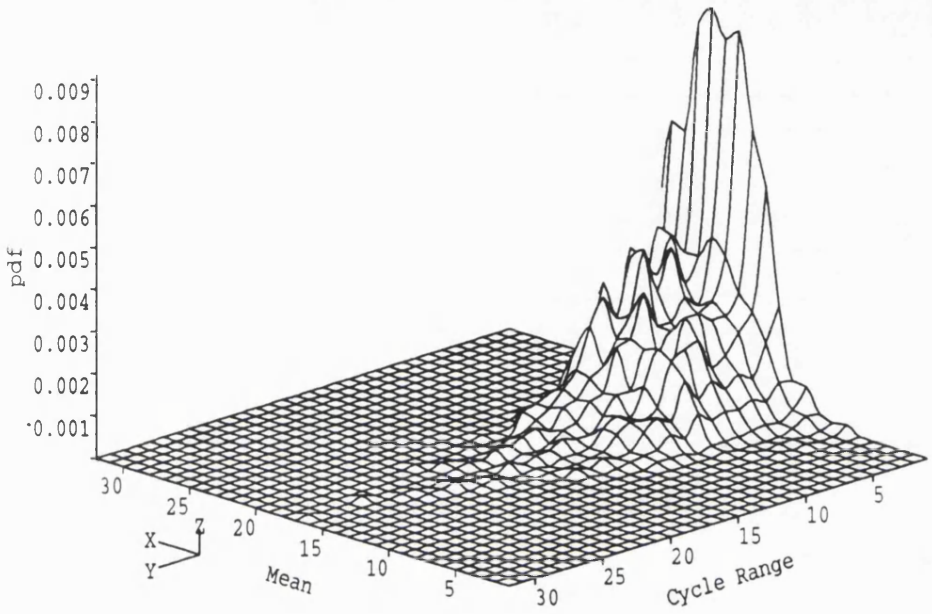

(a). Time domain analysis

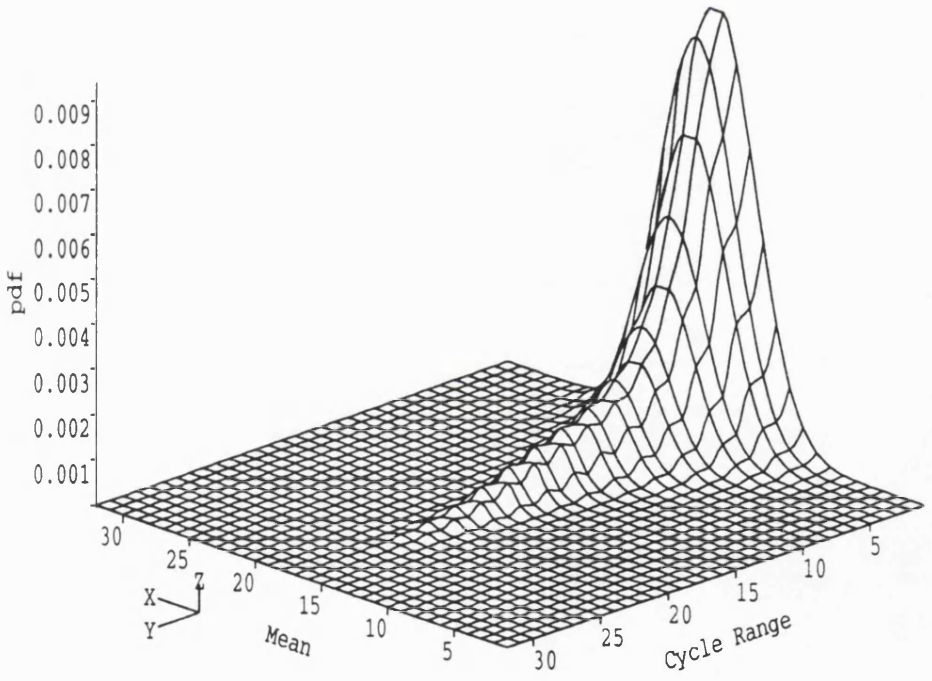

(b). Frequency domain analysis

Figure 6.14: The joint PDF of rainflow range and mean from Howden data tape 26 3m flapwise

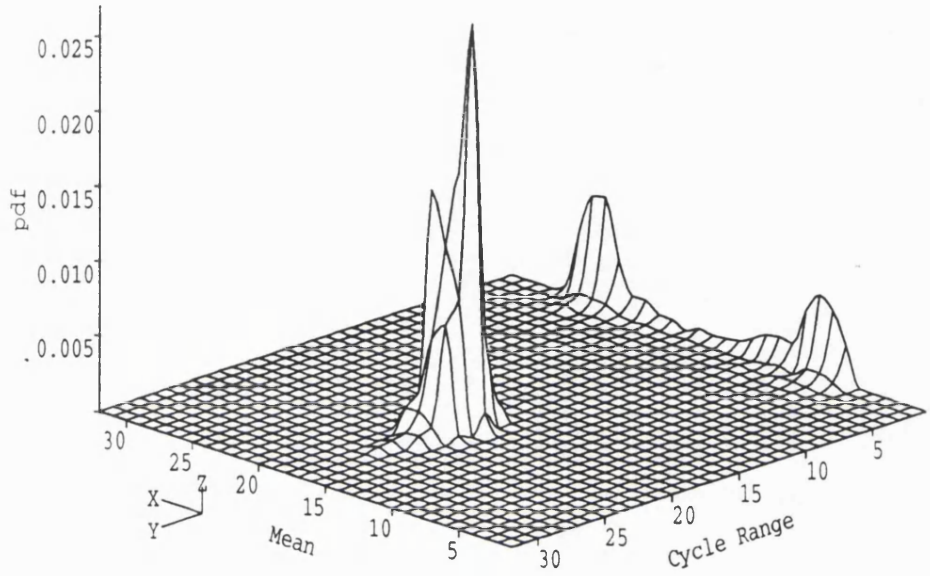

(a). Time domain analysis

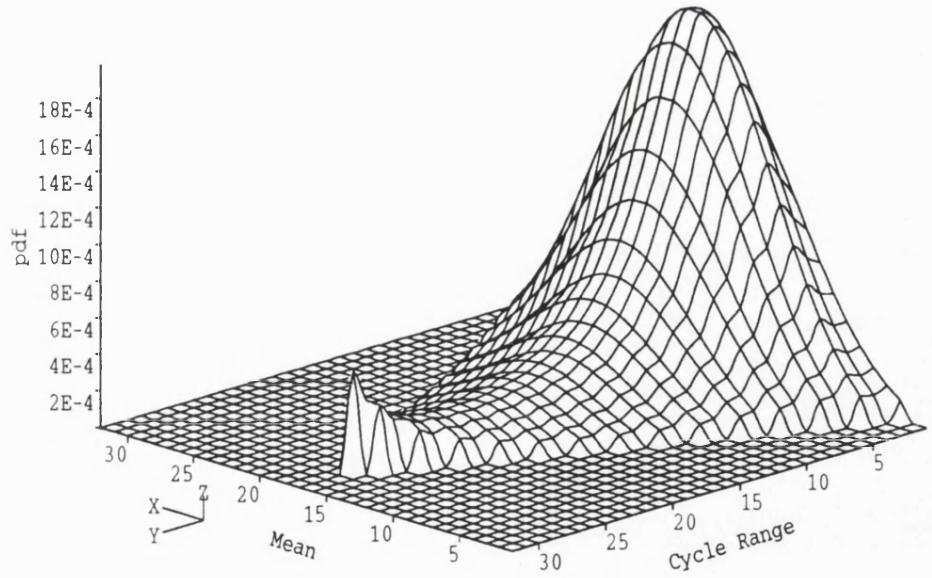

(b). Frequency domain analysis

Figure 6.15: The joint PDF of rainflow range and mean from Howden data tape 26 3m edgewise

Chapter 7

Fatigue analysis for Non-Gaussian response histories

7.1 Introduction

Up to now, the fatigue analysis of stochastic stress histories has focused on situations where the random process is Gaussian. For most engineering problems, assuming the structural response to be Gaussian is reasonable, according to the central limit theorem. However, if structural nonlinearity is an issue, the response may not then conform to the Gaussian assumption as we have seen from the statistical analysis of the Howden HWP330 data. Some other response measurements also reveal the same non-normality [68].

The most difficult problem for non-Gaussian signals is the expression for their probability density functions. Of course it is known that only one parameter, the root mean square, is needed for a Gaussian distribution given that the mean value is zero. This is calculated from the second order central moment of the signal, or the zeroth order moment of its power spectral density function. For a non-Gaussian signal there is no universal expression for its probability distribution nor for the relevant frequency domain information. Some techniques, such as Hermite series, or MacLaurin series, have been employed to express the probability density functions. However, they all have their disadvantages.

Most of the present methods, as we have seen in previous chapters, are unable to deal with the non-Gaussian problem. A method based on Bishop's theoretical method using Markov chain theory is presented in this chapter. It can be used for all kinds of non-Gaussian distributions as long as the peak to trough and trough to peak transition matrices are known. This is often the case when using, for instance, standardised load sequences such as FALSTAFF.

7.2 Mathematical description of non-Gaussian variables

There is no doubt that a random variable is described optimally in terms of its probability density functions. However, this form of description is not available for some situations, for instance, with experimental data. For these practical cases, statistical methods can only provide a limited amount of information such as the statistical moments (i.e. mean,variance, skewness etc). This information may be utilised to approximate the unknown PDF in closed form. Generally, such an approximation can not be unique since a PDF is defined by infinitely many statistical moments. Additional uncertainties about the PDF arise because of limited confidence (in a statistical sense) in these statistical moments because of the short sample lengths used for the calculation.

7.2.1 Characteristic functions

As discussed in Chapter *2*, the nth order moment of a random variable x is defined as[40],

$$\alpha_n = E\{X^n\} = \int_{-\infty}^{\infty} x^n p(x) dx$$

where *p(x)* is the probability density function (PDF).

When the moments are taken about the mean $\overline{x}$, the central moments are defined as

$$\mu_n = \int_{-\infty}^{\infty} (x - \overline{x})^n p(x) dx$$

The characteristic function is defined as

$$\phi(u) = E\{e^{iux}\} = \int_{-\infty}^{\infty} e^{iux} p(x) dx \tag{7.1}$$

Thus, the PDF is obtained by applying the Fourier transformation to the characteristic function.

$$p(x) = \frac{1}{2\pi} \int_{-\infty}^{\infty} e^{-iux} \phi(u) du \tag{7.2}$$

The characteristic function can be expanded as MacLaurin series as follows

$$\phi(u) = \phi(0) + \phi^{'}(0)u + \phi^{"}(0)\frac{u^2}{2} + ... = \sum_{j=0}^{n} \frac{\alpha_j}{j!}(iu)^j + O(u^n) \tag{7.3}$$

From Equation 7.1,

$$\phi^{(n)}(0) = i^n \int_{-\infty}^{\infty} x^n p(x) dx = i^n \alpha_n$$

Equation 7.2 can be taken as the universal expression for the probability density functions. Theoretically, infinite order moments are needed to express the PDF. This makes the expression quite difficult to use. There is no closed form expression which can be derived.

7.2.2 Gram-Charlier Expansion

Several types of expansion have been developed in the past [69], one of the most convenient, in term of computational efficiency, is the Gram-Charlier expansion. In this case, the PDF *p(x)* is approximated by

$$p(x) = \phi(x)[1 + \sum_{k=3}^{n} \frac{C_k}{k!} H_k(x)] \tag{7.4}$$

in which

$$H_k(x) = (-1)^k \exp(\frac{x^2}{2}) \frac{d^k}{dx^k} [\exp(-\frac{x^2}{2})] \quad (k = 0, 1, ...)$$

is the Hermite series.

In the above equation, $\phi(x)$ denotes the normal distribution with given mean and variance, the coefficients C_k are determined from the higher statistical moments and $H_k(x)$ denotes the Hermite polynomials of order k. Since these polynomials are orthogonal with respect to the normal density as weighting function the lower order statistical moments are not influenced by adding additional terms in the series 7.4. This means that, for instance, normalisation is not affected by adding additional terms which, in turn, implies that in some regions *p(x)* may attain negative values. It should therefore be treated quite carefully.

There is another approach based on the fact that for Gaussian variables the cumulants of order > 2 vanish. It is therefore quite reasonable to define non-normal properties in terms of higher order cumulants instead of moments. This so-called cumulant neglect closure method assumes that cumulants higher than a certain order vanish. It can be shown that this is equivalent to an approximating function $P(\omega)$ - which is the Fourier transform of *p(x)* - given by

$$P(\omega) = exp[\sum_{k=3}^{n} \frac{K_k}{k!} (i\omega)^k] \tag{7.5}$$

where the coefficients K_k follow from the cumulants. The PDF *p(x)* can be obtained by applying an inverse Fourier transformation. However, this is generally not feasible in closed form. Upon discretisation and after the FFT the numerical values of *p(x)* may become negative in some regions. In fact, the results are quite similar to those of Equation 7.4.

7.2.3 Maximum Entropy Method(MEM)

A different concept is introduced by this method, i.e. to leave the random variable in as general a form as possible given the known information about the statistical moments. Mathematically, this is achieved by maximising the"entropy" H_p of a PDF *p(x)*

$$H_p = -\int_{-\infty}^{\infty} p(x) \ln p(x) dx \tag{7.6}$$

subject to the constraints:

$$E[x^k] = \int_{-\infty}^{\infty} x^k p(x) dx \qquad k = 0 \cdots n$$

for all given statistical moments up to order n.

This has a solution of the form

$$p(x) = \exp \sum_{k=0}^{n} C_k x^k \tag{7.7}$$

in which the coefficients C_k are determined from the statistical moments, i.e., to satisfy the constraints. It is clearly seen that only positive values can result from this expression. A drawback of the method is that for odd n the PDF may become unbounded at either $x \to \infty$ or $x \to -\infty$. Computationally, there is the problem that each additional term in the series 7.7 alters all the statistical moments. Still the results obtained from this method are in some cases superior to those from other methods.

7.3 Statistical description of non-Gaussian processes

7.3.1 Time domain

Analogously to the autocorrelation function of a random process $x(t)$, the higher moment function, e.g. third correlation (Bi-correlation)

$$R_{xxx}(t_1, t_2, t_3) = E[x(t_1)x(t_2)x(t_3)] \tag{7.8}$$

or fourth order correlation (Tri-correlation)

$$R_{xxxx}(t_1, t_2, t_3, t_4) = E[x(t_1)x(t_2)x(t_3)x(t_4)] \tag{7.9}$$

can be defined. As usual, $E[\cdot]$ in the above equations denotes ensemble average (mathematical expectation), t_k denotes time arguments. If the process is stationary, only the time lags are important, so that:

$$R_{xxx}(\tau_1, \tau_2) = E[x(t)x(t+\tau_1)x(t+\tau_2)] \tag{7.10}$$

and

$$R_{xxxx}(\tau_1, \tau_2, \tau_3) = E[x(t)x(t+\tau_1)x(t+\tau_2)x(t+\tau_3)] \tag{7.11}$$

For a zero mean and with zero time lags, the correlation functions yield the one time central statistical moments of the random process $x(t)$:

$$\mu_{3,x} = R_{xxx}(0,0) = E[x^3(t)] \tag{7.12}$$

$$\mu_{4,x} = R_{xxxx}(0,0,0) = E[x^4(t)] \tag{7.13}$$

While not giving complete information, these two quantities still provide some measure of the non-Gaussian properties of a process $x(t)$.

7.3.2 Frequency domain

Analogously to the above time domain approach, multiple Fourier transforms can be applied to higher order spectra. The Bi-spectrum $S_{xxx}(\omega_1, \omega_2)$ and the Tri-spectrum $S_{xxxx}(\omega_1, \omega_2, \omega_3)$ are defined by the following Fourier transform:

$$S_{xxx}(\omega_1, \omega_2) = \frac{1}{4\pi^2} \int_{-\infty}^{\infty} \int_{-\infty}^{\infty} R_{xxx}(\tau_1, \tau_2) e^{-i\omega_1\tau_1} e^{-i\omega_2\tau_2} d\tau_1 d\tau_2 \tag{7.14}$$

$$S_{xxxx}(\omega_1, \omega_2, \omega_3) = \frac{1}{8\pi^3} \int_{-\infty}^{\infty} \int_{-\infty}^{\infty} \int_{-\infty}^{\infty} R_{xxxx}(\tau_1, \tau_2, \tau_3) e^{-i\omega_1\tau_1} e^{-i\omega_2\tau_2} e^{-i\omega_2\tau_3} d\tau_1 d\tau_2 d\tau_3 \tag{7.15}$$

The inverse relations are given by:

$$R_{xxx}(\tau_1, \tau_2) = \int_{-\infty}^{\infty} \int_{-\infty}^{\infty} S_{xxx}(\omega_1, \omega_2) e^{i\omega_1\tau_1} e^{i\omega_2\tau_2} d\omega_1 d\omega_2 \tag{7.16}$$

$$R_{xxxx}(\tau_1, \tau_2, \tau_3) = \int_{-\infty}^{\infty} \int_{-\infty}^{\infty} \int_{-\infty}^{\infty} S_{xxxx}(\omega_1, \omega_2, \omega_3) e^{i\omega_1\tau_1} e^{i\omega_2\tau_2} e^{i\omega_2\tau_3} d\omega_1 d\omega_2 d\omega_3 \tag{7.17}$$

When time lags are zero, the central moments are obtained:

$$\mu_{3,x} = R_{xxx} = \int_{-\infty}^{\infty} \int_{-\infty}^{\infty} S_{xxx}(\omega_1, \omega_2) d\omega_1 d\omega_2 \tag{7.18}$$

$$\mu_{4,x} = R_{xxxx} = \int_{-\infty}^{\infty} \int_{-\infty}^{\infty} \int_{-\infty}^{\infty} S_{xxxx}(\omega_1, \omega_2, \omega_3) d\omega_1 d\omega_2 d\omega_3 \tag{7.19}$$

The introduction of higher order spectra implies the use of higher order moments of the process. The problem again is determining to what order the spectrum should be computed in order to be able to enough describe the non-Gaussian process? It is hoped that, the Bi-spectrum and Tri-spectrum will contain the most important information about the non-Gaussian properties.

7.4 Present methods for non-Gaussian signal fatigue analysis

7.4.1 Transformation method

Suppose the non-Gaussian response of a structure is denoted as *X(t)*. It can be the result of applying a monotonic transfer function, g, to a standard normal process, *U(t)*: [70] [71] [72]

$$X(t) = g[U(t)]$$

in which $g(u) = F_x^{-1}[\Phi(u)]$ in terms of the cumulative distribution functions, F_x and Φ, of *X(t)* and *U(t)*.

The difficulty in using this equation is that, the transfer function g must be determined numerically, complicating the subsequent fatigue analysis. And, it is not clear how g should be chosen if only certain response moments are available. To overcome these difficulties, a Hermite series approximation to g is constructed based on the known response moments.

$$X(t) = \sum_{n\geq 0} \alpha_n H_n[U(t)]$$

Since $\overline{x} = \alpha_0$, $\sigma_x = \alpha_1$, the above series can be rearranged into a standardised form:

$$X_0(t) \equiv \frac{X(t) - \overline{x}}{\sigma_x} = U(t) + \sum_{n\geq 2} \epsilon_{n+1} H_n[U(t)]$$

and

$$\epsilon_n = \frac{E\{H_n[X_0(t)]\}}{n!}$$

in which it assumed that $\epsilon_{n+1} \equiv \alpha_n/\sigma_x \ll 1 (n > 2)$, so that the $O(\epsilon_n \epsilon_m)$ terms are negligible. Depending on the known moments, a suitable cutoff order can be selected as an approximation of g.

A fatigue analysis can then follow this approximation. If *X(t)* is narrow-band, the peak distribution of *U(t)* would have a Rayleigh distribution. If *U(t)* has a peak at level *S*, *X(t)* would have a peak at level *g(S)* and there would exist a cycle *g(S)-g(-S)*. The fatigue damage is then determined by using the moments of the signal.

7.4.2 Weakly non-Gaussian approximation

The Gram-Charlier approximation of PDF described in the previous section can be developed into another expression for calculating the distribution of signal

peaks. Firstly, the joint probability density function $p(\xi, \dot{\xi})$ of a random variable ξ and $\dot{\xi}$ can be calculated. Then, if the response is narrow-banded, the probability distribution $F(\hat{\xi})$ for the peak values of ξ is approximated by [73]:

$$F(\hat{\xi}) = 1 - \frac{N(\hat{\xi})}{N(0)}$$

where $N(\hat{\xi})$ is the average number of crossing of level $\xi = \hat{\xi}$ per unit time

$$N(\hat{\xi}) = \int_{-\infty}^{\infty} p(\hat{\xi}, \dot{\xi}) |\dot{\xi}| d\dot{\xi}$$

This approximation assumes that the most-often crossed level is $\hat{\xi} = 0$. This holds for a symmetric response, but is just an approximation for an asymmetric response, even with zero mean.

Using this approximation, the probability distribution for the peak values is obtained. The peak range distribution is then found to be $F_a(\hat{\xi}) = \frac{1}{2}[F(\hat{\xi}) + F(-\hat{\xi})]$ because of the narrow-band assumption. The fatigue damage is then evaluated from the cycle probability density function as before.

7.5 Theoretical solution for non-Gaussian stress history analysis

7.5.1 Statistic aspect

As discussed in previous chapters, two symmetrical properties exist for Gaussian stationary signals. One is the symmetry about mean axis the other is about the *t=0* axis as shown in Figure 6.11. A fatigue analysis for Gaussian response histories then can make use of this, as in Bishop's theoretical solution for a Gaussian stress history. For the non-Gaussian signals being discussed here, stationarity is still assumed. Thus, symmetry about the *t=0* axis can still be assumed. Symmetry about mean axis, however, does not exist for non-Gaussian signals. The Markov model for rainflow cycle computation therefore has to be modified.

7.5.2 Theoretical solution for non-Gaussian responses

The theoretical solution described in Section *3.6* and *6.3* assumes the signal is stationary and Markovian. When applied to Gaussian response histories, symmetry about the mean value axis is used to simplify the Markovian model and computation.

For non-Gaussian response histories, this symmetry does not exist. However, the transition from peak to trough and from trough to peak of the process can still be taken as a Markov chain and thus the probability density can still be calculated as before. That is,

$$p_{RR}(h) = \frac{2.0}{dh} \sum_{ip=h+1}^{\infty} Y_1(ip, ip-h) Y_2(ip, ip-h) Y_3(ip, ip-h) p(ip) \qquad (7.20)$$

Event Y_1 and Y_2, representing transitions to *ip* from *kp* and below, are the same as before, and the procedure for its probability calculation remains unchanged. The probability calculation for events Y_3, however, is different. If the signal is turned upside down, that is, every peak becomes a trough and every trough become a peak, the original model can then be used to derive the probability of event Y_3. That is, the probability of event Y_3 can be calculated using the same procedure as Y_1 with the initial transition matrices transposed.

Figure 7.2 shows one example based on such a calculation. The turning point matrix is a combination of two matrices from the Kowalewski formula with different spectral moments. The peak to trough part is based on moments group *(a)* below while the trough to peak part is based on moments group *(b)*. The matrix is plotted in Figure 7.1.

- *(a)* $m_0 = 0.405986, \quad m_2 = 122.708, \quad m_4 = 74833.9, \quad \gamma = 0.703993$
- *(a)* $m_0 = 0.405254, \quad m_2 = 122.959, \quad m_4 = 202541.0, \quad \gamma = 0.429198$

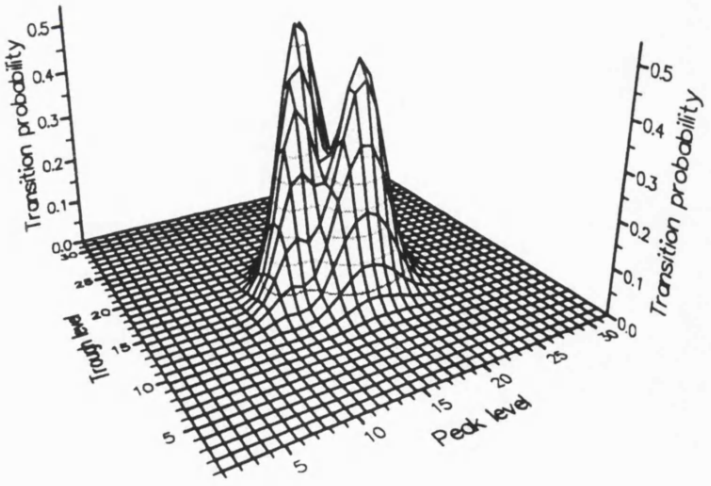

Figure 7.1: Non-Gaussian transition probability matrix

The result obtained by using this new theoretical solution for a non-Gaussian transition matrix is plotted in Figure 7.2 along with the result obtained by applying the original theoretical solution. The result from a peak-trough sequence

regeneration using this transition matrix is also shown. If the simulation result is taken as a reference for other solutions to compare with, it is clear that the solution without the Gaussian assumption works much better than the one with Gaussian assumption. In other words, the non-Gaussian theoretical solution does take the non-Gaussian property in the transition matrix into account.

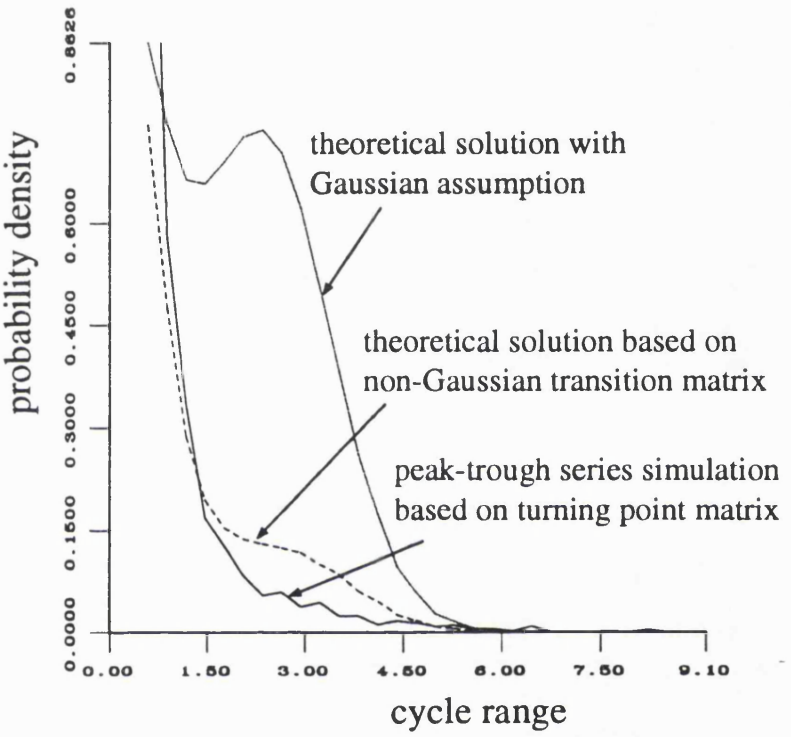

Figure 7.2: Rainflow cycle PDF's from non-Gaussian transition matrix

The difficulty which remains is that currently there is no suitable non-Gaussian replacement for the one-step Gaussian Kowalewski transition formula. And, the peak number in unit time is also another parameter not known because the Gaussian formula is no longer valid. But once such formulae are available, the complete problem would be solved. However, the problem with the representation of a non-Gaussian process arises again. Since the properties of a non-Gaussian process need to be expressed by the high order moments, then how can the spectrum provide such information? Although Bi-spectra and Tri-spectra provide some of this information it is difficult to say how much information is retained in such spectra. Furthermore, such spectra are quite difficult to derive.

Perhaps then, it is advisable to abort the search for a universal solution for non-Gaussian processes. Since there are so many kinds of probability distributions which are non-Gaussian (since the Gaussian distribution is just one special case) it

is practically impossible to deal with all of them together. Therefore, the possible approach is to assume the suitable distribution functions of the response. The spectra can then be employed to determined the parameters in these distribution functions.

7.6 Peak-trough series regeneration

Because of the difficulties which arise in the theoretical solution for non-Gaussian response histories, signal or peak-trough regeneration is usually adopted instead. The methodology used for Standardised Load Sequence regeneration is therefore examined here [74].

7.6.1 Transition matrix

Modern structural fatigue laboratories are usually equipped with computer-controlled servohydraulic machines. A variable amplitude fatigue experiment can then easily be performed using complicated loading histories. One problem which arises with such tests is, if several experiments are conducted with different loading histories in different laboratories, the results are difficult to compare. To overcome this difficulty, standardised load sequences have been developed, such as FALSTAFF for aircraft [75] [76], WASH for offshore structures [77], etc. Generally, the load sequences are stored as a peak trough turning point matrix which denotes the transition probabilities from peak to trough and from trough to peak [78]. Figure 7.3 shows the three FALSTAFF transition matrices for three different aircraft serving conditions.

The requirements for a standardised load sequence are:

- the choice of the essential parameters of the sequence must be well found;
- the sequence must be realisable in a practicable manner on the test equipment.

The basis of a meaningful standardised load history is either strain or load measurements in service, preferably from a number of similar structures. From these many measurements, common features can be extracted; that is, their spectrum shapes must be similar. Based on these strain measurements in service, an "average" spectrum can then be selected.

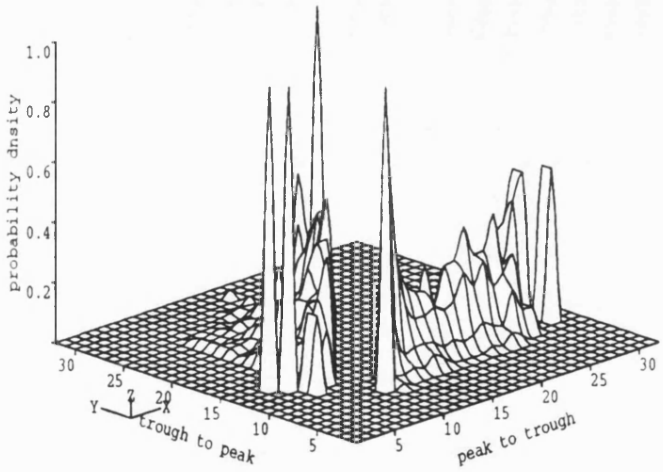

(a). FALSTAFF turning point matrix for service condition type I

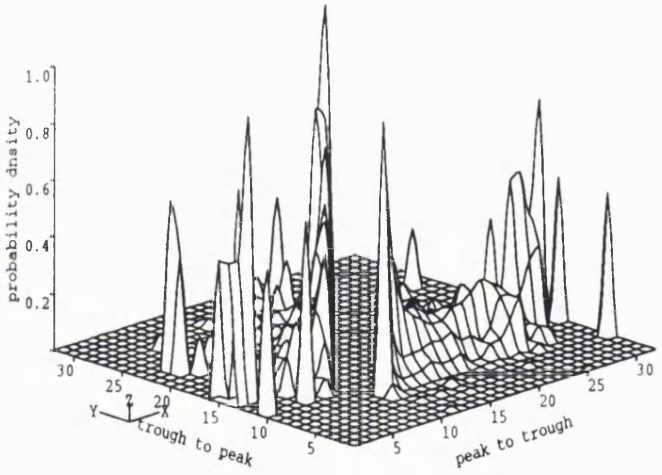

(b). FALSTAFF turning point matrix for service condition type II

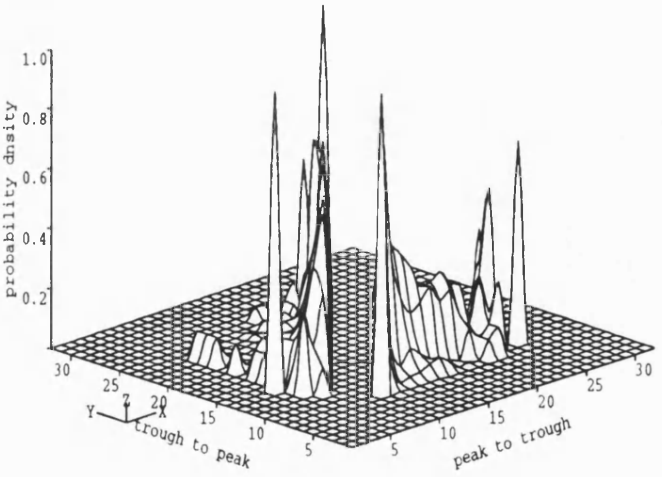

(c). FALSTAFF turning point matrix for service condition type III

Figure 7.3: FALSTAFF matrices

7.6.2 Load sequence generation

To regenerate the load sequence from a transition matrix, a random number generator is needed. Nearly all computers nowadays provide an intrinsic function such as a pseudo random number generator which has a uniform distribution in a given area.

The routine for load sequence generation is then as follows:

(1). Determine the cumulative distribution for each row of the transition matrix, as shown in Figure 7.4.

(2). Generate a random number between 1 and the maximum level of signal as the start point.

(3). Generate another random number inside the range of the cumulative distribution of the starting row. Take the hit column number as the trajectory turning point (next peak or trough).

(4). Repeat procedure 3). until the return period length is reached.

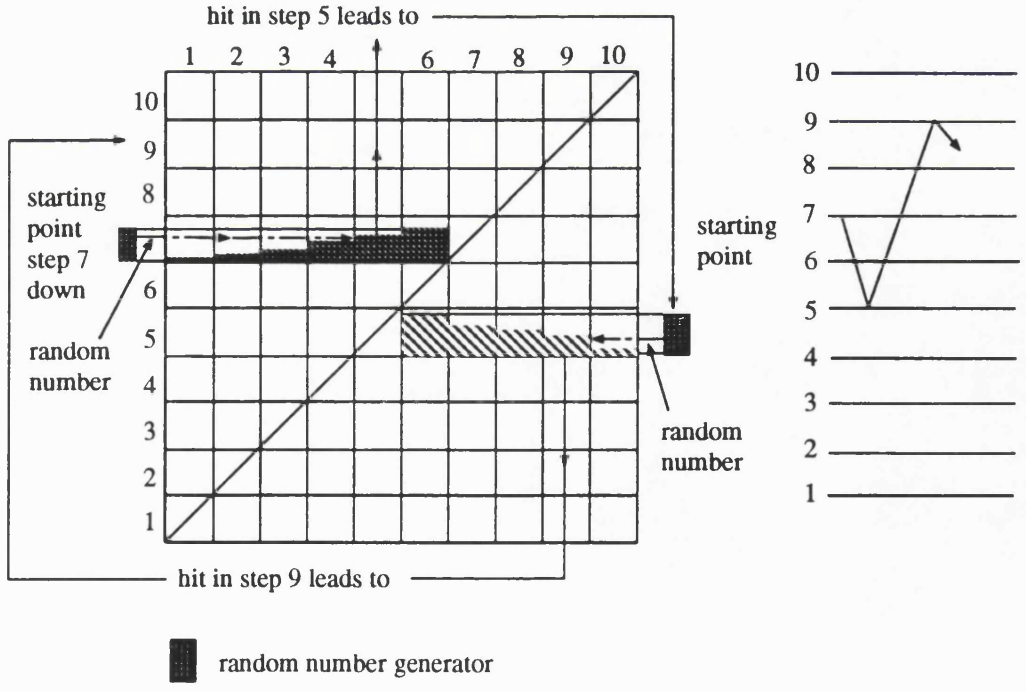

Figure 7.4: Load sequence regeneration

This method has been applied to the WEG MS-1 data with the transition matrices obtained directly from the time histories. Figure 7.5 shows the rainflow

cycle PDF's for such a regenerated load sequence, together with the original time series from which the transition matrix is extracted. This time series was simulated using the turning point matrix of the WEG data *y27d* time history after the noise above *15.625Hz* was filtered out. The results here show good agreement.

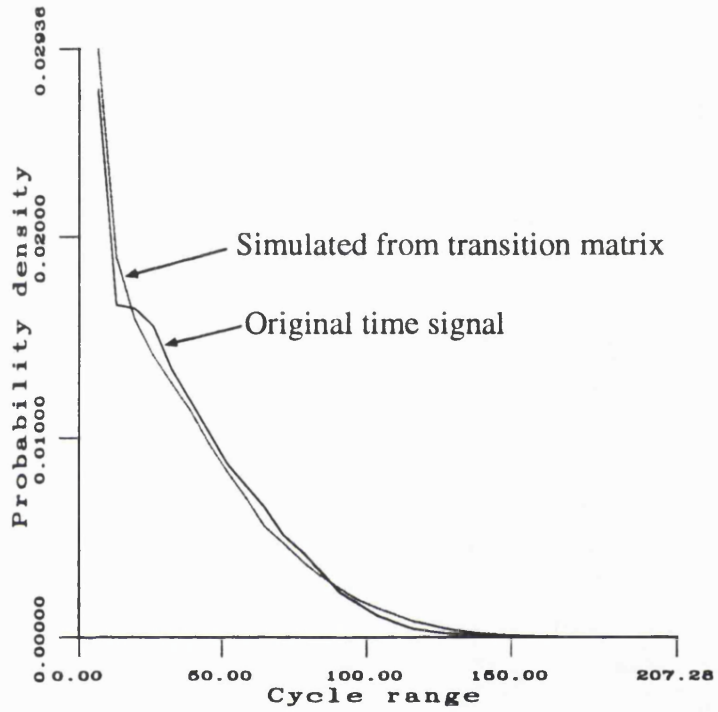

Figure 7.5: PDF's from regenerated load sequence

7.7 Discussion

The possibility of employing the theoretical solution for the fatigue analysis of non-Gaussian response histories is addressed in this chapter. It was found that suitable modifications to the theoretical solution enable it to take account the non-normality in the fatigue loading history provided that the peak trough transition matrix is available. Therefore, the theoretical solution has been extended as a universal tool for fatigue analysis of non-Gaussian response histories. The difficulty which remains for the overall problem is a suitable expression for the peak trough transition matrix.

As shown in Equation 7.2, finite order moments of the signal are never enough to represent the probability distribution for any general class of signal. Some assumption or approximation must be made in any practical computation. On

the other hand, as shown in the Rice's formula for peak rate computation ([40]), the joint distribution of the process and its first and second order differential processes must be known. This simply means that, the number of peaks in unit time of the process is a function of the process moments — all the moments in general non-Gaussian situations. The conclusion therefore is that, there is no universal solution for non-Gaussian stochastic processes.

It is quite easy to reach this conclusion using another argument. If all the possible probability distributions of the stochastic processes are grouped into one set, the Gaussian distribution is just one point in this set. The so-called non-Gaussian distribution is the whole probability distribution set including the Gaussian distribution. In this sense, the so-called non-Gaussian stochastic process is a very wide class of distributions. A universal solution is obviously impossible. There is a simple analogy, there exists one unique solution for a linear equation but it is impossible to have a universal solution for nonlinear equations.

If a fatigue analysis has to be performed for a non-Gaussian situation, the response distribution should be determined first. Some mathematical work based on Rice's formula could be involved to develop a peak-trough and trough-peak one step matrix. Then, the theoretical solution could be applied for the fatigue analysis. Or alternatively, simulation is another choice. No matter what method is used, we have to remember that, there is no universal solution.

Chapter 8

Fatigue analysis for random stress histories with deterministic components

8.1 Background

To date, most of the methods used for random fatigue analysis are based on the assumption that the time history is random and Gaussian. For wind turbine blades, the stress history resulting from the action of the stochastic wind field is definitely random. However, when gravity of the blades is considered, a strong deterministic component is superimposed onto the stochastic component. The response of the blades therefore contains both a deterministic component caused by gravity and a stochastic part caused by wind speed fluctuations. Generally speaking, this time history with a strong deterministic component included is no longer Gaussian. Thus, the analysis methods based on the Gaussian assumption are not valid. The assumption of randomness is also in doubt although this is a complex issue. This is because the whole signal is random but, for instance, with a strong sine wave superimposed onto the signal the ensemble average is not stationary although the temporal one is. In this case we might also say that although the signal is stationary it is not ergodic.

From the previous analysis of the Howden data, the existence of a dominant deterministic component in the stress time history represents an important problem for fatigue life estimation in the frequency domain. For the Howden data edgewise signals, apart from the low and middle range rainflow cycles, the probability density functions show a peak in the high range portion, which can not be predicted by any existing method using frequency domain techniques. When the damage distribution is plotted, this high range peak contributes most to the total damage as shown in Figure 8.1.

Although Madsen's method provided a way of performing such an analysis,

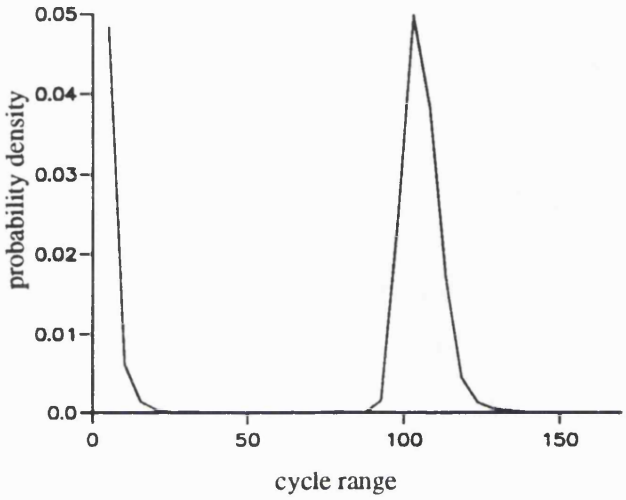

(a). Rainflow cycle probability density
of Howden data tape 26 3m edgewise

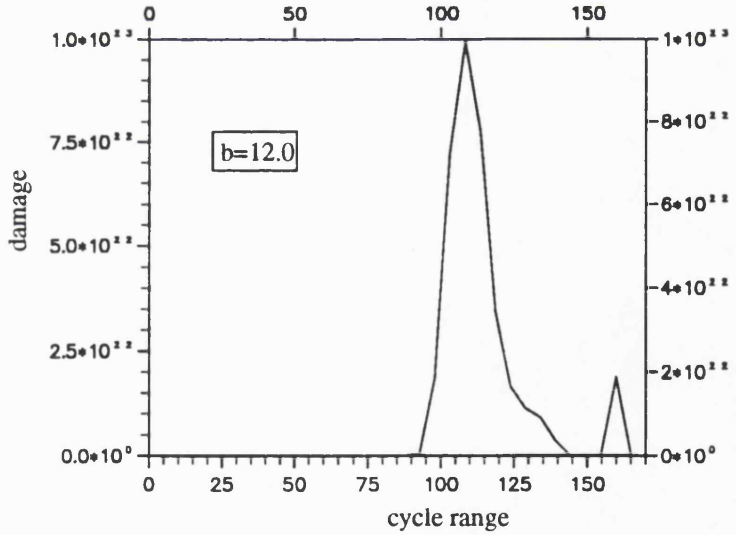

(b). Damage distribution of Howden data tape 26 3m edgewise

Figure 8.1: The effect of deterministic component in stress history

it is far from satisfactory. Other work has focused on this problem but failed to obtain a feasible design tool [79]. In [79], efforts were made to modify Dirlik's formula (because it works well for Gaussian response histories) by increasing the power of z in the third term, or by adding a fourth term to the formula. However, it was found that changing the third term was not very satisfactory and the work of adding the fourth term was not finished.

A method therefore needs to be developed to deal with these situations for a more accurate fatigue analysis of wind turbine blades. This chapter presents a method to predict the rainflow cycle probability distribution and peak rate for such combined stress histories. Due to the complexity of the problem, a simulation method is used to develop the analysis toolbox. This toolbox for spectral fatigue analysis is presented at the end of this chapter. The methodology is quite straight forward as shown in Figure 8.2.

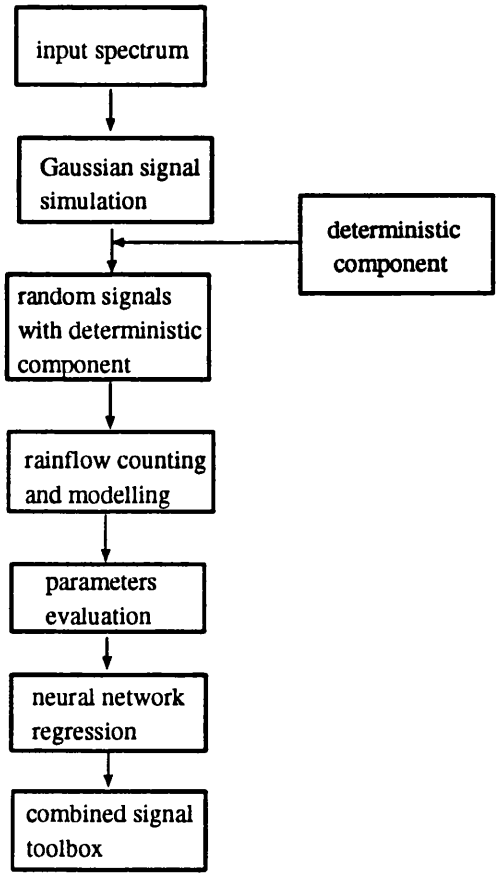

Figure 8.2: The methodology used to develop a combined signal toolbox for fatigue analysis

8.2 Simulation of a stress history with deterministic components

8.2.1 Simulation of a stationary Gaussian process

When a Fourier transform is performed on a time series, the time domain information of the process is transformed into the frequency domain. No information has been lost up to this stage and in fact it is quite straightforward to transform back to the original time signal. When the power spectral density function is formed from the transformed data, however, the phase information is lost. One spectrum can therefore be theoretically derived from an infinite number of time signals in so far as they contain the same amplitude constitution but different phase information. In other words, only one spectrum can be derived from a time series but a lot of time series can be derived from one spectrum given that the phase information is unknown. Since the PSD does not contain all the information from the original signals, it is necessary to assume the probability distribution of the time series. This assumption generally makes it possible to derive a sample time series from a given spectrum.

To simulate a stationary Gaussian process for a given power spectral density function, consider a stationary Gaussian process $x(t)$ with zero mean and power spectral density $S(\omega)$. The process $x(t)$ could be expressed by the form of the spectral representation [80][81]:

$$x(t) = \int_{-\infty}^{\infty} e^{i\omega t} dX(\omega) \tag{8.1}$$

where $X(\omega)$ is an orthogonal random process with zero mean and

$$\begin{aligned} E[dX(\omega_1)dX^*(\omega_2)] &= 0 \\ E[|dX(\omega_1)|^2] &= S(\omega)d\omega \end{aligned} \tag{8.2}$$

The autocorrelation function $R_x(\tau)$ of $x(t)$ and $x(t+\tau)$ is related to the spectral density as follows:

$$R_x(\tau) = \int_0^{\infty} G(\omega)\cos\omega\tau d\omega \tag{8.3}$$

where $G(\omega) = 2S(\omega)$ for $\omega \geq 0$ is the one-sided spectral density function. Since $x(t)$ is a real process, Equation 8.1 can be written as :

$$x(t) = \int_0^{\infty} \cos\omega t dU(\omega) + \sin\omega t dV(\omega) \tag{8.4}$$

where

$$dU(\omega_k) = [2G(\omega_k)\Delta\omega_k)]^{1/2}\cos\psi_k \tag{8.5}$$

$$dV(\omega_k) = -[2G(\omega_k)\Delta\omega_k)]^{1/2} \sin\psi_k$$

where, $\psi_k (k = 1, 2, \cdots)$ are independent and all have uniform distribution in $(0, 2\pi]$.

By substituting Eqn. 8.5 into Eqn. 8.4 and approximating the integral by a summation, the simulated random process can be obtained as :

$$x(t) = \sum_{k=1}^{N} [2G(\omega_k)\Delta\omega_k]^{1/2} \cos(\omega_k t + \psi_k) \tag{8.6}$$

Equation 8.6 actually takes a strip (Figure 8.3) as a harmonic component. The amplitude of each component can be evaluated using the Fourier transform formula. This is an acceptable approximation if the number of strips used for the approximation is large enough to satisfy the condition set by the central limit theorem. Some papers have used this technology to simulate Gaussian signals [82]. However, it will not be adopted in this thesis because with the inverse Fourier method it is easier to guarantee the Gaussian distribution of the simulated signals.

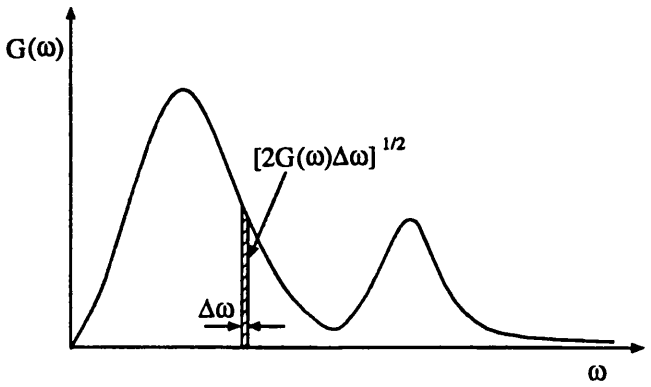

Figure 8.3: Harmonic component from spectrum

In order to do this, the complex inverse Fourier transform is applied to the series $\sqrt{2G(\omega_k)}e^{i\psi_k}$. This produces a complex random process expressed as:

$$Y(t) = \sum_{k=1}^{N} [\sqrt{2G(\omega_k)}e^{i\psi_k}]e^{i\omega_k t} \tag{8.7}$$

The random process described by Equation 8.6 then becomes the real part of $Y(t)$:

$$x(t) = \sqrt{\Delta\omega} Re(Y(t)) \tag{8.8}$$

Using this approach, a sample random process for a given power spectral density function can be simulated by applying an inverse FFT to the relevant

PSD. According to the central limit theorem, the process obtained in this way has a normal distribution as long as the phases ψ_k have a uniform distribution in $(0,\ 2\pi]$. It can also be shown that such a simulated process is ergodic irrespective of N[83]. Thus, a relatively long process can be obtained by putting different simulated samples together.

The procedure for simulating a Gaussian stationary time series for a given PSD can be set out as follows:

1). Generate a series of random phases ψ_k .

2). Perform an inverse FFT on

$$\sqrt{2G(\omega_k)}e^{i\psi_k}$$

to produce a complex time series

$$Y(t) = \sum_{k=1}^{N}[\sqrt{2G(\omega_k)}e^{i\psi_k}]e^{i\omega_k t}$$

3). Take the real part of the time series:

$$x(t) = \sqrt{\Delta\omega}Re(Y(t))$$

4). Repeat 1) to 3) until the desired length of time signal is obtained.

8.2.2 Simulation of a stress history with a deterministic component

Simulation of the stochastic stress history

Seventy spectral density functions were selected to simulate the stress time history of typical wind turbine blades. These spectra were of two types, smooth and rectangular, as shown in Figure 8.4. In this way the PSD's used for simulation covered a very wide range of both irregularity factor and "mean frequency" , as shown in Table 8.1 and 8.2 with the first 14 as smooth spectra and the others as rectangular ones. The smooth spectra have two peaks which have the analytical form:

$$G(f) = \frac{A_i}{\sqrt{1 + (f - f_i)^2/Q_i^2}}$$

Simulation of the deterministic component

The deterministic component can be modelled by a sine wave. The amplitudes of the sine waves were selected between 2σ and 10σ where σ is the root mean square

Table 8.1: 70 PSD's used in stress history simulation (1)

PSD No.	A_1	f_1	Q_1	A_2	f_2	Q_2	fc	γ	x_m
1	32767	98	5	0	0	0	229	0.9235	0.9073
2	23580	90	10	0	0	0	210	0.8684	0.8380
3	22543	82	11	0	0	0	226	0.8124	0.7739
4	21683	74	12	0	0	0	233	0.7559	0.7092
5	20226	65	14	0	0	0	227	0.7004	0.6431
6	26333	40	5	18444	105	3	242	0.6674	0.5877
7	27019	30	5	20264	104	2	231	0.5984	0.4925
8	29204	32	5	17522	108	2	237	0.5624	0.4712
9	30202	30	5	15101	106	1	245	0.5350	0.4497
10	31527	29	5	10404	114	2	237	0.5040	0.4296
11	29680	25	6	7420	108	2	235	0.5040	0.4310
12	30402	20	6	6081	109	2	225	0.4435	0.3650
13	31091	19	6	0	0	0	236	0.2992	0.2283
14	32741	14	5	0	0	0	222	0.2566	0.1804
15	31800	2	17	3572	123	138		0.1674	0.1030
16	31500	2	17	3984	103	134		0.2178	0.1198
17	31000	2	17	5020	93	132		0.2785	0.1477
18	30000	2	17	5324	69	138		0.3557	0.1964
19	29000	2	17	7045	76	134		0.4286	0.2495
20	28000	2	17	11130	94	124		0.4978	0.3058
21	27000	2	17	12758	95	123		0.5482	0.3546
22	25000	2	17	10873	78	131		0.6170	0.4357
23	23000	2	17	12111	78	131		0.6827	0.5166
24	20000	2	17	13008	74	132		0.7553	0.6184
25	18000	2	17	16330	86	1277		0.8159	0.6999
26	12000	2	17	13984	64	135		0.8659	0.8000
27	8000	2	17	16562	76	131		0.9292	0.8954
28	4000	2	17	30801	101	117		0.9888	0.9815
29	16000	2	15	32660	104	115		0.8829	0.7953
30	15850	2	14	21268	94	122		0.8902	0.8112
31	13700	2	17	18290	87	126		0.8895	0.8168
32	11100	2	22	16289	79	130		0.8889	0.8253
33	7840	2	40	15397	74	132		0.8886	0.8353
34	5440	2	62	14036	63	136		0.8862	0.8438
35	0	0	0	13492	49	138		0.8891	0.8573

Table 8.2: 70 PSD's used in stress history simulation (2)

PSD No.	A_1	f_1	Q_1	A_2	f_2	Q_2	fc	γ	x_m
36	23400	2	11	30150	104	115		0.8186	0.6885
37	17020	2	20	23930	100	118		0.8164	0.6963
38	14000	2	30	23130	100	119		0.8132	0.7012
39	12000	2	41	19140	95	123		0.8158	0.7150
40	11000	2	44	14664	80	131		0.8181	0.7274
41	9700	2	53	13296	71	135		0.8189	0.7381
42	7900	2	48	12158	49	139		0.8192	0.7504
43	24700	2	13	27482	104	115		0.7458	0.5838
44	18000	2	24	22276	101	118		0.7440	0.5977
45	17150	2	25	15081	87	127		0.7511	0.6141
46	15900	2	25	12140	66	135		0.7538	0.6312
47	12500	2	49	12826	80	133		0.7495	0.6377
48	11900	2	42	11156	55	139		0.7511	0.6482
49	0	0	0	10818	2	141		0.7507	0.6546
50	22480	2	19	23677	104	116		0.6706	0.4948
51	22300	2	19	17243	97	121		0.6800	0.5081
52	21700	2	19	12452	80	130		0.6853	0.5221
53	20900	2	19	10955	65	135		0.6863	0.5324
54	19700	2	19	10107	48	139		0.6838	0.5408
55	18700	2	19	9897	38	140		0.6841	0.5478
56	14800	2	31	9714	38	141		0.6816	0.5566
57	22000	2	23	21863	105	116		0.6006	0.4209
58	21000	2	25	14392	96	123		0.6100	0.4364
59	19820	2	28	13036	93	126		0.6111	0.4436
60	17980	2	34	11147	86	131		0.6119	0.4561
61	18000	2	32	9319	66	138		0.6119	0.4605
62	17090	2	32	8605	44	142		0.6132	0.4711
63	16000	2	35	8433	36	143		0.6143	0.4788
64	27200	2	17	13764	98	121		0.5390	0.3448
65	26900	2	17	10222	84	129		0.5459	0.3554
66	26400	2	17	8525	65	136		0.5459	0.3625
67	25980	2	17	8154	65	138		0.5396	0.3557
68	25580	2	17	7849	45	140		0.5458	0.3712
69	25000	2	17	7724	35	141		0.5472	0.3769
70	22200	2	20	7586	21	142		0.5462	0.3855

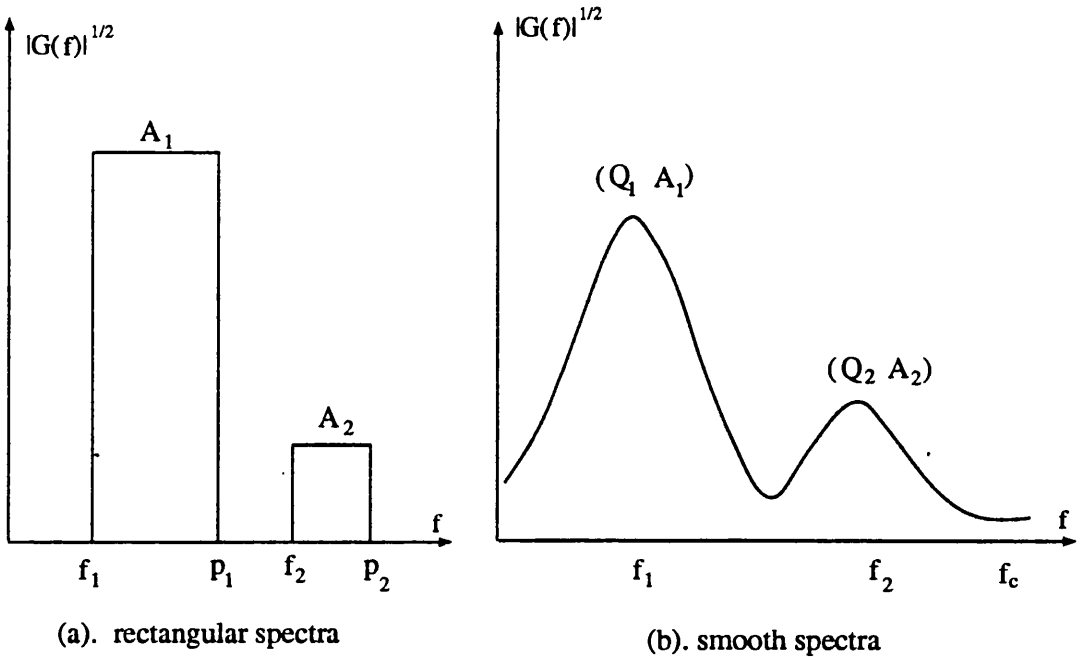

Figure 8.4: Shapes of spectra used

of the time series simulated by inverse FFT. Here we assume a time series with a deterministic component of amplitude less than 2σ is still Gaussian; and, if the amplitude of the deterministic component is bigger than 10σ, the deterministic component completely dominates the damage calculation. The frequency of the sine waves were selected between $0.5Hz$ and $3.0Hz$. If the frequency is lower than *0.5Hz*, it is assumed that the sine wave does not change the statistical property of the stochastic signals. If the frequency is above *3.0Hz*, it is assumed that there would be too many cycles to consider other cycles produced by the stochastic components. The cycles produced by the deterministic component should cause most of the damage.

If all the assumptions here do not hold, it is hoped that the interpolation of the formula will still work well. For most structures, the amplitudes and frequencies used here should be able to cover the main area of dynamic response.

Combination of the stochastic and deterministic components

The random signal with a deterministic component can be obtained simply by superimposing the deterministic component and the random simulated signal. One problem involved in mixing these two signals is a suitable choice of the sine wave phase.

When trying to combine more than two sine waves together, the phase dif-

ferences between them might be important from the point of view of fatigue damage. Since the phase information in the power spectral density function is lost, the phase of the single sine wave should not be important relative to the spectrum, given that the phase information in the spectrum is lost and this is not important for fatigue analysis. Actually, it was found that phase is irrelevant.

Numerical checks on the influence of the phase have been performed. For each check the rainflow cycle PDF's and the corresponding damage of the signals with different phases were calculated. Figure 8.5 shows one example of these rainflow cycle PDF's and the damages against phase with $b = 5.0$. The rainflow cycle PDF's show very little variance and the damage was within 1%. Similar checks were performed for all the spectra. The amplitude of the sine wave added in was selected as 6σ and the frequency was selected as *0.5Hz*. The phases of the sine waves were selected as 0.0, 0.4π, $0.8\pi, 1.2\pi$ and 1.6π. The fatigue damages from these simulated signals were calculated for *b=5.0, 8.0*, and 12.0 respectively. The percentage error of the damages against their mean value was then calculated. Figure 8.6 presents the average taken from the absolute values of these errors. This clearly shows that the errors are less then 1.5%, 2.0% and 2.5% respectively for the three *S-N* curves selected. It can therefore be concluded that the phases of the sine waves added to the Gaussian signals have nearly no effect on the distribution of rainflow cycles and the corresponding fatigue damages.

Thus, the deterministic components can be characterised by their amplitudes and frequencies. Their phases were therefore selected randomly. With these sine waves added into the Gaussian stationary stress histories, the stochastic signals with a deterministic component were obtained. There were 30 sine waves considered for each of the 70 spectra. Thus, the total number of simulated time series is over 2000.

Theoretically, for a sine wave with amplitude A and phase ϕ, given the phase has a uniform distribution in $(0, 2\pi]$, the signal should have a distribution density as :

$$p_x(x) = \frac{1}{\pi\sqrt{A^2 - x^2}}$$

Suppose this signal is added into a Gaussian signal which has a distribution density function as:

$$p_y(y) = \frac{1}{\sqrt{2\pi}\sigma} e^{-\frac{x^2}{2\sigma^2}}$$

the joint distribution density function $p(x, y)$ of sum $z = x + y$ has the form as :

$$p(z) = \int_{-\infty}^{\infty} p(x, y)dx = \int_{-\infty}^{\infty} p(x, z - x)dx$$

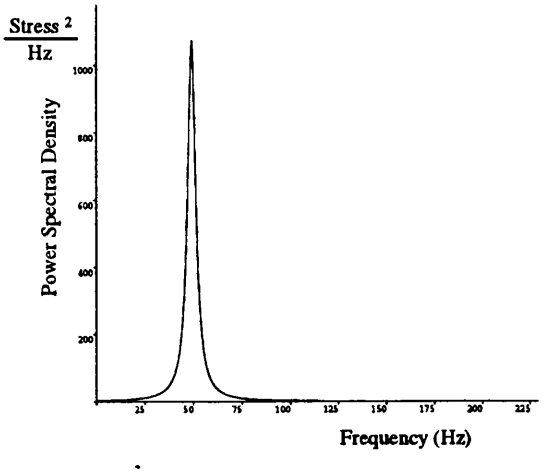

(a). The Power Spectral Density function No. 1

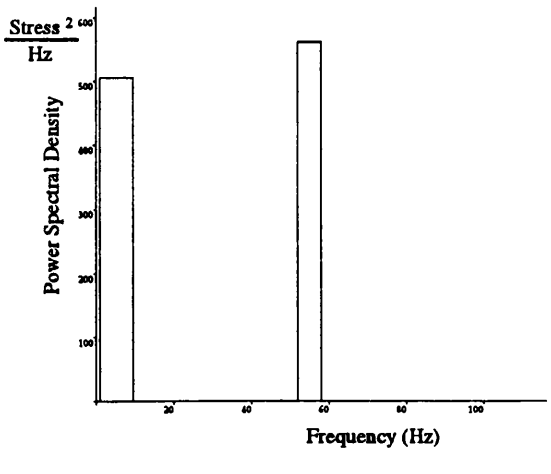

(d). The Power Spectral Density function No. 50

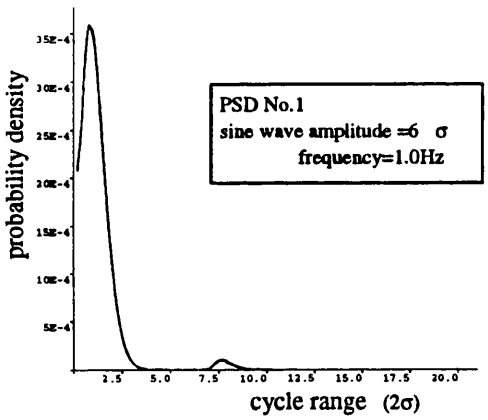

(b). The PDF curves of mixed signals with different phases in sine waves

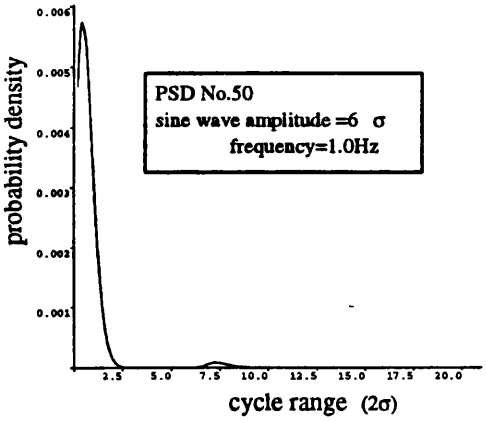

(e). The PDF curves of mixed signals with different phases in sine waves

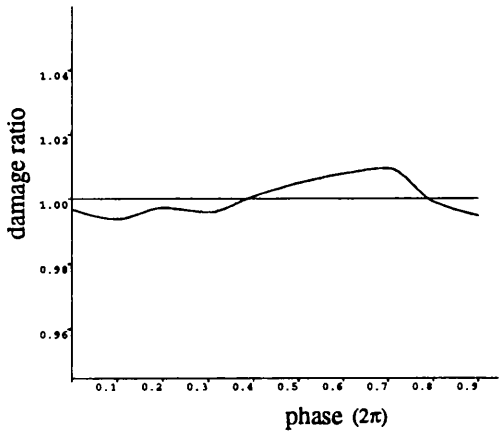

(c). Damage ratios (with mean) from pdfs of different phase shown in (b)

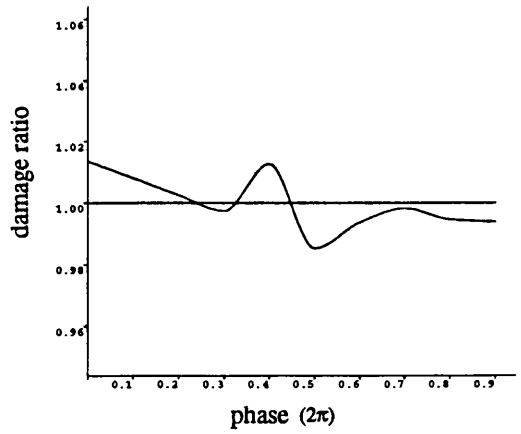

(f). Damage ratios (with mean) from pdfs of different phase shown in (e)

Figure 8.5: Phase check for input sine waves

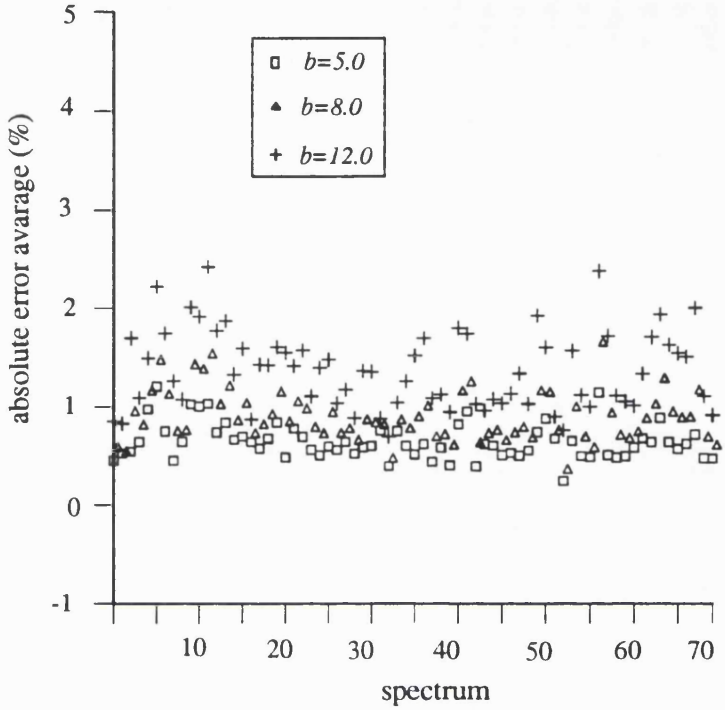

Figure 8.6: Average of absolute percentage errors of fatigue damage with different phase

Since x and y are independent random variables, we have

$$p(x,y) = p_x(x) \cdot p_y(y)$$

$$p(z) = \int_{-\infty}^{\infty} p_x(x) p_y(z-x) dx$$

The stress histories with a deterministic components then have the distribution

$$p(z) = \frac{1}{\sqrt{2\pi}\pi\sigma} \int_{-A}^{A} \frac{1}{\sqrt{A^2 - x^2}} e^{-\frac{(x-z)^2}{2\sigma^2}} dx \tag{8.9}$$

Statistical analysis was performed on all the simulated data. The statistic parameters of the simulated signal from PSD no. 1 combined with various sine waves are listed in Table 8.3 as an example. As expected, the signal is Gaussian before the deterministic components are added in. The stronger the sine wave which is added, the stronger becomes the degree of non-normality. The statistical parameters are irrelevant with the frequency of sine waves as the probability density of these signals are not the function of the frequency as in Equation 8.9.

Table 8.3: Statistical parameters for signals from PSD No.1

amp	frq	mean	rms	X^2_{30}	E[P]	E[0]	γ	K
0.0	0.5	0.03	49.73	30.54	3155.90	2950.20	0.515	0.001
1.0	0.5	0.02	156.78	3454.79	11477.10	4877.70	0.425	-0.664
1.0	1.0	0.02	156.74	3436.92	11466.40	4917.30	0.429	-0.663
1.0	1.5	0.02	156.73	3617.44	11465.50	4886.20	0.426	-0.674
1.0	2.0	0.01	156.75	3422.72	11449.10	4884.00	0.427	-0.659
1.0	2.5	0.00	156.75	3430.34	11445.60	4909.70	0.429	-0.659
1.0	3.0	0.01	156.79	3486.51	11445.40	4900.30	0.428	-0.668
2.0	0.5	0.03	271.52	19447.80	11472.20	2182.60	0.190	-1.184
2.0	1.0	0.05	271.49	19463.22	11449.70	2167.80	0.189	-1.184
2.0	1.5	0.03	271.48	19791.37	11429.30	2193.80	0.192	-1.188
2.0	2.0	0.01	271.50	19364.40	11390.10	2204.00	0.194	-1.182
2.0	2.5	0.00	271.50	19387.120	11353.00	2215.30	0.195	-1.182
2.0	3.0	0.00	271.55	19539.74	11307.80	2220.40	0.196	-1.186
3.0	0.5	0.05	394.51	33732.14	11466.90	1418.20	0.124	-1.346
3.0	1.0	0.07	394.48	33773.72	11425.50	1413.30	0.124	-1.345
3.0	1.5	0.05	394.46	34105.60	11372.50	1440.70	0.127	-1.348
3.0	2.0	0.02	394.49	33612.81	11292.30	1456.50	0.129	-1.345
3.0	2.5	0.00	394.48	33670.52	11207.80	1483.80	0.132	-1.345
3.0	3.0	0.00	394.53	33798.72	11091.80	1496.30	0.135	-1.347
4.0	0.5	0.07	519.91	44665.20	11462.50	1049.10	0.092	-1.410
4.0	1.0	0.09	519.89	44801.94	11396.40	1065.80	0.094	-1.410
4.0	1.5	0.07	519.86	45136.84	11297.60	1091.40	0.097	-1.411
4.0	2.0	0.03	519.89	44544.04	11166.70	1112.70	0.100	-1.410
4.0	2.5	0.00	519.89	44705.58	11007.00	1142.90	0.104	-1.410
4.0	3.0	0.01	519.94	44805.47	10794.00	1166.00	0.108	-1.411
5.0	0.5	0.08	646.33	53271.66	11450.90	838.90	0.073	-1.441
5.0	1.0	0.11	646.31	53387.67	11352.20	855.70	0.075	-1.442
5.0	1.5	0.09	646.28	53729.53	11202.80	888.20	0.079	-1.442
5.0	2.0	0.03	646.31	53098.50	11008.20	913.10	0.083	-1.441
5.0	2.5	0.00	646.31	53242.54	10758.80	946.10	0.088	-1.441
5.0	3.0	0.01	646.36	53385.98	10432.30	994.10	0.095	-1.442

8.3 Modelling the rainflow range probability density

8.3.1 Gaussian time history

When rainflow counting was applied to the 70 Gaussian stochastic time histories (no deterministic component), 70 rainflow cycle PDF's were derived. These PDF's are designed to cover a wide range of Gaussian signals and were described by their irregularity factor and mean frequency. A typical probability density curve is shown as in Figure 8.7.

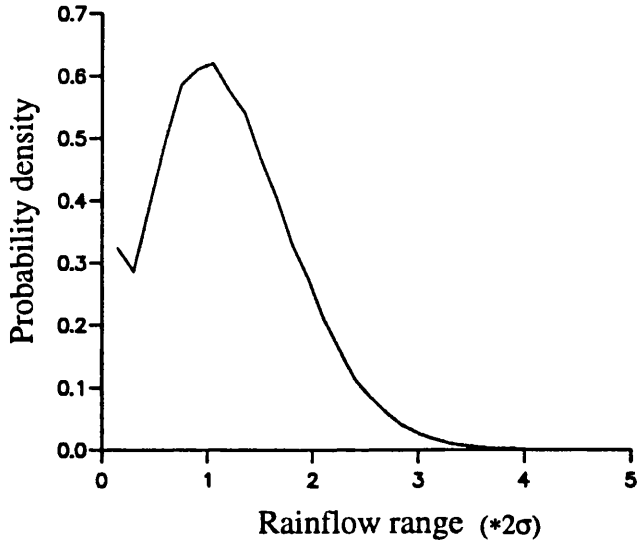

Figure 8.7: Rainflow cycle probability density function from spectrum 1

This type of function can be modelled using three expressions as follows:

$$f_{RR}(z) = C_1 \frac{1}{\tau} e^{\frac{z}{\tau}} + C_2 \frac{1}{\alpha^2} e^{-\frac{z^2}{2\alpha^2}} + C_3 e^{-\frac{z^2}{2}} \tag{8.10}$$

where, C_1, C_2, C_3, τ and α are all parameters to be decided and $C_1+C_2+C_3 = 1.0$, $z = S/2\sigma$ is taken as the normalised cycle range. This model was intended to express the lower, middle and high range portions of the rainflow cycle PDF's by using exponential, Rayleigh and standard Rayleigh distributions.

This model was actually the one used by Dirlik [13]. However, since the model for a random time history combined with a deterministic component is quite different from the one above, a new model was required and this is covered in the next section. The model for Gaussian response histories was still employed to improve accuracy when the deterministic component is very small. This also makes the fatigue analysis toolbox complete.

8.3.2 Random time history with a deterministic component

Rainflow cycle counting was performed on all the combined signals simulated in the previous section. A typical one is shown in Figure 8.8. Like the model for Gaussian response histories, these curves apparently have three portions. The model which was eventually developed is as follows:

$$f_{RR}(z) = C_1 \frac{1}{\tau} e^{\frac{z}{\tau}} + C_2 \frac{1}{\alpha^2} e^{-\frac{z^2}{2\alpha^2}} + C_3 \frac{1}{\sqrt{2\pi}\beta} e^{-\frac{(z-\mu)^2}{2\beta^2}} \tag{8.11}$$

where, $C_1, C_2, C_3, \tau, \alpha, \mu$ and β are all parameters to be decided and $C_1+C_2+C_3 = 1.0$.

This model is intended to express the low range part by a exponential function, the middle range part by a Rayleigh function and the high range part by a Gaussian distribution function as shown in Figure 8.8. Parameters τ, α, and β are the shape control parameters for the three probability density functions employed. C_1, C_2 and C_3 control the distribution of the probability among the three range portions. μ is determined by the location of the peak in the PDF curve caused by the deterministic component.

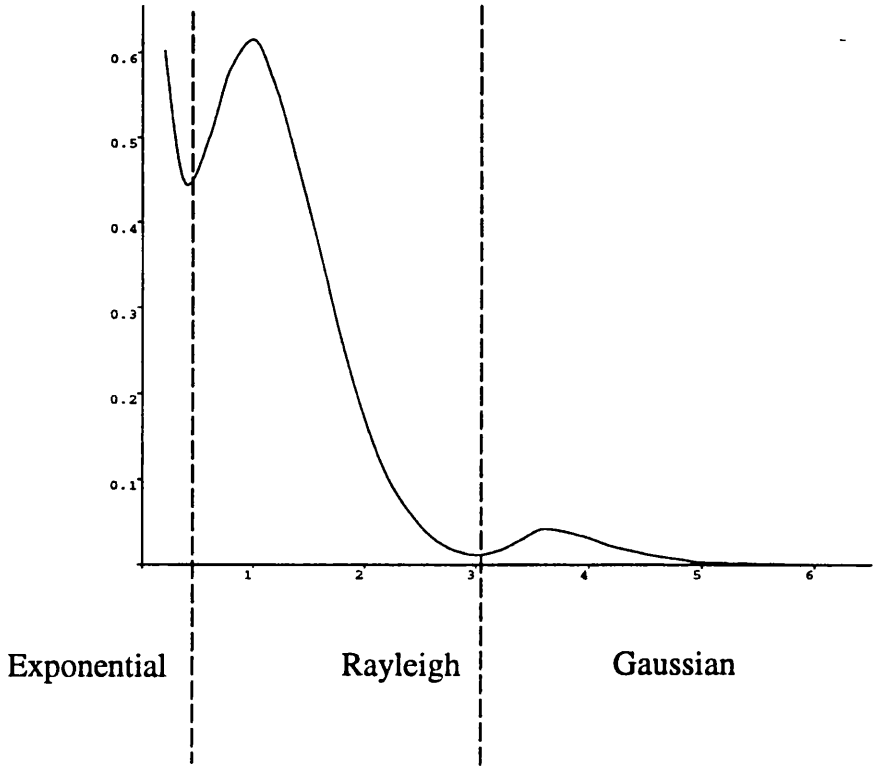

Figure 8.8: Model for the rainflow cycle probability density function

8.4 Parameter evaluation

8.4.1 Least square technique

The procedure of representing data in functional form and then selecting parameter values in the function to best fit the data is called *curve fitting.* The form of the function used is generally determined by the physical process governing the data or by a graphical observation of the data. The process of selecting the parameters in the function to which a best fit is to be applied is called parameter evaluation [84] [85] [86].

The method of least squares is the most widely used curve fitting procedure. At least in the case of pure curve fitting, where the coefficients have no physical significance. In the general case, assume that there are n independent observations y_1, y_2, ..., y_n obtained for various values x_1, x_2, ..., x_n, and a model $y = f(x, \theta)$ is set for fitting the data, the problem reduces to the suitable selection of the parameter θ.

Firstly, the residuals can be defined as

$$e_i(\theta) = y_i - f(x_i, \theta) \tag{8.12}$$

The idea of least squares is to select the parameter θ to minimise the least square error (sum of squares of the residuals),i.e.,

$$\Phi(\theta) = \sum_{i=1}^{n} e_i(\theta)^2 = \sum_{i=1}^{n} (y_i - f(x_i, \theta))^2 \tag{8.13}$$

The difficulty here is deciding how to use nonlinear programming techniques to perform the optimisation in order to search for θ^* values which minimise $\Phi(\theta)$. Many methods, such as the simplex, direction search, or even direct search can be employed. For the problem with constraints, the direction search method is most widely used. The procedure is to perform an iteration $\theta_{i+1} \Leftarrow \theta_i$ along a suitable direct v from the initial guess θ_1. The procedure is as follow

1. Set $i = 1$, an initial guess θ_1 must be provided externally.
2. Determine a vector v_i in the direction of the proposed ith step.
3. Determine a scalar ρ_i such that the step

$$\sigma_i = \rho_i v_i \tag{8.14}$$

is acceptable. That is, take

$$\theta_{i+1} = \theta_i + \rho_i v_i \tag{8.15}$$

whilst ensuring that ρ_i is chosen so that the following equation holds

$$\Phi_{i+1} < \Phi_i \tag{8.16}$$

4. Test whether the termination criterion is met. If not, increase i by one and return to step 2. If yes, accept θ_{i+1} as the value of θ^*.

There are different methods for choosing the step direction v_i and step size ρ_i. The most widely used method for determining the step direction is the so-called *gradient method* which uses the direction which forms a greater than 90° angle with the gradient q_i. The step direction thus chosen is expressed as

$$v_i = -R_i q_i$$

Newton's method, used in nonlinear programming, is to take R_i as the Hessian matrix, which is the matrix of the second partial derivatives of the objective function, i.e.,

$$H_{ij}(\theta) = \frac{\partial^2 \Phi}{\partial \theta_i \partial \theta_j} \tag{8.17}$$

For the least square problem, this special form of the objective function has certain advantages. From Equation 8.13, the gradient vector and the Hessian matrix are expressed by :

$$q_i = \frac{\partial \Phi}{\partial \theta_i} = -2 \sum_{j=1}^{n} e_j \frac{\partial f_j}{\partial \theta_i} \tag{8.18}$$

$$H_{ij} = \frac{\partial^2 \Phi}{\partial \theta_i \partial \theta_j} = -2 \sum_{k=1}^{n} e_k \frac{\partial^2 f_k}{\partial \theta_i \partial \theta_j} + 2 \sum_{k=1}^{n} \frac{\partial f_k}{\partial \theta_i} \frac{\partial f_k}{\partial \theta_j} \tag{8.19}$$

In the Gauss method, the first term is neglected, and N is used in place of H, where N is defined by

$$N_{ij} = 2 \sum_{k=1}^{n} \frac{\partial f_k}{\partial \theta_i} \frac{\partial f_k}{\partial \theta_j} \tag{8.20}$$

The Gauss method can be taken as an approximation of Newton's method. Since the residuals are, hopefully, small, this provides some justification for regarding N as a good approximation of H, particularly near the minimum. However, when a poor initial guess is given, the method may fail to converge. In such a situation an improvement should be obtained by providing suitable constraints.

Some situations need constraints because some physical parameters can not take arbitrary values. The constraints are usually provided by using penalty functions, the projection method or a variable transformation. When penalty functions are adopted, the objective functions (and the corresponding gradient

vector and Hessian matrix) are modified such that the values of the parameters will not leave the feasible region.

For the inequality constraint

$$h_j(\theta) \geq 0$$

the penalty function can be taken as

$$\zeta_j(\theta) = \alpha_j / h_j(\theta)$$

where α_j is a small positive constant called a penalty factor. The objective function can then be modified by adding the penalty functions to it for all the constraints.

$$\Phi^{\dagger}(\theta) = \Phi(\theta) + \sum_j \alpha_j / h_j(\theta) \tag{8.21}$$

Let $\theta^{\dagger}$ and θ^* be the points at which $\Phi^{\dagger}$ and Φ attain their respective minima within the feasible region. It can be proven that

$$\lim_{\alpha_j \to 0} \theta^{\dagger} = \theta^* \tag{8.22}$$

The iteration scheme for an unconstrained θ^* remains nearly unchanged except that another iteration of α_j has to be added for the limiting condition of Equation 8.22.

8.4.2 Parameter evaluation for rainflow cycle models

By applying a rainflow cycle count to each simulated time series, the probability density functions $p_{RR}(z)$ of rainflow cycles are derived. Then by using the model function $f_{RR}(z, \theta)$ established in the previous section, a least square technique was employed to evaluate the parameters in the model equation.

The residuals were defined as :

$$E(\theta) = \sum_{k=1}^{n} e_k^2 = \sum_{k=1}^{n} [p_{RR}(z_k) - f_{RR}(z_k, \theta)]^2 \tag{8.23}$$

where n is the number of points used to discretise the curve.

Optimisation of model for purely random time histories

The model equation which was used is expressed in Equation 8.10. The parameters to be evaluated were $\theta = [C_1\ C_2\ C_3\ \tau\ \alpha\ ]^T$ as explained in Section *8.3.1.*

The full mathematical expression for nonlinear programming is as follows:

$$min\ E(\theta) \tag{8.24}$$

s.t.

$$0.0 \leq C_1 \leq 1.0$$

$$0.0 \leq C_2 \leq 1.0$$

$$0.0 \leq C_3 \leq 1.0$$

$$C_1 + C_2 + C_3 = 1.0$$

$$\tau > 0.0$$

$$\alpha > 0.0$$

Optimisation of model for random time history with a deterministic component

The model equation is expressed as in Equation 8.11. The parameters to be evaluated were $\theta = [C_1\ C_2\ C_3\ \tau\ \alpha\ \mu\ \beta]^T$.

The full mathematical expression for nonlinear programming is as follows:

$$min\ E(\theta) \tag{8.25}$$

s.t.

$$0.0 \leq C_1 \leq 1.0$$

$$0.0 \leq C_2 \leq 1.0$$

$$0.0 \leq C_3 \leq 1.0$$

$$C_1 + C_2 + C_3 = 1.0$$

$$\tau > 0.0$$

$$\alpha > 0.0$$

$$\beta > 0.0$$

$$\mu > 0.0$$

The gradient vector and the Hessian matrix were calculated using the equation presented in Section *8.4.1.*

Accuracy improvement of solution

There are two problems which must be considered in the calculation procedure.

The first one is the possibility of convergence to a local stationery point. To avoid this,

a). Different initial values were given for each case and the computation was repeated to check for consistency of solution.

b). The program was designed to be able to jump out from a stationery point and then be terminated "manually".

c). An "eye-test" was used after each calculation was performed in order to ensure convergence to the global stationery point.

The second possible problem is that a relatively higher accuracy is needed for the higher range cycles. To achieve this, the computation is actually performed on a weighted objective function which incorporates the fatigue damage potential of each cycle range. This is achieved by applying a weight function $\xi(z)$ to the rainflow cycle PDF's calculated from the time series. That is, instead of fitting $f_{RR}(z,\theta)$ to $p_{RR}(z)$ as in Equation 8.23, the computation was performed by fitting $\xi(z)f_{RR}(z,\theta)$ to $\xi(z)p_{RR}(z)$. The residual was then expressed as:

$$E(\theta) = \sum_{k=1}^{n} e_k^2 = \sum_{k=1}^{n} \xi^2(z)[p_{RR}(z) - f_{RR}(z)]^2 \tag{8.26}$$

This modifies the gradient vector and the Hessian matrix into the following form:

$$q_i = \frac{\partial E}{\partial \theta_i} = -2\sum_{j=1}^{n} \xi^2(z) e_j \frac{\partial f_j}{\partial \theta_i} \tag{8.27}$$

$$N_{ij} = 2\sum_{k=1}^{n} \xi^2(z) \frac{\partial f_k}{\partial \theta_i}\frac{\partial f_k}{\partial \theta_j} \tag{8.28}$$

Thus, once $\xi^2(z)$ is selected it can be used as a multiplier to the gradient vector and Hessian matrix. $\xi(z)$ was chosen as z^2 for most computation. This sometimes makes the lower range portion of the probability density function have a poor fit. However, from the point of view of fatigue, the damage potential of each cycle is proportional to the power b of its range. Furthermore, if the cycle range is quite high and its probability is too small for the program to detect (because missing it causes very little error), the weighted fitting will avoid missing such cycles .

Figure 8.9 shows a typical rainflow cycle PDF and damage density from one of the time histories using both weighted and unweighted fitting. The weight function was selected here as $\xi^2(z) = z$. Although there is so little difference between the PDF's which can hardly be detected, the fatigue damage distribution

caused by the PDF's are quite different. The damage is very similar in the low range part but for the medium and higher ranges, weighted fitting gives a much closer fit. A higher powered weight function would have provided an even better fit to the high range part of the damage distribution.

Parameters for Gaussian signals (no deterministic component)

The weight function used to curve fit the 70 Gaussian cases is $\xi^2(z) = z$. This is based on the consideration that, the high range cycle part of the PDF should be given more attention, but on the other hand, some emphasis should remain on keeping the PDF shape generally correct. The 70 sets of fitted parameters for the 70 Gaussian signals are listed in Table 8.4 and 8.5. The generally used "cost" (or residual) is not listed in this table, but instead, the fatigue damage rates of the fitted model curve compared with the damage counted directly from the time signals are listed. The "$D_{b=5}$" listed here are the damage values obtained when inverse *S-N* curve slope $b = 5.0$ is used while "$D_{b=8}$" are the values when $b = 8.0$ is used. Most of them meet well with the time history curves from the point of view of fatigue. The average absolute error is *7%* for $b = 5.0$ and *18%* for $b = 8.0$. The maximum error is *35%* for $b = 5.0$ and *43%* for $b = 8.0$. When the PDF's from both the time series and the curve fitting are plotted together, it was noted that most of them meet quite well. Figure 8.10 shows the curve fitting results for spectrum 1. Figure 8.10(a) shows the rainflow cycle PDF's from the simulated time history and curve fitting. Figure 8.10(b) shows the correspondent damage density of the cycles when *b=5.0* is used.

Parameter for random signals with deterministic components (the combined case)

2100 sets of fitted data were used for the simulated random signals incorporating deterministic components. The fitting was performed using the weight function $\xi^2(z) = z^2$ for most cases. For others $\xi^2(z) = z$ was used. It is impossible to list all this data in the thesis although it can be provided on floppy disk. However, in order to examine quality of the fitting, the ratios of the damage rates between the fitted PDF's with the simulated time history are listed in Table 8.6 to Table 8.11 for *b=5.0.* The second row in these tables refer to the frequency of the deterministic component. It can be seen from these tables that the fitting process is quite successful from the point of view of fatigue damage.

Figure 8.11 shows some PDF's from spectrum No.60 together with the cor-

respondent functions from the time series. The high range part of the functions have been magnified by 10 in order to have a better visualisation.

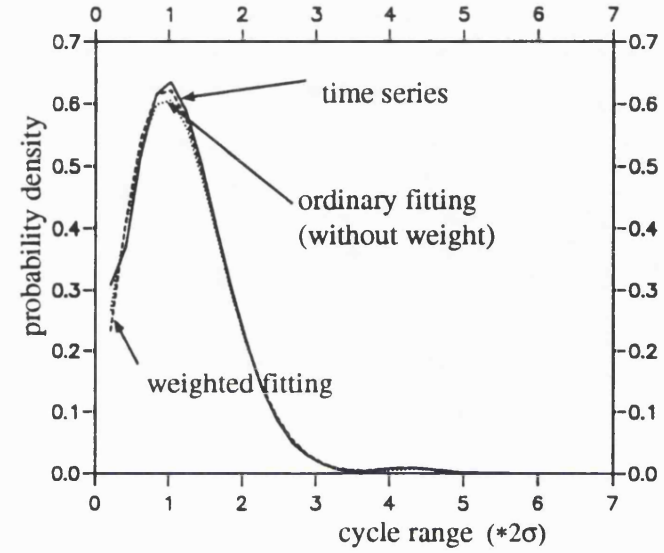

(a). rainflow cycle probability

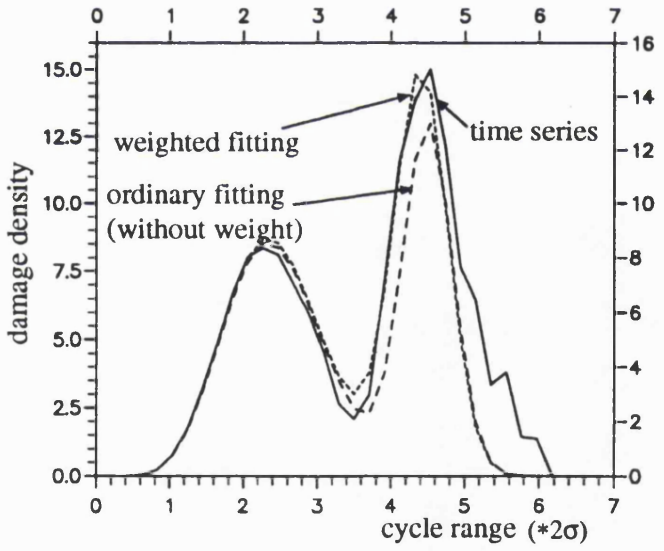

(b). damage density with b=5.0

Figure 8.9: Curve fitting on weighted and unweighted basis

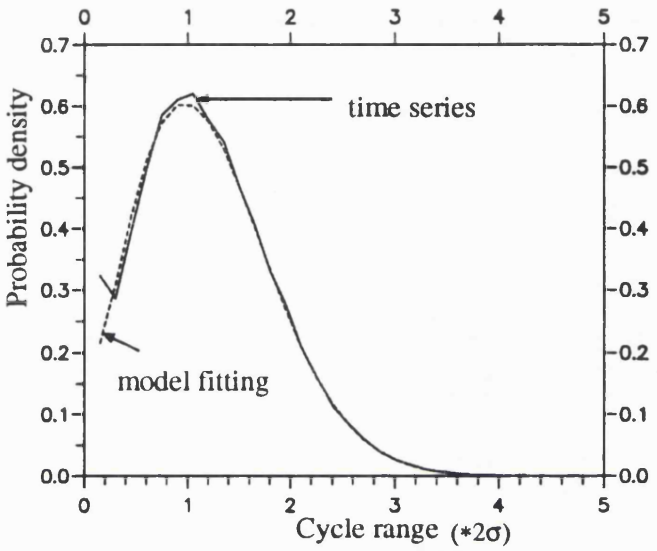

(a). Probability density functions

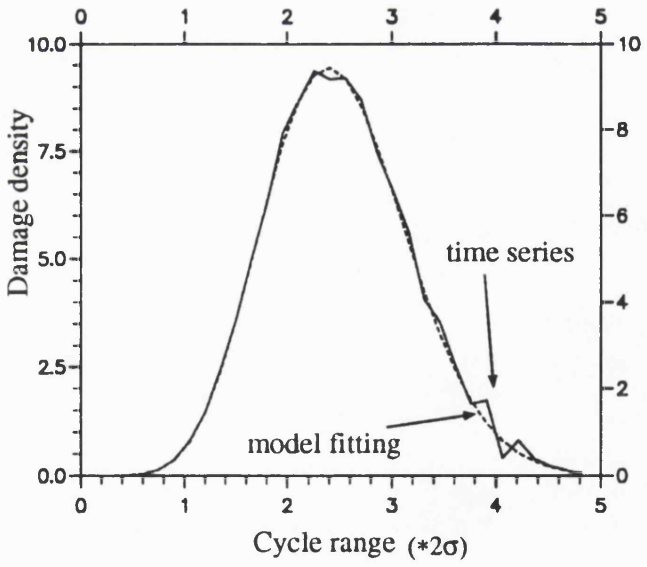

(b). Damage density

Figure 8.10: Curve fitting for spectrum no. 1

Table 8.4: Model parameters by curve fitting with weight $\xi^2(z) = z$ (1)

No.	C_1	C_2	C_3	τ	α	$D_{b=5}$	$D_{b=8}$
1	0.0277	0.7196	0.2527	0.1103	0.9335	0.9889	0.9754
2	0.0782	0.6700	0.2518	0.1498	0.9326	1.0124	1.0332
3	0.0782	0.8796	0.0422	0.1473	0.9645	1.0665	1.1012
4	0.1779	0.4493	0.3728	0.1645	0.9711	1.0328	1.0858
5	0.2499	0.3817	0.3684	0.2006	1.0082	1.0521	1.1361
6	0.4333	0.5589	0.0078	0.3374	1.1054	1.1017	1.3162
7	0.7015	0.2800	0.0185	0.5046	1.2695	1.1321	1.5305
8	0.5789	0.4096	0.0115	0.2994	1.1841	1.0958	1.3752
9	0.5658	0.4326	0.0016	0.2513	1.1509	1.0596	1.2926
10	0.5355	0.4594	0.0051	0.1979	1.1131	1.0321	1.2195
11	0.5054	0.4885	0.0061	0.1910	1.0811	1.0092	1.1426
12	0.5841	0.2130	0.2030	0.2065	1.2175	1.0387	1.2405
13	0.6892	0.1559	0.1550	0.1743	1.2982	1.0791	1.3629
14	0.8037	0.0748	0.1215	0.1788	1.5386	0.9436	1.3016
15	0.8951	0.0494	0.0555	0.1320	1.5281	0.9230	1.3319
16	0.9181	0.0388	0.0431	0.1680	1.6295	0.9383	1.3509
17	0.9281	0.0342	0.0376	0.2327	1.6359	0.8565	1.1910
18	0.1599	0.6897	0.1504	0.2199	0.0763	0.7463	0.6783
19	0.1663	0.6763	0.1574	0.2912	0.1158	0.7366	0.6515
20	0.2868	0.6239	0.0892	0.5600	0.1566	0.8172	0.9161
21	0.2465	0.6367	0.1168	0.5746	0.1958	0.9089	1.0861
22	0.1865	0.6394	0.1741	0.6686	0.2527	0.9975	1.2484
23	0.1332	0.6245	0.2423	0.6464	0.3083	0.9787	1.1065
24	0.0968	0.5776	0.3256	0.6530	0.3804	0.9862	1.0649
25	0.0532	0.5458	0.4010	0.5074	0.4249	1.0469	1.1262
26	0.0595	0.5422	0.3983	0.1582	0.6285	0.9298	0.9000
27	0.0246	0.4999	0.4755	0.1138	0.6765	0.9879	1.0117
28	0.0243	0.5653	0.4104	1.0244	0.7189	1.0620	1.2500
29	0.0588	0.6460	0.2952	0.5825	0.5668	1.0412	1.1523
30	0.0428	0.5431	0.4141	0.5723	0.5378	1.0582	1.1818
31	0.0416	0.4772	0.4812	0.5313	0.5229	1.0631	1.1724
32	0.0309	0.4369	0.5323	0.1728	0.5237	1.0385	1.1268
33	0.0974	0.4870	0.4156	0.4155	0.7006	0.9817	0.9992
34	0.1261	0.6367	0.2372	0.2624	0.8325	0.9554	0.9462
35	0.0925	0.9013	0.0062	0.1778	0.9102	1.0309	1.0463

Table 8.5: Model parameters by curve fitting with weight $\xi^2(z) = z$ (2)

No.	C_1	C_2	C_3	τ	α	$D_{b=5}$	$D_{b=8}$
36	0.0593	0.6957	0.2450	0.5197	0.4787	1.0602	1.1783
37	0.0876	0.5979	0.3145	0.5371	0.4595	1.0393	1.1360
38	0.1165	0.5018	0.3817	0.5170	0.4295	1.0431	1.1421
39	0.1705	0.3899	0.4396	0.5395	0.4353	1.0612	1.1961
40	0.1708	0.3266	0.5026	0.4852	0.4557	1.0433	1.1390
41	0.2411	0.3507	0.4082	0.5813	0.6280	1.0182	1.1537
42	0.2244	0.4458	0.3297	0.4386	0.8171	0.9926	1.0050
43	0.0897	0.7039	0.2064	0.5510	0.3916	1.0485	1.1740
44	0.1389	0.5662	0.2949	0.5235	0.3593	1.0257	1.1167
45	0.1447	0.5017	0.3537	0.5522	0.3545	1.0409	1.1346
46	0.1199	0.4630	0.4171	0.3694	0.3695	0.9492	0.9534
47	0.2582	0.2729	0.4689	0.5090	0.3287	1.0310	1.1042
48	0.2931	0.2459	0.4610	0.5164	0.4265	1.0022	1.1070
49	0.3993	0.3128	0.2879	0.6132	0.7332	1.0579	1.3072
50	0.1647	0.6317	0.2036	0.5378	0.2979	0.9972	1.1125
51	0.1547	0.6266	0.2186	0.5432	0.3086	0.9647	1.0121
52	0.1344	0.5950	0.2706	0.5607	0.3027	0.9426	0.9559
53	0.1993	0.5701	0.2306	0.7460	0.3297	1.0996	1.5507
54	0.2958	0.4576	0.2465	0.6642	0.3776	1.0521	1.3839
55	0.2071	0.4719	0.3210	0.3184	0.3901	0.8045	0.7362
56	0.3498	0.2542	0.3959	0.5160	0.3016	0.9745	1.0663
57	0.2542	0.5639	0.1819	0.5534	0.2186	0.9649	1.0999
58	0.2610	0.5325	0.2065	0.5470	0.2265	0.9349	1.0134
59	0.2974	0.4815	0.2211	0.5537	0.2215	0.9438	1.0394
60	0.3273	0.4024	0.2703	0.5442	0.1966	0.9529	1.0608
61	0.3259	0.3912	0.2829	0.5475	0.2064	0.9312	1.0522
62	0.3964	0.2947	0.3089	0.5233	0.2141	0.9095	0.9615
63	0.4268	0.2353	0.3379	0.5197	0.1891	0.9376	1.0115
64	0.2265	0.6438	0.1297	0.5015	0.1893	0.8206	0.8471
65	0.2317	0.6420	0.1263	0.6121	0.1922	0.9189	1.0988
66	0.2686	0.6220	0.1093	0.6967	0.2021	1.0467	1.5008
67	0.2817	0.6236	0.0947	0.7131	0.1998	1.1090	1.7068
68	0.1882	0.6198	0.1919	0.2528	0.2291	0.6517	0.5620
69	0.2413	0.5593	0.1994	0.2995	0.2388	0.6527	0.5695
70	0.4650	0.3815	0.1536	0.5849	0.2043	0.8684	1.0475

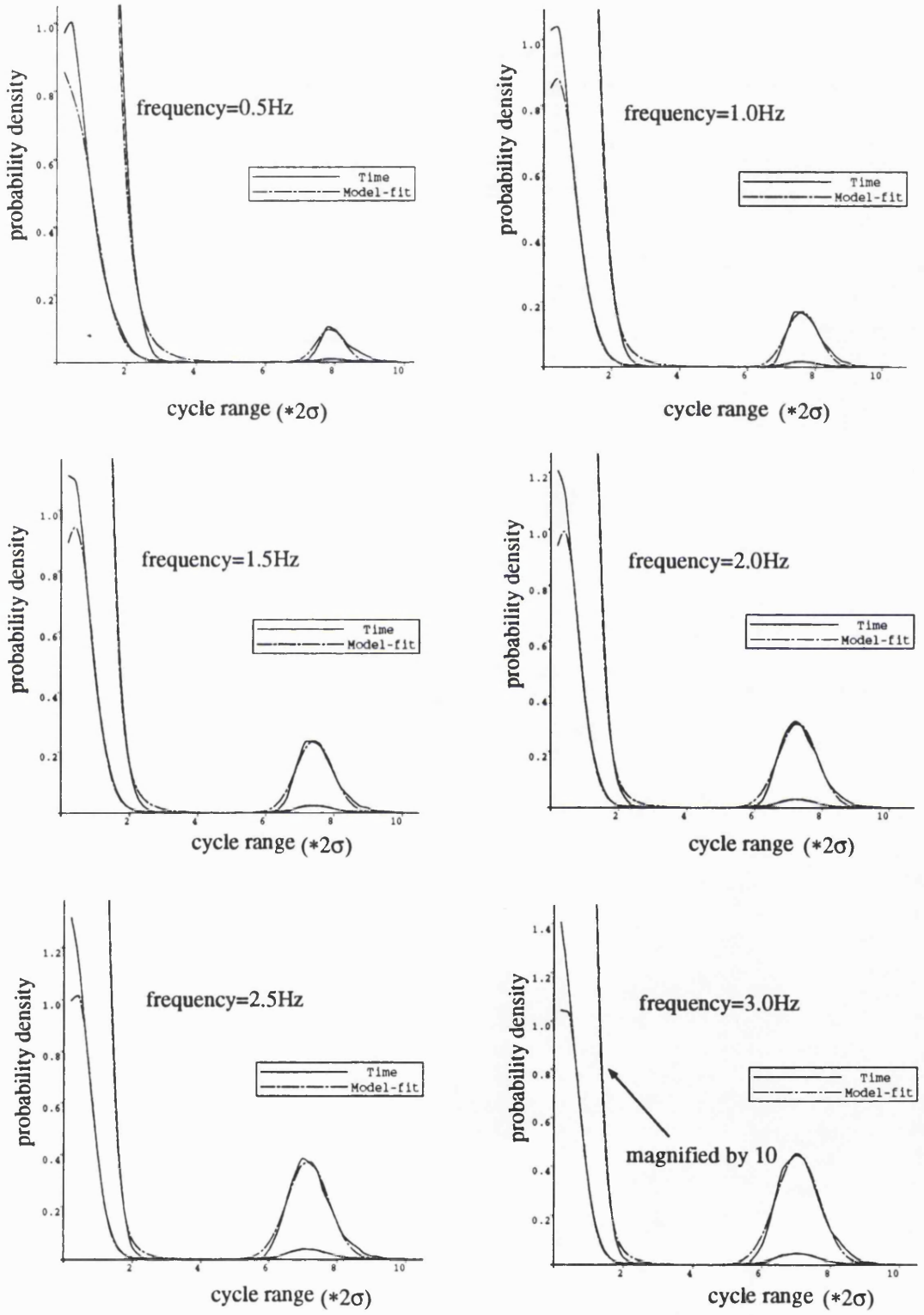

Figure 8.11: Least-square fitting results for spectra 60

Table 8.6: Fatigue damage rates for fitted model curve with $b = 5.0$ (1)

PSD No.	amplitude=1.0						amplitude=2.0			
	0.5	1.0	1.5	2.0	2.5	3.0	0.5	1.0	1.5	2.0
1	1.11	1.12	1.11	1.29	1.22	1.15	1.09	1.10	1.14	1.15
2	1.04	1.05	1.08	1.06	1.12	1.13	1.08	1.10	1.10	1.11
3	1.02	1.16	1.10	1.12	1.10	1.13	1.07	1.10	1.09	1.11
4	1.03	1.07	1.12	1.12	1.13	1.12	1.07	1.10	1.11	1.11
5	1.09	1.11	1.12	1.13	1.13	1.15	1.10	1.10	1.11	1.12
6	1.08	1.09	1.12	1.14	1.18	1.15	1.11	1.10	1.11	1.12
7	1.08	1.12	1.13	1.15	1.16	1.15	1.08	1.06	1.09	1.11
8	1.10	1.11	1.19	1.16	1.17	1.17	1.12	1.04	1.10	1.14
9	1.09	1.10	1.03	1.15	1.14	1.15	1.11	1.08	1.09	1.12
10	1.05	1.11	1.18	1.17	1.18	1.18	1.10	1.06	1.12	1.14
11	1.13	1.28	1.28	1.23	1.28	1.32	1.12	1.12	1.10	1.13
12	1.10	1.28	1.22	1.29	1.19	1.19	1.10	1.11	1.12	1.13
13	1.07	1.10	1.11	1.17	1.28	1.38	1.12	1.00	1.12	1.12
14	1.06	1.12	1.33	1.20	1.16	1.20	1.11	1.11	1.10	1.13
15	1.16	1.18	1.13	1.12	1.13	1.36	1.14	1.11	1.08	1.09
16	1.14	1.79	1.14	1.13	1.30	1.32	1.17	1.12	1.11	1.08
17	1.21	1.14	1.26	1.28	1.49	1.49	1.15	1.11	1.09	1.10
18	1.24	1.31	1.13	1.14	1.15	1.09	1.26	1.09	1.06	1.07
19	1.23	1.22	1.16	1.12	1.08	1.11	1.17	1.15	1.06	1.08
20	1.12	1.19	1.15	1.08	1.09	1.06	1.18	1.15	1.09	1.08
21	1.08	1.27	1.17	1.09	1.09	1.08	1.19	1.17	1.11	1.09
22	1.04	1.27	1.21	1.12	1.11	1.07	1.17	1.12	1.12	1.08
23	1.04	1.19	1.17	1.11	1.10	1.03	1.15	1.13	1.11	1.08
24	1.08	1.16	1.12	1.10	1.10	1.24	1.10	1.11	1.10	1.09
25	1.10	1.22	1.09	1.10	1.08	1.08	1.11	1.16	1.10	1.10
26	1.07	1.07	1.04	1.09	1.06	1.09	1.10	1.09	1.08	1.09
27	1.02	1.08	1.00	1.10	1.09	1.08	1.08	1.09	1.10	1.11
28	0.94	0.99	0.98	0.97	0.99	1.00	1.13	1.06	1.20	1.15
29	1.05	1.11	1.23	0.89	1.06	1.11	1.17	1.14	1.12	1.11
30	1.09	1.10	1.12	1.14	1.21	1.09	1.15	1.13	1.11	1.11
31	1.11	1.11	1.09	1.11	1.09	1.23	1.13	1.11	1.14	1.10
32	1.07	1.11	1.09	1.08	1.09	1.11	1.10	1.11	1.13	1.11
33	1.05	1.09	1.09	1.08	1.09	1.10	1.08	1.09	1.12	1.11
34	1.02	1.14	1.10	1.10	1.26	1.28	1.12	1.09	1.20	1.11
35	1.01	1.08	1.19	1.22	1.26	1.26	1.11	1.09	1.09	1.10

Table 8.7: Fatigue damage rates for fitted model curve with $b = 5.0$ (2)

PSD No.			amplitude=3.0							
	2.5	3.0	0.5	1.0	1.5	2.0	2.5	3.0	0.5	1.0
1	1.14	1.09	1.09	1.12	1.12	1.16	1.14	1.12	1.11	1.15
2	1.11	1.14	1.09	1.16	1.27	1.11	1.33	1.17	1.08	1.08
3	1.11	1.13	1.08	1.09	1.08	1.09	1.10	1.11	1.07	1.08
4	1.13	1.11	1.06	1.08	1.10	1.09	1.10	1.10	1.07	1.08
5	1.11	1.13	1.08	1.07	1.09	1.10	1.08	1.10	1.08	1.07
6	1.14	1.12	1.13	1.11	1.10	1.11	1.11	1.10	1.04	1.08
7	1.22	1.11	1.09	1.13	1.14	1.14	1.08	1.09	1.09	1.06
8	1.12	1.11	1.07	1.09	1.09	1.12	1.10	1.10	1.12	1.07
9	1.12	1.12	1.08	1.07	1.09	1.10	1.10	1.11	1.09	1.06
10	1.13	1.13	1.10	1.07	1.10	1.11	1.11	1.10	1.09	1.06
11	1.25	1.24	1.10	1.18	1.16	1.10	1.19	1.17	1.07	1.10
12	1.12	1.12	1.10	1.16	1.09	1.17	1.08	1.08	1.09	1.14
13	1.14	1.26	1.12	1.07	1.10	1.08	1.18	1.18	1.11	1.04
14	1.11	1.13	1.10	1.09	1.08	1.08	1.07	1.09	1.10	1.07
15	1.07	1.06	1.12	1.08	1.06	1.06	1.05	1.05	1.10	1.06
16	1.07	1.14	1.13	1.09	1.06	1.06	1.05	1.05	1.09	1.07
17	1.09	1.09	1.14	1.08	1.06	1.05	1.04	1.04	1.10	1.07
18	1.06	1.05	1.28	1.06	0.96	1.05	1.04	1.04	1.21	1.05
19	1.07	1.07	1.13	1.11	1.07	1.05	1.05	1.04	1.13	1.08
20	1.07	1.04	1.17	1.12	1.06	1.06	1.04	1.03	1.14	1.08
21	1.06	1.06	1.17	1.13	1.08	1.07	1.04	1.29	1.14	1.08
22	1.07	1.05	1.15	1.10	1.08	1.05	1.05	1.04	1.11	1.08
23	1.07	1.06	1.12	1.09	1.08	1.06	1.05	1.05	1.11	1.09
24	1.08	1.07	1.11	1.08	1.07	1.06	1.05	1.05	1.09	1.06
25	1.08	1.09	1.07	1.10	1.07	1.07	1.07	1.07	1.07	1.08
26	1.09	1.09	1.09	1.08	1.07	1.08	1.07	1.07	1.09	1.07
27	1.11	1.09	1.08	1.09	1.10	1.11	1.08	1.08	1.09	1.08
28	1.15	1.14	1.15	1.12	1.12	1.12	1.11	1.12	1.12	1.11
29	1.10	1.10	1.14	1.13	1.11	1.08	1.07	1.07	1.13	1.11
30	1.10	1.10	1.13	1.10	1.10	1.08	1.07	1.07	1.13	1.08
31	1.09	1.10	1.09	1.07	1.09	1.08	1.07	1.08	1.08	1.07
32	1.11	1.09	1.10	1.10	1.09	1.07	1.07	1.08	1.10	1.08
33	1.13	1.12	1.07	1.08	1.10	1.09	1.09	1.08	1.13	1.08
34	1.21	1.21	1.08	1.08	1.13	1.13	1.10	1.13	1.07	1.03
35	1.13	1.13	1.07	1.07	1.07	1.09	1.09	1.10	1.08	1.06

Table 8.8: Fatigue damage rates for fitted model curve with $b = 5.0$ (3)

PSD No.	amplitude=4.0				amplitude=5.0					
	1.5	2.0	2.5	3.0	0.5	1.0	1.5	2.0	2.5	3.0
1	1.11	1.10	1.09	1.09	1.12	1.09	1.10	1.10	1.10	1.08
2	1.09	1.08	1.08	1.08	1.08	1.08	1.08	1.07	1.08	1.07
3	1.07	1.08	1.08	1.11	1.07	1.07	1.06	1.07	1.08	1.10
4	1.07	1.07	1.09	1.09	1.06	1.07	1.08	1.07	1.08	1.07
5	1.07	1.08	1.07	1.09	1.07	1.07	1.06	1.10	1.07	1.08
6	1.08	1.09	1.09	1.08	1.05	1.06	1.07	1.07	1.08	1.11
7	1.05	1.08	1.13	1.13	1.08	1.05	1.06	1.07	1.06	1.06
8	1.07	1.10	1.09	1.08	1.14	1.06	1.07	1.09	1.08	1.06
9	1.08	1.09	1.08	1.09	1.07	1.04	1.08	1.08	1.08	1.08
10	1.08	1.10	1.10	1.09	1.08	1.05	1.07	1.09	1.08	1.07
11	1.06	1.09	1.15	1.14	1.07	1.13	1.11	1.08	1.07	1.07
12	1.08	1.13	1.06	1.06	1.09	1.07	1.07	1.06	1.06	1.05
13	1.08	1.07	1.08	1.14	1.06	1.06	1.07	1.06	1.07	1.06
14	1.06	1.07	1.05	1.07	1.08	1.06	1.06	1.06	1.04	1.06
15	1.05	1.04	1.04	1.04	1.08	1.05	1.03	1.04	1.03	1.03
16	1.05	1.05	1.04	1.04	1.08	1.05	1.04	1.03	1.02	1.03
17	1.05	1.04	1.03	1.03	1.08	1.06	1.04	1.03	1.02	1.00
18	1.04	1.04	1.03	1.03	1.16	1.04	1.03	1.03	1.02	1.03
19	1.06	1.04	1.03	1.03	1.12	1.07	1.05	1.03	1.03	1.03
20	1.05	1.04	1.03	1.02	1.12	1.07	1.04	1.03	1.02	1.02
21	1.06	1.06	1.03	1.03	1.13	1.07	1.04	1.05	1.02	1.03
22	1.06	1.04	1.04	1.03	1.11	1.08	1.05	1.03	1.03	1.03
23	1.06	1.04	1.04	1.04	1.10	1.08	1.05	1.03	1.03	1.03
24	1.05	1.05	1.04	1.04	1.09	1.06	1.05	1.04	1.03	1.03
25	1.06	1.06	1.05	1.05	1.05	1.07	1.06	1.05	1.04	1.04
26	1.07	1.06	1.06	1.06	1.10	1.09	1.06	1.05	1.05	1.05
27	1.09	1.08	1.07	1.07	1.08	1.07	1.07	1.07	1.06	1.06
28	1.09	1.11	1.09	1.09	1.12	1.11	1.09	1.10	1.09	1.09
29	1.08	1.06	1.05	1.06	1.11	1.08	1.07	1.05	1.05	1.05
30	1.09	1.06	1.06	1.07	1.12	1.07	1.08	1.05	1.05	1.05
31	1.08	1.06	1.06	1.07	1.07	1.06	1.07	1.05	1.05	1.06
32	1.07	1.06	1.07	1.06	1.10	1.07	1.07	1.05	1.05	1.05
33	1.09	1.09	1.07	1.07	1.10	1.06	1.08	1.07	1.06	1.06
34	1.08	1.07	1.11	1.12	1.01	1.07	1.08	1.06	1.07	1.06
35	1.06	1.08	1.08	1.09	1.07	1.08	1.06	1.07	1.07	1.09

Table 8.9: Fatigue damage rates for fitted model curve with $b = 5.0$ (4)

PSD No.	amplitude=1.0						amplitude=2.0			
	0.5	1.0	1.5	2.0	2.5	3.0	0.5	1.0	1.5	2.0
36	1.07	1.15	1.10	1.06	1.01	1.07	1.14	1.12	1.10	1.09
37	1.13	1.34	1.31	1.06	1.08	1.17	1.12	1.12	1.11	1.08
38	1.13	1.22	1.12	1.10	1.09	1.09	1.13	1.11	1.11	1.09
39	1.11	1.13	1.12	1.11	1.10	1.09	1.15	1.12	1.12	1.11
40	1.05	1.09	1.10	1.24	1.26	1.25	1.07	1.05	1.11	1.20
41	1.07	1.09	1.12	1.26	1.28	1.29	1.08	1.07	1.10	1.10
42	1.08	1.08	1.22	1.15	1.25	1.28	1.07	1.19	1.10	1.10
43	1.09	1.17	1.28	1.08	1.08	1.11	1.12	1.15	1.11	1.08
44	1.07	1.14	1.14	1.09	1.09	1.02	1.12	1.11	1.11	1.09
45	1.12	1.14	1.10	1.10	1.11	1.10	1.15	1.11	1.10	1.09
46	1.09	1.15	1.10	1.10	1.11	1.09	1.11	1.15	1.09	1.09
47	1.10	1.13	1.14	1.12	1.12	1.13	1.12	1.11	1.12	1.09
48	1.10	1.10	1.11	1.12	1.10	1.12	1.09	1.11	1.09	1.09
49	0.98	1.10	1.11	1.13	1.12	1.12	1.08	1.11	1.09	1.10
50	1.04	1.17	1.15	1.10	1.08	0.99	1.11	1.12	1.10	1.08
51	1.06	1.23	1.17	1.09	1.07	1.13	1.18	1.11	1.11	1.08
52	1.05	1.24	1.16	1.07	1.09	1.05	1.18	1.12	1.10	1.09
53	1.03	1.22	1.12	1.07	1.10	1.04	1.15	1.12	1.08	1.08
54	1.05	1.15	1.11	1.06	1.08	1.10	1.13	1.13	1.09	1.07
55	1.10	1.11	1.08	1.10	1.10	1.05	1.12	1.12	1.07	1.06
56	1.09	1.14	1.14	1.11	1.09	1.05	1.12	1.13	1.07	1.09
57	0.99	1.19	1.22	1.11	1.08	1.08	1.13	1.13	1.10	1.08
58	1.01	1.24	1.20	1.11	1.08	1.05	1.16	1.13	1.10	1.09
59	1.01	1.18	1.16	1.12	1.10	1.10	1.14	1.13	1.09	1.07
60	1.08	1.18	1.18	1.12	1.09	1.10	1.13	1.13	1.10	1.08
61	1.11	1.18	1.19	1.13	1.09	1.07	1.14	1.12	1.11	1.09
62	1.11	1.17	1.16	1.12	1.11	1.08	1.12	1.13	1.11	1.09
63	1.01	1.15	1.17	1.12	1.13	1.06	1.09	1.12	1.10	1.09
64	1.05	1.25	1.19	1.07	1.02	1.01	1.16	1.15	1.08	1.07
65	1.02	1.22	1.21	1.08	1.06	1.09	1.17	1.16	1.09	1.07
66	0.97	1.21	1.18	1.09	1.07	1.02	1.18	1.13	1.09	1.07
67	0.97	1.21	1.18	1.10	1.05	1.00	1.18	1.15	1.08	1.08
68	0.98	1.24	1.15	1.08	1.05	1.06	1.13	1.14	1.09	1.06
69	0.98	1.19	1.14	1.10	1.04	1.07	1.12	1.14	1.08	1.08
70	1.06	1.21	1.17	1.11	1.08	1.09	1.12	1.13	1.10	1.08

Table 8.10: Fatigue damage rates for fitted model curve with $b = 5.0$ (5)

PSD No.			amplitude=3.0							
	2.5	3.0	0.5	1.0	1.5	2.0	2.5	3.0	0.5	1.0
36	1.07	1.06	1.16	1.10	1.07	1.06	1.06	1.04	1.13	1.08
37	1.09	1.20	1.14	1.08	1.09	1.07	1.07	1.06	1.12	1.07
38	1.09	1.09	1.14	1.09	1.08	1.07	1.07	1.07	1.12	1.07
39	1.10	1.10	1.13	1.09	1.10	1.07	1.07	1.08	1.11	1.08
40	1.10	1.20	1.08	1.11	1.09	1.10	1.08	1.06	1.15	1.11
41	1.10	1.11	1.15	1.09	1.08	1.08	1.09	1.16	1.12	1.08
42	1.19	1.20	1.08	1.09	1.15	1.09	1.08	1.15	1.09	1.08
43	1.08	1.07	1.16	1.11	1.08	1.06	1.06	1.05	1.13	1.11
44	1.09	1.08	1.13	1.08	1.08	1.07	1.07	1.05	1.12	1.07
45	1.09	1.08	1.14	1.08	1.08	1.07	1.08	1.06	1.12	1.08
46	1.10	1.08	1.15	1.12	1.08	1.07	1.07	1.06	1.10	1.10
47	1.10	1.10	1.16	1.11	1.08	1.08	1.08	1.08	1.13	1.10
48	1.08	1.10	0.94	1.12	1.08	1.08	1.06	1.07	1.14	1.10
49	1.10	1.09	1.10	1.08	1.07	1.08	1.08	1.07	1.13	1.09
50	1.06	1.07	1.12	1.10	1.08	1.06	1.04	1.04	1.09	1.08
51	1.07	1.06	1.21	1.09	1.08	1.06	1.05	1.05	1.17	1.08
52	1.08	1.06	1.20	1.11	1.08	1.06	1.05	1.05	1.11	1.09
53	1.07	1.06	1.17	1.09	1.06	1.06	1.05	1.04	1.09	1.08
54	1.07	1.07	1.15	1.10	1.07	1.06	1.05	1.05	1.11	1.08
55	1.07	1.06	1.11	1.09	1.06	1.06	1.06	1.04	1.10	1.10
56	1.08	1.07	1.15	1.09	1.08	1.07	1.07	1.06	1.06	1.09
57	1.07	1.07	1.10	1.09	1.08	1.06	1.06	1.04	1.10	1.09
58	1.07	1.07	1.13	1.10	1.08	1.07	1.06	1.05	1.12	1.09
59	1.08	1.08	0.92	1.10	1.07	1.06	1.05	1.06	1.15	1.08
60	1.08	1.08	1.19	1.09	1.08	1.06	1.06	1.06	1.15	1.08
61	1.08	1.08	1.16	1.09	1.08	1.07	1.06	1.06	1.12	1.07
62	1.08	1.08	1.15	1.10	1.07	1.07	1.07	1.06	1.12	1.10
63	1.08	1.09	1.13	1.13	1.08	1.07	1.06	1.06	1.10	1.10
64	1.05	1.06	1.18	1.11	1.06	1.05	1.04	1.04	1.16	1.09
65	1.06	1.06	1.19	1.13	1.06	1.05	1.04	1.04	1.14	1.10
66	1.06	1.05	1.19	1.09	1.07	1.05	1.04	1.04	1.14	1.08
67	1.06	1.05	1.21	1.09	1.06	1.07	1.04	1.04	1.18	1.08
68	1.05	1.04	1.15	1.11	1.08	1.05	1.03	1.04	1.12	1.07
69	1.06	1.06	1.09	1.10	1.07	1.06	1.04	1.04	1.14	1.09
70	1.07	1.06	1.14	1.10	1.08	1.06	1.05	1.04	1.12	1.08

Table 8.11: Fatigue damage rates for fitted model curve with $b = 5.0$ (6)

PSD No.	amplitude=4.0				amplitude=5.0					
	1.5	2.0	2.5	3.0	0.5	1.0	1.5	2.0	2.5	3.0
36	1.06	1.05	1.05	1.03	1.12	1.07	1.05	1.04	1.04	1.03
37	1.08	1.05	1.05	1.04	1.10	1.06	1.07	1.05	1.05	1.04
38	1.07	1.05	1.05	1.05	1.11	1.07	1.06	1.05	1.04	1.05
39	1.08	1.06	1.06	1.06	1.10	1.08	1.07	1.06	1.05	1.05
40	1.08	1.07	1.08	1.05	1.01	1.08	1.06	1.05	1.06	1.04
41	1.07	1.07	1.08	1.12	1.04	1.08	1.07	1.07	1.07	1.10
42	1.07	1.07	1.06	1.13	1.08	1.06	1.07	1.07	1.06	1.06
43	1.06	1.04	1.05	1.04	1.11	1.09	1.05	1.03	1.04	1.04
44	1.07	1.05	1.05	1.04	1.09	1.05	1.05	1.04	1.04	1.03
45	1.07	1.05	1.06	1.05	1.10	1.08	1.06	1.05	1.05	1.04
46	1.05	1.06	1.06	1.05	1.09	1.08	1.05	1.04	1.05	1.04
47	1.08	1.06	1.06	1.06	1.14	1.09	1.07	1.06	1.06	1.05
48	1.07	1.06	1.05	1.06	1.13	1.08	1.06	1.05	1.05	1.05
49	1.06	1.07	1.07	1.06	1.12	1.07	1.05	1.06	1.06	1.05
50	1.06	1.04	1.03	1.03	1.08	1.07	1.05	1.03	1.02	1.03
51	1.07	1.04	1.04	1.04	1.14	1.07	1.06	1.04	1.03	1.03
52	1.06	1.05	1.04	1.04	1.16	1.07	1.05	1.05	1.03	1.03
53	1.05	1.05	1.04	1.03	1.14	1.07	1.04	1.04	1.04	1.03
54	1.05	1.05	1.04	1.04	1.09	1.08	1.05	1.04	1.03	1.04
55	1.05	1.05	1.04	1.03	1.09	1.08	1.05	1.04	1.04	1.03
56	1.07	1.06	1.06	1.05	1.05	1.08	1.06	1.05	1.05	1.04
57	1.07	1.05	1.04	1.03	1.12	1.07	1.06	1.04	1.04	1.03
58	1.05	1.06	1.04	1.04	1.10	1.07	1.04	1.05	1.04	1.03
59	1.06	1.05	1.05	1.05	1.12	1.06	1.05	1.04	1.04	1.04
60	1.06	1.05	1.05	1.04	1.12	1.07	1.05	1.04	1.05	1.04
61	1.06	1.05	1.05	1.05	1.10	1.07	1.06	1.05	1.04	1.04
62	1.06	1.06	1.05	1.04	1.10	1.08	1.05	1.05	1.04	1.03
63	1.07	1.06	1.05	1.05	1.10	1.08	1.07	1.05	1.04	1.04
64	1.05	1.04	1.03	1.03	1.13	1.07	1.04	1.03	1.02	1.03
65	1.05	1.04	1.03	1.03	1.14	1.08	1.05	1.03	1.03	1.03
66	1.05	1.04	1.03	1.03	1.11	1.07	1.04	1.03	1.02	1.02
67	1.05	1.05	1.03	1.03	1.14	0.83	1.04	1.04	1.02	1.03
68	1.06	1.04	1.03	1.03	1.11	1.07	1.05	1.03	1.02	1.02
69	1.06	1.05	1.03	1.03	1.07	1.07	1.05	1.05	1.02	1.03
70	1.06	1.05	1.04	1.03	1.10	1.07	1.06	1.04	1.04	1.03

8.5 An introduction to neural computation

8.5.1 Basic structure of neural network

Introduction

Neural computing is a new computer information processing technique quite different to conventional *programmed computing* [87] [88]. Programmed computing approaches are based on devising an algorithm and a set of rules for solving the problem and then correctly coding these in software. If the required algorithm and set of rules are not known, then they must be developed — even if it is very difficult and time consuming. Neural computing is a new approach that does not require the algorithm to be known or any rule development. For some types of problems such as pattern recognition or data analysis and control where rule development is impossible or too difficult, Neural computing offers many possibilities.

Definition of a neural network

The primary structures in neural computing is the *neural network* which is defined as follows.

• DEFINITION • A neural network is a parallel, distributed information processing structure consisting of processing elements (which can process a local memory and can carry out localised information processing operations) interconnected via undirectional signal channels called connections. Each processing element has a single output connection that branches ("fans out") into as many collateral connections as desired; each carries the same signal – the processing element output signal. The processing element output signal can be of any mathematical type desired. The information processing that goes on within each processing element can be defined arbitrarily with the restriction that it must be completely local; that is, it must depend only on the current values of the input signals at the processing element via impinging connections and on values stored in the processing element's local memory.

According to this definition, neural networks are composed of processing elements and connections. It is therefore a parallel distributed information processing structure in the form of directed graph, i.e., a geometrical object consisting of a set of points (called *nodes*) along with a set of directed line segments (called *links* between them), with the following sub-definitions and restrictions:

1. The nodes of the graph are called *processing elements* (or *neurons*).

2. The links of the graph are called *connection.* Each connection function as an instantaneous undirectional signal-conduction path.

3. Each processing element can receive any number of incoming connections (also called *input connections*).

4. Each processing element can have any number of outgoing connections, but the signals in all these must be the same. In effect, each processing element has a single *output connection* that can branch or *fan out* into copies to form multiple output connections, each of which carries the same identical signal (the processing element's *output signal*).

5. Processing elements can have *local memory.*

6. Each processing element possesses a *transfer function* which uses local memory on the input signals, thereby producing the processing element's output signal. In other words, the only inputs allowed to the transfer function are the values stored in the processing element's local memory and the current value of the input signals in the connections received by the processing element. The only output allowed from the transfer function is the value stored in the processing element's local memory and the processing element's output signal. Transfer functions can operate *continuously* or *episodically.* If they operate episodically, there must be an input called "*activate*" that causes the processing element's transfer function to operate on the current input signal and local memory value to produce an *updated* output signal (and possibly to modify the local memory value). Continuous processing elements are always operating. The "activate" input arrives via a connection from a *scheduling* element that is part of the network.

7. Input signals to a neural network from outside the network arrive via connections that originate in the outside world. Outputs from the network to the outside world are connections that leave the network.

Figure 8.12 shows a typical neural network architecture and Figure 8.13 shows the internal details of a neural network processing element. The processing element transfer function receives, as input, the signals arriving via the incoming connections which impinge upon the processing element, as well as values from local memory. Given these inputs, the transfer function outputs values to be stored in specified locations in local memory, as well as supplying the processing element's output signal. The output signal then branches into copies after leaving the processing element.

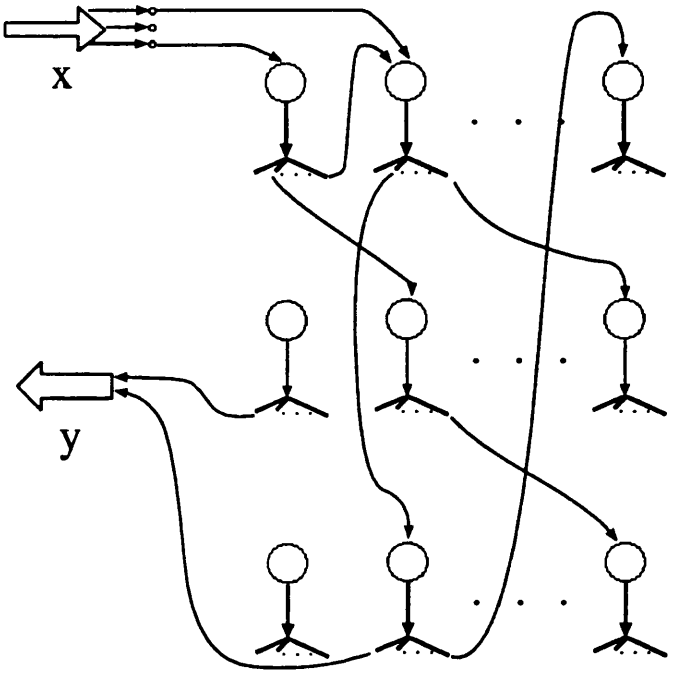

Figure 8.12: A typical neural network architecture

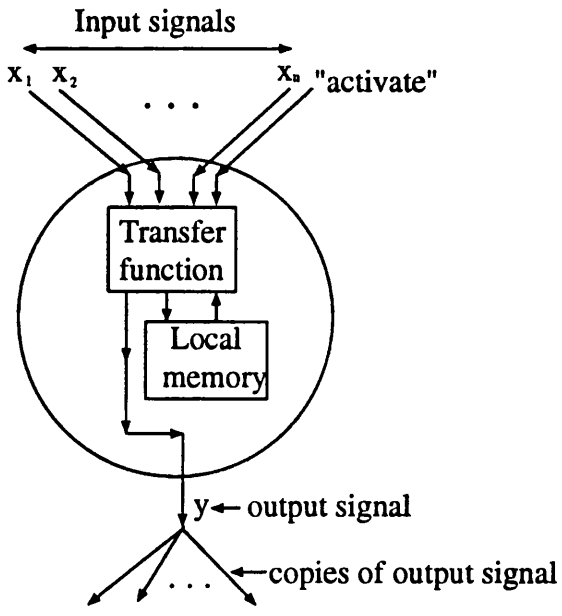

Figure 8.13: A generic processing element

Transfer functions and local memories

The transfer function receives values from the incoming connections and from local memory. It produces outputs from the processing element and values from storage in the local memory. Each time an active signal is sent, these operations are performed. If the neural network is not continuously running, the processing element ceases to function after each operation is performed.

A typical example of such a transfer function is a case where the input signal (assumed to be a floating point number) of the connections are combined to form a weighted sum of the form $I_k = \mathbf{w_k} \cdot \mathbf{x_k}$ for input class k with $\mathbf{x_k}$ as the input vector and $\mathbf{w_k}$ as the *weight.* A weight is a local memory variable of a specified data type assigned to input connections. A vector which has weights as components is known as a *weight vector.*

Training of a neural network

Weight plays a very important rule in most neural networks that have learning capabilities. Learning is accomplished through a modification of the processing element weights. There are many kinds of training methods for different types of networks which depend on different learning laws. There can be divided into *supervised training, graded training* , and *self-organised training* at the fundamental level.

Supervised training is used in this thesis. This type of training is generally used for the situation where the network is functioning as an input/output system. In other words, the network receives an input vector $\mathbf{x}$ and emits a vector $\mathbf{y}$. Supervised training for such a system implies a regimen in which the network is supplied with a sequence of examples $(\mathbf{x_1}, \mathbf{y_1}), (\mathbf{x_2}, \mathbf{y_2}), ..., (\mathbf{x_k}, \mathbf{y_k}),...$ of "desirable" or "correct" input/output pairs. As each input $\mathbf{x_k}$ is entered into the neural network, the "correct output" $\mathbf{y_k}$ is also supplied to the network. The network is thus told precisely what it should be emitting as its output. The actual output is then taken as an estimation of the correct output.

In many supervised training situations the $(\mathbf{x_k}, \mathbf{y_k})$ pairs used during training are assumed to be examples of a fixed function f. The neural network is then used to identify the system. It is generally of use for situations where examples can be obtained but where the function is difficult to establish using traditional regression methods. This type of network is introduced in the following section.

8.5.2 Mapping Networks

The approximation of mathematical functions is an important issue in many fields. Numerous methods have been developed to solve this problem. Essentially, all of them can be regarded as variants of regression analysis. Neural networks are more capable of doing this kind work. Neural networks can be viewed as a type of regression that in some ways generalises traditional regression approaches. One kind of multi-layer data transformation network is back propagation neural network(BPN). This is the method used in this thesis and is introduced here.

The Structure of a back propagation network

The typical structure of a back propagation network is shown in Figure 8.14 [89]. Basically, this type of neural network has a fully interconnected multi-layer structure. It uses supervised training.

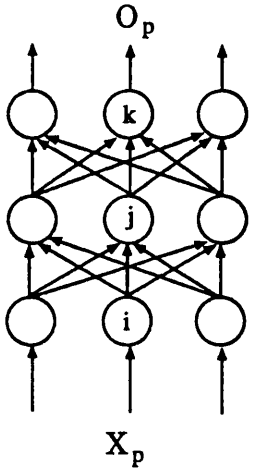

Figure 8.14: Layout of back propagation network

Along with the arrow direction of the connections, the first layer is the input layer which read in the inputs $\mathbf{x_p}$ from the input/output pairs $(\mathbf{x_1}, \mathbf{y_1})$, $(\mathbf{x_2}, \mathbf{y_2})$, ..., $(\mathbf{x_k}, \mathbf{y_k})$. The last layer, the output layer, gives the estimation results of $\mathbf{y_p}$. The layers in between are the so-called *hidden layers.* The size of the input and output layers is determined by the function which the network is modelling. The number of hidden layers and the sizes for each layer, however, can in theory be arbitrary. According to the Kolmogorov's mapping neural network existence theorem [87] (p122), any continuous function of n variables can be implemented exactly by a three layer network with *(2n+1)* processing elements in the hidden layer. This theorem provides some guidance for the selection of the hidden layer

size.

The work of a back propagation network can be divided into a *forward pass* and a *backward pass*. The backward pass only occurs on training trials. This forward and backward pass form a loop during the network training which is used to search for a set of weights which gives the network its optimum performance. Mathematically, the optimum performance means the best estimation of the desired output (or least error between them). After the training process, this set of weights can be regarded as one special regression of the function relationship between the input and output. The trained network can then be used for further computation using an input for which the desired output is not known.

Forward pass

The inputs for the processing elements in the input layer are determined by the system input. For any processing elements in the hidden layer and output layer, the input from the connections are taken as the weighted sum, that is,

$$net_{pj} = \sum_i w_{ji} o_{pi} \tag{8.29}$$

The output from each processing element j can be assumed as any differentiable monotonic function,

$$o_{pj} = f_j(net_{pj}) \tag{8.30}$$

From the output layer, the estimation for function value $\mathbf{y_p}$ can then be obtained :

$$net^o_{pk} = \sum_j w^o_{kj} o_{pj} \tag{8.31}$$

$$o_{pk} = f^o_k(net^o_{pk}) \tag{8.32}$$

The superscript "o" here refers to the quantities on the output layer.

Backward propagation

During the network training, the mean square error of the output vector is taken as an objective function which need to be minimised. The error can be defined as $\delta_{pk} = (y_{pk} - o_{pk})$. The total error of the output layer is

$$E_p = \frac{1}{2} \sum_k \delta^2_{pk} \tag{8.33}$$

The value $\frac{1}{2}$ here is used to make the calculation process easier. The values of the weights can be adjusted such that the total error reduces. This can be done

by using a gradient direction search, such as

$$\frac{\partial E_p}{\partial w_{kj}^o} = -(y_{pk} - o_{pk}) \frac{\partial f_k^o}{\partial net_{pk}^o} \frac{\partial net_{pk}^o}{\partial w_{kj}^o} \tag{8.34}$$

As $\frac{\partial net_{pk}^o}{\partial w_{kj}^o} = o_{pj}$, the negative gradient direction is:

$$-\frac{\partial E_p}{\partial w_{kj}^o} = (y_{pk} - o_{pk}) f_k^{o'}(net_{pk}^o) o_{pj} \tag{8.35}$$

If the sigmoid function is used, then

$$f(net_{jk}^o) = \frac{1}{1 + e^{-\mu \cdot net_{jk}^o}} \tag{8.36}$$

and

$$f^{o'} = \mu f_k^o (1 - f_k^o) = \mu o_{pk}(1 - o_{pk}) \tag{8.37}$$

where μ is a constant.

By defining a step size η and a quantity as

$$\delta_{pk}^o = (y_{pk} - o_{pk}) f_k^{o'}(net_{pk}^o) \tag{8.38}$$

The weights can be upgraded as

$$w_{kj}^o \Leftarrow w_{kj}^o + \eta_{pk}^o \delta_{pk}^o o_{pj} \tag{8.39}$$

Following on further, the weights of the hidden layers can be upgraded by changing δ_{pk}^o to

$$\delta_{pj}^h = f_j^{h'}(net_{pj}^h) \sum_k \delta_{pk}^o w_{kj} \tag{8.40}$$

Considerations in network training

The back propagation algorithm described previously provides a way of network training. Implementation of the algorithm is, in many ways, a more difficult problem. Since the weights are generally assigned as random initial values at the beginning of the training loop, the problem which arises is how can the network find a global minimum in the error space. As shown in Figure 8.15, it is quite possible for a network to cease its training loop at a local stationery point.

This is a general problem for nonlinear programming and there is no universal panacea. Four steps have been taken to avoid such problems arising.

1). Different initial values for the weight and bias were used;

2). Different size of network were tested;

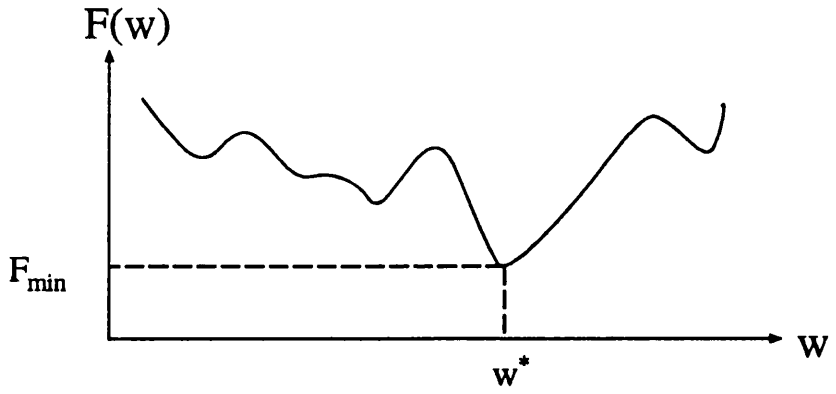

Figure 8.15: A typical error surface.

3). The iteration was allows to jump out from a stationary point and search in a wider area;

4). An "eye test" (plot checking) was used to compare the results with the time domain analysis results.

Some results have also been compared with least square fitted results.

8.6 The use of neural networks for fatigue analysis

8.6.1 Toolbox for fatigue analysis of random stress histories with deterministic component

The fatigue damage for a situation where a stochastic stress history is combined with a deterministic components can be calculated using model Equation 8.11. The problem which remains is how should the model parameters be calculated using the frequency domain and deterministic component information instead of following the whole procedure. This is the task of regression. The spectrum can be well characterised by its mean frequency f_m and its irregularity factor γ and the deterministic component can be described by its amplitude A and frequency f_d.

Thus, the task remaining is the determination of the relationship between the following parameters:

- *input* : f_m, γ, A, f_d
- *output*: C_1, C_2, C_3, τ, α, β, μ, $E[P]$

Once the model parameters have been evaluated by employing least square

techniques, examples between model parameters and the stress history information are obtained. The relationship could then be established using traditional regression methods. However, for the multi-input situation and with such a large number of cases, regression is not an easy task. Moreover, regression analysis has to be performed for each output parameter. The neural network approach is therefore a much better alternative in this situation.

A four-layer network was established for each of the output parameters. These subnets worked together just like one network in order to perform the calculation. The network training, of course, is performed on each subnetwork. As mentioned earlier during the network training, the network was allowed to "get off" the local stationery point. This made the search for the global minimum possible but results in a longer training time.

Some networks converged monotonically, while others had to be pulled out from local stationary points. Figure 8.16 shows the convergence path of μ, σ, C_2 and $E[P]$ for a typical network.

Some rainflow cycle PDF's calculated using this neural network toolbox are plotted in Figure 8.17, together with the time domain analysis results. As with least square fitting, the higher range part is magnified by 10 and plotted on the same graph for visualisation purpose.

The residual of the neural network output with the training data was not checked directly. Again, they were checked using a comparison of the fatigue damage rates with the time domain results. For an S-N curve slope b=5.0, the results are listed in Table 8.14 to Table 8.19. The values in the second row of these tables refer to the frequency of the deterministic component. These tables show that the neural network toolbox can give results which meet quite well with the time domain solution.

8.6.2 Toolbox of fatigue design for Gaussian stress histories

A regression analysis on the model parameters evaluated by least square curve fitting in the previous section leads to a formula for the PDF when the stress responses are assumed to be Gaussian. However, this regression analysis has been performed using multilayer neural network in order to maintain consistency with the toolbox developed for the situation when the random signals are combined with one significant deterministic component. As stated before, such a neural network approach needs no model for the output data.

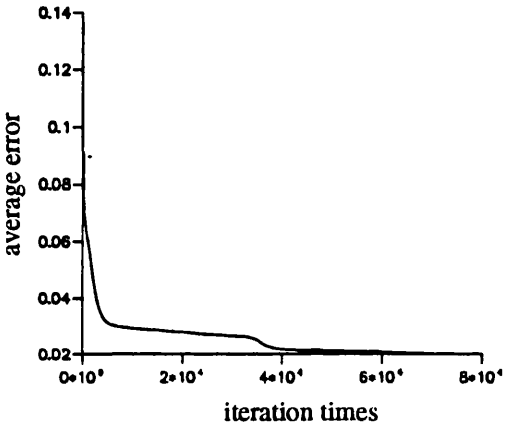

(a). convergence path of σ

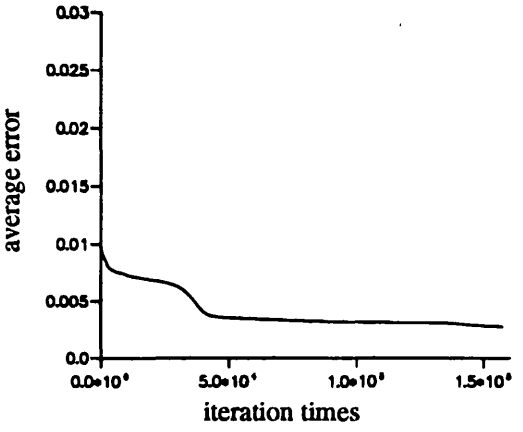

(b). convergence path of μ

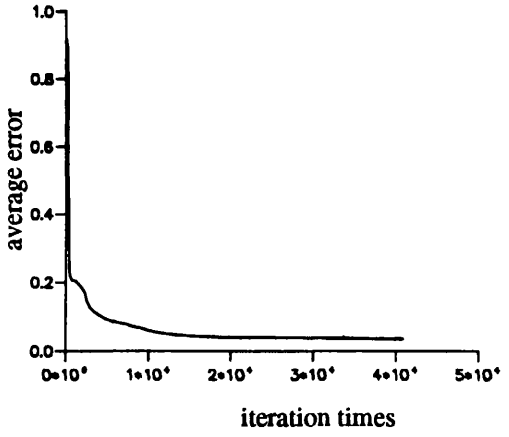

(c). convergence path of C_2

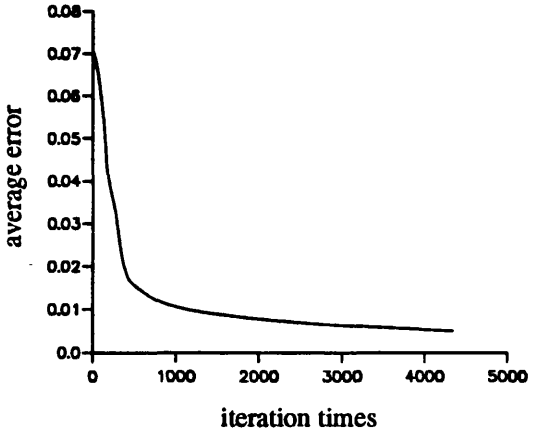

(b). convergence path of E[P]

Figure 8.16: Convergence path of μ, σ, C_2 and $E[P]$

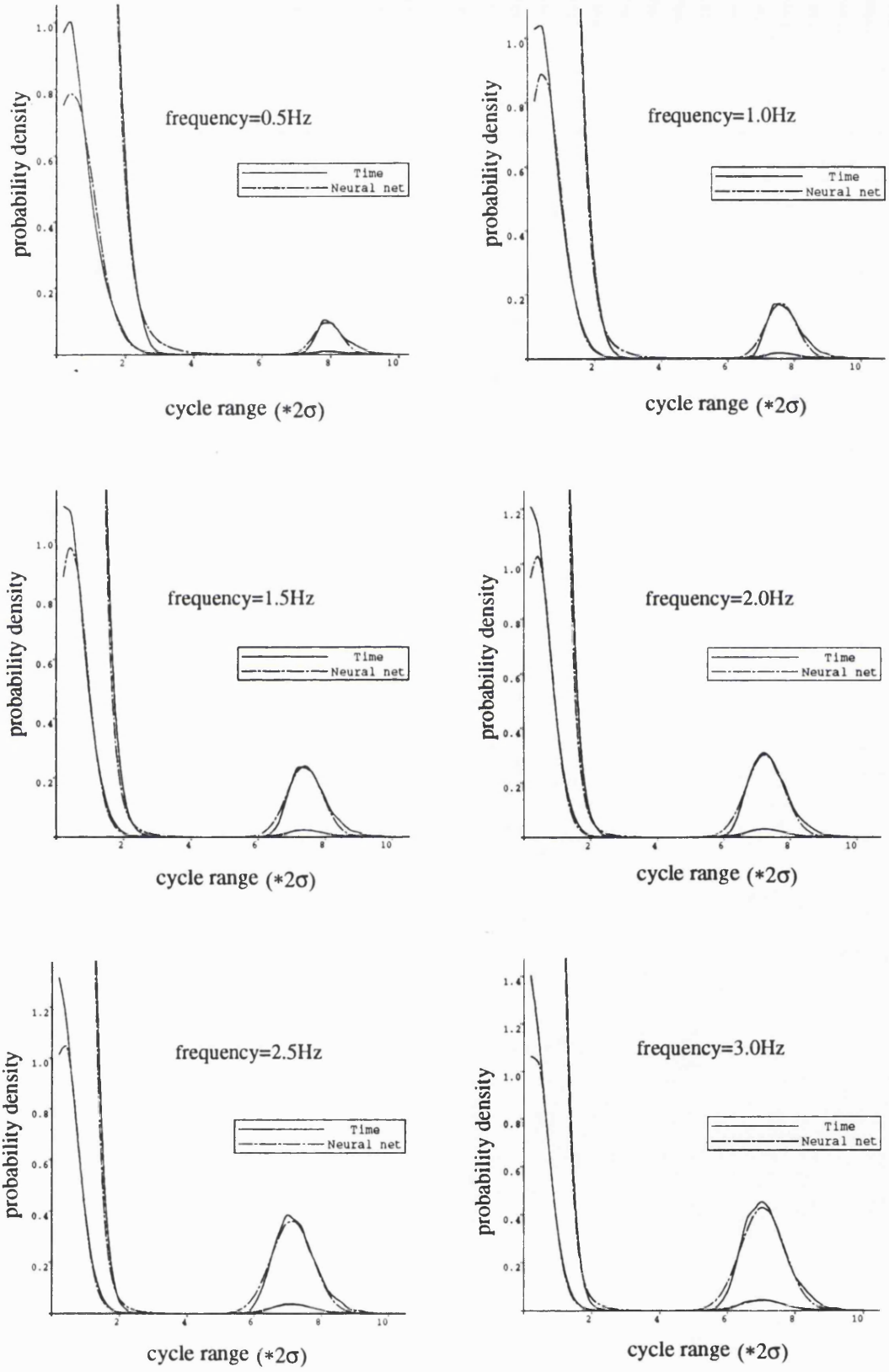

Figure 8.17: Neural network prediction for spectra 60

The input and output layer of the network are:

- *input* : f_m, γ
- *output* : C_1, C_2, C_3, τ, α

The peak rate is calculated as $E[P] = \sqrt{m_4/m_2}$ as the signal is assumed as Gaussian.

Four three layer networks were established for this problem. They were separately intended to perform a regression analysis for C_2, C_3, τ, and α. C_1 is calculated as $C_1 = 1.0 - C_2 - C_3$. Once training of the networks was completed, the data was used together with the combined signal results to form a complete toolbox for doing fatigue analysis. The convergence paths for the four parameters are shown in Figure 8.18.

Figure 8.19 shows the rainflow cycle PDF's from both the time domain analysis and neural network computation, together with the corresponding damage densities.

The model parameters obtained for the 70 sets of data used for training are given in Tables 8.12 and 8.13 along with the damage rates when *b=5.0* and *b=8.0* are used. These damage rates show that the fatigue damage calculated from the neural network has a reasonable consistency with the time domain analysis.

8.7 Discussion

Some previous research work has been devoted to the fatigue analysis of random response histories which contain one deterministic component [79] [53]. However, most of them are unsatisfactory for different reason [79]. Madsen's formula can not be expected to work well [53] because this method simply employs a correction factor method for the random response and an interpolation using confluent hypergeometric functions which has no theoretical background. The most important conclusion is, that it does not make sense to interpolate the damage between the purely stochastic and deterministic component.

A neural network toolbox for the fatigue analysis of a random response history which contains one deterministic component is developed in this chapter. A typical application of this toolbox is the fatigue analysis of wind turbine blades. Analysis of the monitored response histories in the previous chapters has shown that the existence of deterministic component cause serious problem when other

methods are employed in the analysis. The toolbox developed in this chapter is of particular significance for such structures.

Because of the complexity involved in developing a theoretical solution for the combined signal problem, a numerical simulation method was adopted instead to solve this problem. As seen from the output results of the neural network toolbox developed in this chapter, the simulation worked successfully. This means that both the parameter evaluation and neural network training were successful.

In principle, the toolbox can be extended to the situation where there are more than one deterministic components existing in the response history. The procedure would be the same as in this chapter but more attention should be paid to the selection of models and parameters. The relative phase between the sine wave would also be important for such situations.

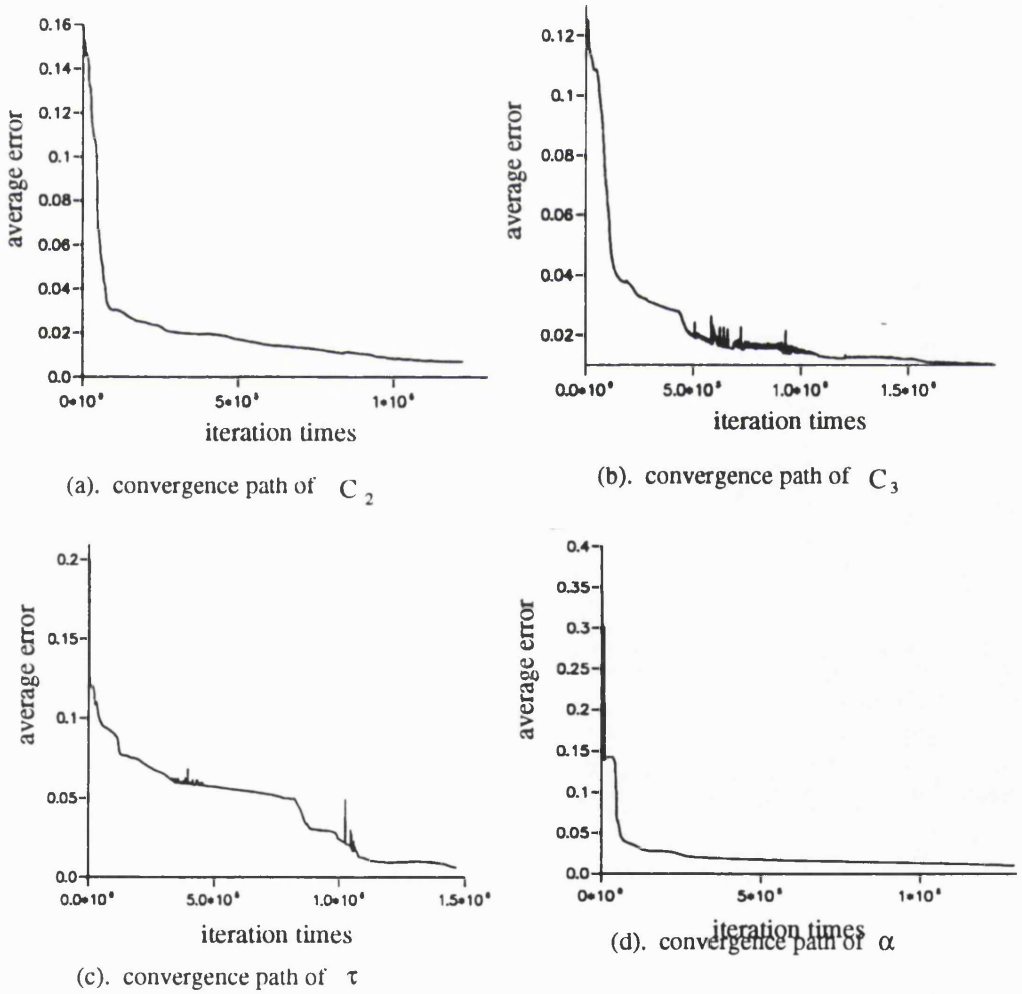

Figure 8.18: Convergence path of the parameters for Gaussian model

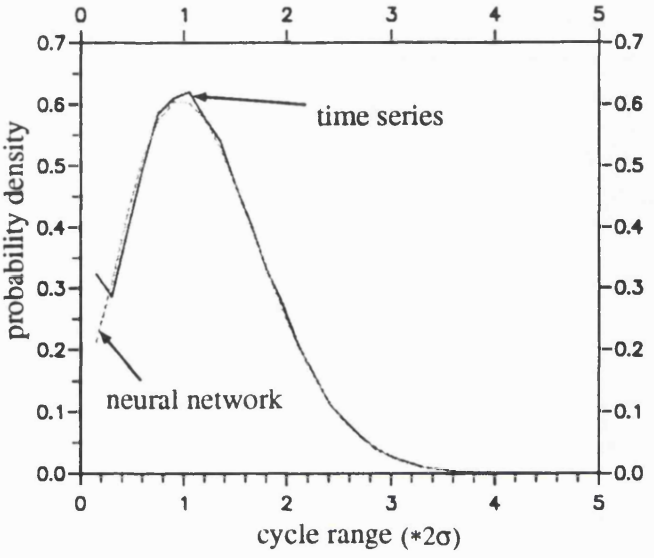

(a). rainflow cycle probability density

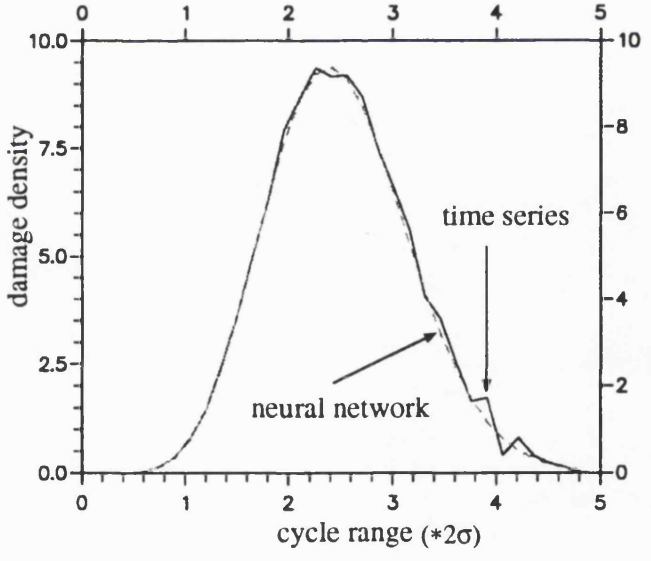

(a). fatigue damage density

Figure 8.19: The rainflow cycle PDF's and fatigue damage density functions from time domain analysis and neural network computation

Table 8.12: Model parameters calculated from neural network toolbox for the 70 PSD's use.

No.	C_1	C_2	C_3	τ	α	$D_{b=5}$	$D_{b=8}$
1	0.0263	0.7187	0.2550	0.1111	0.9286	0.9816	0.9636
2	0.0685	0.6691	0.2623	0.1545	0.9386	1.0357	1.0640
3	0.0806	0.8795	0.0399	0.1635	0.9608	1.0537	1.0820
4	0.1781	0.4494	0.3725	0.1689	0.9743	1.0369	1.0927
5	0.2506	0.3822	0.3672	0.2005	1.0072	1.0497	1.1327
6	0.4343	0.5594	0.0063	0.3368	1.1072	1.1047	1.3232
7	0.7022	0.2785	0.0192	0.4992	1.2739	1.1258	1.5224
8	0.5744	0.4145	0.0112	0.3008	1.1835	1.1071	1.3888
9	0.5692	0.4292	0.0017	0.2520	1.1560	1.0625	1.3031
10	0.5226	0.4748	0.0027	0.1959	1.0997	1.0317	1.2019
11	0.5069	0.4867	0.0064	0.1901	1.0919	1.0305	1.1816
12	0.5802	0.2176	0.2022	0.2106	1.2180	1.0524	1.2590
13	0.6888	0.1560	0.1553	0.1739	1.2995	1.0819	1.3677
14	0.8029	0.0753	0.1218	0.1770	1.5392	0.9492	1.3107
15	0.8942	0.0495	0.0563	0.1330	1.5286	0.9298	1.3409
16	0.9196	0.0379	0.0425	0.1709	1.6305	0.9200	1.3236
17	0.9258	0.0355	0.0386	0.2310	1.6361	0.8848	1.2337
18	0.9851	0.0073	0.0077	0.3533	1.6786	0.3240	0.3289
19	0.2324	0.6420	0.1256	0.3651	0.1118	0.6239	0.5453
20	0.2858	0.6246	0.0896	0.5572	0.1712	0.8171	0.9030
21	0.2337	0.6418	0.1245	0.5490	0.2015	0.8682	0.9642
22	0.1761	0.6388	0.1851	0.6640	0.2360	0.9939	1.2231
23	0.1326	0.6143	0.2531	0.6294	0.3135	0.9915	1.0915
24	0.1163	0.5404	0.3432	0.6528	0.3630	1.0303	1.1468
25	0.1107	0.5287	0.3606	0.5300	0.4397	0.9998	1.0865
26	0.0645	0.5282	0.4073	0.1630	0.6321	0.9412	0.9161
27	0.0362	0.4899	0.4739	0.1150	0.6991	1.0035	1.0307
28	0.0306	0.5563	0.4130	1.0278	0.7282	1.0938	1.3307
29	0.0741	0.6281	0.2978	0.5843	0.5643	1.0463	1.1802
30	0.0649	0.5318	0.4032	0.5747	0.5525	1.0624	1.1959
31	0.0504	0.4605	0.4892	0.5414	0.5250	1.0786	1.1988
32	0.0581	0.4261	0.5158	0.1713	0.5427	1.0207	1.1023
33	0.0885	0.4739	0.4376	0.4197	0.6841	0.9894	1.0139
34	0.1475	0.6256	0.2269	0.2647	0.8426	0.9478	0.9448
35	0.0335	0.8945	0.0721	0.1797	0.9052	1.1036	1.1258

Table 8.13: Model parameters calculated from neural network toolbox for the 70 PSD's use.

No.	C_1	C_2	C_3	τ	α	$D_{b=5}$	$D_{b=8}$
36	0.0772	0.6717	0.2510	0.5180	0.4767	1.0733	1.2122
37	0.0956	0.5771	0.3273	0.5277	0.4464	1.0499	1.1623
38	0.1139	0.4864	0.3996	0.5265	0.4288	1.0816	1.1953
39	0.1739	0.3619	0.4642	0.5107	0.4164	1.0772	1.2083
40	0.1976	0.3238	0.4786	0.5039	0.4504	1.0148	1.1205
41	0.2531	0.3255	0.4214	0.5750	0.6277	1.0274	1.1682
42	0.2361	0.4322	0.3317	0.4541	0.8170	0.9909	1.0113
43	0.1016	0.6855	0.2129	0.5375	0.3744	1.0425	1.1876
44	0.1608	0.5457	0.2934	0.5209	0.3510	1.0217	1.1251
45	0.1330	0.5225	0.3445	0.5489	0.3640	1.0191	1.0959
46	0.1213	0.4551	0.4236	0.3607	0.3774	0.9645	0.9680
47	0.2527	0.2704	0.4769	0.5007	0.3272	1.0374	1.1060
48	0.2937	0.2473	0.4591	0.5092	0.4412	0.9971	1.0921
49	0.3975	0.3103	0.2922	0.6046	0.7332	1.0455	1.2710
50	0.1542	0.6294	0.2163	0.5084	0.3087	1.0116	1.0749
51	0.1473	0.6219	0.2308	0.5161	0.3181	0.9805	0.9915
52	0.1239	0.6111	0.2651	0.5481	0.3164	0.9218	0.9108
53	0.1994	0.5641	0.2365	0.7335	0.3300	1.0889	1.5005
54	0.2832	0.4638	0.2530	0.6596	0.3707	1.0367	1.3381
55	0.2152	0.4669	0.3179	0.3124	0.3919	0.7974	0.7291
56	0.3431	0.2577	0.3992	0.5081	0.3024	0.9691	1.0496
57	0.2593	0.5618	0.1789	0.5511	0.2222	0.9562	1.0875
58	0.2611	0.5396	0.1993	0.5414	0.2225	0.9007	0.9713
59	0.2852	0.4885	0.2263	0.5527	0.2200	0.9475	1.0365
60	0.3161	0.4017	0.2822	0.5355	0.2211	0.9684	1.0533
61	0.3453	0.3772	0.2776	0.5369	0.2223	0.9153	1.0212
62	0.3648	0.3226	0.3126	0.5228	0.2153	0.9031	0.9473
63	0.4324	0.2291	0.3385	0.5128	0.1871	0.9301	0.9965
64	0.2481	0.6395	0.1125	0.5075	0.1968	0.7771	0.8209
65	0.2407	0.6417	0.1176	0.6136	0.2010	0.9082	1.0989
66	0.2484	0.6330	0.1186	0.6996	0.2038	1.0413	1.4639
67	0.2600	0.6319	0.1081	0.7082	0.2015	1.0840	1.6058
68	0.2378	0.5932	0.1690	0.2914	0.2103	0.5750	0.4966
69	0.2416	0.5536	0.2048	0.3117	0.2147	0.6600	0.5845
70	0.4637	0.3839	0.1524	0.5861	0.2272	0.8737	1.0505

Table 8.14: Fatigue damage rates from neural toolbox $b = 5.0$ (1)

PSD No.	amplitude=1.0						amplitude=2.0			
	0.5	1.0	1.5	2.0	2.5	3.0	0.5	1.0	1.5	2.0
1	1.16	1.23	1.23	1.26	1.28	1.30	1.16	1.24	1.22	1.22
2	1.05	1.13	1.13	1.13	1.15	1.19	1.07	1.17	1.15	1.13
3	0.99	1.06	1.08	1.08	1.11	1.15	1.00	1.11	1.10	1.08
4	1.01	1.10	1.12	1.15	1.19	1.23	1.03	1.13	1.13	1.12
5	1.05	1.16	1.19	1.23	1.27	1.32	1.07	1.18	1.17	1.18
6	1.02	1.07	1.09	1.12	1.17	1.21	1.01	1.08	1.08	1.10
7	0.98	1.05	1.08	1.11	1.13	1.15	1.01	1.08	1.08	1.08
8	1.03	1.11	1.12	1.16	1.19	1.21	1.03	1.10	1.09	1.10
9	1.04	1.11	1.14	1.19	1.23	1.24	1.05	1.10	1.10	1.11
10	1.06	1.17	1.20	1.25	1.29	1.28	1.08	1.14	1.13	1.14
11	1.15	1.22	1.26	1.34	1.36	1.29	1.17	1.17	1.17	1.19
12	1.03	1.13	1.19	1.22	1.20	1.10	1.08	1.11	1.11	1.11
13	0.92	1.03	1.09	1.15	1.19	1.20	1.01	1.06	1.06	1.07
14	0.97	1.12	1.21	1.25	1.25	1.25	1.03	1.11	1.10	1.09
15	1.00	1.10	1.12	1.15	1.12	1.08	0.98	1.03	1.02	1.03
16	0.93	1.06	1.10	1.07	1.07	1.06	1.01	1.03	1.00	0.99
17	0.75	0.89	0.96	0.98	0.98	0.96	1.02	1.06	1.01	0.98
18	1.13	1.25	1.20	1.14	1.07	1.04	1.20	1.16	1.07	1.02
19	1.09	1.26	1.18	1.08	1.03	0.98	1.21	1.17	1.07	1.00
20	0.86	1.04	1.09	1.05	0.99	0.93	1.16	1.13	1.06	1.01
21	0.84	0.99	1.04	1.04	0.98	0.96	1.13	1.14	1.07	1.04
22	0.78	0.96	1.04	1.06	1.05	1.04	1.13	1.20	1.16	1.11
23	0.82	0.99	1.05	1.07	1.06	1.06	1.13	1.22	1.18	1.13
24	0.85	1.07	1.14	1.14	1.14	1.12	1.14	1.24	1.20	1.15
25	0.92	1.12	1.19	1.20	1.18	1.18	1.16	1.24	1.23	1.19
26	1.10	1.22	1.24	1.25	1.26	1.27	1.15	1.26	1.24	1.22
27	1.18	1.31	1.36	1.36	1.38	1.40	1.26	1.37	1.37	1.34
28	1.06	1.11	1.11	1.12	1.13	1.17	1.15	1.23	1.23	1.25
29	0.94	1.07	1.07	1.06	1.04	1.05	1.05	1.13	1.11	1.10
30	1.16	1.27	1.27	1.25	1.24	1.23	1.20	1.29	1.25	1.22
31	1.18	1.29	1.31	1.29	1.29	1.29	1.22	1.32	1.29	1.25
32	1.15	1.28	1.30	1.31	1.30	1.31	1.20	1.32	1.29	1.27
33	1.10	1.22	1.25	1.26	1.28	1.29	1.18	1.29	1.27	1.25
34	1.06	1.17	1.19	1.21	1.23	1.25	1.14	1.25	1.24	1.23
35	1.03	1.12	1.15	1.17	1.20	1.23	1.11	1.22	1.22	1.21

Table 8.15: Fatigue damage rates from neural toolbox $b = 5.0$ (2)

PSD No.			amplitude=3.0							
	2.5	3.0	0.5	1.0	1.5	2.0	2.5	3.0	0.5	1.0
1	1.22	1.22	1.08	1.20	1.20	1.19	1.18	1.18	1.02	1.16
2	1.13	1.14	1.03	1.16	1.15	1.13	1.12	1.12	0.99	1.13
3	1.09	1.10	0.98	1.12	1.12	1.09	1.10	1.11	0.97	1.11
4	1.14	1.15	1.02	1.14	1.15	1.13	1.14	1.14	1.00	1.13
5	1.20	1.21	1.07	1.19	1.18	1.18	1.18	1.19	1.05	1.17
6	1.11	1.13	1.02	1.10	1.10	1.10	1.11	1.12	1.02	1.10
7	1.08	1.08	1.02	1.09	1.08	1.07	1.07	1.07	1.02	1.08
8	1.10	1.11	1.04	1.10	1.09	1.08	1.08	1.08	1.05	1.09
9	1.13	1.11	1.07	1.10	1.09	1.09	1.10	1.08	1.08	1.09
10	1.15	1.13	1.10	1.13	1.11	1.11	1.11	1.09	1.12	1.13
11	1.17	1.10	1.18	1.15	1.13	1.14	1.12	1.06	1.19	1.13
12	1.08	0.98	1.12	1.11	1.08	1.08	1.05	0.98	1.14	1.11
13	1.07	1.07	1.10	1.12	1.08	1.06	1.05	1.05	1.10	1.13
14	1.07	1.07	1.10	1.13	1.08	1.04	1.03	1.02	1.08	1.10
15	1.01	1.02	1.03	1.05	1.02	1.02	1.02	1.03	1.00	1.04
16	1.00	1.00	1.06	1.06	1.00	0.97	0.98	0.98	1.04	1.04
17	0.98	0.99	1.09	1.08	1.01	0.98	0.98	1.00	1.06	1.07
18	0.99	1.00	1.12	1.10	1.01	0.97	0.96	0.99	1.05	1.07
19	0.99	0.98	1.12	1.10	1.01	0.96	0.96	0.97	1.04	1.06
20	0.99	0.98	1.10	1.07	1.01	0.97	0.97	0.98	1.03	1.03
21	1.00	1.01	1.10	1.09	1.03	1.00	0.99	1.01	1.04	1.05
22	1.07	1.06	1.13	1.17	1.12	1.07	1.05	1.06	1.08	1.13
23	1.09	1.08	1.11	1.18	1.14	1.10	1.07	1.07	1.09	1.15
24	1.12	1.10	1.10	1.19	1.15	1.11	1.09	1.08	1.08	1.17
25	1.16	1.15	1.08	1.17	1.16	1.12	1.10	1.10	1.05	1.15
26	1.20	1.20	1.08	1.20	1.19	1.17	1.15	1.14	1.05	1.17
27	1.32	1.33	1.16	1.29	1.30	1.26	1.25	1.24	1.09	1.24
28	1.28	1.33	1.09	1.21	1.23	1.24	1.26	1.29	1.03	1.19
29	1.10	1.12	0.97	1.06	1.06	1.07	1.07	1.10	0.95	1.07
30	1.20	1.21	1.08	1.19	1.16	1.14	1.14	1.14	1.04	1.16
31	1.24	1.24	1.11	1.22	1.20	1.17	1.16	1.16	1.06	1.18
32	1.25	1.24	1.11	1.23	1.21	1.19	1.17	1.17	1.06	1.19
33	1.25	1.24	1.10	1.23	1.22	1.20	1.18	1.17	1.05	1.19
34	1.22	1.22	1.08	1.21	1.20	1.19	1.18	1.17	1.03	1.17
35	1.20	1.20	1.07	1.19	1.20	1.19	1.17	1.17	1.02	1.16

Table 8.16: Fatigue damage rates from neural toolbox $b = 5.0$ (3)

PSD No.	amplitude=4.0				amplitude=5.0					
	1.5	2.0	2.5	3.0	0.5	1.0	1.5	2.0	2.5	3.0
1	1.16	1.15	1.14	1.13	1.00	1.15	1.14	1.12	1.10	1.09
2	1.12	1.10	1.09	1.09	1.01	1.14	1.13	1.09	1.08	1.06
3	1.11	1.08	1.08	1.08	1.01	1.15	1.13	1.08	1.07	1.06
4	1.13	1.11	1.11	1.11	1.05	1.17	1.15	1.11	1.10	1.09
5	1.16	1.14	1.14	1.14	1.09	1.20	1.17	1.14	1.12	1.11
6	1.08	1.08	1.08	1.09	1.06	1.13	1.09	1.07	1.06	1.06
7	1.07	1.05	1.04	1.05	1.05	1.11	1.08	1.04	1.03	1.02
8	1.06	1.05	1.05	1.06	1.08	1.12	1.07	1.04	1.03	1.03
9	1.07	1.06	1.06	1.06	1.11	1.12	1.08	1.05	1.04	1.03
10	1.09	1.07	1.08	1.07	1.15	1.15	1.10	1.06	1.06	1.05
11	1.09	1.11	1.10	1.06	1.21	1.15	1.08	1.08	1.07	1.04
12	1.07	1.07	1.06	1.00	1.17	1.13	1.07	1.05	1.03	0.98
13	1.09	1.06	1.04	1.04	1.04	1.08	1.03	1.00	0.99	0.98
14	1.05	1.00	0.99	0.99	0.96	0.99	0.96	0.94	0.96	0.99
15	1.05	1.09	1.08	1.08	0.79	0.96	1.08	1.09	1.00	1.00
16	0.98	0.95	0.97	0.96	0.84	0.91	0.93	0.97	1.01	1.03
17	1.01	0.98	0.98	0.98	0.95	0.99	0.96	0.94	0.94	0.96
18	1.01	0.98	0.98	1.00	1.02	1.06	1.02	1.00	0.99	1.00
19	0.99	0.96	0.97	0.99	1.01	1.06	1.02	0.99	1.00	1.02
20	0.99	0.96	0.97	0.99	0.99	1.03	1.00	0.98	0.99	1.02
21	1.00	0.98	0.98	1.01	1.00	1.04	1.00	0.99	0.99	1.02
22	1.08	1.04	1.03	1.05	1.06	1.12	1.07	1.03	1.03	1.04
23	1.11	1.07	1.06	1.07	1.08	1.15	1.11	1.07	1.05	1.06
24	1.14	1.10	1.08	1.08	1.09	1.18	1.14	1.10	1.08	1.08
25	1.14	1.11	1.09	1.09	1.06	1.16	1.14	1.11	1.09	1.09
26	1.16	1.14	1.12	1.11	1.05	1.17	1.16	1.13	1.10	1.09
27	1.24	1.21	1.19	1.18	1.06	1.20	1.20	1.17	1.15	1.13
28	1.21	1.22	1.23	1.25	0.97	1.13	1.16	1.17	1.17	1.18
29	1.07	1.07	1.08	1.10	0.95	1.07	1.08	1.08	1.08	1.10
30	1.14	1.12	1.12	1.12	1.03	1.15	1.13	1.11	1.10	1.10
31	1.17	1.14	1.13	1.13	1.05	1.17	1.16	1.13	1.11	1.11
32	1.18	1.15	1.14	1.13	1.05	1.18	1.16	1.13	1.11	1.10
33	1.18	1.16	1.14	1.13	1.05	1.18	1.17	1.14	1.12	1.10
34	1.17	1.15	1.14	1.13	1.04	1.17	1.17	1.14	1.11	1.10
35	1.17	1.15	1.13	1.13	1.02	1.16	1.16	1.13	1.11	1.09

Table 8.17: Fatigue damage rates from neural toolbox $b = 5.0$ (4)

PSD No.	amplitude=1.0						amplitude=2.0			
	0.5	1.0	1.5	2.0	2.5	3.0	0.5	1.0	1.5	2.0
36	0.74	0.88	0.94	0.96	0.98	1.01	1.04	1.12	1.09	1.07
37	0.84	1.03	1.08	1.08	1.09	1.08	1.10	1.19	1.15	1.11
38	0.87	1.06	1.11	1.11	1.10	1.09	1.08	1.17	1.14	1.11
39	0.96	1.11	1.15	1.15	1.13	1.13	1.09	1.16	1.15	1.13
40	1.06	1.16	1.18	1.16	1.15	1.16	1.08	1.18	1.17	1.14
41	1.03	1.12	1.14	1.14	1.15	1.16	1.05	1.15	1.15	1.14
42	0.98	1.08	1.08	1.10	1.11	1.13	1.03	1.15	1.12	1.12
43	0.74	0.88	0.90	0.90	0.91	0.96	1.04	1.12	1.09	1.06
44	0.76	0.94	0.99	1.00	1.01	1.01	1.05	1.15	1.11	1.06
45	0.81	1.00	1.08	1.09	1.08	1.08	1.09	1.18	1.15	1.11
46	0.87	1.08	1.13	1.13	1.12	1.11	1.08	1.17	1.15	1.12
47	0.91	1.07	1.09	1.07	1.08	1.07	1.02	1.12	1.11	1.08
48	0.95	1.08	1.06	1.07	1.07	1.09	1.02	1.13	1.10	1.08
49	0.96	1.04	1.05	1.07	1.07	1.09	1.01	1.10	1.09	1.08
50	0.72	0.87	0.91	0.90	0.90	0.92	1.03	1.11	1.08	1.04
51	0.77	0.92	0.96	0.95	0.96	0.98	1.08	1.15	1.12	1.07
52	0.81	0.98	1.04	1.07	1.05	1.05	1.12	1.21	1.16	1.12
53	0.81	1.00	1.08	1.10	1.10	1.08	1.12	1.20	1.16	1.13
54	0.81	1.04	1.09	1.09	1.08	1.07	1.09	1.19	1.14	1.10
55	0.83	1.04	1.08	1.09	1.08	1.06	1.07	1.16	1.12	1.09
56	0.87	1.04	1.07	1.08	1.07	1.09	1.04	1.13	1.10	1.09
57	0.70	0.88	0.95	0.96	0.94	0.93	1.02	1.11	1.06	1.02
58	0.72	0.90	1.00	1.02	1.00	0.99	1.06	1.13	1.09	1.06
59	0.72	0.93	1.03	1.04	1.01	1.01	1.06	1.13	1.10	1.06
60	0.78	1.01	1.08	1.07	1.04	1.03	1.07	1.15	1.11	1.07
61	0.81	1.04	1.11	1.09	1.08	1.07	1.08	1.16	1.13	1.09
62	0.86	1.05	1.10	1.09	1.09	1.09	1.06	1.14	1.13	1.10
63	0.87	1.04	1.09	1.10	1.10	1.08	1.05	1.14	1.12	1.10
64	0.84	0.98	1.03	1.00	0.96	0.93	1.14	1.14	1.07	1.01
65	0.86	1.03	1.08	1.06	1.02	0.99	1.17	1.18	1.10	1.05
66	0.89	1.08	1.14	1.13	1.07	1.04	1.19	1.20	1.14	1.10
67	0.89	1.10	1.16	1.13	1.07	1.03	1.19	1.22	1.15	1.09
68	0.91	1.14	1.16	1.14	1.09	1.04	1.18	1.23	1.15	1.10
69	0.92	1.14	1.16	1.16	1.10	1.08	1.16	1.20	1.15	1.12
70	0.95	1.15	1.17	1.13	1.10	1.08	1.13	1.20	1.15	1.09

Table 8.18: Fatigue damage rates from neural toolbox $b = 5.0$ (5)

PSD No.			amplitude=3.0							
	2.5	3.0	0.5	1.0	1.5	2.0	2.5	3.0	0.5	1.0
36	1.08	1.12	0.98	1.06	1.05	1.05	1.06	1.10	0.97	1.06
37	1.10	1.09	1.02	1.13	1.10	1.07	1.06	1.07	1.01	1.12
38	1.09	1.08	1.02	1.12	1.10	1.08	1.06	1.06	1.01	1.11
39	1.10	1.10	1.03	1.12	1.12	1.10	1.08	1.07	1.02	1.12
40	1.12	1.12	1.04	1.15	1.14	1.11	1.09	1.09	1.02	1.14
41	1.13	1.12	1.02	1.14	1.14	1.12	1.11	1.10	1.00	1.13
42	1.11	1.10	1.01	1.14	1.12	1.12	1.10	1.10	1.00	1.13
43	1.05	1.08	1.01	1.08	1.06	1.04	1.05	1.08	1.00	1.08
44	1.05	1.04	1.02	1.12	1.09	1.05	1.04	1.04	1.01	1.11
45	1.08	1.08	1.05	1.14	1.12	1.08	1.06	1.06	1.04	1.14
46	1.10	1.08	1.06	1.15	1.13	1.10	1.08	1.07	1.05	1.15
47	1.07	1.06	1.01	1.13	1.11	1.08	1.07	1.06	1.01	1.13
48	1.07	1.07	1.02	1.14	1.11	1.09	1.08	1.07	1.02	1.14
49	1.07	1.07	1.01	1.11	1.11	1.09	1.08	1.08	1.01	1.12
50	1.01	1.02	1.03	1.10	1.06	1.03	1.02	1.03	1.02	1.08
51	1.04	1.05	1.07	1.13	1.10	1.05	1.04	1.05	1.05	1.11
52	1.08	1.07	1.11	1.18	1.13	1.10	1.07	1.07	1.08	1.15
53	1.10	1.08	1.10	1.17	1.13	1.10	1.08	1.07	1.09	1.15
54	1.08	1.06	1.07	1.17	1.13	1.09	1.07	1.06	1.07	1.16
55	1.08	1.06	1.07	1.16	1.12	1.09	1.08	1.06	1.06	1.15
56	1.07	1.07	1.04	1.14	1.11	1.10	1.08	1.07	1.04	1.14
57	1.00	0.99	1.04	1.09	1.04	1.01	1.00	1.01	1.02	1.07
58	1.02	1.02	1.07	1.11	1.07	1.04	1.02	1.03	1.05	1.09
59	1.03	1.03	1.06	1.12	1.08	1.05	1.03	1.03	1.05	1.10
60	1.04	1.03	1.07	1.13	1.09	1.06	1.04	1.03	1.05	1.11
61	1.07	1.05	1.08	1.15	1.12	1.08	1.06	1.05	1.06	1.13
62	1.08	1.07	1.07	1.14	1.12	1.09	1.07	1.07	1.06	1.13
63	1.09	1.07	1.07	1.14	1.12	1.10	1.08	1.07	1.06	1.13
64	0.99	0.99	1.09	1.09	1.03	0.98	0.97	0.99	1.03	1.05
65	1.03	1.03	1.12	1.12	1.05	1.01	1.01	1.02	1.07	1.08
66	1.06	1.05	1.15	1.15	1.08	1.05	1.03	1.04	1.09	1.10
67	1.05	1.04	1.14	1.16	1.09	1.04	1.02	1.03	1.08	1.11
68	1.08	1.05	1.15	1.17	1.09	1.06	1.05	1.04	1.10	1.13
69	1.08	1.07	1.14	1.16	1.10	1.07	1.05	1.06	1.10	1.13
70	1.07	1.06	1.11	1.16	1.11	1.06	1.05	1.05	1.08	1.13

Table 8.19: Fatigue damage rates from neural toolbox $b = 5.0$ (6)

PSD No.	amplitude=4.0				amplitude=5.0					
	1.5	2.0	2.5	3.0	0.5	1.0	1.5	2.0	2.5	3.0
36	1.06	1.07	1.08	1.11	0.98	1.08	1.08	1.08	1.09	1.11
37	1.10	1.07	1.06	1.07	1.02	1.13	1.11	1.07	1.07	1.08
38	1.10	1.08	1.06	1.06	1.02	1.13	1.11	1.08	1.06	1.06
39	1.11	1.09	1.07	1.07	1.04	1.14	1.12	1.09	1.07	1.06
40	1.13	1.10	1.08	1.07	1.04	1.16	1.14	1.10	1.08	1.07
41	1.13	1.11	1.09	1.08	1.03	1.16	1.14	1.11	1.09	1.07
42	1.11	1.10	1.09	1.08	1.03	1.16	1.13	1.11	1.08	1.07
43	1.06	1.05	1.06	1.09	1.01	1.08	1.06	1.06	1.07	1.10
44	1.08	1.05	1.04	1.05	1.03	1.13	1.09	1.05	1.05	1.06
45	1.11	1.08	1.06	1.06	1.06	1.15	1.12	1.08	1.06	1.06
46	1.13	1.10	1.08	1.07	1.07	1.17	1.14	1.10	1.07	1.07
47	1.11	1.08	1.07	1.06	1.05	1.16	1.13	1.09	1.07	1.06
48	1.11	1.09	1.07	1.07	1.06	1.17	1.13	1.09	1.07	1.06
49	1.11	1.09	1.08	1.07	1.05	1.16	1.13	1.10	1.08	1.07
50	1.05	1.02	1.02	1.04	1.02	1.09	1.05	1.02	1.03	1.05
51	1.08	1.04	1.03	1.05	1.04	1.11	1.07	1.04	1.03	1.05
52	1.10	1.07	1.06	1.07	1.08	1.15	1.10	1.06	1.05	1.06
53	1.11	1.08	1.07	1.07	1.09	1.16	1.11	1.08	1.06	1.07
54	1.11	1.08	1.07	1.06	1.08	1.17	1.12	1.08	1.06	1.06
55	1.11	1.08	1.07	1.06	1.08	1.17	1.12	1.08	1.07	1.06
56	1.11	1.09	1.07	1.07	1.07	1.16	1.12	1.09	1.06	1.06
57	1.02	1.00	0.99	1.01	1.00	1.07	1.03	1.00	1.00	1.02
58	1.05	1.02	1.01	1.03	1.03	1.09	1.05	1.02	1.01	1.03
59	1.06	1.03	1.02	1.03	1.04	1.10	1.06	1.03	1.01	1.03
60	1.07	1.04	1.03	1.03	1.05	1.12	1.08	1.04	1.02	1.03
61	1.09	1.06	1.04	1.04	1.06	1.14	1.09	1.05	1.03	1.03
62	1.10	1.06	1.05	1.06	1.07	1.14	1.11	1.06	1.04	1.05
63	1.10	1.08	1.06	1.06	1.07	1.15	1.11	1.07	1.06	1.05
64	1.00	0.96	0.97	1.00	0.99	1.04	1.00	0.98	0.98	1.02
65	1.02	0.99	0.99	1.01	1.02	1.07	1.02	0.99	1.00	1.03
66	1.05	1.02	1.01	1.03	1.05	1.09	1.05	1.01	1.01	1.04
67	1.05	1.01	1.00	1.02	1.04	1.10	1.05	1.01	1.01	1.03
68	1.06	1.03	1.03	1.03	1.06	1.12	1.06	1.03	1.03	1.04
69	1.07	1.04	1.03	1.05	1.07	1.12	1.06	1.04	1.03	1.05
70	1.08	1.03	1.02	1.04	1.06	1.13	1.08	1.03	1.02	1.03

Chapter 9

Assessment of the neural network toolbox

9.1 Introduction

Loadings on most engineering structures are generally complex. Apart from deterministic loading which can be described mathematically, there generally exists some loading which can not be described this way. This is the so-called random loading for which only statistical parameters are known. Wind turbine blades are one such kind of structure. The loading acting on the turbine includes deterministic components as well as random ones. The following kinds of deterministic loads for wind turbines generally exist[20].

- Wind shear.
- Skew wind.
- Tower interference.
- Mean wind.
- Gravity loading.
- Centrifugal forces.

The stochastic loading, of course, results from wind turbulence.

Among all the deterministic components, the most important is undoubtably the one caused by gravity. Its value is usually so big that all the others can be classified into the stochastic part. There may be some situations where more than one deterministic component is important. For this situation an extended form of the toolbox presented in this thesis would be required. In principle, this should pose few problems for a future work programme. It would simply require additional parameters to be included in the training process such as the second sine wave's frequency and amplitude. In this case, phase would also be needed.

9.2 Extraction of deterministic components

The bending moments on a wind turbine blade at different sections (or stress at hot spots) are the sum of the effects caused by the wind and gravity of the blade itself. The response to wind is a stochastic process and the response to gravity is generally a sine wave. At the design stage, these two responses are computed separately. Based on this information, the fatigue analysis can now be performed using the toolbox developed in the previous chapter. In order to assess the accuracy of this neural network toolbox, it is necessary to extract the deterministic components from the mixed signals. This data can then be used to test the toolbox.

As seen from the spectra shown in previous chapters, the gravity induced response is the main deterministic component in the bending moment history. Thus, a single sine wave situation can be considered. Let *X(t)* be the response caused by the wind turbulence, and *Y(t)* be the one caused by the gravity of the blade. The monitored signal is then *Z(t)=X(t)+Y(t)*. Together with the bending moment histories in Howden HWP330 data files, the azimuth of the turbine blade is also recorded, which is generally measured as shown in Figure 9.1. Thus, the gravity induced response takes the following form:

$$Y(t) = A\sin(\phi + \xi) + D \tag{9.1}$$

where A is the amplitude of the sine wave, D is the global mean value of the signal, ϕ is the azimuth, and ξ is a suitable phase.

9.2.1 Band pass filter

The task of separating the sine wave from the stochastic signal is then to determine the value A and ξ in Equation 9.1 given that the azimuth is known. This can be done in many ways. The first method tried in this thesis was a band pass filter which was intended to filter the stochastic signal but let the single sine wave (or a very narrow band of signal around it)pass. Unfortunately, this method did not work well because of the leakage problem with FFT calculations. This is inevitable in discrete FFT computation, regardless of type of window used. The sine wave becomes a narrow band signal because of this leakage. Also, there is no guarantee that the blade is always rotating at a constant frequency during the time period in which the data is acquired. This ruled out the possibility of using such a band pass filter.

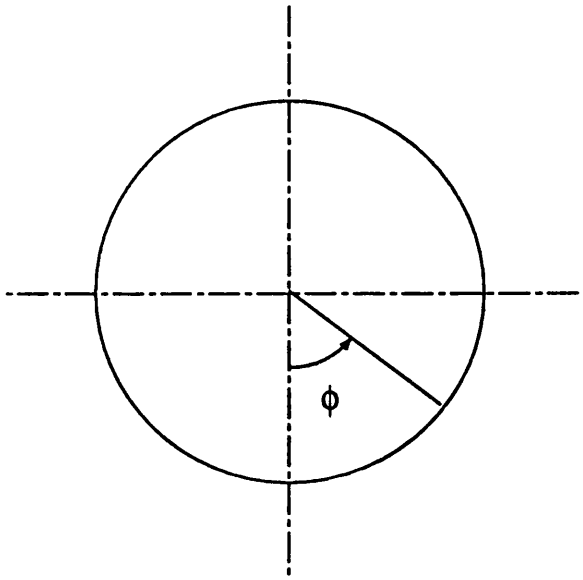

Figure 9.1: Azimuth of turbine blade

9.2.2 Least square sine wave fitting

We can assume the global mean of *Z(t)* is zero without losing generality. The stochastic response *X(t)* is also a process with zero mean. This implies that, when the stochastic component is added into a sine wave *Y(t)*, it still has a zero mean if this mean value is taken around the sine wave. Thus, we have

$$\sum_{k=1}^{N}[Z(t_k) - Y(t_k)] = 0.0$$

This expression shows that, for a signal such as *Z(t)* which contains a significant deterministic component expressed as Equation 9.1, a sine wave could be best fitted to the signal to make the average around the sine wave zero. This highlights the possibility of employing a least square technique. Although theoretically a zero mean can not guarantee a minimum least square error, the least square fitting can be expected to produce acceptable results. The smaller the stochastic component is, the better the results are likely to be obtained since the fact of zero mean will more likely tend to meet the least square error assumption.

A better strategy for calculating the parameters of the sine wave is to apply a band pass filter to the original signal and then apply a least square error fitting to the filtered signal. Since the task is only to determine a few parameters, this work can be performed on part of the signal instead of the whole.

The mathematical model for sine wave extracting can be established as

$$\min \sum_{k=1}^{N} [Z(t_k) - Y(t_k)]^2$$

$$s.t. \quad A > 0$$

$$D > 0$$

All of the computation can be performed with the same program that was used for curve fitting in the previous chapter. A band pass filter was employed on the original signal in order to focus the fitting work towards the sinusoidal part. Since the Howden data contains not only the moments of the blades during rotating but some control induced loads such as braking etc., it is necessary to extract a suitable portion of the signal which contains the sine wave.

9.2.3 Some comments about the azimuth averaging method

It is necessary to give a brief comment on the so-called "Azimuth averaging" method [90] [79]. The idea of this method is that, if every point which is one period of the sine wave away from the previous one is taken from the combined signal, the average of this new series will give the value of the sine wave at this azimuth angle. To make this true, it must be assumed that the stochastic component is absolutely stationary and ergodic. The signal is grouped in accordance with its azimuth angle and each group must have a zero mean. This assumption proved to be too rigorous for the wind response history. The least square fitting method here only assumes the error between the sine wave and stochastic component is at its minimum. If the fact that the overall average around the sine wave is zero is considered, this assumption is not difficult to satisfy. Thus, there is reason to believe that the least square fitting method gives better results. Accuracy can be improved by combining the analysis with a band pass filter (see next section).

9.3 Separation of the Howden data

The azimuth information included in the Howden HWP330 data is recorded on channel 4 for all the tapes. A typical azimuth from tape 18 is shown in Figure 9.2.

Using the azimuth information and the technique introduced in the previous section, the sine waves in the edgewise signals of HWP330 data files were extracted

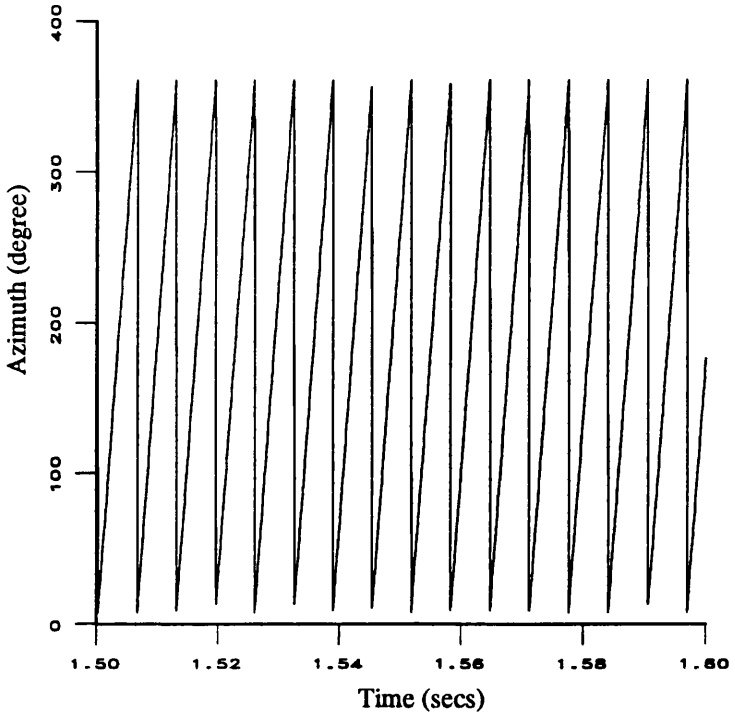

Figure 9.2: A sample of azimuth record from HWP330 tape 18

out. In the practical computation, the phase angle was introduced in order to adjust the possible lag. Before using the program developed in the previous chapter, the azimuth information was analysed in order to find the time when the rotor began normal operation because the beginning and the end often included such control operations as braking. In terms of fatigue analysis, only the amplitudes and frequencies of the sine waves were important.

Before the least-square sine wave fitting procedure was applied to the signals, a band pass filter was used to get rid of irrelevant frequency information in order to improve the accuracy. As can be seen from the spectra of the signals, the frequencies of the deterministic components in the edgewise signals are in the range *0.5Hz* to *0.6Hz*. Two frequency bands were selected for the filter. The first one is *0.2Hz* to *2.0Hz* and the second one *0.4Hz* to *0.8Hz*. Further narrowing of the frequency band is not used in order to avoid the possibility of leakage. In any case it did not prove necessary because the results with different frequency bands met very well.

The amplitudes of the sine waves existing in all the edgewise signals are listed in Table 9.1 and 9.2 for the filtered and raw signals. The least-square sine wave fitting method works very well for the Howden edgewise signals because the errors between the results from filtered and raw signals are all nearly negligible. The

other reason is that the sine waves are so dominant that the stochastic components are simply acting like noise. But anyway, this consistency inferred the reliability of the results.

Table 9.1: Amplitudes of deterministic components in Howden data edgewise signals

filter band	tape 18			tape 26		
	3m	8m	13m	3m	8m	13m
raw	42.126	9.720	3.179	49.195	17.223	3.028
0.2-2.0(Hz)	42.196	9.743	3.187	49.143	17.176	3.040
0.4-0.8(Hz)	42.190	9.734	3.185	49.114	17.165	3.038

Table 9.2: Amplitudes of deterministic components in Howden data edgewise signals

filter band	tape 27			tape 30		
	3m	8m	13m	3m	8m	13m
raw	49.027	17.145	3.011	49.643	17.191	3.020
0.2-2.0(Hz)	49.156	17.316	3.065	50.262	17.463	3.040
0.4-0.8(Hz)	49.328	17.367	3.074	50.395	17.512	3.046

The stochastic component can then be separated from the original signal by deducting the sine wave. A sample of the stochastic component extracted from tape 18 3m edgewise signal is shown in Figure 9.3.

9.4 Reanalysis of Howden data

Once the deterministic components were extracted from the edgewise signals, the neural network toolbox was used for a fatigue analysis using these signals. Figure 9.4 shows the rainflow cycle probability density function calculated from the neural network toolbox and the one from the time signal directly for tape 18 3 meter edgewise signal. It can be seen that, despite the over prediction of the low range cycles, the high range part of the frequency domain result agree quite well with the time domain solution. Table 9.3 shows the results for the damage rates between the neural network calculation and time domain solutions when a value of $b=5.0$ is used.

The results shown in this table are in some ways disappointing since better solutions were expected. However, when the flapwise results in Chapter 4 are referred to, it is easy to see that the reason for this discrepancy is in the signals

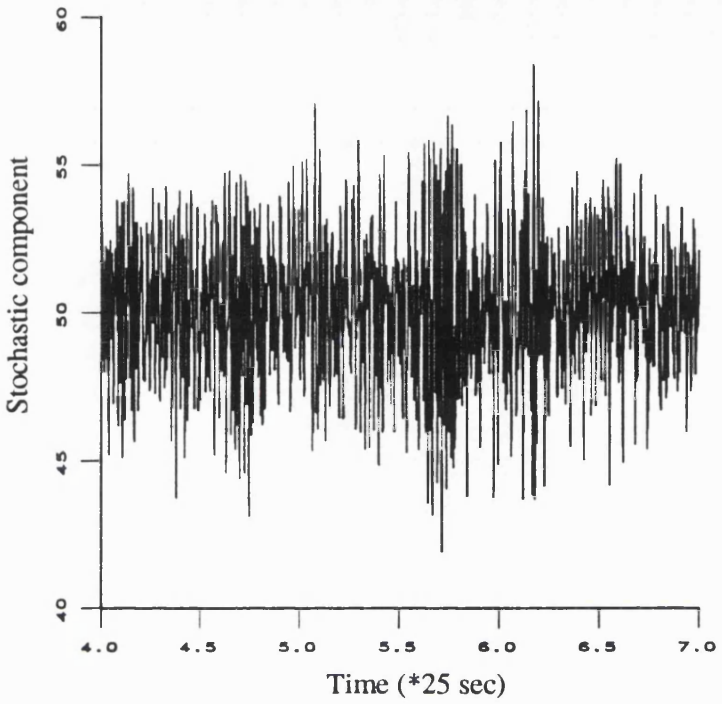

Figure 9.3: The stochastic component of tape 18 3m edgewise signal

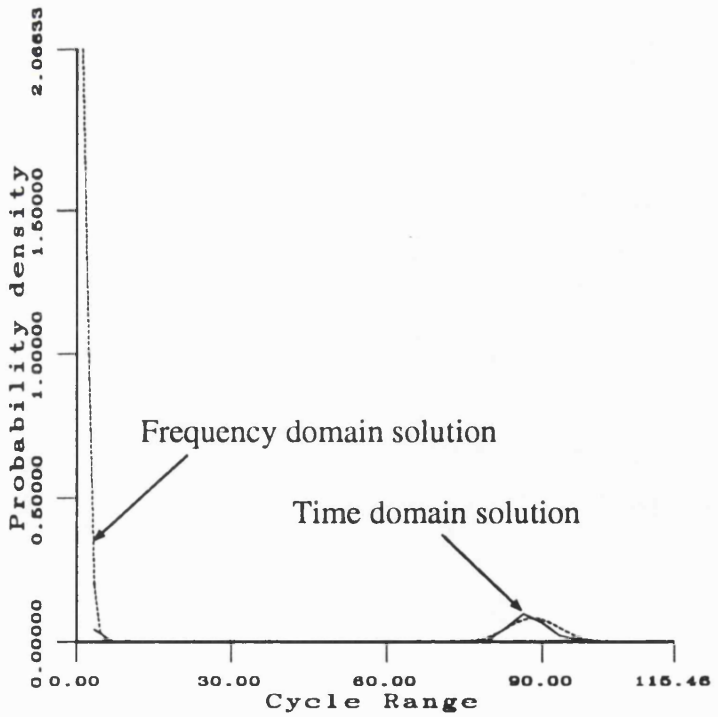

Figure 9.4: Rainflow cycle probability density function from time and frequency domain analysis

Table 9.3: Damage rates of frequency domain results with time domain results for Howden data edgewise signals with b=5.0

Tape	3 meter	8 meter	13 meter
18	1.610	0.958	0.8781
26	2.711	2.085	0.624
27	4.767	3.567	4.554
30	5.453	2.908	1.240

themselves. Because the results in the frequency domain for the flapwise signals do not agree, there is no reason to expect the neural network toolbox here to give better results than the flapwise signals containing no significant deterministic component. Apart from the nonstationarity in the time histories, it was found from the stochastic components that, nearly all the signals contain some strange spikes.

Figure 9.5(a) shows a very long segment of the stochastic component from tape 26 3 meter edgewise signal which contains this type of fault. It is seen from this figure that some extraordinarily high spikes exist in the stochastic component. Figure 9.5 (b), (c), (d), and (e) show the details of the spikes in both the stochastic component and the original signal. It can be seen that these spikes exist in the signals as isolated points. For a signal acquired at 40Hz, it is hard to believe that these spikes are anything other than recording errors. Such spikes are not found in the wind speed signals at the same time duration. Therefore, they must be caused by equipment faults.

If the signal contains both a stochastic component and a deterministic component, these spikes would have less influence on the fatigue estimation since they can hardly change the high range part of the PDF. However, since the two kinds of components are separated, the spikes remained in the stochastic part. The spectra from the stochastic components is then seriously influenced.

Thus, these spikes have two aspects of influence on the fatigue analysis. The first one is that they produce false cycles in the time domain analysis. Secondly, they completely distorted the spectra from the stochastic components. Since the damage rates produced are at about the same level as the flapwise results, it may be concluded that the neural network toolbox will work perfectly well for signals with a deterministic component. In addition, the nonstationarity is still a problem here. This is addressed in the next section for more realistic signals.

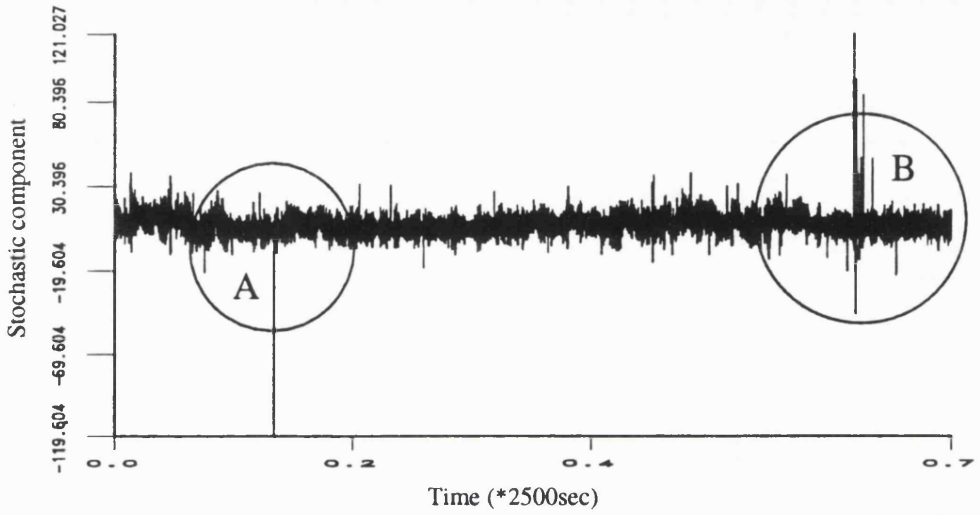

(a). Stochastic component of Howden data tape 26 3m edgewise signal.

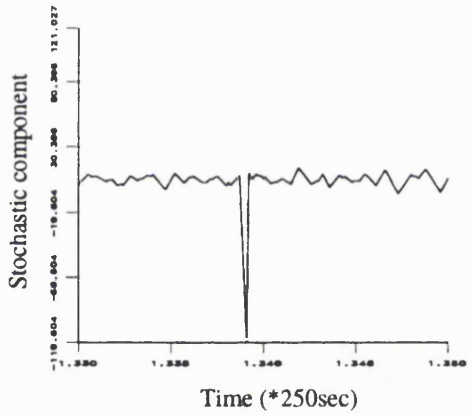

(b). Details of A in stochastic component

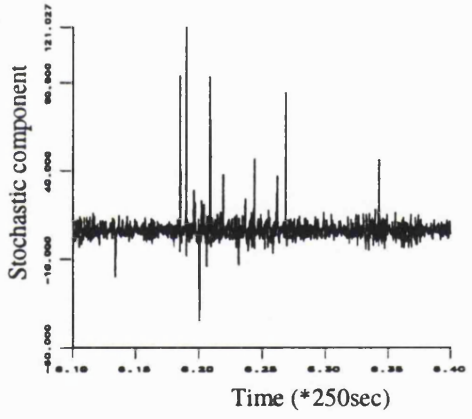

(c). Details of B in stochastic component

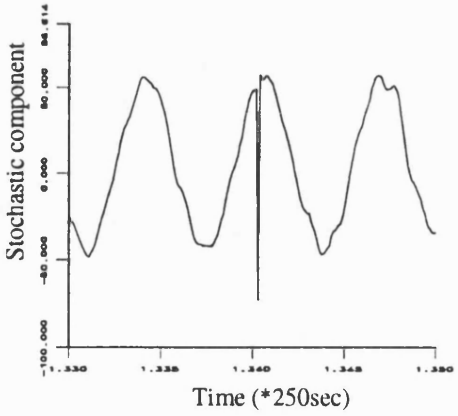

(d). Details of A in original signal

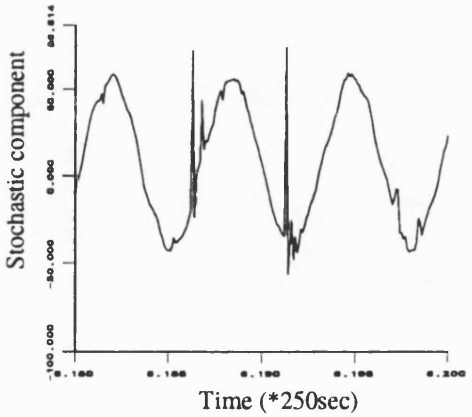

(e). Details of B in original signal

Figure 9.5: Howden data tape 26 3m edgewise

9.5 Result for simulated signals

Further simulated time signals different from the signals used in the previous chapter was produced in order to provide an assessment of the neural network toolbox. The PSD used for signal simulation is shown in Figure 9.6.

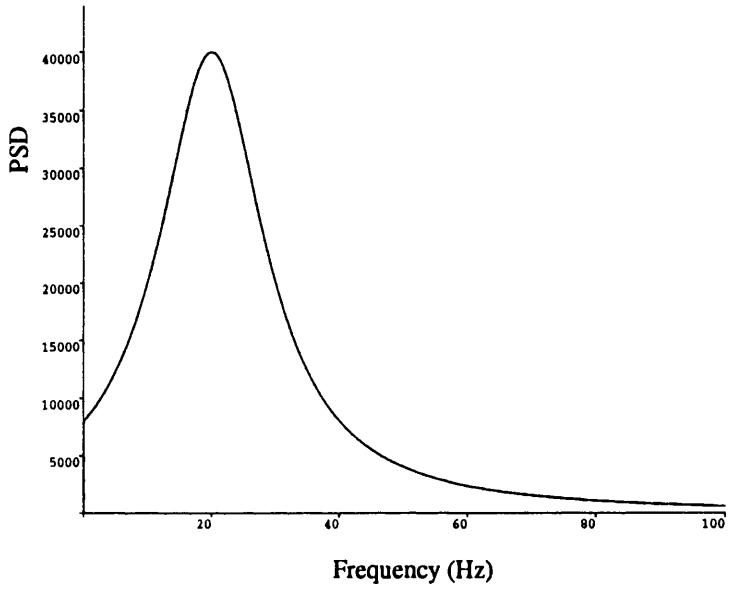

Figure 9.6: New simulated signal

Because different deterministic components were added into the signal, different rainflow range PDF's are obtained. Figure 9.7 shows one of these PDF's when the amplitude of the deterministic component is 2σ and frequency is *1.0Hz* with σ as the *rms* of the stochastic component. Together with the time domain solution, the one from neural network toolbox and Dirlik's formula were also presented in the same figure. It is seen from this figure that the result from neural network toolbox can meet the time domain solution very well for the cycle ranges produced by the deterministic component. Dirlik's formula was unable to produce such a peak in the PDF curve. The result attempted to derive in [79] was achieved by the neural network toolbox developed in this thesis.

The damage rates from neural network toolbox for a value of b=*5.0* are shown in Table 9.4. It can be seen from this table that the results from the neural network meet well with the time domain results.

The damage rates from Dirlik's formula are listed in Table 9.5. The damage rate for the purely stochastic signal is 1.13, which can be taken as a reasonable prediction. However, it is seen that when the deterministic components are added into the stochastic signal, Dirlik's formula failed to give a good prediction,

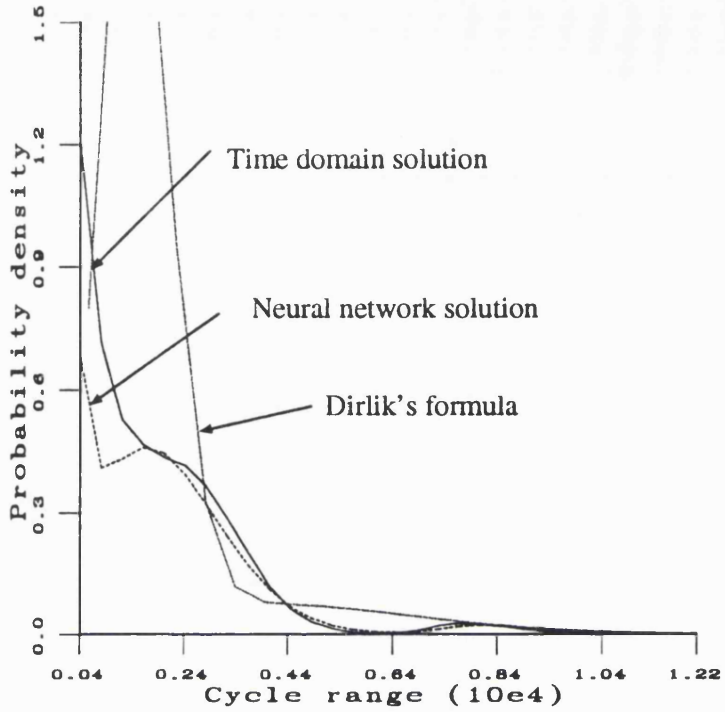

Figure 9.7: Rainflow cycle PDF's from new simulated signal

especially when the deterministic component becomes bigger.

Table 9.4: Damage rates of frequency domain results compared with the time domain results for the new simulated signals with b=5.0

	1	2	3	4	5
1	0.973	0.918	0.863	0.820	0.782
2	0.980	0.914	0.855	0.806	0.757
3	0.913	0.863	0.838	0.801	0.787

Table 9.5: Damage rates of Dirlik's formula compared with the time domain results for the new simulated signals with b=5.0

	1	2	3	4	5
1	1.44283	1.58510	1.76641	1.95076	2.10519
2	1.27628	1.49100	1.76277	1.98683	2.17223
3	1.22268	1.52935	1.84667	2.10761	2.30154

9.6 Conclusions

The neural network toolbox developed in the previous chapter has been examined in this chapter with the Howden data edgewise signals and new simulated signals. The assessment on the monitored data was seriously influenced by the faults existing in the recorded data, especially when the deterministic component was extracted from the combined response history. The faults distorted the stochastic part and the results from neural networks, even though they have nearly no influence on the combined signals. Assessment using new simulated signals indicate good performance of the toolbox developed.

Effort was also made to separate the deterministic component from the combined signal. The method used here incorporate a band pass filter and the least square techniques. It has a higher efficiency than the conventionally used azimuth averaging method.

Chapter 10

Conclusions and Suggested Future Work

10.1 Conclusions

The work presented in this thesis makes a number of significant advances in spectral fatigue analysis techniques. Current methods which have previously been developed are reviewed and assessed here. The theoretical solution developed by Dr. Bishop is extended to consider the influence of mean stress for random fatigue analysis. It is also extended for the fatigue analysis of non-Gaussian response histories provided that the peak-trough and trough-peak matrices are known. A toolbox for fatigue analysis of wind turbine blades is developed based on numerical simulation and neural network technique. This toolbox should have made wide applicability than wind turbine loadings but this has not been assessed.

Fatigue analysis of two sets of monitored response histories, the WEG MS-1 and Howden HWP330, was performed in **Chapter 4**, both in the time and frequency domains. The frequency domain results include most of the present methods in use and are compared with the time domain results, which are taken as a reference solution. The narrow band solution is always conservative due to the narrow band assumption. The two methods which meet best with the time domain results are Dirlik's empirical formula and Bishop's theoretical solution. The former one is based on numerical simulation and regression. The later one is based on Markov chain theory and thus has a better theoretical background. Most of the methods now in use assume the response histories have a Gaussian distribution mainly because of the limited information provided by the ordinary power spectral density function.

Chapter 5 presents some important results concerning the parameters choices involved in the computation work of **Chapter 4**. The first parameter investigated is the cutoff frequency of the power spectral density function. This problem is mainly concerned with the high frequency noise problem but more generally the

truncation problem of other spectrum is of relevance. The high frequency noise in the spectrum can seriously influence the fourth moment of the spectrum and thus influence the irregularity factor. Most of the spectral methods are seriously affected by this high frequency noise. The length requirement of the response histories was also investigated for both sets of data. The Howden HWP330 data is much longer than the WEG MS-1 data. Because of this the rainflow cycles counted from Howden data form continuous PDF's which are more representative of the process. The WEG MS-1 data, on the other hand, is too short to give such continuous functions. Thus, the signal length needs to be carefully considered when response monitoring work is performed. The clipping ratio problem is discussed here for the first time and some guidance is given for selecting this parameter for fatigue analysis. It is interesting to find that, the consistency between fatigue predictions is affected by the material characteristic, i.e. the slope of *S-N* curve. This means that the same spectral method can give an equivalent stress very close to the correct value for some materials but may give very poor predictions for some other materials with different *S-N* curve slopes. The deterministic component in the Howden edgewise response presented a serious problem with the calculation of fatigue damage. One of the main parts of this thesis is concerned with development of a toolbox for the fatigue analysis of such responses. This is presented in **Chapter 8**.

Chapter 6 presents a method for taking the mean stress influence into account in a frequency domain analysis for the first time. This method is based on Bishop's theoretical solution which uses Markov chain theory for the rainflow cycle probability calculation. Since the spectrum can not provide information of the the global mean level of response, the mean level of rainflow cycle relative to the global mean is calculated and a joint rainflow range PDF of relative mean stress and cycle range is obtained using this method. The requirement of needing the global mean to be specified does not normally represent a problem since this global mean level is usually known at the design stage. Once this value is combined with the relative mean from the spectral solution, a damage estimation can then be performed by employing Goodman's relationship, or any other formulae used to convert cycle range with mean into equivalent cycle range without mean. This method is applied to the two sets of data used in **Chapter 4** to analyse the influence of mean stress on the fatigue damage.

A number of possible approaches to deal with non-Gaussian responses are discussed in **Chapter 7**. A method for calculating the rainflow cycle PDF is

developed based on Markov chain theory. This approach assumes the peak to trough and trough to peak transition matrices are known. Because the general non-Gaussian class of distributions is such a huge set of probability distributions, it is impossible to find any method which can deal with the general non-Gaussian situations.

Since most of present methods cannot give satisfactory results for the edge-wise response of wind turbine blades where significant deterministic components are present, this thesis addresses such situations in **Chapter 8**. Seventy power spectral density functions were selected to cover a wide range of engineering spectra. Signal simulation work was then performed using an inverse FFT technique. After examined the rainflow range PDF's derived from the signals, a mathematical model was established. By employing least-square technique for curve fitting, more than 2000 sets of model parameters were obtained. To improve the accuracy of the fatigue damage calculation, the least squares calculation were performed on the weighted PDF's according to their cycle ranges. A neural network with back propagation was established to perform the regression work. After training the network, the neural network is capable of calculating the model parameters from the spectrum statistics and deterministic component parameters. Since the peak number in unit time can no longer be calculated from the formula which is suitable for Gaussian signals, the network was also developed to calculate the peak rate. Thus, a neural network toolbox was developed and presented in **Chapter 8.**

Some reassessment work using the neural network toolbox was performed on the Howden data and new simulated data in **Chapter 9.**

10.2 Suggested future work

Generally speaking, the future work of spectral fatigue analysis should be concentrated on the non-Gaussian problem and nonstationary problem. For future research work on the spectral fatigue analysis of wind turbine blades, the nonstationary problem should be the most important because the deterministic component problem reduces the importance of non-normality of the response history. It has been shown in the statistical analysis of the WEG MS-1 data and Howden HWP330 data that, the turbine blade response is strongly non-Gaussian and nonstationary. This phenomena can be seen quite clearly from the statistical results of the Howden data. A suitable technique to deal with this problem is needed.

One approach might be to divide the response history into small blocks to reduce the influence of nonstationarity. Such techniques can reduce the influence but can not eliminate it. Furthermore, there is the risk of reducing the blocks to a point where they are not long enough to see the important fatigue damaging rainflow cycles. A frequency domain approach maybe necessary to deal with such situations.

The spectral method presented in **Chapter 6** made the theoretical method capable of considering the mean stress. It would be desirable to find the distribution of mean, together with rainflow cycle ranges. It is then possible to modify all the method to consider the mean stress influence in spectral fatigue analysis. The formula developed by Kowalewiski would provide a clue for this work.

The theoretical solution described in **Chapter 7** provided a useful tool for solving the non-Gaussian problem but the peak-trough and trough-peak transition matrices have to be provided first. It is necessary to develop the peak trough turning point matrix based on frequency domain information to derive a complete solution. As stated in **Chapter 7**, such a turning point matrix would be very difficult to derive for universal non-Gaussian process. Therefore, suitable assumption should be adopted according to the concerned application.

Another direction in future research is the developing of spectral method for multiaxial fatigue evaluation. Much work has been devoted to multiaxial fatigue analysis and experiments [91]. However, there is no efficient way to evaluate the fatigue damage using frequency domain information.

References

[1] N.W.M.Bishop. *The Use of Frequency Domain Parameters to Predict Structural Fatigue.* PhD thesis, University of Warwick, 1988.

[2] L. P. Pook N. E. Frost, K. J. Marsh. *Metal Fatigue.* Oxford:Clarendon Press, 1974. Oxford engineering science series.

[3] R. I. Stephens H. O. Fuchs. *METAL FATIGUE IN ENGINEERING.* Wiley-Interscience Publication, John Wiley & Sons, 1980.

[4] James L. Handrock Julie A. Bannantine, Jess J. Comer. *FUNDAMENTALS OF METAL FATIGUE ANALYSIS.* Prentice Hall, INC., Englewood Cliffs, 1990.

[5] F. Sherratt. Vibration and fatigue: Basic life estimation methods. *Journal of the Society of Environmental Engineers*, December 1983.

[6] D.F.Socie. Fatigue life estimation techniques. Technical Report Tech-Report-145, Department of Mechanical Engineering, Illinois University.

[7] F. Sherratt. Fatigue life estimation using simple fracture mechanics. *Journal of the Society of Environmental Engineers*, March 1983.

[8] F. Sherratt. Fatigue life estimation by local stress-strain methods. *Journal of the Society of Environmental Engineers*, September 1983.

[9] J.Domingu J.Zapatero. A statistical approach to fatigue life predictions under random loading. *Int J. of Fatigue*, 12 No 2:107–114, March 1990.

[10] F. Sherratt. Fatigue life estimation: A review of traditional methods. *Journal of the Society of Environmental Engineers*, January 1982.

[11] S.O.Rice. Mathematical analysis of random noise, January 1954. Selected papers on Noise and Stochastic process.

[12] J.S.Bendat. Probability functions for random responses. Technical report, NASA Report NAS-5-4590, January 1964.

[13] T.Dirlik. *Application of computers in Fatigue Analysis.* PhD thesis, University of Warwick, January 1985.

[14] J. M. Tunna. Fatigue life prediction for Gaussian random loads at the design stage. *Fatigue and Fracture of Engineering Material and Structures*, September 1986. Vol 9 No. 3.

[15] Professor K J Miller. Metal fatige - past,current and future. In *Proceedings of the Institution of Mechanical Engineers*, 27 March 1991.

[16] R.E.Little and E.H. Jebe. *Statistical Design of Fatigue Experiments.* Applied Science Publishers LTD., 1975.

[17] M.A. Miner. Cumulative damage in fatigue. *J. of Applied Mechanics*, September 1945.

[18] N E Dowling. Fatigue failure predictions for complicated stress-strain histories. *J. of Materials MISA Vol.7,No.1*, March 1972.

[19] Frank Sherratt. Cumulative damage laws and statistical calculations. (Private communication).

[20] P.H. et al Madsen. The significance of dynamic loads w.r.t. lifetime of wind turbine rotors. Technical report, Project final report, Denmark, 1984, January 1984.

[21] Eli Altus. Fatigue,fractals,and a modified miner's rule. *J of Applied Mechanics*, 58, March 1991.

[22] J.Livesey and D. Webber. Recording and interpretation of strain measurements in military bridges. J.B.C.S.A. conference, 1972.

[23] T. Haas. Loading statistics as a basis of structural and mechanical design. *Engineers Digest*, 23(3,4 and 5), 1962.

[24] J.Schijve. The analysis of random load-time histories with relation to fatigue tests and life calculations. In *2nd ICAF-AGARD symposium*, Paris, May 1961.

[25] J.Taylor. Measurement of gust loads in aircraft. *J. Roy. Aero. Soc.*, 57,58, 1953.

[26] R.M.Wetzel. *A method of fatigue damage analysis.* PhD thesis, University of Waterloo, Canada, 1971.

[27] M.Matsuishi and T. Endo. Fatigue of metals subject to varying stress. *JSME*, 1968.

[28] T. Endo *et al.* Damage evaluation of metals for random or varying loads. In *Symposium on mechanical behaviour of matterials*, Japan, August 1974. Soc. Mats. Sci.

[29] I.Rychlik. A new definition of the rainflow cycle counting method. *Int. J. Fatigue, 9(2), p119-121, 1987*, January 1987.

[30] Y. Murakami, editor. *The Rainflow Method in Fatigue.* Oxford:Butterworth-Heinemann, 1991. The Tatsuo Endo Memorial Volume: The papers presented at the International Symposium on Fatigue Damage Measurement and Evaluation under Complex Loadings.

[31] N W M Bishop. Fatigue life prediction from psd data. Part I: traditional approaches. *Envirenmental Engineers, pp11-14*, March 1989.

[32] N W M Bishop. Fatigue life prediction from psd data. Part II: recent developments. *Envirenmental Engineers, pp11-14*, March 1989.

[33] S.D.Downing and D.F. Simple rainflow counting algorithms. *Int.J.Fatigue*, January 1982.

[34] G.Lindgren and I.Rychlik. Rainflow cycle distribution for fatigue life prediction under Gaussian load. *Fatigue Fract.Eng'g mater.Struct.,10(3),pp251-260*, January 1987.

[35] N.W.M.Bishop and F.Sherratt. A theoretical solution for the estimation of rainflow ranges from psd data. *Fatigue Fract.Eng.Mater.Struc.,13(4), pp311-326*, January 1990.

[36] D.E.Newland. *An Introduction to Rabdom vibrations, Spectral & Wavelet Analysis, Third edition.* Longman Scientific & Technical, 1993.

[37] Neil Conway Hay. *The Simulation of Random Environments for Structural Synamics Testing.* PhD thesis, Napier Polytechnic of Edinburgh, 1989.

[38] Robert Colin Pumphery. *The Dynamic Response of Water Pumping Windmills.* PhD thesis, University of Sheffield, October 1994.

[39] Joseph Penzien Ray W. Clough. *Dynamics of structures, second edition.* McGraw-Hill, INC,, 1993.

[40] T. T. Soong. *Random Differential Equations in Science and Engineering,* volume 103 of *Mathematics in Science and Engineering.* Academic Press, 1973.

[41] J.C.P.Kam and W.D.Dover. Advanced tool for fast assessment of fatigue under offshore random wave stress histories. In *Proc. Instn Civ.Engrs,Part 2,* pages 539–556, December 1989.

[42] G.K.Chaudhury. Fatigue analysis of offshore platforms subjected to sea wave loadings. *Int J Fatigue,* 7 No. 1, January 1985.

[43] J.Solin. Methods for comparing fatigue lives for spectrum loading. *Int. J. of Fatigue,* 12 No 1, January 1990.

[44] Mark C. Light Paul H. Wirsching. Fatigue under wide band random stresses. *ASCE J of ST.,* 106,No.ST7, July 1980.

[45] A.Moh P.H.Wirschhing. fatigue under wide band random stress using the rainflow method. *J. of Engineering Material and Technology,* July 1977.

[46] J.C.P.Kam and W.D.Dover. Fast fatigue assessment procedure for offshore structures under random stess history. In *Proc.Instn. Civ.Engrs,Part 2,* pages p689–700, December 1988.

[47] Hancock J.W. and Gall D.S. Fatigue under narrow and broad band stationary loading. Technical report, Marine Technology Directorate Ltd., December 1985. Final report of the Cohesive Programme of research and Development into the Fatigue of Offshore Structures (July 83-June 85).

[48] J M Tunna. Random load fatigue: Theory and experiment. In *Proc. Instn. Mech. Engrs. Vol. 199 No. C3,* January 1985.

[49] F Sherratt N.W.M.Bishop and Hu Zhihua. The analysis of non-Gaussian loadings from wind turbine blades using frequency domain techniques. In *British Wind Energy Conference.* BWEC'91, Swansea, April 1991.

[50] N.W.M.Bishop and Hu Zhihua. The fatigue analysis of wind turbine blades using frequency domain techneques. In *Proceedings of the European Wind Energy Conference, EWEC'91.* Amsterdam, The Netherlands, October 1991.

[51] Hu Zhihua N.W.M. Bishop and R Wang. Fast frequency domain fatigue life assessment of wind turbine blades. In *Proceedings of the 14th British Wind Energy Association Conference.* BWEC'92, Nottingham, March 1992.

[52] Andrea Carpinteri, editor. *Handbook of Fatigue Crack Propagation in Metallic Structures*, volume 2, pages 1685–1720. ELSEVIER, 1994.

[53] P. Madsen and S. Frandsen. Dynamic analysis of wind turbine rotors for lifetime prediction. Technical report, RISO Contract report 102-43-51, 1983.

[54] Zhao.W and M.J. Baker. On the p.d.f. of rainflow stress range for stationary Gaussian process. *Int. J. of Fatigue, 14(2)*, pages 121–135, March 1992.

[55] British Standards Institution, London. *BS5400: Part 10: 1980, Steel, Concrete and Composite Bridges, Code of practice for fatigue.*

[56] J. S. Bendat and A. G. Piersol. *Random Data: Analysis and Measurement Procedures (2nd ed.).* John-Wiley & Son, 1986.

[57] K. A. BROWNLEE. *Statistical Theory and Methodology In Science and Engineering.* Wiley, New York, 2nd edition, 1965.

[58] D. Middleton. *An Introduction to Statistical Communication Theory.* McGraw Hill Book Company, 1960.

[59] J G Warre R E Hoskin. Prediction of fatigue damage in wind turbine rotors. Technical report, report of BWEC'89, January 1989.

[60] MICHAEL A. STEPHENS RALPH B. D'AGOSTINO, editor. *Goodness-of-fit Techniques*, volume 68 of *STATISTICS:textbooks and monographs.* Marcel Dekker, INC., 1986.

[61] P Bonfield and MP Ansell. Fatigue testing of wood composites for aerogenerator rotor blades. Part VI. life prediction and hysteresis. In TD Davies et al., editor, *Wind Energy Conversion*, 1990.

[62] R.D.Hibberd W.D. Dover. The influence of mean stress and amplitude distribution on random load fatigue. *Engineering fracture Mechanics, Vol.9*, January 1977.

[63] J.Kowalewski. On the relationship between component life under irregularly fluctuating. Technical report, DVL Report 249,1963,Mira Translation no.60/66, January 1963.

[64] M.J. Newby. Markov models for fatigue crack growth. *Eng'g Fracture Mechanics*, 27(4):477–482, January 1987.

[65] K. Sobczyk and Jr. B. F. Spencer. *RANDOM FATIGUE, From Data to Theory.* ACADEMIC PRESS, INC., 1992.

[66] D.R.Cox and H.D.Miller. *The theory of stochastic process.* London, Chapman and Hall, 1977.

[67] N W M Bishop, Z Hu, R Wang. Methods for the Rapid Evaluation of Fatigue Damage on the HOWDEN HWP330 Wind Turbine. In *Proc of EWEC'93*, York, UK., October 1993.

[68] Jørgen Højstrup. Measurements of structural loads in the Nørrekerengær windfarm. In *Proc of BWEC'91,*, April 1991.

[69] G.T. Schueller. *STRUCTURAL DYNAMICS - Recent Advances.* Springer_Verlag, 1991.

[70] Achintya Haldar Hari B. Kanegaonkar. Non-Gaussian responses of offshore platforms: Dynamics. *ASCE J. ST Div.*, January 1989.

[71] Steven R. Winterstein. Non-normal responses and fatigue damage. *ASCE J. EM Div. vol 111*, October 1985.

[72] H.B. et Kanegaonkar. Non-Gaussian response of offshore platforms: Fatigue. *J.Struct.Eng'g,ASCE*, 113(9):1883–1908, September 1987.

[73] J. Juncher Jensen. Fatigue damage due to non-Gaussian responses. *ASCE J. EM Div.*, January 1991.

[74] Dorothy M.Holford. Synthesis of loading sequences from a range-mean-pairs (rainflow) count or fatigue load meter data. Technical Report Technical report 82080, Royal Aircraft EST., July 1982.

[75] M.Hück and W.schütz. Genarating the falstaff load history by digital mini computers. Technical report, Industrieanlagen-Betriebsgesellschaft mbH, 1975. Part II.

[76] G.M.Van Dijk and J.B. Introduction to a fighter aircraft loading standard for fatigue evaluation. Technical report.

[77] H.Klatschke W.Schütz. Standardized load sequence for offshore structures–WASH1. *Fract.Engng Mater.Struct.Vol.13.No.1.pp15-29*, January 1990.

[78] E.Haibach R.Fischer. A standard random load sequence of Gaussian type recommended for general application in fatigue testing: its mathematical background and digital generation. In *Fatigue Testing and Design*, volume 2, April 1976.

[79] J. Draper R.E.Hoskin, J.G. Warren. Prediction of fatigue damage in wind turbines, Phase II. Technical Report WEG T-4132, Wind Energy Group, February 1992.

[80] J.N.YANG. Simulation of random envelope process. *Journal of Sound and Vibration 21(1),73-85*, 1972.

[81] Matej Bily Jozef Cacko and Juraj Bukoveczky. *Random Processes: Measurement, Analysis and Simulation.* Publishing House of the Slovak Academy of Science, Bratislava, 1988.

[82] Curtis Loren D.Lutes. Improved spectral method for variable amplitude fatigue prediction. *ASCE J., ST. Div.*, 116,No. 4, April 1989.

[83] J N Yang. On the normality and accuracy of simulated random processes. *J. of Sound and Vibration*, 26(3):417–428, January 1973.

[84] Yonathan Bard. *Nonlinear Parameter Estimation.* Academic Press, 1974.

[85] Harold W. Sorenson. *Parameter Estimation.* Marcel DeKKER, INC., 1980.

[86] Donald G. Watts Douglas M. Bates. *Nonlinear Regression analysis & its Applications.* John Wiley & Sons, 1988.

[87] Robert Hecht-Nielsen. *NEUROCOMPUTING.* Addison-Welsley Publishing Company, 1990.

[88] R Beale and T Jackson. *Neural Computing: An Introduction.* Adam Hilger.

[89] James A. Freeman and David M. Skapura. *Neural Network: Algorithms, Applications, and Programming Techniques.* Addison-Wesley Publishing Company, 1991.

[90] J Draper R E Hoskin, J G Warren. prediction of fatigue damage in wind turbine rotors. In *Proc of BWEC'91*, April 1991.

[91] K.J.Miller and M.W.Brown, editors. *Multiaxial Fatigue.* Dept. of Machenical Engineering, University of Sheffield, UK, ASTM Special Technical Publication 853, December 1982. A Symposium Sponsored by ASTM Comittees E-9 on Fatigue and E-24 on Fracture Testing, San Francisco.

Appendix A

Spectral fatigue analysis program for Gaussian responses

This is the program used in Chapter 3. The fowchart is shown as in Figure A.1.

```
c
c  Main program for spectral fatigue analysis. Some SUN FORTRAN functions are used
c
c   variable list:
c   bb, bk:  S-N curve parameters
c   nos    :  signal length
c   nchk   :  number of blocks to be used
c   npos   :  interval numbers to divide the signal
c   nl     :  power of 2 of the window size in FFT
c   samp   :  sampling frequency of the signal
c   fc     :  cutoff frequency to be used
c
      PROGRAM FATIG
      PARAMETER (MP=520,MALN=1024000,MHF=60000)
      DIMENSION SIG(MALN),G(MHF)
      COMMON /DENSITY/NPOS,DN,RS(MP),RN(MP),RD(MP),RT(MP)
      COMMON XMEAN,AD,AX,VAR,RMS,BO,B1,B2,B4,GAMMA,BB,BK
      CHARACTER FSP*15,INPUTMODE*1
      WRITE(*,'(5X///,15X,A)')' FORTRAN PROGRAM FOR FATIGUE ESTIMATION'
      NARGS=IARGC()
      IF(NARGS.NE.2)THEN
      WRITE(*,'(10X,A,$)')'Usage :'
      CALL GETARG(0,FSP)
      WRITE(*,'(A,$)')FSP(1:8)
      WRITE(*,'(A)')'task_type  filename'
      CALL EXIT(1)
      ENDIF
      CALL GETARG(1,INPUTMODE)
      IF((INPUTMODE.NE.'2').AND.(INPUTMODE.NE.'1'))THEN
      WRITE(*,'(21X,A)')' Unknown task. '
      CALL EXIT(2)
      ENDIF

c  read in system file

      WRITE(*,'(5X/////)')
      CALL GETARG(2,FSP)
      M=INDEX(FSP,' ')
      FSP(M:M+3)='.sys'
      OPEN(7,FILE=FSP(1:M+3),STATUS='OLD')
      REWIND 7
      READ(7,*)BB,BK
      READ(7,*)NOS,NCHK,NPOS,NL,SAMP,FC
      CLOSE(7)
      FSP(M:M+3)='.psd'
      OPEN(10,FILE=FSP(1:M+3))
```

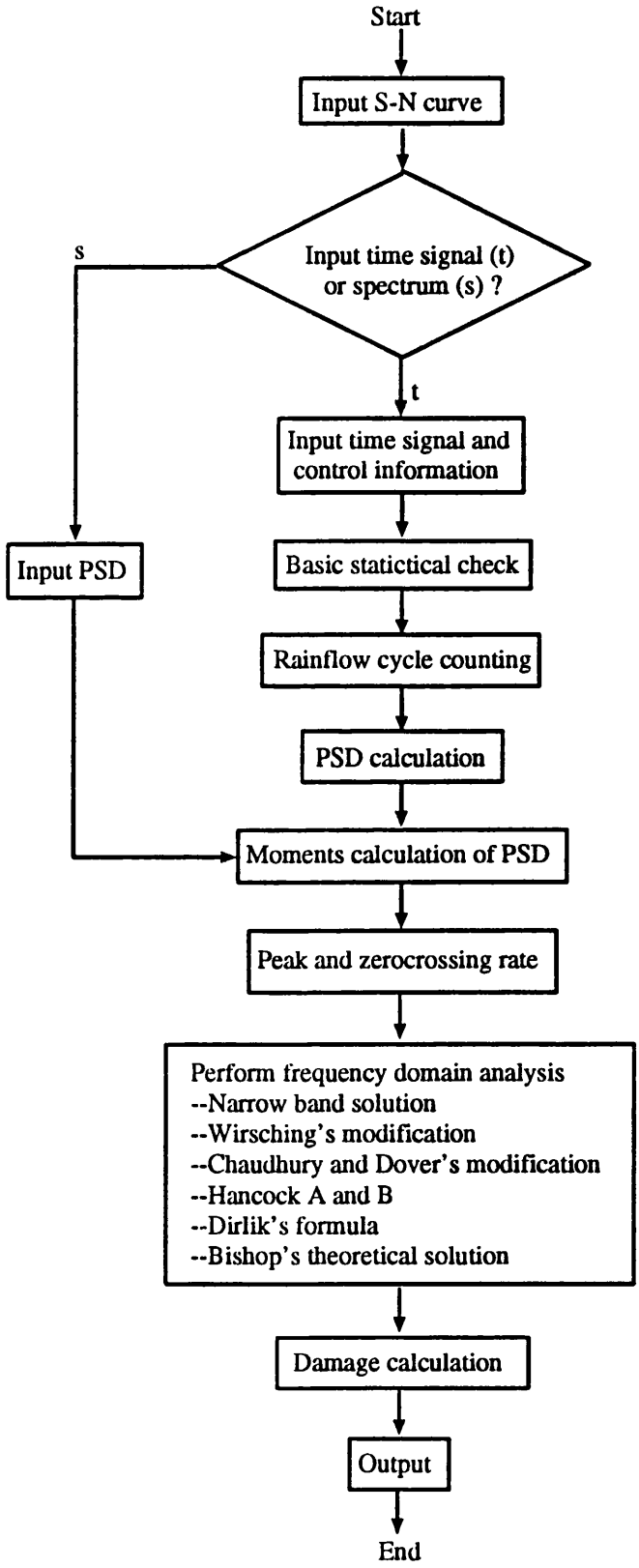

Figure A.1: Flowchart of the program for random fatigue analysis

```
      FSP(M:M+3)='.out'
      OPEN(9,FILE=FSP(1:M+3))
      REWIND 9
      WRITE(9,'(5X/////)')
c
c   if PSD only, read in PDF
c
      IF(INPUTMODE.EQ.'2')THEN
      READ(10,*)FC,NOP,DN,SAMP
      READ(10,*)(G(I),I=1,NOP)
      TK=1.0
      CALL AFTER(SIG,MALN,MHF,G,NOP,SAMP,FC,TK,inv)
      GOTO 500
      ENDIF
c
c   computation when signal history is provided
c
      INV=1
      FC=FC/INV
      MKDS=NOS/NCHK
      IF(NL.EQ.0)THEN
20    NL=NL+1
      MAXT=2**NL
      IF(MKDS/MAXT.NE.0)GOTO 20
      NL=NL-1
      ENDIF
      MAXT=2**NL
      NOP=MAXT/2
c
c   signal read in
c
      FSP(M:M+3)='.bin'
      OPEN(8,FILE=FSP(1:M+4),STATUS='OLD',ACCESS='DIRECT',RECL=4)
      WRITE(*,'(15X,A,I8)')'Length of time signal:  ',NOS
      DO 200 L=1,NCHK
      DO 80 I=1,NPOS
80    RS(I)=0.0
      IF(NCHK.NE.1)THEN
      WRITE(*,'(20X,A,I2,5X,I6/)')' Block  ',L,MKDS
      WRITE(9,'(20X,A,I2/)')' Block  ',L
      WRITE(10,'(20X,A,I2/)')' Block  ',L
      ENDIF
      XMEAN=0.0
      AD=-9E+20
      AX=-AD
      DO 18 I=1,MKDS
      READ(8,REC=I+(L-1)*MKDS)SIG(I)
      XMEAN=XMEAN+SIG(I)
      AD=AMAX1(AD,SIG(I))
      AX=AMIN1(AX,SIG(I))
18    CONTINUE
      XMEAN=XMEAN/MKDS
      CALL PSDG(G,MHF,SIG,MKDS,XMEAN,NL,INV,SAMP)
      CALL TSERIS(SIG,MKDS,SAMP,TK)
      WRITE(10,*)FC,NOP,DN,SAMP
      WRITE(10,*)(G(I),I=1,NOP)
      CALL AFTER(SIG,MALN,MHF,G,NOP,SAMP,FC,TK,inv)
200   CONTINUE
500   CONTINUE
      CLOSE(9)
      WRITE(*,'(5X///)')
      WRITE(*,'(10X,20(1H-),A)')'THE END.'
      STOP
      END

c
c Subroutine for rainflow cycle counting on time series
c
      SUBROUTINE TSERIS(SIG,NOS,SAMP,TK)
      PARAMETER (MP=520,MPKS=300000)
```

```
      DIMENSION SIG(NOS),PKTR(MPKS),IE(MPKS)
      COMMON XMEAN,AD,AX,VAR,RMS,BO,B1,B2,B4,GAMMA,BB,BK
      COMMON /DENSITY/NPOS,DN,RS(MP),RN(MP),RD(MP),RT(MP)
      WRITE(*,'(5X/////,15X,A///)')'Working on the Time Signal'
      DN=(AD-AX)/(NPOS-1.0)
      DO 5 I=1,NOS
      SIG(I)=INT((SIG(I)-AX)/DN+0.5)+1
      IF(SIG(I).LT.1.0)THEN
      WRITE(*,*)' Signal Lower Than the Lowest Limit.',I,sig(i)
      SIG(I)=1.0
      ENDIF
      IF(SIG(I).GT.NPOS)THEN
      WRITE(*,*)' Signal Higher Than the Highest Limit.',I,sig(i)
      SIG(I)=NPOS
      ENDIF
5     CONTINUE
      DO 10 I=1,NPOS
10    RS(I)=0.0
      J=1
      DO 20 I=2,NOS
      IF(SIG(I).NE.SIG(J))THEN
      J=J+1
      SIG(J)=SIG(I)
      ENDIF
20    CONTINUE
      K=J-1
      LN=1
      PKTR(1)=SIG(1)
      DO 30 I=2,K
      JS=INT(SIG(I)-SIG(I-1))
      JL=INT(SIG(I+1)-SIG(I))
      IF(JS*JL.LT.0)THEN
      LN=LN+1
      PKTR(LN)=SIG(I)
      ENDIF
30    CONTINUE
      JS=PKTR(1)-PKTR(2)
      JL=PKTR(LN-1)-PKTR(LN)
      MAXSIG=INT(PKTR(1))
      K=1
      DO 40 I=2,LN
      IF(INT(PKTR(I)).GT.MAXSIG)THEN
      MAXSIG=INT(PKTR(I))
      K=I
      ENDIF
40    CONTINUE
      DO 50 I=1,LN
50    IE(I)=PKTR(I)
      J=1
      IF(JL.GT.0)THEN
      IF(JS.GT.0)THEN
      IF(IE(1).LE.IE(LN))THEN
      IE(LN)=IE(2)
      J=3
      ENDIF
      ELSE
      J=2
      IE(LN)=MIN(IE(LN),IE(1))
      ENDIF
      ELSE
      IF(JS.LT.0)THEN
      IF(IE(1).GE.IE(LN))THEN
      IE(LN)=IE(2)
      J=3
      ENDIF
      ELSE
      J=2
      IE(LN)=MAX(IE(LN),IE(1))
      ENDIF
      ENDIF
```

```
      KK=LN-K+1
      DO 60 I=1,KK
60    PKTR(I)=IE(I+K-1)
      DO 70 I=J,K
      KK=KK+1
      PKTR(KK)=IE(I)
70    CONTINUE
      LN=LN+2-J
      NN=1
      KK=1
      IE(NN)=PKTR(KK)
90    KK=KK+1
      NN=NN+1
      IE(NN)=PKTR(KK)
      IF(NN.LT.4)GOTO 90
100   I=IABS(IE(NN-2)-IE(NN-3))
      J=IABS(IE(NN-1)-IE(NN-2))
      K=IABS(IE(NN)-IE(NN-1))
      IF((J.GT.I).OR.(J.GT.K))GOTO 90
      RS(J)=RS(J)+1.0
      NN=NN-2
      IE(NN)=IE(NN+2)
      IF(NN.GE.4)GOTO 100
      IF(KK.LT.LN)GOTO 90
      J=NPOS-1
      RS(J)=RS(J)+1.0
      NOC=0
      DO 110 I=1,NPOS
110   NOC=NOC+RS(I)
      DO 120 I=1,NPOS
120   RS(I)=RS(I)/NOC/DN
      WRITE(*,'(15X,A,I8,5X/////)')'Cycle Counting End.',LENGH
      write(*,*)'cycles after filter',NOC
      TK=NOC*SAMP/(NOS)
      RETURN
      END

c
c subroutine for PSD calculation
c
      SUBROUTINE PSDG(G,MHF,SIG,NOS,XMEAN,NL,INV,SAMP)
      PARAMETER(MALN=160000)
      DIMENSION G(MHF),SIG(NOS)
      COMPLEX F(MALN)
      MAXT=2**NL
      NOP=MAXT/2
      IBLOCK=NOS/INV/MAXT
      T=FLOAT(MAXT)
      DO 10,K=1,NOP
10    G(K)=0.0
      WRITE(*,'(5X///,12X,A,I3)')' Calculating P.S.D ',IBLOCK
      DO 40 I=1,IBLOCK
      WRITE(*,'(20X,A,I4,5X,I5)')' Block No. ',I,MAXT
      DO 20,J=1,MAXT
      KJ=(J-1)*INV+1+(I-1)*MAXT*INV
      F(J)=CMPLX((SIG(KJ)-XMEAN)/T,0.0)
20    CONTINUE
      CALL FFT(F,MAXT,NL)
      DO 30 K=1,NOP
30    G(K)=G(K)+(REAL(F(K))**2+AIMAG(F(K))**2)
40    CONTINUE
      T=2.0*INV*MAXT/FLOAT(IBLOCK)/SAMP
      DO 50 K=1,NOP
50    G(K)=G(K)*T
      WRITE(*,'(5X//,10X,A//////)')'  P.S.D. Calculating End'
      RETURN
      END

c
C FFT subroutine
```

```
c
      SUBROUTINE FFT(A,N,NN)
      COMPLEX A(N),W,T,U
      J=1
      DO 40 L=1,N-1
10    IF(L.LT.J)THEN
      T=A(J)
      A(J)=A(L)
      A(L)=T
      ENDIF
      K=N/2
20    IF(K.GE.J)GOTO 30
      J=J-K
      K=K/2
      GOTO 20
30    J=J+K
40    CONTINUE
      DO 80 M=1,NN
      U=(1.0,0.0)
      K=2**(M-1)
      PI=3.1415926589793/K
      W=CMPLX(COS(PI),-SIN(PI))
      DO 70 J=1,K
      I=J
60    T=A(I+K)*U
      A(I+K)=A(I)-T
      A(I)=A(I)+T
      I=I+2**M
      IF(I.LE.N)GOTO 60
      U=U*W
70    CONTINUE
80    CONTINUE
      RETURN
      END

c
c Subroutine for calculating the rainflow PDF's
c
      SUBROUTINE DENST
      PARAMETER (MP=520)
      COMMON XMEAN,AD,AX,VAR,RMS,B0,B1,B2,B4,GAMMA,BB,BK
      COMMON /DENSITY/NPOS,DN,RRANGE(MP),RN(MP),RD(MP),RT(MP)
      WRITE(*,'(5X/////15X,A///)')'Probability Densities  '
      L=NPOS+1
c
c  narrow band
c
      DO 10 I=1,L
      S=(I-0)*DN
      RN(I)=EXP(-S*S/8.0/B0)*S/4.0/B0
10    CONTINUE
c
c   Dirlik's formula
c
      XM=B1*SQRT(B2/B4)/B0
      write(*,*)'mm',b0,b1,b2,b4,gamma
      D1=2.0*(XM-GAMMA*GAMMA)/(1.0+GAMMA*GAMMA)
      R=(GAMMA-XM-D1*D1)/(1.0-GAMMA-D1+D1*D1)
      D2=(1.0-GAMMA-D1+D1*D1)/(1.0-R)
      D3=1.0-D1-D2
      Q=1.25*(GAMMA-D3-D2*R)/D1
      XC=0.5/SQRT(B0)
      DO 20 I=1,L
      Z=(I-1)*DN*XC
      C=D1*EXP(-Z/Q)/Q+D2*Z*EXP(-Z*Z/2.0/R/R)/R/R
      RD(I)=(C+D3*Z*EXP(-Z*Z/2.0))*XC
      write(*,*)i,rd(i)
20    CONTINUE
      WRITE(*,'(15X,A//////)')'  Densities End'
      RETURN
```

```
      END

c
c Bishop's theoretical solution
c
      SUBROUTINE SRAIN
      PARAMETER(MP=520,NSQ=20)
      DIMENSION ARR(MP,MP),BRR(MP,MP),SPKS(MP)
      DIMENSION PPPT(MP,MP),XNEW(MP,MP),WX(MP,MP)
      COMMON XMEAN,AD,AX,VAR,RMS,BO,B1,B2,B4,GAMMA,BB,BK
      COMMON /DENSITY/NPOS,DN,RRANGE(MP),RN(MP),RD(MP),SRR(MP)
      XC=DN*(NPOS)/2.0
      SUM=BO*(1.0-GAMMA**2)
      SUMD=DN*DN
      DO 10 J=1,NPOS
      DO 10 K=1,J-1
      YP=(DN*(J-0.5)-XC)
      YT=(DN*(K-0.5)-XC)
      XRR=(YP-YT)/(4.0*BO*GAMMA**2)
      YRR=SUMD/(SQRT(6.284*SUM))
      ZRR=-1/(8*SUM*GAMMA**2)*(YP**2+YT**2+2.0*YP*YT*(2.0*GAMMA**2-1))
      PPPT(J,K)=XRR*YRR*EXP(ZRR)
10    CONTINUE
      DO 15 I=1,NPOS
      DO 15 J=I+1,NPOS
15    PPPT(I,J)=PPPT(J,I)
      SUMD=0.0
      DO 40 I=1,NPOS
      PPPT(I,I)=0.0
      SUM=0.0
      DO 20 J=1,I-1
      SUM=SUM+PPPT(I,J)
20    CONTINUE
      SPKS(I)=SUM
      SUMD=SUMD+SUM
      IF(SUMD.EQ.0.0)GOTO 40
      DO 30 J=1,I-1
      PPPT(I,J)=PPPT(I,J)/SUM
30    CONTINUE
40    CONTINUE
      DO 50 IR=1,NPOS
      SPKS(IR)=SPKS(IR)/SUMD
50    CONTINUE
      DO 80 I=1,NPOS
      SUM=0.0
      DO 60 J=I+1,NPOS
      SUM=SUM+PPPT(I,J)
60    CONTINUE
      DO 70 J=I+1,NPOS
      PPPT(I,J)=PPPT(I,J)/SUM
70    CONTINUE
80    CONTINUE
      DO 90 I=1,NPOS
      DO 90 J=1,NPOS
      ARR(I,J)=0.0
      BRR(I,J)=0.0
90    CONTINUE
      DO 220 IP=4,NPOS
      WRITE(*,'(16X,A,I5)')'  Peak  :  ',IP
      DO 210 KP=2,IP-2
      IA=KP-1
      IB=KP+1
      IC=IP-IA
      IE=3
      DO 100 I=1,IC
      DO 100 J=1,IC
      XNEW(I,J)=0.0
100   CONTINUE
      DO 120 LA=IE,IC
      DO 110 LB=1,IA
```

```
      XNEW(LA,1)=XNEW(LA,1)+PPPT(LA+IA,LB)
110   CONTINUE
      XNEW(LA,2)=PPPT(LA+IA,KP)
120   CONTINUE
      XNEW(1,1)=1.0
      XNEW(2,2)=1.0
      DO 150 LA=IE,IC
      JCNT=LA+IA
      DO 140 LB=IE,IC
      KCNT=LB+IA
      LCNT=MINO(KCNT,JCNT)-1
      DO 130 MA=IB,LCNT
      XNEW(LA,LB)=XNEW(LA,LB)+PPPT(JCNT,MA)*PPPT(MA,KCNT)
130   CONTINUE
140   CONTINUE
150   CONTINUE
      DO 200 III=1,NSQ
      DO 180 LA=1,IC
      DO 180 LB=1,IC
      SUM=0.0
      DO 170 LC=1,IC
      IF(III.EQ.1.AND.LC.EQ.IC)GO TO 160
      SUM=SUM+XNEW(LA,LC)*XNEW(LC,LB)
160   CONTINUE
170   CONTINUE
      WX(LA,LB)=SUM
180   CONTINUE
      DO 190 I=1,IC
      DO 190 J=1,IC
190   XNEW(I,J)=WX(I,J)
200   CONTINUE
      ARR(IP,KP)=XNEW(IC,1)+XNEW(IC,2)
      BRR(IP,KP)=XNEW(IC,2)
210   CONTINUE
220   CONTINUE
      DO 230 I=1,NPOS
      SRR(I)=0.0
230   CONTINUE
      DO 240 IP=4,NPOS
      DO 240 KP=2,IP-2
      I=NPOS+1-KP
      K=NPOS+1-IP
      DRR=2.0*ARR(IP,KP)*BRR(IP,KP)*ARR(I,K)*SPKS(IP)/DN
      SRR(IP-KP)=SRR(IP-KP)+DRR
240   CONTINUE
      RETURN
      END

c
c Damage calculation
c
      SUBROUTINE EDAMAGE(SH,SIG,M,TK,EP)
      PARAMETER(MP=520)
      DIMENSION SIG(M),SH(10)
      COMMON XMEAN,AD,AX,VAR,RMS,BO,B1,B2,B4,GAMMA,BB,BK
      COMMON /DENSITY/NPOS,DN,RS(MP),RN(MP),RD(MP),RT(MP)
      WRITE(*,'(5X/////,15X,A/////)')'Expected Damage Life'
      L=NPOS+1
      EO=SQRT(B2/BO)
      EP=SQRT(B4/B2)
      RT(L)=0.0
      RS(L)=0.0
      do 10 i=1,5
10    sh(i)=0.0
      DO 109 I=1,NPOS
      XTOT=((I*DN)**BB)
      XT=(((I-1)*DN)**BB)
      RS(I)=RS(I)*XTOT
      RN(I)=RN(I)*XT
      RD(I)=RD(I)*XTOT
```

```
      RT(I)=RT(I+1)*((i+1)*dn)**bb
      sh(1)=sh(1)+rs(i)*dn*tk/bk
      sh(2)=sh(2)+rn(i)*dn*ep/bk
      sh(3)=sh(3)+rd(i)*dn*ep/bk
      sh(5)=sh(5)+rt(i)*dn*ep/bk
109   continue
      AB=0.0
      k=npos-1
      CALL SIMPSON1(RS,L,ab,dn,ab,ER)
      CALL SIMPSON1(RN,L,ab,dn,ab,EN)
      CALL SIMPSON1(RD,L,ab,dn,ab,ED)
      CALL SIMPSON1(RT,k,ab,dn,ab,ET)
      WRITE(*,*)ER,EN,ED,ET
      WRITE(*,*)TK,EP,'   psd/time ',EP/TK
      SH(1)=ER*TK/bk
      SH(2)=EN*EP/bk
      SH(3)=ED*EP/bk
      SH(5)=ET*EP/bk
      EPS=SQRT(1.0-GAMMA*GAMMA)
      AB=0.926-0.033*BB
      CB=1.587*BB-2.323
      DLAM=AB+(1.0-AB)*(1.0-EPS)**CB
      SH(4)=SH(2)*DLAM
      ZZ=BB/2.0+1.0
      CALL GAMA(ZZ,SIG,M,GB)
      SH(6)=(DLAM*GB)**(1.0/BB)
      SH(6)=SH(6)*2.0*SQRT(2.0*BO)
      ZZ=(BB+1.0)/2.0
      CALL GAMA(ZZ,SIG,M,GB1)
      ERF=0.5
      CC=GB1*EPS**(BB+2.0)/SQRT(3.1415927)+GB*(1.0+ERF)*GAMMA
      SH(7)=2.0*SQRT(2.0*BO)*(CC/2.0)**(1.0/BB)
      ERF=0.3012*GAMMA+0.4916*GAMMA*GAMMA+0.9181*GAMMA**3
      ERF=ERF-2.3534*GAMMA**4-3.3307*GAMMA**5
      ERF=ERF+15.6524*GAMMA**6-10.7846*GAMMA**7
      CC=GB1*EPS**(BB+2.0)/SQRT(3.1415927)+GB*(1.0+ERF)*GAMMA
      SH(8)=2.0*SQRT(2.0*BO)*(CC/2.0)**(1.0/BB)
      SH(9)=SQRT(8.0*BO)*(GAMMA*GB)**(1.0/BB)
      ZZ=BB/(2.0-EPS*EPS)+1.0
      CALL GAMA(ZZ,SIG,M,GB)
      EPS=0.02
      SH(10)=SQRT((2.0*BO)*(2.0-EPS**2))*GB**(1.0/BB)
      DO 20 I=6,10
20    SH(I)=(SH(I)**BB)*EP/BK
4     RETURN
      END

c
c Gamma function
c
      SUBROUTINE GAMA(ZZ,F,M,GB)
      DIMENSION F(M)
      H=1.0/(M-1)
      F(1)=-ALOG(0.00001)
      F(M)=0.0
      DO 10 I=2,M-1
      X=(I-1)*H
      R=-ALOG(X)
      F(I)=R**(ZZ-1.0)
10    CONTINUE
      H=1.0/(M-1)
      a=0.0
      w=0.0
      CALL SIMPSON1(F,M,a,H,w,GB)
      RETURN
      END

c
c PSD moments calculation
c
```

```
      SUBROUTINE AFTER(SIG,MALN,MHF,G,NOP,SAMP,FC,TK,inv)
      PARAMETER (MP=520)
      DIMENSION SIG(MALN),G(MHF),SH(10)
      COMMON /DENSITY/NPOS,DN,RRANGE(MP),RN(MP),RD(MP),RT(MP)
      COMMON XMEAN,AD,AX,VAR,RMS,BO,B1,B2,B4,GAMMA,BB,BK
      G(NOP+1)=0.0
      H=SAMP/2.0/inv/(NOP-1)
      knd=0
1     knd=knd+1
      if(knd*h.ge.fc)goto 2
      goto 1
c      KND=INT(FC/H)
c      IF(MOD(KND,2).EQ.0)KND=KND+1
2      J=INT(0.0/H)
      DO 3 I=1,J
3     G(I)=0.0
      G(1)=0.0
      A=0.0
      WL=0.0
      CALL SIMPSON1(G,KND,A,H,WL,BO)
      WL=1.0
      CALL SIMPSON1(G,KND,A,H,WL,B1)
      WL=2.0
      CALL SIMPSON1(G,KND,A,H,WL,B2)
      WL=4.0
      CALL SIMPSON1(G,KND,A,H,WL,B4)
      EP=SQRT(B4/B2)
      GAMMA=SQRT(1.0/(BO*B4))*B2
      WRITE(*,*)(KND-1)*H,' MOMENTS',BO,B1,B2,B4,GAMMA
      CALL DENST
      CALL SRAIN
      J=NPOS+1
      WRITE(9,*)NPOS,DN
      WRITE(9,*)(RRANGE(I),I=1,NPOS)
      WRITE(9,*)
      WRITE(9,*)(RN(I),I=1,J)
      WRITE(9,*)
      WRITE(9,*)(RD(I),I=1,J)
      WRITE(9,*)
      WRITE(9,*)(RT(I),I=1,NPOS)
      J=MALN-1
      IF(MALN.GE.200000)J=199999
      CALL EDAMAGE(SH,SIG,J,TK,EP)
c
c  results output to file .out
c
      write(9,*)'At Frequency = ',KND,'   *',H,'   =',h*(knd-1)
      WRITE(9,*)'Moments = ',BO,B1,B2,B4,GAMMA
      WRITE(9,*)'Expected peaks (PSD / TIME)= ',EP,'   /',TK
      WRITE(9,'(5X///,15X,A//)')'Expected Damage Life '
      WRITE(9,*)'   Probability density     Damage Life'
      WRITE(9,*)'       Time Signal       ',SH(1),SH(1)/SH(1)
      WRITE(9,*)'       Narrow Band       ',SH(2),SH(2)/SH(1)
      WRITE(9,*)'      Dirlic Theory      ',SH(3),SH(3)/SH(1)
      WRITE(9,*)'      Dirlic Theory      ',SH(3),SH(3)/SH(1)
      WRITE(9,*)'    Wirsching Modified   ',SH(4),SH(4)/SH(1)
      WRITE(9,*)'   Theoretical Rainflow  ',SH(5),SH(5)/SH(1)
      WRITE(9,'(5X///)')
      WRITE(9,*)'    Equivalent Stress  '
      WRITE(9,*)' Wirsching  : ',SH(6),SH(6)/SH(1)
      WRITE(9,*)' Chaudhury1 : ',SH(7),SH(7)/SH(1)
      WRITE(9,*)' Chaudhury2 : ',SH(8),SH(8)/SH(1)
      WRITE(9,*)' Hancock A  : ',SH(9),SH(9)/SH(1)
      WRITE(9,*)' Hancock B  : ',SH(10),SH(10)/SH(1)
      write(9,*)'mean=',xmean,'dn=',dn
      WRITE(9,*)'       Time Signal       ',SH(1),SH(1)/SH(1)
      WRITE(9,*)'      Dirlic Theory      ',SH(3),SH(3)/SH(1)
      WRITE(9,*)'   Theoretical Rainflow  ',SH(5),SH(5)/SH(1)
      WRITE(9,'(5X///)')
      WRITE(9,'(10X,20(1H-),A)')'THE END.'
```

```
      WRITE(*,'(10X///)')
      WRITE(*,'(5X///,15X,A//)')'Expected Damage Life '
      WRITE(*,*)'   Probability density     Damage Life'
      WRITE(*,*)'       Time Signal       ',SH(1),SH(1)/SH(1)
      WRITE(*,*)'       Narrow Band       ',SH(2),SH(2)/SH(1)
      WRITE(*,*)'      Dirlic Theory      ',SH(3),SH(3)/SH(1)
      WRITE(*,*)'    Wirsching Modified   ',SH(4),SH(4)/SH(1)
      WRITE(*,*)'   Theoretical Rainflow  ',SH(5),SH(5)/SH(1)
      WRITE(*,'(5X///)')
      WRITE(*,*)'    Equivalent Stress  '
      WRITE(*,*)' Wirsching  : ',SH(6),SH(6)/SH(1)
      WRITE(*,*)' Chaudhury1 : ',SH(7),SH(7)/SH(1)
      WRITE(*,*)' Chaudhury2 : ',SH(8),SH(8)/SH(1)
      WRITE(*,*)' Hancock A  : ',SH(9),SH(9)/SH(1)
      WRITE(*,*)' Hancock B  : ',SH(10),SH(10)/SH(1)
      WRITE(7,*)KND,KND*H,(SH(I),I=1,10)
      WRITE(*,'(5X///)')
      RETURN
      END

c
c integration by Simpson's rule
c
      SUBROUTINE SIMPSON1(FUNC,M,A,H,WL,RSLT)
      DIMENSION FUNC(M)
      FUNC(1)=FUNC(1)/2.0
      FUNC(M)=FUNC(M)/2.0
      R1=0.0
      DO 10 I=2,M-1,2
      TE=A+(I-1)*H
10    R1=R1+FUNC(I)*TE**WL
      R2=0.0
      DO 20 I=1,M,2
      TE=A+(I-1)*H
20    R2=R2+FUNC(I)*TE**WL
      RSLT=(R1*4.0+R2*2.0)*H/3.0
      RETURN
      END
```

Appendix B

Computer program for neural network training

This appendix includes the for neural network training. It is a multi-layer network with back propagation. The structure of the program is described in **Chapter 8.**

```
/*
     C program for neural network training
     variable list:
   nl     :  number of layers
   n      :  number of training data
   layer  :  layout of the net
   ita    :  iteration step size
   alp    :  momentum size
   bj,bx  :  transform factor
   ep     :  accuracy criterion

   */
#define  nd  2200
#define  ln    5
#define  nu    30
#include  <stdio.h>
#include  <math.h>
#include  <stdlib.h>
#include  <string.h>
main(argc,argv)
int argc;
char *argv[];
{
  int i,j,k,n,nl,st,m,ni,kk,jj,no,layer[ln],count,cnts;
  float wt[ln][nu][nu],theta[ln][nu],x[nu][nd],dth[ln][nu];
  float dw[ln][nu][nu],eps,de,t[nu],s[nu],ep,tal,es;
  float ita,net[ln][nu],nout[ln][nu],delt[ln][nu],old;
  float pth[ln][nu],pw[ln][nu][nu],y[nu][nd],alp,bj,bx;
  FILE *fi,*fo;
  if(argc != 2)
    {
      printf("usage: %s filename \n",argv[0]);
      exit(1);
    }

/*
    data read in
*/

  m=strlen(argv[1]);
  strcpy(argv[1]+m,".sys");
  if((fi=fopen(argv[1],"r")) == NULL)
    {
      printf("%s: can't open %s\n",argv[0],".sys file");
       exit(2);
    }
  fscanf(fi,"%d%d",&nl,&n);
```

```
  for(i=0;i<=nl;i++)
    fscanf(fi,"%d",&layer[i]);
  fscanf(fi,"%g%g",&ita,&alp);
  fscanf(fi,"%g%g",&bj,&bx);
  fscanf(fi,"%g",&ep);
  fclose(fi);

  ni=layer[0];
  no=layer[nl];

  strcpy(argv[1]+m,".in");
  if((fi=fopen(argv[1],"r")) == NULL)
    {
      printf("%s: can't open %s\n",*argv,argv[1]);
       exit(3);
    }

  strcpy(argv[1]+m,".out");
  fo=fopen(argv[1],"w");
  for(i=1;i<=n;i++)
    {
    for(j=0;j<ni;j++)
      fscanf(fi,"%g",&x[j][i]);
    for(j=1;j<=no;j++)
      fscanf(fi,"%g",&y[j][i]);
    }
  eps=9e+10;old=-eps;
  for(i=1;i<=n;i++)
    for(j=1;j<=no;j++)
      {
        y[j][i]=(y[j][i]+bj)*bx;
        if ( y[j][i] > old )
          old=y[j][i];
        if ( y[j][i] < eps )
          eps=y[j][i];
      }

  for(st=1;st<=n;st++)
   {
    printf("%5d ",st);
    for(i=0;i<ni;i++)
      printf("%8.3f ",x[i][st]);
    for(i=1;i<=no;i++)
      printf("%8.5f ",y[i][st]);
    printf("\n");
   }

/*
   network initial setting, random
*/

  for(k=1;k<=nl;k++)
    for(j=1;j<=layer[k];j++)
      {
        for(i=1;i<=layer[k-1];i++)
          wt[k][j][i]=(0.02*i+0.01*j-0.08*k)/layer[k];
        theta[k][j]=(0.02*k-0.01*j)/layer[k];
      }
  for(k=1;k<=nl;k++)
    for(j=1;j<=layer[k];j++)
      {
        pth[k][j]=0.0;
        for(i=1;i<=layer[k-1];i++)
          pw[k][j][i]=0.0;
      }

/*
    iteration training
    forward computation first
*/
```

```
  old=9e+20;
  count=0;
  cnts=0;
  do {
  eps=0.0;
  tal=0.0;
  for(st=1;st<=n;st++)
    {
      for(i=1;i<=ni;i++)
        nout[0][i]=x[i-1][st];
      for(k=1;k<=nl;k++)
        for(j=1;j<=layer[k];j++)
          {
            net[k][j]=theta[k][j];
            for(i=1;i<=layer[k-1];i++)
              net[k][j]+=wt[k][j][i]*nout[k-1][i];
            nout[k][j]=val(net[k][j]);
          }

/*
    back propagation
*/

      for(j=1;j<=no;j++)
        {
          de=y[j][st]-nout[nl][j];
          delt[nl][j]=de*slp(nout[nl][j]);
          es=fabs(de/y[j][st]);
          tal+=es/n;
          if ( eps < es )
            eps= es;
        }

      for(k=1;k<=nl-1;k++)
        for(i=1;i<=layer[k];i++)
          {
            for(j=1;j<=layer[k+1];j++)
              t[j]=wt[k+1][j][i]*slp(nout[k][i]);
            for(kk=k+2;kk<=nl;kk++)
              {
                 for(jj=1;jj<=layer[kk];jj++)
                   {
                      s[jj]=0.0;
                      for(m=1;m<=layer[kk-1];m++)
                        s[jj]+=wt[kk][jj][m]*slp(nout[kk-1][m])*t[m];
                   }
                 for(jj=1;jj<=layer[kk];jj++)
                   t[jj]=s[jj];
              }
            delt[k][i]=0.0;
            for(j=1;j<=no;j++)
              delt[k][i]+=delt[nl][j]*t[j];
          }

      for(k=1;k<=nl;k++)
        for(j=1;j<=layer[k];j++)
          {
            for(i=1;i<=layer[k-1];i++)
              dw[k][j][i]=ita*delt[k][j]*nout[k-1][i];
            dth[k][j]=ita*delt[k][j];
          }
      for(k=1;k<=nl;k++)
        for(j=1;j<=layer[k];j++)
          {
            for(i=1;i<=layer[k-1];i++)
              wt[k][j][i]+=dw[k][j][i]+alp*pw[k][j][i];
            theta[k][j]+=dth[k][j]+alp*pth[k][j];
          }
      for(k=1;k<=nl;k++)
```

```
        for(j=1;j<=layer[k];j++)
          {
            for(i=1;i<=layer[k-1];i++)
              pw[k][j][i]=dw[k][j][i];
            pth[k][j]=dth[k][j];
          }

    }
    count++;
    if(count >=1000)
      {
        cnts++;
        k=cnts*1000;
        printf("%8d maximam error=%10.6f   average=%10.6f\n",k,eps,tal);
        count=0;
      }
    if( fabs(1.0-old/eps) > 1.0e-20)
      old=eps;
    else
      break;

     }while((eps > 100.0*ep) || (tal > ep ));
/*
  results output
*/

  printf("  end with maximam error %10.7f  and average %g\n",eps,tal);
  fprintf(fo,"%d\n",nl);
  for(i=0;i<=nl;i++)
    fprintf(fo," %d ",layer[i]);
  fprintf(fo,"\n");
  fprintf(fo,"%g %g\n",bj,bx);
  for(i=1;i<=nl;i++)
    for(j=1;j<=layer[i];j++)
      {
        for(k=1;k<=layer[i-1];k++)
          fprintf(fo," %g",wt[i][j][k]);
        fprintf(fo," %g\n",theta[i][j]);
      }

  eps=0.0;
  tal=0.0;
  printf(" No.");
  for(i=1;i<=ni;i++)
    printf("     X%d  ",i);
  for(i=1;i<=no;i++)
    printf("    Y%d   ",i);
  for(i=1;i<=no;i++)
    printf("   Out%d",i);
  for(i=1;i<=no;i++)
    printf("      de%d",i);
  for(i=1;i<=no;i++)
    printf("       error%d",i);
  printf("\n");
  for(i=1;i<=85;i++)
    printf("_");
  printf("\n");
  for(st=1;st<=n;st++)
    {
    for(i=1;i<=ni;i++)
      nout[0][i]=x[i-1][st];
      for(k=1;k<=nl;k++)
        for(j=1;j<=layer[k];j++)
          {
            net[k][j]=theta[k][j];
            for(i=1;i<=layer[k-1];i++)
              net[k][j]+=wt[k][j][i]*nout[k-1][i];
            nout[k][j]=val(net[k][j]);
          }
    for(j=1;j<=no;j++)
```

```
      {
        y[j][st]=y[j][st]/bx-bj;
        nout[nl][j]=nout[nl][j]/bx-bj;
      }

    for(i=1;i<=no;i++)
      {
        de=y[i][st]-nout[nl][i];
        es=fabs(de/y[i][st]);
        tal+=es/n;
        if ( eps < es )
          eps= es;
      }
    printf("%3d ",st);
    for(i=0;i<ni;i++)
      printf("%8.3f ",x[i][st]);
    for(i=1;i<=no;i++)
      printf("%8.5f ",y[i][st]);
    for(i=1;i<=no;i++)
      printf("%8.5f ",nout[nl][i]);
    printf("%10.7f %10.7f%s\n",de,es*100.0,"%");
    }
  for(i=1;i<=85;i++)
    printf("_");
  printf("\n");
  eps*=100.0;tal*=100.0;
  printf("maximax error = %10.6f%s average error = %10.6f%s\n",eps,"%",tal,"%");
}
```